University of Reading

Department of Meteorology

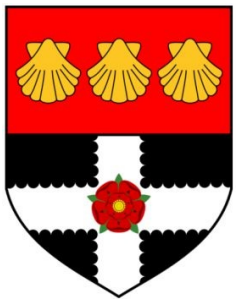

Nicholas Williams

Arctic Sea Ice Reduction: Gaining New Knowledge from Data Assimilation

This dissertation is submitted for the degree of
Doctor of Philosophy

June 2023

Declaration

I confirm that this is my own work and the use of all material from other sources has been properly and fully acknowledged.

Nicholas Williams
June 2023

Acknowledgements

I would like to thank the following for their guidance and support:

- Firstly, my supervisors Daniel Feltham, Peter Jan Van Leeuwen, David Schroeder, Ross Bannister and Andy Shepherd for their invaluable guidance, support and patience throughout my PhD.
- Nick Byrne, Lars Nerger and Maria Broadridge for their help and support in the use of the PDAF framework and producing this research.
- My monitoring committee, Keith Haines, Elena Tarnavsky and Ed Hawkins, who provided me with constructive feedback, support and advice regularly throughout my PhD.
- The sea ice group in Reading for their constructive feedback, discussions and advice.
- My fellow PhD students and the staff in the Department of Meteorology, for being such a friendly and supportive community and creating such a great environment for research.
- Finally, my family for their understanding and support, especially in the final year of my PhD.

Abstract

The evolution of Arctic sea ice thickness and volume over the satellite era are poorly understood because of the difficulties in both modelling and observing the sea ice. The intricate coupling that occurs between the ice, the ocean and the atmosphere makes modelling the sea ice cover accurately a very complex task. The harsh conditions and remoteness of the polar regions as well as the continual changes in the sea ice cover mean that sea ice thickness is difficult to observe consistently year-round. Further work is needed in understanding the changes that have occurred in the Arctic sea ice cover, not only to understand where the changes have occurred, but how and why they have occurred, so that we can understand what is driving these changes, and what changes are likely to occur in the future. In this thesis, we produce a new Arctic sea ice reanalysis in an attempt to ascertain where sea ice models are performing poorly, why this is happening, and identify possible areas of focus for future sea ice model development in order to obtain better estimates of regional and Pan Arctic changes in the sea ice cover.

In the past decade groundbreaking new satellite observations of the Arctic sea ice cover have been made, allowing researchers to understand the state of the Arctic sea ice system in greater detail than before. The derived estimates of sea ice thickness are useful but limited in time and space. In this thesis the results from a new sea ice data assimilation system are presented. Observations assimilated (in various combinations) are monthly mean sea ice thickness and monthly mean sea ice thickness distribution from Cryosat-2, and NASA Team and Bootstrap daily sea ice concentration. This data assimilation system couples the Centre for Polar Observation and Modelling's (CPOM) version of the Los Alamos Sea Ice Model (CICE) to the Localised Ensemble Transform Kalman Filter (LETKF) from the Parallel Data Assimilation Framework (PDAF) library. The impact of assimilating a sub-grid scale sea ice thickness distribution is of particular novelty. The sub-grid scale sea ice thickness distribution is a fundamental component of sea ice models, playing a vital role in the dynamical and thermodynamical processes, yet very little is known of its true state in the Arctic. Observations of summer sea ice thickness are assimilated for the first time, which has not previously been possible in Arctic sea ice reanalyses.

We find that assimilating Cryosat-2 products for the mean thickness and the sub-grid scale thickness distribution can have significant consequences on the modelled distribution of the ice thickness across the Arctic and particularly in regions of thick multi-year ice. The assimilation of sea ice concentration, mean sea ice thickness and sub-grid scale sea ice thickness distribution together performed best when compared to a subset of Cryosat-2 observations held back for validation. Regional model biases are reduced: the thickness of the thickest ice in the Canadian Archipelago is decreased, but the thickness of the ice in the Central Arctic is increased. When comparing the assimilation of mean thickness with the assimilation of sub-grid scale thickness distribution, it is found that the latter leads to a significant change in the volume of ice in each category. Estimates of the thickest ice improve significantly with the assimilation of sub-grid scale thickness distribution alongside mean thickness.

We find that our reanalyses of Arctic sea ice over the satellite era (1981-2020) substantially improve the estimates of sea ice extent, primarily in winter where the model estimates of sea ice concentration are much too high in the Arctic peripheral seas, causing an overestimation of sea ice extent in the stand-alone model. The differences in estimated sea ice concentration in two different sets of observations (NASA Team and Bootstrap) lead to very different estimates of sea ice volume depending on which is assimilated. These differences are reduced when ice thickness is also assimilated, demonstrating both the importance of assimilating ice thickness, and the drawbacks of only using sea ice concentration observations to make reanalysis estimates of short or long term changes in ice volume. We find that the distribution of the ice thickness in the Arctic is considerably different in our reanalyses in comparison to a model simulation that does not use assimilation, with a reduction in very thick ice and a reduction in the overall range of grid cell mean ice thickness. We also find strong disagreement between the free run of the model, observation and reanalysis on the timing of the seasonal sea ice cycle, with observations favouring earlier starts to both the melt and growth season. The assimilation of recently produced year-round sea ice thickness estimates is performed for the first time and shows the greatest improvement for ice thickness estimates in comparison with independent observations. Our work demonstrates the importance of, and need for, further work in sea ice observations and sea ice data assimilation in order to improve our understanding of the Arctic sea ice cover.

Table of contents

List of figures

List of tables

Chapter 1

Introduction

The primary objective of this thesis is to produce and analyse a new Arctic sea ice reanalysis over the satellite era (1981-2020) using recently developed observations from the Cryosat-2 (CS2) satellite. This includes assimilating a sub-grid scale sea ice thickness distribution and year-round observations of mean sea ice thickness. The impacts and potential benefit of assimilating these new observational records in a new sea ice data assimilation product are investigated. Also of particular interest is the identification of incorrect model physics in CICE from the data assimilation product, which could be used to improve sea ice models in future. In section 1.1 we give an overview of the Arctic and the changes which have been occurring in the 21st century. In section 1.2 we discuss the potential for a new sea ice reanalysis and the usefulness of data assimilation in climate studies. In section 1.3 we lay out the aims and outline for this thesis.

1.1 Arctic Ocean

The Arctic Ocean is an environment unlike anywhere else on Earth. It is a vast ocean almost completely surrounded by continental landmass (figure 1.1). Year-round, the Arctic Ocean is partially covered in sea ice. The sea ice cover waxes and wanes seasonally, covering between a maximum of around 15 million km^2 in March to a minimum of around 5 million km^2 in September. The sea ice cover is not a homogeneously thick slab of ice but is instead characterised by a number of important features. Sea ice in the Arctic first forms on the surface of the ocean as frazil ice, ice crystals that are up to a few millimetres across. Thin frazil ice then accumulates to form pancake ice that then freeze together to form a continuous cover. In the Arctic this ice most often thickens by congelation (freezing at the bottom). Under the influence of the Beaufort Gyre and Transpolar Drift, ice is packed up against the Greenland Coast and Canadian Archipelago, where ridging and rafting will occur, further thickening

the ice. Newly formed ice has substantially different properties to that of thick ridged sea ice. Firstly, the thick ice will have a layer of snow up to 40 cm deep, which in summer may melt to form ponds (see figure 1.2), further decreasing the ice albedo and strengthening the albedo feedback cycle (Schröder et al., 2014). Thicker ice is also less smooth, and ridges caused by ice floe collisions can be several metres taller than the surrounding surface. The thick ice is also substantially less saline than thin ice. As ice forms the salt in the seawater becomes trapped within the crystalline matrix of the ice, and so called 'brine pockets' are formed. These brine pockets significantly alter the thermodynamic properties of the ice and it behaves like a mushy layer: a combination of a solid matrix of ice and brine melt (Feltham et al., 2006). The brine is slowly drained away from the ice through a number of mechanisms, primarily gravity drainage. This means that thicker multiyear ice is much less saline than thin and newly formed ice, particularly at the surface. These differences in dynamical and thermodynamical properties highlight the importance of a good understanding of the sea ice thickness distribution in the Arctic.

The Arctic sea ice cover is not a self-contained piece of the global climate, it interacts with the atmosphere and oceans, driving changes in both the local and global climate. The snow and ice on its surface reflects between 50% and 80% of incoming solar energy, significantly more than the surrounding ocean (Curry et al., 1995). This layer of snow and ice impedes exchanges of sensible and latent heat, moisture and momentum between the atmosphere and the ocean surface. The brine rejected during ice formation and the increase of freshwater caused by sea ice melt play important roles in the thermohaline circulation (Mauritzen and Häkkinen, 1997). The ridging process of sea ice introduces atmospheric wind drag and momentum exchange between the atmosphere and ocean - the ridges on the surface of ice floes act like sails, and the keels underneath transfer this momentum to the ocean (Castellani et al., 2014).

The Arctic, more so than any other region on Earth, has felt the effects of man-made climate change. 'Arctic amplification' has meant that the Arctic is experiencing an increase in surface air temperatures at double the rate of the rest of the planet. The primary (but not sole) mechanism driving this change is Arctic sea-ice decline observed during the satellite era (Dai et al., 2019). The Arctic sea ice cover is declining substantially, especially during summer and early autumn. This is happening at a rate of around -13% in September, and -3% in April intra-annually (National Snow and Ice Data Center). The overall trend between 1979 and the

Fig. 1.1 A geographic map of the Arctic Ocean, labelling many of the important seas in the Arctic for sea ice. Source: ECMWF.

Fig. 1.2 An image of Arctic sea ice in the Chukchi Sea from July 2011. Melt ponds are visible and on the LHS of the picture the water on the surface is beginning to refreeze and form frazil ice. Source: NASA.

present is around 5%, with a larger decreasing trend occurring since the beginning of the 21st century (Cavalieri and Parkinson, 2012). Arctic amplification would not be possible without the ice albedo feedback effect but this is a complicated mechanism with direct effects on surface temperature during the summer but also the delayed effects this has on the Arctic sea ice melting season and the exposed dark water surface causing warming of the mixed ocean layer (Serreze and Barry, 2011). Increased sea ice loss in summer causes excess heat to be stored in the Arctic Ocean, which is released into the atmosphere as the freezing-up season begins. The increase of near-surface air temperature causes changes to Arctic geopotential heights which in turn effect global circulation, and feeds back into the troposphere and stratosphere (Coumou et al., 2018). These changes could lead to weakened storm tracks and jet streams due to decreases in the temperature gradient between the mid-latitudes and the Arctic circle, and cause modifications to planetary waves (Cohen et al., 2014). Arctic sea ice loss could also affect global oceanic circulation patterns, the Atlantic Meridional Overturning Circulation is sensitive to changes to freshwater and heat flux changes in the Arctic and is weakening, which it has been suggested is due to a declining sea ice cover (Sévellec et al., 2017). The links between the declining sea ice cover and its wider effects on climate are difficult to prove and widely disputed. For example, observations strongly support a link between Arctic amplification and mid-latitude weather, but model results show little connection between Arctic amplification and its potential consequences in other regions of the globe (Cohen et al., 2020). The impacts of Arctic amplification on a global scale and the mechanisms driving these changes are only beginning to be understood (Francis et al., 2017).

The Arctic sea ice, although inhospitable to ourselves and many forms of life we are familiar with, is a fundamental environment for many bacterial, plant and animal species, forming its own unique ecosystem. The sea ice is home to large colonies of algae and phytoplankton which form the basis of the food web and contribute to the cycling of important organic nutrients (Zhang et al., 2010). There are many species of fish that live under the sea ice surviving on the algae that forms underneath it, the most common of which being the Polar Cod (David et al., 2016). However the most visible group of animals that have made sea ice their home are the marine mammals. A number of seal species use the sea ice as feeding grounds with which to hunt these fish, and in winter use the thick snow to form lairs. This means they require stable ice year-round. Polar bears use sea ice as a platform for hunting these seals, but rapidly declining sea ice cover means that they need to venture further to hunt (possibly increasing likelihood of contact with humans), and may need to fast for longer periods (Kovacs et al., 2011). Polar bear population on an inter-annual basis has been linked

to sea ice extent, and projections show that the Arctic sea ice decline could lead to significant population loss (Hunter et al., 2010). Arctic sea ice decline is also expected to have an impact on human activity. Sea ice poses a significant hazard to ships in higher latitudes, preventing shipping routes from crossing the Arctic. Sea ice decline may however open up the Arctic for passage, allowing shipping routes to shortcut between Atlantic and Pacific ports and within the Arctic, opening up trading opportunities (Melia et al., 2016). The sea ice is also important for indigenous communities living in the Arctic circle. The sea ice is used not only as a place to hunt but also provides important mental health, physical health, social and cultural benefits to the peoples living there (Durkalec et al., 2015). Some participants in the study by Durkalec et al. (2015) already cited negative health impacts as a result of changing environmental conditions. Sea ice is not only an vital component of the global climate, but also one of a global ecosystem.

Observations of the Arctic sea ice (and its polar cousin, the Antarctic), in comparison with the rest of the world, are sparse in both space and time because of its remoteness. The Arctic is largely inhospitable to humans due to its climate and terrain, and the sparseness of human activity in this region means that long term climate records are almost non-existent. The most widely known source consists of 1000-year long records of atmospheric methane from air bubbles trapped in ice cores in Greenland (Rhodes et al., 2013). Observations of the Arctic sea ice are made even more difficult because of its position in the Arctic Ocean, and its evolution throughout the changing seasons. The longest and most consistent records of Arctic sea ice have been made by passive microwave satellites, observing the sea ice concentration initially bi-daily from the early 1970s and now daily since the late 1980s (Cavalieri et al., 1984, Comiso et al., 1992). In the second half of the 20th century, observations of Arctic sea ice were limited in scope, there were a few programmes carried out to establish manned stations on the sea ice which made atmospheric and oceanic observations. The biggest programme by far was a Soviet campaign consisting of 28 stations which provides a record of snow depth on the sea ice between 1954 and 1991, and was later used to provide a climatological snow depth for the Arctic (Warren et al., 1999). However with the threat of global warming and Arctic amplification better understood, significant efforts have been made since the 1990s to improve the observational record of the Arctic sea ice. A record of sea ice motion since 1979 has been derived from satellites, buoys and reanalysis wind fields and of particular focus has been sea ice thickness. The Ice Cloud and land Elevation Satellite ICESat (Schutz et al., 2005) and Cryosat-2 (CS2) (Laxon et al., 2013) satellites (and their predecessors) are now both in operation, with CS2 providing a record of Arctic sea ice thickness since October 2010. The SMOS satellite (Kerr et al., 2010), while not

primarily designed for observations of Arctic sea ice, has also been useful for providing observations of the thinnest sea ice, which have proved difficult. Recent efforts also include the Multidisciplinary drifting Observatory for the Study of Arctic Climate (MOSAiC), a recent field campaign which took place between September 2019 and October 2020, undertaken by an international and interdisciplinary team to survey the changing ice cover for a full year. The new observational records that have become available over the past two decades mean that we now have access to an unprecedented amount of sea ice data which can be used in climatological studies, in our case for reanalysis.

1.2 A New sea ice data assimilation system

Reanalyses are vital tools for climate study, because they allow us to combine state-of-the-art climate models with observations to create a spatially and temporally continuous climate record. This can be extremely useful as both sources of information have associated errors. Climate models can have sources of error such as those arising from lack of resolution, non-inclusion or incorrect parametrisations of climate processes, poor initialisation or boundary conditions. Errors occurring early in the model may also be propagated into and accumulate at future times. Stand-alone models of individual systems of the climate, such as the Arctic sea ice are also dependent on forcing data obtained from atmospheric reanalyses or climatological data of the atmosphere and oceans, which are imperfect themselves. Observational records are similarly troubled, with uncertainties arising from human error, instrument issues, and uncertainties in conversion from the observed parameter to the quantity that we want to observe (for example from brightness temperature to concentration). The internal variability in the sea ice cover also limits comparisons between models and observations, and this internal variability is also non-uniform (England et al., 2019) and has an important influence on the recent sea ice loss. The internal variability requires the use of statistical approaches for direct comparisons between models and observations, such as in Swart et al. (2015), which finds that observed and model trends between 1997 and 2013 are not inconsistent, but there is a need for additional large ensemble models that can capture the internal variability as the variability could mask or enhance trends greatly over short periods. Observations are also unable to provide a completely consistent picture of the climate, even with the advent of satellites. Not everything is observable using satellite technology, so remote areas like the Arctic are still an issue. Considering the issues with each source of information, the best way to study the climate will be to combine them, accounting for the errors in each separately.

This is where a the reanalysis is born, and why it is so vital for the study of the environment. Reanalyses are used to monitor both short and long term changes to the climate regionally and globally, most importantly for the monitoring of climate change (Santer et al., 2004). As they use the same models that are used for numerical weather prediction, reanalyses can help to improve weather forecasting (Dee et al., 2011). Reanalyses can answer questions about unobserved quantities - of particular interest in the Arctic is sea ice volume - which can help provide important insight in the changes in the climate which either cannot be observed or are difficult to fully quantify from observations. Reanalyses are also a vital tool for climate prediction, where they can provide a better initialisation of the state of the climate before the prediction step occurs. Prediction is of particular importance in Arctic sea ice because of shipping (Melia et al., 2017), which is becoming increasingly relevant in the Arctic due to the reduction of ice extent in the Arctic (Melia et al., 2016). Sea ice prediction is also important for fishing and extraction of resources and resource management in the Arctic Ocean. Sea ice prediction is also of importance to communities living in these regions. The predictability of sea ice thickness has a high potential for up to 2 years, but extent is harder to predict and only shows potential for up to 1 year (Holland et al., 2011). Winter generally shows high predictability, with summer sea ice predictability depending on the changes in the internal variability in the sea ice. If the September sea ice extent varies strongly from the linear trend prediction can be poor in summer (Stroeve et al., 2014). Massonnet et al. (2015) showed that ensemble Kalman filter assimilation of ice concentration had strong prospects for future improvement of short-term sea ice prediction. Reanalyses and data assimilation can also be used to answer questions about model processes, in particular parameter estimation can be a useful tool for the calibration of poorly-constrained parameters in the sea ice model, e.g. ice strength and ice-air/ocean fluxes (Massonnet et al., 2014). Reanalyses can be used for the development and placement of renewable energy sources, and for agriculture (Nezhad et al., 2021). They are also used in both business and government for decision and policy making reasons.

In comparison to other research areas in climate science, sea ice has not generally been the primary focus of much long-term reanalysis research, though there have been a number of works looking into the usefulness of data assimilation on sea ice reanalysis and prediction in shorter timescales (up to a decade). This may be due to both a lack of observational data, and that the uncertainties on these observations are unusually difficult to quantify. Modern state-of-the-art sea ice models would also be difficult to linearise and are non-Gaussian. These factors would have made producing a sea ice reanalysis difficult, especially before the recent development of ensemble data assimilation techniques. Nevertheless, there has been

much focus in sea ice research on the feasibility of long-term reconstructions of sea ice over the satellite era, and of sea ice observation assimilation. In 2003 two seminal papers in sea ice reanalysis research were published, the first, Lisæter et al. (2003), showed the benefits of the assimilation of sea ice concentration in a dynamic-thermodynamic sea ice model (coupled to an ocean model), and this was also the first study of sea ice assimilation using the ensemble Kalman filter. The second paper, Zhang and Rothrock (2003), introduced the most widely-known sea ice data assimilation system, the Pan Arctic Ice Ocean Modelling and Assimilation System (PIOMAS). PIOMAS uses a coupled ocean-sea ice system with a 12 category Eulerian thickness and enthalpy distribution. This first paper primarily introduced the model reanalysis system, but in 2006 the assimilation of ice concentration was introduced (Lindsay and Zhang, 2006), whereby ice concentration was assimilated using a nudging method which prioritised the sea ice extent, and improvements were found in both extent and concentration. Though it uses this simple data assimilation method, it has been extensively validated with thickness observations from submarines, buoys, ICESat and CS2, which were studied and verified (Schweiger et al., 2011). The work of Dulière and Fichefet (2007) also used the assimilation of ice concentration and velocity in a simpler model of the sea ice cover, using optimal interpolation. Assimilation of ice velocity was found to be much less useful, though it could improve the sea ice state estimation if the ice dynamics is quite poor. They found that assimilation of ice concentration needed to be handled with care due to correlations with other state variables, but the overall impact was very positive. The sensitivity of the sea ice model in data assimilation to the correlations between the state variables within the sea ice model, and to the coupling to the ocean and atmospheric models, means that some studies have focused on assimilating sea ice observations into global climate models, avoiding unphysical updates to the system. For example, Toyoda et al. (2016) applied corrections to both the atmospheric and ocean in a 3D-var system. Tietsche et al. (2013) finds that the addition of sea ice concentration assimilation in a global climate model, even with a relatively simple nudging scheme, reduces errors in concentration and extent significantly, though care was needed to reduce unphysical effects from the updates. Both studies found that the improved sea ice initialisation was effective, though the impacts on the ocean and atmosphere were minimal.

Within the past decade a growing number of ocean-sea ice DA systems and reanalyses have been produced and are in operation, including the UK Met Office's Forecast Ocean Assimilation Model (FOAM) (Blockley et al., 2014), The Nansen Environmental and Remote Sensing Center's (NERSC) Towards an Operational Prediction system for the North Atlantic European coastal Zones (TOPAZ4) (Sakov et al., 2012), ECMWF's Ocean ReAnalysis Pilot

5 (ORAP5) (Zuo et al., 2017), the Modern-Era Retrospective analysis for Research and Applications (MERRA) Ocean product (Rienecker et al., 2011), The Canadian Global Ice Ocean Prediction System (Smith et al., 2016) and the US Navy's Arctic Cap Norwcast/Forecast System (ACNFS) (Hebert et al., 2015). Many of these use 3D-Var or (OI) and assimilate only sea ice concentration. TOPAZ4 uses an Ensemble Kalman Filter (EnKF) for sea ice concentration and has tested the assimilation of SMOS-CS2 sea ice thickness (Ricker et al., 2017). The Met Office has tested sea ice thickness assimilation in its FOAM system with OI assimilation of CS2 monthly mean ice thickness (Blockley and Peterson, 2018), and recently using 3D-Var assimilation of its daily sea ice thickness data (Fiedler et al., 2022). They have also recently tested the model with assimilation of the combined CS2-Soil Moisture and Ocean Salinity (CS2-SMOS) product (Mignac et al., 2022). There are also a number of Arctic sea ice reconstruction studies which do not assimilate any sea ice variables but are using atmospheric reanalyses to force their ocean-sea ice models, in particular a number of studies looking at either the Arctic sea ice interannual or intra-annual variability or the long term trends in the Arctic sea ice extent and volume, including (Cavalieri and Parkinson, 2012, Hilmer and Lemke, 2000, Kwok, 2018)

In a comparison of 14 ocean-sea ice reanalyses it has been found that the spatial pattern of ice volume varies widely between products, with no reanalysis standing out as clearly superior when compared to altimetry estimates (Chevallier et al., 2017). Chevallier et al. (2017) found that the majority of sea ice reanalyses do a good job at representing the monthly and interannual variability of the ice velocity, primarily due to the use of surface forcing from atmospheric reanalyses. In most reanalyses, sea ice concentration is consistent, with most differences appearing at the ice edge, due to the uncertainties here. In terms of the sea ice thickness Chevallier et al. (2017) notes that most reanalyses suffer from ice too thick in the Beaufort Sea and CAA and too thin around the North Pole, something we hope this thesis can address by using the assimilation of not only mean ice thickness, but sub-grid scale ice thickness distribution.

1.3 Thesis Aims and Outline

There is a clear need for a better understanding of the mechanisms driving long term changes in the Arctic sea ice cover. Currently available sea ice reanalyses do not take advantage of the new observational records of Arctic sea ice available, they use models which have not kept pace with the advances in sea ice modelling, they use relatively simple data assimilation

techniques, and/or sea ice is not the primary focus of the reanalysis product. The primary objective of this thesis is to use the state-of-the-art Centre for Polar Observation and Modelling (CPOM) version of the Los Alamos Sea Ice Model (CICE) (Hunke et al., 2015), with new long-term observational records that are available and a robust data assimilation method to produce a new Pan-Arctic sea ice reanalysis over the satellite era. This is then used to improve our understanding of long term changes in the sea ice cover. Of particular interest is the assimilation of the sub-grid scale sea ice thickness distribution (Schröder et al., 2019) and a summer record of the mean ice thickness (Landy et al., 2022), two observation types which have not been assimilated in any previous study. The sub-grid scale thickness distribution is a fundamental component of sea ice models, playing a vital role in the dynamical and thermodynamical processes, yet very little is known of its true state in the Arctic. The observational products from CS2 are limited, they are monthly mean observations of the thickness distribution of sea ice with a mean thickness above 1 m. By producing a reanalysis, we can produce a consistent record of the thickness distribution and can analyse how this distribution has changed in the past decade. Using an ensemble based data assimilation method means that much more information can be extracted from the observation. Not only can we use the information of the observed variable but also information about how it is correlated to other variables in the sea ice system as a whole, which is used to update the full model state. This means that even though we only assimilate sea ice concentration between 1981 and 2009, we still obtain information about other aspects of the sea ice state. In this chapter we provide background on the Arctic Ocean, sea ice, reanalysis studies and data assimilation in sea ice, for a more complete background and outlook in these fields, see Thomas (2017) and Buehner et al. (2017).

In chapter 2, we present currently available observations of the Arctic sea ice, including discussion of how their uncertainties are to be used in the data assimilation. Background information of the CPOM-CICE model, data assimilation and the Local Ensemble Transform Kalman Filter (LETKF) are presented in Chapter 3, including details of currently available sea ice reanalyses, which we compare with our own methods. The methodology of how the sea ice data assimilation system was produced is presented in chapter 4, which includes discussion of the Parallelised Data Assimilation Framework (PDAF), the importance of the post-analysis step processing and how an ensemble spread in a stand-alone CICE model is generated. Case studies and discussion of some important parameters for the data assimilation system, and our choices for these parameters are also discussed. An intercomparison of four-year reanalyses, assimilating different configurations of observations, is presented in chapter 5. The impacts and consequences of assimilating each type of sea ice observation are

discussed, and we use this study to decide the observations that will be assimilated in the satellite era reanalysis to constrain the reanalysis setup further. This study also includes a comparison of these different configurations to independent data. We present and discuss the results of our satellite era reanalyses in chapters 6 and 7. The reanalyses are compared to independent observations of concentration and thickness, and the PIOMAS reanalysis. The findings, consequences and outcomes of this thesis are discussed and summarised in chapter 8.

Chapter 2

Observations of the Arctic Sea Ice

2.1 Overview

In this chapter we discuss observations of sea ice currently available which could be used in a sea ice data assimilation system and give a brief overview of their development and their uncertainties. This is done so that we can choose what observations will be useful to assimilate in our reanalysis and what their uncertainties are. This is important because the scientific robustness of our reanalysis depends on choosing observations that have a good spatial and temporal coverage and quantifying the uncertainties appropriately. In section 2.2 we discuss observations of sea ice concentration, in section 2.3 we discuss observations of sea ice thickness, in section 2.4 we discuss observations of sea ice thickness distribution, in section 2.5 we discuss observations of sea ice motion, and we discuss other observations available in section 2.6.

2.2 Sea Ice Concentration

The most widely available observations of Arctic sea ice over the satellite era have been sea ice concentration, observations of which have been available since the 1970s from passive microwave sensing satellites. This data came initially from the Scanning Multichannel Microwave Radiometer (SMMR) which was launched in 1978 on the Nimbus 7 Satellite, and continued with the Special Sensor Microwave/Imager (SSM/I) launched in 1987 as well as the Special Sensor Microwave Imager/Sounder (SSMI/S) beginning in 2003 which were both placed on board United States Defense Meteorological Satellite Program (DMSP) satellites. These data sets are extremely useful as they provide a continuous time series of brightness temperature and hence sea ice concentration data sets since 1978, providing an important

insight into the long term trends of the sea ice concentration and extent (see Figure 2.1) for more than 40 years. The year of lowest sea ice extent, and volume (see figure 3.1) occurred in 2012. The causes of the anomalously low 2012 Arctic sea ice state were the increased vulnerability of sea ice due to decades of reduction and thinning of the sea ice cover, which made it particularly vulnerable to a strong storm which entered the Arctic in August 2012 (Parkinson and Comiso, 2013). The previous record in 2007 was the result of strong cloud anomalies in the Arctic, there was reduced the cloudiness over the Arctic and as a result the downwelling shortwave and longwave radiation increased substantially during summer 2007 (Kay et al., 2008). The overall trend of a thinning and weakening ice pack has made it more vulnerable in future to anomalous weather patterns such as these which occurred in 2007 and 2012 (Perovich and Richter-Menge, 2009).

The Advanced Microwave Scanning Radiometer for EOS (AMSR-E) and its successor satellites, launched in 2002, provide daily sea ice data products and may also be used in formulation or validation of sea ice concentration retrieval algorithms. Sea ice concentration is retrieved from passive microwave satellites by using observations of the brightness temperature over different surface types. The satellites provide vertically and horizontally polarized brightness temperatures at various different frequencies, for example SSMI provides data at 19, 37 and 85 GHz frequencies (Hollinger et al., 1990). The 19V (19 GHz, vertically polarized) frequency channel is particularly important in distinguishing between sea ice and water surfaces due to the emissivity differences between the two on this channel. Different types of ice can also be distinguished especially in the 37V channel - usually first year and multiyear ice are distinguished as these are important for understanding the changing sea ice cover. Consequently almost all sea ice concentration retrieval algorithms use these channels. The key equation for sea ice concentration retrieval is

$$T_b = \sum_{j=1}^{n_s} T_{bs_j} C_{aj}, \tag{2.1}$$

where T_b is the observed brightness temperature, T_{bs_j} is the reference brightness temperature over the surface (these are also known as tie-points) and C_{aj} is the fractional concentration of the grid cell covered by surface j over all surfaces n_s, which must total 1. If you choose two surfaces: ice cover and open-water then you end up with

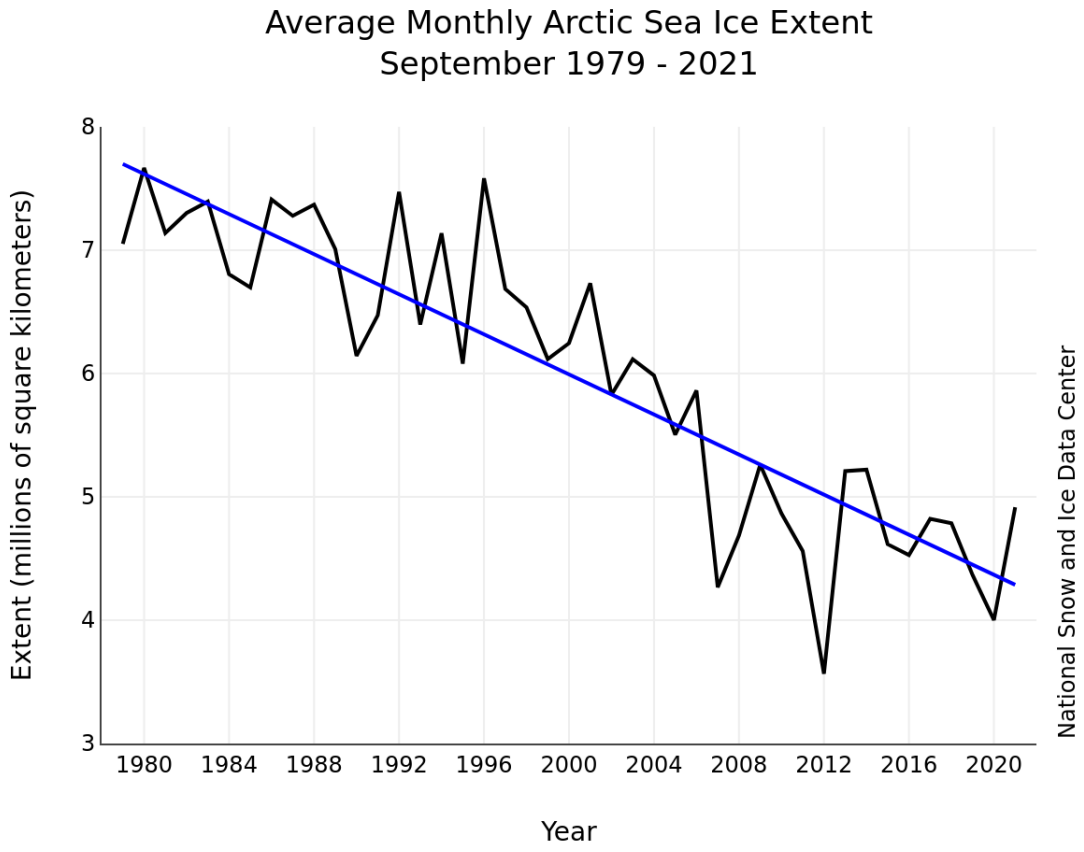

Fig. 2.1 Monthly average September Sea ice extent from 1979 to 2021 with trend line shown in blue. Source: National Snow and Ice Data Center, US

$$T_b = T_{bi}C_{ai} + T_{bw}C_{aw}, \tag{2.2}$$

with T_{bi} and T_{bw} the brightness temperatures observed over ice cover and open water, and C_i and C_w the concentrations of sea ice and open wate respectively. This means we can find sea ice concentration using

$$C_i = \frac{T_b - T_{bw}}{T_{bi} - T_{bw}}. \tag{2.3}$$

The retrieval of sea ice concentration then, is reduced to being able to correctly evaluate reference brightness temperatures (known as tie-points) for each of the surface types when 100% of the surface is dominated by that type. Some of the most widely used algorithms are the NASA Team algorithm (Cavalieri et al., 1984), Bootstrap (Comiso, 1995), Bristol (Smith, 1996) and the ARTIST Sea Ice (ASI) algorithm upon which the AMSR-E and AMSR-2 retrieval algorithms are based (Kaleschke et al., 2001, Spreen et al., 2008). Although based upon the same key principle the algorithms differ in a number of key ways: different choices in both frequency channels and polarizations, choice of reference brightness temperatures, and their sensitivity to surface temperature and other surface characteristics.

The NASA Team algorithm looks at contributions from three different surface types: multiyear ice, first-year ice and ice-free ocean (Cavalieri, 1991), and uses the 19V, 19H and 37V channels from the SSM/I, SSMR and SSMIS sensors with a resolution of 25km. The radiances from these channels are then used to calculate a polarization ratio and spectral gradient ratio from which sea ice concentration can be retrieved. The NASA Team algorithm uses different tie points for measuring concentration in the different hemispheres but they are non-dynamic within these domains. The Bootstrap algorithm also uses the SSM/I, SSMR and SSMIS but instead takes advantage of the correlated distributions of the brightness temperatures over the Arctic, specifically over the 37GHz channels, using the 19V 37V and 37H channels instead. Unlike the NASA Team algorithm however, it only derives a single sea ice concentration rather than separate first-year ice (FYI) and multi-year ice (MYI) concentrations. The Bootstrap algorithm uses dynamic (daily) tie-points, which means it takes more time to process the data, and cannot be used for a near real-time product. The Bristol algorithm is similar to the Bootstrap algorithm, except that it additionally uses the 19H channel. The AMSR-E and AMSR-2 products are derived using the ASI algorithm, with

a smaller spatial resolution than that of the NASA Team and Bootstrap datasets of 12.5km, which is the main advantage of this product. Also unlike the NASA algorithms the ASI algorithm uses high frequency channels to derive sea ice concentration. It uses the 90GHz frequency, where the differences in emissivities between the horizontal and vertical channels are much larger for sea ice than for water. The concentration can then be calculated by taking the difference in brightness temperatures between these two channels.

Many evaluation and intercomparison studies (Comiso et al., 1997, Ivanova et al., 2015, Kern et al., 2016, Nose et al., 2020) of sea ice concentration retrieval algorithms have been conducted. The different retrieval algorithms are all useful, and generally show similar ice-edge positions for the Arctic. The NASA Team algorithm finds smaller ice concentrations in general than the Bootstrap algorithm, especially during January and around the inner ice pack. High temperature and emissivity fluctuations in the marginal ice pack can also produce discrepancies (Comiso, 1995). These discrepancies can lead to large differences in sea ice concentration calculations. The NASA Team algorithm is better at handling the brightness temperature fluctuations. Another difference is also in their handling of melt ponds, which appear as open water in the satellite data. The Bootstrap algorithm tries to offset this bias by synthetically increasing sea ice concentrations more than the NASA algorithm does (Bunzel et al., 2018). The Bristol algorithm is affected most by melt ponds, but also performs best in areas of high ice concentration (Ivanova et al., 2015). It has been shown that the use of the vertically polarized 19GHz and 37GHz channels, such as by the Bootstrap algorithm, are the least sensitive to uncertainty effects that can be caused by atmospheric conditions, in particular from wind and liquid water content of clouds (Andersen et al., 2006). This sensitivity to both surface and atmospheric variability has led to the use of weather filters during the retrieval, where extra frequency channels are used solely to identify where surface or atmospheric properties may interfere with the retrieval, and possible erroneous data can then be filtered out. The use of weather filters on the higher frequency channels where spatial resolution is better can have a smearing effect as the weather filters use low frequency channels, this can cause ice concentrations along the marginal ice zone to be higher than the truth (Spreen et al., 2008). The higher frequency channels however are less susceptible to surface effects that can arise from melt ponds and ridging (Tonboe et al., 2006). The variety of the algorithms means that the differences between the derived products can be significant, when deriving sea ice extent they can differ in up to 0.5 million square kilometres (Ivanova et al., 2014), however all are in good agreement with the decreasing trend of sea ice extent.

In terms of uncertainty in the products an important factor was found to be the differ-

ing derivation of the reference brightness temperatures or tie-points. The tie-points also cause difficulties in deriving the errors in the sea ice concentration products because the tie-points are newly derived at daily or longer time periods, which causes a discontinuity in the ice concentration time series. However using these dynamic tie points reduces systematic biases and reduce problems of seasonal variability in the accuracy of the sea ice concentration retrieval (Ivanova et al., 2015) An important problem which affects all the algorithms is the underestimation of the concentration in areas with high concentrations of thin ice. This can lead to a higher gradient of sea ice concentration at the ice edge than in truth, especially in the Bootstrap algorithm where almost all of the ice pack is evaluated to have close to 100% ice concentration cover. As there is limited data available of in-situ sea ice concentration observations it is difficult to verify which of these algorithms is the most accurate and therefore the best to assimilate in our sea ice data assimilation system. I have chosen to assimilate the Bootstrap sea ice concentration data (Comiso, 2017), because it attempts to account for the presence of melt ponds, which are key to understanding changes in the sea ice cover during the melting season, and it uses dynamic tie points which reduce systematic biases and problems with the seasonal variability of the ice cover.

Observation errors for sea ice concentration retrievals in the Bootstrap and NASA Team algorithms are similar, and estimated to be on average between 5 and 10% of the total fraction, but up to 30% in grid cells with high percentages of thin ice or during the summer melt season when the sea ice surface is dominated by melt ponds (Comiso, 2017). In CICE-PDAF, and for months May-September (inclusive) we use a sea ice concentration uncertainties of 0.2 for all observations. Outside of these months we use a 0.1 error for observations with ice concentration above 0.8, and 0.15 error otherwise. We choose this error formulation to account for the increased uncertainty in ice concentration retrieval at both the ice edge and during the summer melt season (Ivanova et al., 2015). Additional errors in sea ice concentration retrieval algorithms can also be caused by atmospheric effects, where water vapour and cloud liquid water can alter the observed brightness temperature. High winds and storms can also cause sea ice to be anomalously observed in open water (ice detected where none is there in truth). This is caused by the water surface being roughened by the winds causing surface emissivity to move towards values seen over sea ice (Maslanik, 1992).

The data assimilation requires a model version of the observation, which in this case will be the sum of the ice concentrations in each of the thickness categories. The ensemble Kalman filter then works by updating the ice concentrations in each of these categories through the correlations between themselves and the total sea ice concentration, as it does with all

CICE state variables. As this relies on linear correlations it means that values for the ice concentrations in each thickness category can be moved out of bounds, or their total can, which is unphysical. This is accounted for in the post-processing, which will be discussed in section 4.3.

2.3 Sea Ice Thickness

Sea ice thickness observations were not possible until the advent of the Synthetic Aperture Radar or a Lidar ranging instrument that could be used for continuous satellite observations. These have a resolution which is small enough to allow for for the detection of small leads in sea ice, essentially cracks in the sea ice cover. This allows for the detection of small leads in sea ice - meaning freeboard measurements (the elevation difference between the ice and ocean surface) could now be made because of its high spatial resolution compared to passive microwave observation techniques. In this sea ice reanalysis, we use CS2 measurements of sea ice thickness for assimilation and evaluation and we use observation data from Operation IceBridge (OIB) to evaluate the reanalyses, which are described within this section. We also describe other sea ice thickness products available here.

2.3.1 Cryosat-2

Cryosat-2 (CS2) is a European Space Agency (ESA) mission whose primary aim is to observe trends in Earth's continental and marine ice fields (Wingham et al., 2006). It uses a Synthetic Aperture Interferometric Radar Altimeter (SIRAL) to monitor a coverage region of a latitude of up to 88 degrees North. This works by transmitting microwave pulses at regular intervals defined by a pulse repetition frequency towards the Earth and measuring the time taken by the pulse to reflect off the Earth's surface and return to the satellite. The Centre for Polar and Ocean Modelling (CPOM) uses radar altimeter data from CS2 and processes it to produce Arctic sea ice thickness and volume datasets (Tilling et al., 2018). The raw data used is the CS2 Baseline-C L1b SAR and SARIn mode data (Scagliola et al., 2015). This dataset contains information along the orbit ground track of each 20 Hz waveform, comprising 3000 waveforms on average. The L1b product provides time and orbit information, confidence and error estimates, external corrections, transmit and echo power, window delayed and numerous other measurements typically provided by SIRAL instruments. (Cryosat Ice netCDF L1b Product Format Specification).

The CPOM method of processing radar altimeter data from the European Remote sensing Satellite (ERS), Envisat and Cryosat has been in development since the 1990s (Laxon, 1994) (Peacock and Laxon, 2004) (Giles et al., 2008) (Laxon et al., 2013), and described most recently by Tilling et al. (2018). There are two important steps in this process; the differentiation between measurements of surface elevation of the leads between ice floes and surface elevation of the sea ice, and the process which then converts the calculated freeboard to thickness. In order to process the CS2 data other available products must be used. Daily sea ice concentration data generated by the NASA Goddard Space Flight Centre using brightness temperature observations from passive satellite microwave sensors. A climatology (Warren et al., 1999) generated from in-situ measurements of snow depth and density between 1954-1991 is used, where spatial variability of the depth is represented through a 2d-fitted quadratic function. Also used is sea ice type data available from the Norwegian Meteorological Service OSISAF system (Lavergne et al., 2019), where measurements of brightness temperature in two vertically polarised channels (19 GHz and 37 GHz) are combined and a gradient ratio is used to distinguish between first-year ice (FYI) and multi-year ice (MYI).

Identifying leads and floes

In order to calculate sea ice freeboard and hence thickness, we first need to be able to distinguish between satellite return waveforms from the sea ice and the ocean. This is possible because different types of radar returns (echoes) occur depending on the smoothness of the surface from where the radar deflected. Diffuse echoes occur when a radar burst is reflected off a rougher surface, such as an ice floe or the open ocean, whereas specular echoes are found when the radar deflects off a smoother surface such as a lead or newly formed thin ice (which commonly forms in leads). Radar echoes from specular reflections look like spikes, whereas those from diffuse echoes will spike but then gently decay. These returns can be identified by the pulse peakiness - the ratio between the maximum power of the waveform and its mean (Peacock and Laxon, 2004). Ice floes are differentiated from the open ocean in diffuse echoes by using ice concentration data from the NSIDC (National Snow and Ice Data Center) processed from passive satellite microwave sensors, where greater than 75% ice concentration within a grid cell indicates a floe return. We need to then identify the location on each waveform that represents the average surface elevation within the satellite footprint identified - this is known as retracking. CPOM uses a Gaussian plus exponential waveform fit to retrack echoes from leads (Giles et al., 2008) and a 70% leading edge threshold from

the 1st peak to retrack floe echoes. This two-way travel time is then converted to a range and a few corrections are then applied; tidal and other geophysical effects are removed and the geoid (mean sea surface used as reference ellipse of ocean surface) which is itself derived from CS2 data is also used to remove spatially highly variable ocean topography (Armitage et al., 2016).

Sea Ice Freeboard

With the surface types distinguished, the sea ice freeboard can be calculated. To calculate sea ice freeboard, every waveform which is classified as containing an ice floe is identified. The ocean surface elevation at these points is then found by interpolating the elevation between leads. A floe must have a lead present on either side of it and extending 100km outwards from the floe location. We are assuming that the CS2 synthetic aperture radar bursts penetrate the snow layer and deflects off the snow-ice interface as shown in (Beaven, 1995). Finally we must apply a correction to the freeboard to account for the reduced speed of light through snow cover on the sea ice. This freeboard is given by:

$$f_c = f_i + h_s \left(\frac{c_v}{c_s} - 1 \right), \tag{2.4}$$

where f_c is the corrected freeboard, f_i is the original freeboard, h_s is the snow depth, c_v is speed of light in a vacuum and c_s is the speed of light propagation through snow (Tiuri et al., 1984). The speed of light in snowpack can be calculated by

$$c_s = \frac{c}{\sqrt{1 + 1.7\rho_s + 0.7\rho_s^2}}, \tag{2.5}$$

where ρ_s is snow density in gcm^{-3}. Snow density in the Arctic circle (Warren et al., 1999) ranges from between 100 and 450 kg m^{-3} and so we determine speed of light in snow values range between $2.17x10^8$and $2.77x10^8$ m s^{-1}. CPOM has chosen to use 2.4×10^8 m s^{-1} (Tilling et al., 2018).

Sea ice thickness

Sea ice thickness is calculated from the sea ice freeboard using

$$h_i = \frac{f_c\rho_w + h_s\rho_s}{\rho_w - \rho_i}, \tag{2.6}$$

where h_i is sea ice thickness, f_c is the corrected sea ice freeboard, ρ_w is the density of seawater, h_s is snow depth, ρ_s is snow density and ρ_i is sea ice density. The sea ice density is different depending on whether it is first-year ice (FYI) or multi-year ice (MYI), with 916.7 kg m^{-3} used for FYI and 882.0 kg m^{-3} for MYI (Alexandrov et al., 2010), calculated using typical freeboard values and assumed densities of different layers of the sea ice and ocean water. Ice densities decrease significantly in MYI due to drainage of brine inclusions and also an increased presence of air pockets.

Uncertainty in Cryosat-2 products

The CS2 monthly mean sea ice thickness product is produced using over 100 individual measurements of sea ice thickness taken within a grid cell each month, this averaging takes place to reduce the error in the product, which originates from multiple different sources, and is very difficult to quantify. When processing CS2 data we assume that the radar returns from the top of the snow/ice interface (Beaven, 1995), however it has been shown (Willatt et al., 2011) that the penetration of the radar into the snow cover can depend on the temperature and density of the snow. Beaven (1995) also requires that the snow be dry and cold but during the summer the Arctic sea ice is covered with melt ponds, hence CS2 thickness observations are not possible during the summer months (May-Sept). The melt ponds on the surface also cause specular returns from ice floes, meaning ice floes and leads cannot be discriminated. This means we lack data during the melting period, and this could be the most important period for understanding sea ice loss as this is where we have seen the most substantial long term ice loss.

Another possible source of error in CS2 data processing is from the use of snow data (depth and density) drawn from a climatology (Warren et al., 1999) (referred to from now on as Warren). This is a climatology of snow depth derived from in-situ data gathered from Soviet drifting stations on MYI from 1954-1991. There is a possibility this climatology may no longer be valid due to the large observed loss of Arctic sea ice in the past 2 decades - and in particular loss of MYI. Use of the Warren climatology is necessary because snow depth satellite retrievals are not currently feasible, and there are still large problems to overcome in snow loading models such as uncertainties from magnitude of precipitation (Serreze and Hurst, 2000), snow compaction issues and difficulties in estimating snow loss caused by leads. Kurtz and Farrell (2011) showed that the snow cover is much more variable on regional scales than found in Warren but a good match on larger synoptic (1000km+) scales. They also found

the Warren climatology was still useful over MYI, but for FYI snow depths were roughly 52% of that reported by Warren. In many places MYI has disappeared and been replaced by FYI (Tilling et al., 2015) since the time period of the Warren climatology. This detail has been incorporated into the CPOM CS2 thickness processing where snow depth data over FYI is multiplied by a factor of 0.5 before freeboard is converted to thickness (Tilling et al., 2016). A further issue with the Warren climatology is that its region where the snow data is well constrained by the drifting station observations is smaller than any maximum winter sea ice extent in the satellite record. Processing freeboard and thickness from CS2 observations outside this region may not necessarily be valid. Other properties of the snow and ice can also cause issues, particularly variabilities in the snow and ice densities can affect the radar returns.

CS2 uses a synthetic aperture radar (SAR) instrument to make its altimetry measurements, and as such is subject to "speckle" which is a granular interference that is borne out of multiple backscattering constituents randomly combining. Estimated speckle noise for individual echoes is between 0.1 and 0.14m depending on the operating mode employed and affects both lead and floe retrievals. To compare and validate CS2 data with in-situ data a sufficient number of measurements must be averaged to ensure error in sea-ice thickness due to noise is not dominating the uncertainty estimates (Giles et al., 2007). This requirement will limit the spatio-temporal resolution of CS2 data. We are limited by the number of measurements which can be made in a grid cell such that the aforementioned errors can be sufficiently reduced. Generally we need 100 measurements to make a reasonable estimate of the sea ice thickness in a grid cell (as monthly averaging decreases random uncertainties of individual freeboard measurements by the square root of the number of measurements) (Ricker et al., 2014). Ideally we want to have monthly averages thus we need CS2 to pass over each grid cell enough times in a thirty day period to be able to produce a result - this limits our minimum grid cell size to around 1km by 1km. Sea-ice thickness measurements will also vary significantly depending on the retracker algorithm we choose, this is how we obtain the two-way delay time of the averaged radar echoes (Ricker et al., 2014). Different groups have developed a variety of possible algorithms, Kurtz et al. (2013) found effective retracking near the peak of the waveform and a mean difference of 12cm (MYI) or 6cm (FYI) between a 50% threshold and this method. Helm et al. (2014) focused on a lower part of the leading edge to minimize spatial and temporal variations of the volume scattering contribution. The CPOM method uses a leading edge position taken as the point on the echo that first crosses the amplitude where the scaling factor is currently set to 0.5 (for 50%) (Tilling et al., 2018). There also exists a tracker offset which results from the radar altimeter's on board tracking system being unable to maintain the echo waveform due to rapid range

variations in the smoothness of the surface. We must also deal with a problem which exists in many oceanography applications, namely errors arising from our imperfect knowledge of the geoid and variations in sea topography and tides. Errors arising from unmodelled tidal variation and the variability of the dynamic topography can be as much as 9.4cm in thickness (Peacock and Laxon, 2004). As observations of the sea level are only available at leads, we must consider also that between leads the local sea-level may vary by a considerable amount as a result of geoid and topography variations which can be missed by simply interpolation between leads, though mean sea surface is removed when processing the CS2 data using CS2 Baseline-C data (Laxon et al., 2013).

As errors are introduced through the processing of CS2 data from freeboard to thickness, it is useful to consider assimilating freeboard instead. The main advantage of assimilating sea ice freeboard over thickness is that it is a more direct measurement and thus less errors are introduced when deriving it as opposed to the thickness. Errors in freeboard become magnified in thickness because we multiply freeboard by a factor of up to 10 to produce ice thickness data as much of the sea ice is obscured beneath the ocean. All errors in freeboard are therefore magnified by this factor when our thickness data is produced, though freeboard error can be reduced down from 0.03m (uncertainty limit from CS2) to 0.01m by the averaging of measurements from CS2 (Alexandrov et al., 2010). This means our error in ice thickness observations can be as much as 0.3m, without accounting for the other previously mentioned sources of error. The error in snow depth dominates the error in both freeboard and ice thickness calculations (Kwok and Cunningham, 2015). If freeboard observations are assimilated, fewer errors may be introduced through our poor knowledge of Arctic snow cover. Snow density is less important to calculate freeboard than it is for thickness, as processing the thickness requires more detailed knowledge of snow and ice densities. However error in snow density is significantly smaller than that of the snow depth which is used in processing both freeboard and thickness. Assimilating freeboard may ultimately be a better choice as we are reducing our observation error compared to thickness significantly which should be helpful when we assimilate the data. Studies conducted by Mathiot et al. (2012), Sandu et al. (2021) and Sievers et al. (2023) show that freeboard assimilation may perform slightly worse or slightly better, which may depend on model setup, data used and other factors. Generally however there has been good success in model improvement in comparison to observations when sea ice concentration and thickness are assimilated with the Ensemble Kalman Filter (Evensen, 1994, Zhang, Bitz, Anderson, Collins, Hendricks, Hoar, Raeder and Massonnet, 2018, Fritzner et al., 2019). Here we have chosen to assimilate sea ice thickness within the CICE-PDAF model, although assimilating freeboard may provide benefits in reduced

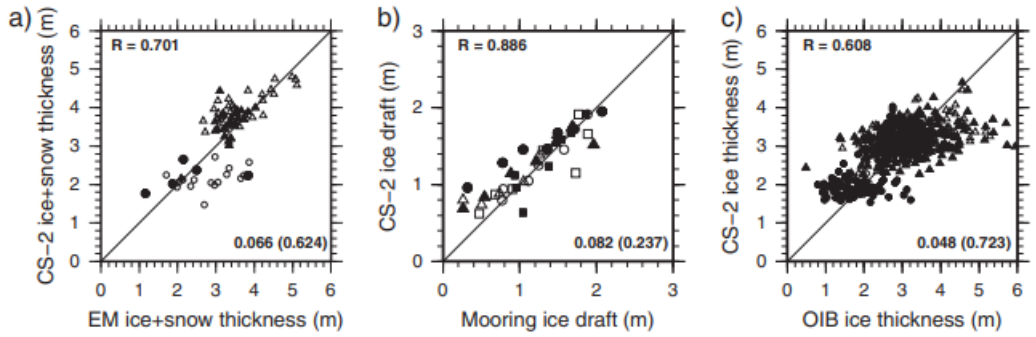

Fig. 2.2 Comparisons of Cryosat-2 data with three different in-situ sources: a) Polar-5 aircraft EM b) BGEP upward-looking sonar moorings and c) Operation IceBridge (Laxon et al., 2013).

observation error, it is also a less direct comparison with the sea ice model state vector.

In Laxon et al. (2013), there is an attempt to validate the Cryosat-2 data with three different sources, from drone sources using electromagnetic radar (Polar-5 aircraft EM) (Haas et al., 2010), from upward looking sonars from the Beaufort Gyre Exploration Project (BGEP) (Krishfield et al., 2014), and from Operation IceBridge (Kurtz et al., 2012), results from these comparisons are shown in figure 2.2. In general the comparisons show agreement of CPOM CS2 ice thickness data is within 0.1 m of the in-situ data, with the BGEP data comparing best to the CS2 data. However there are some issues with the comparisons due to highly different spatial and temporal resolutions of the in-situ projects in comparison to the monthly averaged CPOM CS2 ice thickness. The Operation IceBridge data does not compare so well to the Cryosat-2 estimates, with an increased scatter and CS2 measuring thinner ice as thicker in comparison to OIB, but also measuring ice that is thicker in Operation IceBridge to be thinner, showing evidence of a possible bias in one or both of these sources, possibly due to one or more of the sources of error described earlier in this section which are possible in either CS2 or which we will later describe when discussing Operation IceBridge, the lack of knowledge about the Arctic snow depth on the sea ice will certainly cause some differences between CS2 and in-situ estimates.

The errors in the CS2 sea ice thickness product are extremely difficult to quantify, due to the reasons (the many different sources of area) discussed above, however some attempts have been made to do so. Tilling et al. (2018) does this by estimating the length scales over which the factors (particularly snow depth, density and sea ice density) contribute towards the

error in sea ice thickness measurements de-correlate. For the central Arctic region thickness uncertainty is estimated to be 13.5%, additionally accounting for errors in freeboard due to interpolation of sea surface heights, a relative error of 25% for the CS2 sea ice thickness gridded product is found. We use this as the observation error in the monthly mean sea ice thickness for measurements greater than 1 metre. Measurements of ice thickness less than 1 m are subject to greater error contributions, and thus we use 100% relative error for any measurements of ice thickness below this threshold.

2.3.2 ICESat, ICESat-2 and Operation IceBridge

The first Ice Cloud and land Elevation Satellite (ICESat) was launched by NASA in 2002 with the primary goal of studying both inter-annual and longer term changes in polar ice sheet volume using narrow beam laser altimetry (Schutz et al., 2005). One of ICESat's secondary goals was to provide estimates of sea ice thickness. Kwok et al. (2004) derived sea ice freeboard from a small sample of ICESat data (14 days) however there were significant uncertainties in converting the freeboard to thickness for the data which made making estimates of the sea ice thickness difficult. This was compounded by the short operating lifespan of the ICESat lasers, which could only operate for periods of 33 days every 91 days of the satellite's orbit. This meant that a continuous long-term dataset of ice thickness observations was not possible with ICESat, though further studies of the ice freeboard within these operating periods were conducted such as in Kwok et al. (2007). When ICESat came to the end of its operating lifespan in 2009 a successor mission, which would be able to make continuous measurements of the Arctic sea ice was proposed. This mission, however, would not be ready for launch for almost a decade (ICESat-2 eventually launched in 2018). Operation IceBridge was proposed to fill the gap between the 2 satellites.

Operation Icebridge (OIB) is a NASA airborne mission which has been in operation since 2009, the aeroplanes used are equipped with various measurement equipment, including a Ku-band radar altimeter just as in ESA's CS2, and has also been used to test and early calibration and validation of ICESat-2's laser altimeter, the Advanced Topographic Laser Altimeter System (ATLAS). A number of flight surveys over sea ice are undertaken each year in March and April. These aircraft fly at an altitude of 460 metres, using along track smoothing of 40 metres and sampling frequency of 1 metre. The oversampling allows for statistical smoothing and reduce noise (Farrell et al., 2011). Equipped with a wide range of sensors including laser and radar altimeters, OIB has provided a sparse but significant set of freeboard and thickness data. OIB is also equipped with a frequency-modulated-continuous-wave (FMCW) snow radar, which can be used to measure snow depth. The snow depth is calculated by retrieval

of the air-snow and snow-ice interfaces and taking the difference (Farrell et al., 2011), which can be detected by the radar return as two different maxima due to the difference between the dielectric constants of air, snow and ice. The time difference between the air-snow and snow-ice returns are then converted into a distance by multiplying by the speed of light in snow. The data gathered by this radar has been highly correlated (0.95) with in situ snow depth measurements from Kanagaratnam et al. (2007). The OIB estimates of snow depth and ice thickness have been evaluated to be consistent with measurements from ICESat, CS2 and other in-situ data (Kurtz et al., 2013) (King et al., 2015). In this study we use OIB estimates of sea ice thickness as validation data for our results. Both the quick-look version 1 dataset (Kurtz et al., 2016) and the more reliable Level 4 product (Kurtz et al., 2015) are used, as the Level 4 product not cover the whole time period of the experiment. These data are available in short periods in March and April between 2009 and 2013 primarily over the Greenland and Lincoln Seas to compare with and validate the sea ice thickness from our sea ice assimilation experiments. The observational data are of a different resolution to our model, so it has been interpolated onto the ORCA 1 degree tripolar grid that our model uses.

The successor to ICESat, ICESat-2 launched in September 2018. One of ICESat-2's primary scientific objectives is to estimate and study sea ice thickness. It has similar orbital characteristics to that of CS2, using an inclination of 92 degrees which allows it to survey up to 88 degrees north latitude, identical to that of CS2. It also provides similarly extensive coverage with a 91 day repeat ground track coverage, with a monthly subcycle for the polar regions and oceans in order to produce monthly sea ice data (Markus et al., 2017). ICESat-2 is equipped with the Advanced Topographic Laser Altimeter System (ATLAS), a lidar, as its measuring instrument. The laser altimeter uses a 2x3 laser array (Markus et al., 2017) to provide much better spatial resolution along its measuring track and also discriminate elevation changes. The laser uses a wavelength of 532 nm and transmits a laser pulse with a repetition frequency of 10 KHz. Although using the 532nm wavelength can produce scattering in the ice, snow and water and contribute photons from subsurface heights, it offers a more stable laser and better photon return rates (Kwok and Cunningham, 2015).

As ICESat-2 uses lidar instead of radar measurements, ICESat-2 does not retrieve a waveform but instead uses a photon counting technique to measure surface elevation. This technique is used to differentiate between solar background photons and those from the surface through filtering. One of the important steps in obtaining sea ice thickness estimates is distinguishing surface elevation measurements over sea ice and those over leads (gaps in the sea ice cover). For ICESat-2, this is done using a decision tree algorithm with input variables for photon

rate, width of the Gaussian photon distribution, and calculated background photon rate (Petty et al., 2020). The ratio between background photons returned by snow covered ice and that of water is 7-8, which is expected as this is the ratio between the albedos of ice and water, while surface signal photons peak 4-5 times higher over leads compared to sea ice due to specular returns from leads (Kwok and Morison, 2016). Of particular importance is that background photon returns of melt pond covered ice show tracks of surface photons with much higher variability than ice without melt ponds. This means that ICESat-2 is also able to obtain sea ice freeboard and thickness data during the summer months because some of the photons from the laser bursts will be able to penetrate the surface water of the melt ponds and hence they are not affected by the high percentage of Arctic area covered by melt ponds during the summer months. ICESat-2 can sample both the surface and subsurface of a melt pond of maximum depth 2 metres with this technique. (Brunt et al., 2016). This means that not only can it provide freeboard estimates during the melting season but it could also provide details about the melting season, such as melt pond fractional area and also information about melt pond depth. This ability to provide data during the summer months is ICESat-2's main advantage over CS2.

The second advantage of the multi-beam approach used in ICESat-2 is the greater detection of leads in particular and also ridges when working with sea-ice, allowing for a much better understanding of sea-ice floe surface and as such its freeboard and thickness. This is because of the high level of both cross sampling, by using a beam width of 90m, and along track sampling by using a Pulse Repetition Frequency (PRF) of 10 KHz (Brunt et al., 2016) which gives us a much better smaller-scale profile of the surface of the ice pack. As with CS2, one of the primary challenges of obtaining sea ice thickness from ICESat-2 freeboard measurements is the presence of snow on sea ice. ICESat-2 uses the snow accumulation model NESOSIM (Petty et al., 2018) in conjunction with the modified Warren climatology that is used for CS2 sea ice thickness.

CS2 uses a microwave radar altimeter to measure the surface height, which means that the photons are not attenuated even by thick atmosphere. ICESat-2 uses a lidar, which uses much shorter wavelengths than radar, meaning it is more sensitive to small particles. This means that although it can model the surface better, it is highly susceptible to uncertainty induced by clouds, as a lidar beam can be attenuated by thick clouds (Yang and Christensen, 2012) and also be scattered by them, causing us to observe smaller surface measurements than the truth (Zwally et al., 2008). Mahesh et al. (2002) showed that you could correct for this by filtering out clouds with a higher than acceptable optical depth and also through

estimating biases using a Gaussian fit method with observations from clouds of similar depth. Cloud cover in the Arctic is particularly high in the summer - mainly in May/June, where it can be as high as 90% in some years (Walsh et al., 2009) so although ICESat-2 can make measurements in summer retrieving reliable sea ice freeboard and thickness data may be difficult at times.

Although you can filter out measurements containing cloud cover a similar problem can occur from a different source which is much harder to correct for - snow blown around near the surface can also cause multiple scattering and cause measurement bias. The blowing snow layer is usually not very thick and can occur as high as 300m from the surface. The snow layer has a very small optical depth typically around 0.1, which means a layer of blowing snow 50-100m thick will cause a bias of around 2-4cm in altimetry data using a snow particle radius of 10 μm (Mahesh et al., 2002). As is the case with CS2 data, sea surface uncertainty which results from uncertainty in the Geoid will be a source of error as will the uncertainties found in the snow depth and density. This is still a problem when calculating the freeboard even though the laser will reflect from the snow/air interface rather than the snow/ice interface from which the CS2 radar altimeter reflects off as we still need to know the amount of snow on the ice and its density. It may be possible to use data from radar observations and ICESat-2 to estimate snow depth. Recent papers have looked at using data from CS2, AltiKa (Verron et al., 2015) and OIB which showed good potential, though hindered by a lack of coincident data (Lawrence et al., 2018).

The main drawback of using ICESat-2 thickness for this study is only the lack of data available in the period we are studying (1980-2020). As it was only launched in September 2018, ICESat-2 monthly mean sea ice thickness is currently only available between November 2019 and April 2021. This short time series means that it is less useful when trying to further our understanding of the inter-annual variability of the Arctic sea ice as assimilating such a short period of observations into the model will only improve our model forecast in the short term and not invoke changes for longer time scales within our model. As ICESat-2 has only been collecting data for a very short time it also means that the satellite's ATLAS instrument has not yet benefited from thorough calibration and valuation (although NASA's OIB, which used research aircraft to fly over the polar regions, was equipped with an early version of the ATLAS instrument and was used to test and calibrate the ICESat-2 instrument before launch). CS2 on the other hand has been subject to extensive measurement calibration, data processing and evaluation. However the ICESat-2 data is useful for potential evaluation and validation of our reanalysis for the brief time period when our study and the ICESat-2

data overlap.

2.3.3 Summer Sea Ice Thickness

Assimilation of the CPOM processed CS2 sea ice thickness estimates is restricted to months outside summer because of the inability of the radar altimetry to differentiate melt ponds from leads on the surface of the sea ice cover. However recent work by Landy et al. (2022) using a form of machine learning has managed to retrieve summer estimates of sea ice thickness from CS2. Landy et al. (2022) follows on work by Dawson et al. (2022), which used data from six different satellites, three optical and three equipped with synthetic aperture radar, to train a 1D convolutional neural network to separate CS2 returns from leads with those from floes and melt ponds. The accuracy of this algorithm was around 80%. With this machine learning method, the radar freeboards are calculated in a different way than the CPOM CS2 data. Usually freeboard is calculated by taking the difference between sea ice floe elevations and sea level elevations interpolated from along-track lead elevations. However in summer the presence of leads in the sea ice cover can be very sparse and would lead to interpolation of lead elevation data over too large a distance for the freeboard calculation. The freeboards are instead calculated by using each lead point to produce one freeboard estimate using the mean ice floe elevation surrounding that lead, with floe elevation measurements chosen if they were within 7 km of the lead point and fitted using a 2nd order polynomial.

In Landy et al. (2022), this work is continued by converting the estimated freeboard to thickness, and importantly correcting for bias in the CS2 radar altimeter. This observed bias in the CS2 radar altimeter causes an underestimation of the thickest ice in the Central Arctic, and is corrected for by assessing the radar response over melt pond covered sea ice and simulations to characterise the EM response. To do this, observations of sea surface roughness and melt pond coverage are necessary over the observation period (2010-2020), but this is difficult as there are no consistent observations of either over the period. Melt pond fraction observations from SENTINEL-3 which cover 2017-2020 are used to extract a climatology that can be used over the whole period. For the summer sea ice surface roughnesss observations, the standard deviation is estimated by propagating CS2 estimates in winter using the Lognormal Altimeter Retracker Model (LARM) dataset. Observations of sea ice drift from the NSIDC Polar Pathfinder dataset are used (see section 2.5). The bias-corrected freeboard measurements are then converted to ice thickness using a Lagrangian snow loading model. The sea ice thickness measurements are averaged and produced on 80 km grid cell size at 15 day intervals, we have interpolated these into monthly mean sea ice thickness estimates

on the CPOM 1 degree tripolar grid - the same grid as for the CPOM CS2 sea ice thickness observations. The sea ice thickness measurements calculated in May and September have patterns that closely resemble the April and October CPOM processed sea ice thickness respectively. The Landy CS2 thickness estimates are underestimated compared to OIB by 0.28 to 1 m. This data is provided with individual error statistics for each observation, which are supplied for the observation error covariance matrix for the assimilation.

2.4 Sea Ice Thickness Distribution

The fundamental problem that CICE and all sea ice models seek to solve is the evolution of the sea ice thickness distribution

$$\frac{\partial g}{\partial t} = -\nabla \cdot (g\mathbf{u}) - \frac{\partial}{\partial h}(fg) + \psi \tag{2.7}$$

where g is the ice thickness distribution function, **u** is the ice velocity, f is the rate of thermodynamic ice growth and ψ is the ridging distribution function. This equation is solved in sea ice models by splitting the ice in each grid cell into thickness categories and replacing the thickness distribution function g in the equation above with a_n, the fractional ice concentration in thickness category n (there is also an open water fraction a_0). The five thickness categories h_n we use have lower bounds (in metres) of 0, 0.6, 1.4, 2.4 and 3.6. When we refer to the sea ice thickness distribution assimilation in this paper we mean the assimilation of ten different variables; a_n^*, the concentration of ice in category 1-5, where the open water fraction a_0 in that grid cell is unknown which means

$$\sum_n a_n^* = 1, \tag{2.8}$$

and h_n, the thickness of ice in category 1-5. These are related to the state variables a_n and v_n by

$$a_n = a_n^* a \tag{2.9}$$

$$h_n = \frac{v_n}{a_n}, \tag{2.10}$$

where a is the total fraction of sea ice in a grid cell and v_n is the volume of ice in category n in a grid cell. The ice thickness distribution observations assimilated here are derived from

the CS2 monthly mean thickness observations, with the individual measurements (of which there must be 100 to derive a monthly mean sea ice thickness) binned according to the ice thickness distribution used in our CICE model (Schröder et al., 2019). Precise errors on these measurements are extremely difficult to derive due to the nature of the sea ice cover and several error sources contributing. To find an error approximately consistent to the error used in the CS2 mean thickness we can do some error analysis. The mean ice thickness of a grid cell is

$$h = \sum_{n=0}^{5} a_n h_n, \tag{2.11}$$

where h is mean thickness of the sea ice in the grid cell, a_n is ice concentration in grid cell in category n and h_n is the thickness of ice in a grid cell in category n. If all the quantities in the above equation are in error such that $h = h^{true} + \varepsilon_h$, $a_n = a_n^{true} + \varepsilon_{an}$ and $h_n = h_n^{true} + \varepsilon_{hn}$. Then we find

$$h^{true} + \varepsilon_h = \sum_{n=0}^{5} (a_n^{true} + \varepsilon_{an})(h_n^{true} + \varepsilon_{hn}) h^{true} + \varepsilon_h = \sum_{n=0}^{5} a_n^{true} v_n^{true} + a_n^{true} \varepsilon_{hn} + h_n^{true} \varepsilon_{an} + \varepsilon_{an} \varepsilon_{hn}. \tag{2.12}$$

The 'true' values satisfy the above equation so this reduces to

$$\varepsilon_h = \sum_{n=0}^{5} a_n^{true} \varepsilon_{hn} + h_n^{true} \varepsilon_{an} + \varepsilon_{an} \varepsilon_{hn}. \tag{2.13}$$

We do not know these errors, but assuming we know their root mean square expected errors using

$$\overline{\varepsilon_x^2} = \sigma_x^2, \tag{2.14}$$

where overline indicates average over realisations. Neglecting the triple and quadruple products leaves us with

$$\overline{\varepsilon_h^2} = \sum_{n=0}^{5}\sum_{n'=0}^{5}(a_n^{true}a_{n'}^{true}\overline{\varepsilon_{hn}\varepsilon_{hn'}} + a_n^{true}h_{n'}^{true}\overline{\varepsilon_{hn}\varepsilon_{an'}} + h_n^{true}a_{n'}^{true}\overline{\varepsilon_{an}\varepsilon_{hn'}}) + h_n^{true}h_{n'}^{true}\overline{\varepsilon_{an}\varepsilon_{an'}}. \tag{2.15}$$

To simplify this and be able to use it to make an estimation of the errors we make two necessary assumptions, first we assume that the errors in area and height are uncorrelated, and secondly we must assume that the errors of ice concentration and thickness are uncorrelated between categories. Of course this is untrue, especially considering that the sum of the ice concentrations in each category cannot exceed 1, however without these assumptions it would be impossible to approximate the errors in the ice concentration and thickness in each category. With these assumptions we find

$$\sigma_h^2 = \sum_{n=0}^{5}(a_n^{true^2}\sigma_{hn}^2 + h_n^{true^2}\sigma_{an}^2) \tag{2.16}$$

As we are dealing with relative errors in the case of the mean thickness measurements it is difficult to find errors for ice concentration and ice thickness in each category that work for all values of mean ice thickness. However we find that using a total error of 0.3 for category ice concentration and 0.8 m for category ice thickness leads at least to errors that are close to, or slightly worse than the mean ice thickness error equivalent.

In figure 2.3 we show the observations of thickness in each category in March and October derived from CS2 observations. It is firstly noticeable that the mean thicknesses in categories 4 and 5 in most areas of the Arctic is close to 3.6 m. This is because there is relatively little thick ice here, and of course the ice that is thickest within the category will peak towards the lower bound. This is also true, to a lesser extent, in category 3. Category 1 and Category 2 ice thickness shows generally no spatial pattern across the Arctic, though in a few cases there is very thick category 1 ice at the edges of where CS2 has enough observations, closest to the ice edge. Category 4 and 5 show clear spatial patterns towards thicker ice in these categories closer to the northern coast of Greenland and the Canadian Archipelago, as expected and also what is seen in grid cell mean thickness observations. Category 3 also shows this pattern in October, but not at the end of winter in March. As expected we see thicker ice in each category across the Arctic at the end of winter (March) than at the beginning (October) from the observations. These observations are difficult to compare to, or validate with other observations of ice thickness distribution, because there

are no publicly available observations of ice thickness distribution, though other studies have derived ice thickness distributions from other products using different statistical methods, such as Operation IceBridge (Tian-Kunze et al., 2014) or from upward looking sonars (Thomas, 2017). However because these observations are in-situ or from aeroplane/drone campaigns, they do not have the spatial patterns with which we can compare to the CS2 derived observations of thickness distribution.

In this thesis we assimilate categories 1-4 in the thickness distribution alongside the mean thickness. Since the sum of the elements of the thickness distribution is constrained, errors must be correlated between elements. Although we have observations in all ice thickness categories, instead of assimilating observations of a_n^* and h_n for $1 \leq n \leq 5$, with the approximation of uncorrelated errors, we assimilate these observations only for $1 \leq n \leq 4$, plus the mean thickness. Assuming that errors in the latter data are uncorrelated is presumably a less damaging approximation than the first. In this thesis, reference to the assimilation of observations of the thickness distribution is shorthand for the latter collection of data.

2.5 Sea Ice Motion

Another observation of sea ice has seen a significant amount of development over the past decade, and that is sea ice motion (or drift). There are a few observational datasets of sea ice motion available, but the one with the most spatial and temporal coverage is the Polar Pathfinder daily 25 km sea ice motion vectors (Tschudi et al., 2019). This product has been in development in the last decade and is currently on its 4th iteration. This product is produced using data from three types of sources; satellite imagery, buoys and NCEP-NCAR reanalysis wind fields. Sea ice motion is derived from satellite imagery using the maximum cross-correlation method (Emery et al., 1991). In this process, 2 satellite images of an identical location, taken between 1-3 days apart are selected and the later image is then translated relative to the earlier image, producing a correlation for each possible translation. The translation with the highest correlation between the two images is then selected and sea ice vectors in the x and y direction are derived. The Polar Pathfinder sea ice motion uses satellite data from SMMR, SSMI/I and SSMIS passive microwave sensors and the Advanced Very High Resolution Radiometer (AVHRR), which operates in the visible and near-infrared ranges. Buoys are the second source of sea ice motion data and buoys from the International Arctic Buoy Program (IABP) can provide sea ice motion by their transmitted locations. Sea ice motions from the NCEP-NCAR reanalysis wind fields are produced by assuming that

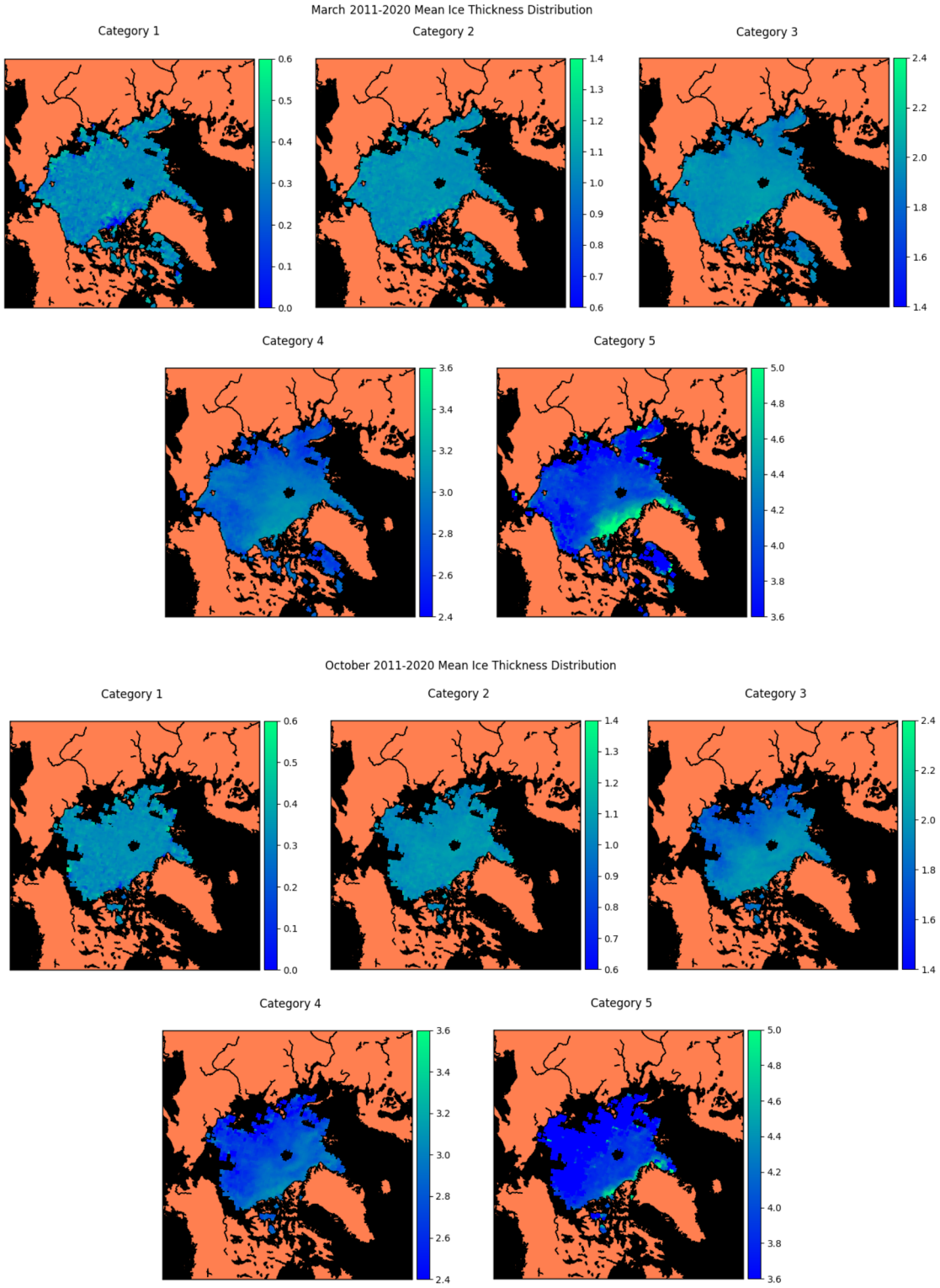

Fig. 2.3 Observations of the ice thickness distribution: the mean thickness in categories 1-5 (lower limits 0 m, 0.6 m, 1.4 m, 2.4 m, 3.6 m) in March and October between 2011 and 2020 (in metres).

the sea ice moves in the geostrophic wind direction at a magnitude of 1% of the wind speed. The sea ice motions are derived independently from each of these sources and combined using an optimal interpolation method and mapped onto a 25 km grid. Some grid cells are masked out, namely grid cells located close to shorelines, which will be affected by land, and those which occur in narrow channels, such as in the Canadian Archipelago. Finally only sea ice motion in grid cells which have an ice concentration equal to or greater than 15% are produced, where they use sea ice concentrations from SMMR, SSMI/I and SSMIS derived using the NASA Team algorithm.

Another notable dataset for sea ice motion comes from Ocean and Sea Ice Satellite Application Facilities (OSISAF) based on Lavergne et al. (2010). They currently produce two products; a medium resolution (20 km grid) and a low resolution (65 km grid) version. The low resolution product is on a 62.5 km at 2 day time intervals using satellite data from DMSP/SSMIS, AMSR-2 and ASCAT. It uses a similar maximum cross correlation method to derive sea ice motion. The medium resolution product uses AVHRR and ASCAT data only. Both products have a time coverage of 2005 to the present day, though they only cover the freeze-up season between October and April. Sea ice motion observations can often have large relative error observations associated with them, particularly in the melt season. This was primarily due to the poor spatial resolution of the passive microwave satellites, for example the Polar Pathfinder product theoretically is limited to a precision of 0.0723 ms^{-1}. In validation studies however it has been shown that these errors are often lower because the sources of error offset one another (Tschudi et al., 2020). A recent study by Gui et al. (2020) which attempted to validate the Pathfinder and OSISAF products over a 4-year period in the Western Arctic, found that Pathfinder tended to slightly underestimate daily sea ice motion, while the OSISAF product overestimated it. The minimum and maximum absolute errors recorded for Pathfinder between 2014 and 2017 were $0.015ms^{-1}$ and $0.056ms^{-1}$. The largest errors tend to occur during the melting season, especially during the July-September period. This is because sea ice motion is at its fastest during this period, but sea ice cover is also difficult to identify due to surface melt. Overall, Gui et al. (2020) found that both the Pathfinder and OSISAF products could be used for assimilation purposes. One issue with the assimilation of sea ice motion is its lack of memory (how its value in one time step can be related to its values at previous time steps) in sea ice models - this would mean that the assimilation would be useless because the model would likely revert to the same ice drift values it would have if no assimilation occurred within a very short time period. Previous studies in assimilation of sea ice motion from the 2000s found that it was not useful due to the lack of memory in this variable in sea ice models e.g. (Zhang et al., 2003, Stark et al.,

2008), though the TOPAZ4 reanalysis (Sakov et al., 2012), which assimilates ice drift, found that the assimilation could correct some biases in the ice thickness. However, in this study we will not consider the assimilation of sea ice motion, but instead focus on assimilating thickness and thickness distribution.

2.6 Other Observations

In this section we have reviewed the observations of Arctic sea ice that are most useful for the purposes of reanalysis - those with good spatiotemporal coverage and with uncertainties that are not too large or difficult to ascertain. However there are a large number of further sea ice observations available which have been assimilated in other studies or could be useful for shorter term reanalyses. Rostosky et al. (2018) was able to produce Pan-Arctic snow depth from passive microwave satellite measurements, with good agreement over FYI in spring against OIB data. Differences over MYI were larger. This data has already been assimilated by Fritzner et al. (2019) with the assimilation of snow depth leading to greater ice thicknesses than assimilating concentration or thickness because of positive correlations and the model generally having lower snow depths than the observations.

There are additionally a number of in-situ observations that have been made by submarine, ships and buoys/moorings that are very sparse in both space and time and with no parametrisation of their uncertainty. This makes these observations difficult to use in a reanalysis, though many have been used for validation of observations or reanalyses. Sea ice records from submarines and moorings, both equipped with upward-looking sonar, have been used to validate the PIOMAS reanalysis (Schweiger et al., 2011). This includes upward looking sonar measurements from the Beaufort Gyre Exploration Project (Krishfield et al., 2014), and from US Navy submarines (Wensnahan and Rothrock, 2005).

2.7 Summary

In this chapter we have considered a wide range of sea ice observations for reanalysis purposes. We discuss their suitability for use in a reanalysis and any previous data assimilation studies where the observations have been assimilated. The observations we find are the most interesting for a reanalysis study are the CS2 sea ice thickness and thickness distribution. Although the usefulness of assimilating sea ice thickness from CS2 has been tested and proved, it has not been assimilated in a long term (30+ year) study previously. The thickness distribution is interesting because it has not been assimilated before, and is closely related

to the model description of sea ice, and it should potentially provide new insights into the thickness distribution of the sea ice with the use of data assimilation, because the . Bootstrap sea ice concentration is also chosen for assimilation because we have a long term record with good spatial and temporal coverage, the Bootstrap data is carefully processed and has been determined to be appropriate for data assimilation, but has not been assimilated previously. The uncertainties in these observational records are discussed, and we have established the observation errors that will be used for the data assimilation. Although the scope of this thesis did not allow for further investigation into assimilation of the sea ice motion and snow depth, many sea ice motion assimilation studies have shown limited promise, although there is potential usefulness in combination with sea ice thickness assimilation. Snow depth assimilation could also provide additional reliability for sea ice thickness estimates (Fritzner et al., 2019), but these are difficult to determine with the large uncertainties in snow depth observations.

Chapter 3

Sea Ice Models and Reanalyses

3.1 Overview

In this chapter we discuss two of the three key pieces in a reanalysis system; the forecast model, and the data assimilation scheme that are used in this study. The third piece is the observation network discussed in chapter 2. Here we also discuss previously available sea ice reanalyses. This will be important when discussing the reanalysis produced in thesis, as it will inform us about the comparisons we make to these reanalyses, and the differences in our sea ice data assimilation systems that could cause these differences. In section 3.2 we discuss the sea ice model CICE, and in particular the parametrisations developed by CPOM unique to this model. In sections 3.3 and 3.4 we give some background in data assimilation and the development of the Local Ensemble Transform Kalman filter (LETKF) that we use in this study. In section 3.5 the currently available sea ice reanalyses are investigated.

3.2 The CPOM-CICE Model

The sea ice cover in the Arctic is not just a homogeneous sheet of ice which expands and contracts throughout the year but is made up of newly formed frazil ice, floes formed from first year ice colliding and splitting, and thick multi-year ice, some of which has formed pressure ridges over 5 metres high. Due to this inhomogeneity, sea ice is described in numerical models not just with a mean sea ice thickness in each grid cell, but with a sea ice thickness distribution. The CPOM-CICE model discretises the sea ice in a particular grid cell into categories of thickness. This distribution is fundamentally important as the dynamic and thermodynamic properties of sea ice depend strongly on its thickness. Hence the essential equation that sea ice models solve is that describing the evolution of the sea ice thickness

distribution

$$\frac{\partial g}{\partial t} = -\nabla \cdot (g\mathbf{u}) - \frac{\partial}{\partial h}(fg) + \psi, \tag{3.1}$$

where $g(h)$ is the ice thickness distribution function, $\mathbf{u}$ is the ice velocity, f is the rate of thermodynamic ice growth and ψ is the ridging distribution function. As already explained in chapter 2, this equation is solved by partitioning the ice in each grid cell into discrete thickness categories. We use the default five categories (with lower limits of 0, 0.6, 1.4, 2.4 and 3.6 metres) which are ordinarily sufficient to simulate the seasonal cycles of the sea ice thickness and other important variables (Bitz et al., 2001). The terms on the right hand side of equation 3.1, from left to right, describe the advection and divergence of ice on the horizontal plane, the transport of ice in thickness space due to thermodynamic melting and growth, and the transport of ice in thickness space due to mechanical processes such as ridging. The horizontal transport is solved using the incremental remapping scheme of Lipscomb and Hunke (2004), with ice velocity $\mathbf{u}$ determined using the sea ice momentum balance equation,

$$m\frac{\partial \mathbf{u}}{\partial t} = \nabla \cdot \sigma + \tau_a + \tau_w + \tau_b - \hat{k} \times mf\mathbf{u} - mg\nabla H_0, \tag{3.2}$$

where m is the mass of ice and snow per unit area, τ_a, τ_w are wind and ocean stresses, τ_b is the seabed stress, which represents interaction of ridged ice floes with shallow water seabed, σ is the internal stress tensor, which represents the internal ice stresses such as ice deformation, $\hat{k} \times mf\mathbf{u}$ is the Coriolis force and $mg\nabla H_0$ is the pressure gradient force arising from the sea surface slope. The internal stress tensor is formulated using an Elastic-Plastic-Anisotropic (EPA) sea ice rheology (Tsamados et al., 2013). This rheology accounts for the highly anisotropic nature of sea ice over a wide range of length scales.

The ice transport in thickness space due to thermodynamic changes is resolved using the remapping method of Lipscomb (2001). The thermodynamic process in the CICE model functions in three steps; the energy flux from atmosphere to ice is computed using surface forcing. New temperatures are then computed using an enthalpy equation, and then top and basal ice and snow growth/melt are computed. In CPOM-CICE the Delta-Eddington approach is used for computing the sea ice albedo and shortwave surface forcing. In this approach the optical properties of the snow and sea ice are prescribed based on physical

measurements (Briegleb and Light, 2007). A topographical melt pond scheme, in which melt pond area, depth and volume are carried on each thickness category as tracers (Flocco et al., 2010), which is used in conjunction with the Delta-Eddington approach. Melt ponds are a key component of the surface energy balance in sea ice models as they can significantly alter the ice albedo. CPOM-CICE also uses a "bubbly brine" thermal conductivity parametrization (Pringle et al., 2007) which increases the thermal conductivity of colder sea ice, which from in-situ observations was found to be 10-15% higher than previous model formulations.

The term describing the rate of thermodynamic ice growth f is found using the 1-dimensional vertical Bitz and Lipscomb thermodynamic model (Bitz and Lipscomb, 1999). This model solves heat flux balance equations for the ice and snow (where it exists) in each thickness category and accounts for the effects of brine pocket melting and freezing and is energy-conserving. The ice in each thickness category in a grid cell is conceptualized as a horizontally uniform column with seven layers and an additional snow layer, with a surface temperature that cannot exceed zero degrees Celsius and a base ice temperature which must be equivalent to the freezing temperature of the ocean mixed layer. Each of the ice (snow) layers has an associated enthalpy q_{ik} (q_{sk}). The sea ice enthalpy is defined as minus the amount of energy required to melt a unit of ice volume and is a function of temperature and salinity,

$$q_i = -\rho_i[c_i(T_m - T) + L_0(1 - \frac{T_m}{T}) - c_w T_m] \tag{3.3}$$

where ρ_i is the sea ice density, c_i and c_w are the specific heats of ice and water respectively, T is the temperature and T_m is the melting temperature of sea ice which is a function of the salinity. The expression for the enthalpy of snow (and fresh ice) is a function of temperature alone,

$$q_s(T) = -\rho_s(-c_i T + L_0) \tag{3.4}$$

where ρ_s is the snow density. Since the salinity is prescribed the enthalpy has a one-to-one relationship with the temperature.

The final term in equation 3.1, ψ describes the mechanical redistribution of the sea ice in thickness space. This function converts thinner ice to thicker ice and is applied after the horizontal transport of the sea ice. When sea ice converges in the model, it ridges such that

the fractional ice area in a grid cell does not exceed the grid cell area. CPOM-CICE uses the mechanical redistribution formulation of Lipscomb et al. (2007) in which the ice thickness distribution of ridged ice is described in a negative exponential, and a weighting function which favours the ridging of thin ice and closing of open water area in preference to ridging thick ice. CPOM-CICE uses the ice strength formulation of Rothrock (1975) whereby the ice strength is proportional to the change in potential energy from ice deformation due to its compression.

Although CICE was designed for use in a global climate model, in this research we use it in stand-alone mode, uncoupled to an atmospheric or ocean model. The model has been used in this way to produce realistic estimates of the sea ice state, e.g. Schröder et al. (2019), and its computational efficiency facilitates physical and technical model development. CICE contains a thermodynamic slab mixed layer ocean model with a prognostic ocean temperature. This model is initialised with ocean temperature and salinity (3m depth) from a 1993-2010 climatology based on an ocean reanalysis (Ferry et al., 2011). The mixed layer salinity is prescribed from the climatology and the prognostic temperature is restored to the monthly climatology with a 20 day timescale to account for heat advection in the ocean. The ocean currents (also at 3m depth) are also taken from the same reanalysis. The atmospheric forcing data used are NCEP-2 (Kanamitsu et al., 2002) comprising daily downward shortwave and longwave radiation fluxes and 6-hourly 2m temperature and humidity and 10m wind velocity. These atmospheric forcing fields are perturbed to generate ensemble spread as described in section 4.4. We also take monthly mean precipitation from the same reanalysis, which is not perturbed. We use a Nucleus for European Modelling of the Ocean (NEMO) 1 degree (a roughly 40km by 40km grid size) tripolar grid, covering the whole Arctic region. A time step of 1 hour is used.

3.3 Data Assimilation

Current state-of-the-art models of the climate have been continuously updated, and work is always ongoing to include newly understood climate processes and physics, or to update existing parametrizations of climate processes into modern standards. However the sheer complexity of the climate, or even a section or subsection of the climate, is too great to account for all the processes which take place. To capture many processes completely accurately would require a model resolution which modern computational processing power could

not accomplish in any reasonable amount of time. In addition to numerical models we have access to a multitude of observations, but these have their own shortcomings (see chapter 2). Observations can be irregularly distributed and sparse in both time and space, providing an incomplete picture of the true state, and often large regions can be completely lacking observations of important climate indicators due to geography or terrain. This especially applies to in-situ observations, for example rainfall measurements in the Amazon rainforest, or snow depth in the Arctic, which is of particular importance to this work. Observations may also be processed from more fundamental data in a highly complex non-linear way, for example observations of sea ice concentration from passive microwave satellites use observed brightness temperatures to produce the final observational sea ice concentration product. Human error, instrument error and errors arising from the processing of the observations must all be accounted for in the observation products. Therefore modern operational climate reanalyses and weather forecasts take advantage of both numerical models and observations and combine them in a process known as data assimilation.

Data assimilation is an extremely useful tool because it allows us to combine models and observations to produce better estimates of the model state. To combine these two sources of information in a statistically coherent way requires the use of probability density functions (representing the uncertainty) and Bayes' theorem, which states

$$p(\mathbf{x}|\mathbf{y}) = \frac{p(\mathbf{x})p(\mathbf{y}|\mathbf{x})}{p(\mathbf{y})}, \tag{3.5}$$

where $p(\mathbf{x}|\mathbf{y})$ is the conditional probability of $\mathbf{x}$ given $\mathbf{y}$, $p(\mathbf{y}|\mathbf{x})$ is the conditional probability of $\mathbf{y}$ given $\mathbf{x}$, $p(\mathbf{x})$ and $p(\mathbf{y})$ are the marginal probabilities of $\mathbf{x}$ and $\mathbf{y}$ respectively (see below). The vector $\mathbf{x}$ represents a general state of a system being analysed, and the vector $\mathbf{y}$ represents a general set of observations. In data assimilation we have $p(\mathbf{x})$, the prior density, which describes the probability of possible states that the system can have, in terms of our knowledge before observations are made. $p(\mathbf{y}|\mathbf{x})$ is the conditional density that observations take the values $\mathbf{y}$, given that $\mathbf{x}$ is the system's true state. $p(\mathbf{y}|\mathbf{x})$ is a function of $\mathbf{y}$ for a fixed $\mathbf{x}$, but in data assimilation, we turn this around and consider it a function of $\mathbf{x}$ for a fixed (given) set of observed values, $\mathbf{y}$, where this function becomes known as the likelihood. $p(\mathbf{y})$ is often treated as a normalising constant, as we will do here (it does not depend on the state $\mathbf{x}$).

We seek to calculate $p(\mathbf{x}|\mathbf{y})$ the posterior density. There are two special states that often arise in data assimilation. One is called the background state, which can be defined as the

mean of $p(\mathbf{x})$. The other is called the analysis state, which can be defined as the mean of $p(\mathbf{x}|\mathbf{y})$. In this thesis though we use an ensemble data assimilation method, which does not have a single background or analysis state at any time, but an ensemble of backgrounds and analyses, which themselves define the respective densities $p(\mathbf{x})$ and $p(\mathbf{x}|\mathbf{y})$ and from which we can derive the ensemble means and covariances.

Turning attention now to general density functions, a problem arises: numerical models used for weather prediction and climate reanalysis are extremely high dimensional and this means it is not plausible to store and calculate the full probability density functions. However what we can do is calculate an estimate of the probability density functions. This has lead to development of a number of data assimilation methods, all of which seek to solve this same problem. These can be divided into four categories; traditional variational methods, ensemble Kalman filters, hybrids (a combination of variational and ensemble Kalman filter), and other Monte Carlo methods. Each method has its own advantages and drawbacks.

Traditional variational methods such as 3D-var and 4D-var are efficient and produce an analysis consistent with the model, and have been widely studied and applied. They are the most commonly used data assimilation approach in operational weather forecasting and climate reanalyses. This includes the ECMWF and the Japanese Meteorological Agency (JMA) climate models, and many other centres use a hybrid approach. Traditional variational methods, and some hybrid methods, require the development of tangent linear and in the case of 4D-var an adjoint model, which are time consuming to develop and maintain. Ensemble Kalman filters avoid the difficulties of having to develop a tangent linear and adjoint models. Other drawbacks of variational methods include the near-linear and Gaussian assumption, which are not always valid and can restrict the length of the assimilation window. Also it is more difficult to account for the background error, which is often taken to be predominantly constant in time. On the other hand, Ensemble Kalman filters can also be easy to parallelise and develop separately from the model. Here, the CPOM-CICE model has been coupled to the Parallelised Data Assimilation Framework (PDAF) (Nerger et al., 2005). PDAF is one example of a few software environments developed to facilitate the use of ensemble data assimilation methods in numerical models. Additionally it is also easier to account for the state uncertainties in ensemble Kalman filters, which are measured by the ensemble spread.

The ensemble Kalman filter also has some drawbacks, some of which arise due to its sensitivity to ensemble size (Houtekamer and Zhang, 2016). Undersampling in ensemble Kalman filters can lead to filter divergence (collapse of the ensemble), which can reduce the

ensemble spread to effectively zero. This means that the observations are virtually ignored at assimilation time. If the spread is too large the inverse can happen, with the analysis ensemble over fitting to the observations. The covariances (the second moment of $p(\mathbf{x})$, described by the covariance matrix $\mathbf{P}_n^f$) are also impacted by sampling error, leading to the assimilation having unwanted effects on some state variables or regions, especially in regions located far from observations. These are known as spurious correlations. Like variational methods, ensemble Kalman filters also require a Gaussian assumption, which again may not be valid for some models. Unlike 4D variational methods, the analysis ensemble produced by ensemble Kalman filters may not necessarily be consistent with the model physics. An earlier developed Kalman filter method, the extended Kalman filter, would explicitly evolve the mean and covariance of the ensemble forward using the model, but this still requires a tangent linear model and thus it still had the problem of storing and forward integration of the forecast error covariance matrix $\mathbf{P}_n^f$. In the next section I will give a brief summary of the ensemble Kalman filter methods.

3.4 Ensemble Kalman Filter and the LETKF

The Ensemble Kalman Filter (Evensen, 1994) differs from variational data assimilation in a number of key ways. It does not require a tangent linear model or adjoint model, it uses an ensemble of forecasts to estimate the model background error statistics, which means that it can also evolve in time, which cannot be achieved easily in variational methods between assimilation cycles. Between assimilation cycles, the model is used to evolve each state forward, and then an ensemble mean and covariance are found. Instead of assimilating all observations within a time window, as in variational DA, the ensemble Kalman filter can assimilate them sequentially in time.

We start our exploration with the Kalman Filter (KF) (Kalman, 1960) (a further introduction is in Welch et al. (1995)). The forecast stage of the KF uses the model to evolve the mean and covariance of the posterior distribution forward in time from the previous analysis at time n

$$\mathbf{x}_n^f = \mathbf{M}\mathbf{x}_{n-1}^a \tag{3.6}$$

$$\mathbf{P}_n^f = \mathbf{M}\mathbf{P}_{n-1}^a\mathbf{M} + \mathbf{Q} \tag{3.7}$$

where x_{n-1}^a is the analysis at previous time step $n-1$, x_n^f is the forecast at current time step

n, $\mathbf{P}_n^a$ is the analysis error covariance matrix, $\mathbf{P}_n^f$ is the forecast error covariance matrix and $\mathbf{Q}$ is the model error covariance. The evolved forecast mean and covariance are then updated during the current analysis stage by Bayes' theorem as follows. If we assume Gaussian probability distribution functions then we find

$$p(\mathbf{x}) = C\exp(-\frac{1}{2}(\mathbf{x}-\mathbf{x}^f)^T\mathbf{P}_n^{f\,-1}(\mathbf{x}-\mathbf{P}_n^f)) \tag{3.8}$$

$$p(\mathbf{y}|\mathbf{x}) = C\exp(-\frac{1}{2}(\mathbf{y}-\mathbf{H}(\mathbf{x}))^T\mathbf{R}^{-1}(\mathbf{y}-\mathbf{H}(\mathbf{x}))) \tag{3.9}$$

where C is a constant, $\mathbf{H}$ is the observation operator, $\mathbf{y}$ are the observations, $\mathbf{H}^T$ is the transpose of $\mathbf{H}$, and $\mathbf{R}$ is the observation error covariance matrix. Plugging this into Bayes' theorem gives us

$$p(\mathbf{x}|\mathbf{y}) \sim \exp\left\{-\frac{1}{2}\left[(\mathbf{x}-\mathbf{x}_n^f)^T\mathbf{P}_n^{f\,-1}(\mathbf{x}-\mathbf{x}^f)+(\mathbf{y}-\mathbf{H}(\mathbf{x}))^T\mathbf{R}^{-1}(\mathbf{y}-\mathbf{H}(\mathbf{x}))\right]\right\} \tag{3.10}$$

the maximum probability occurs when we maximise $p(\mathbf{x}|\mathbf{y})$, which is equivalent to minimizing $\ln(p(\mathbf{x}|\mathbf{y}))$:

$$J(\mathbf{x}) \sim \frac{1}{2}(\mathbf{x}-\mathbf{x}_n^f)\mathbf{P}_n^{f\,-1}(\mathbf{x}-\mathbf{x}_n^f)+\frac{1}{2}(\mathbf{y}-\mathbf{H}(\mathbf{x}))^T\mathbf{R}^{-1}(\mathbf{y}-\mathbf{H}(\mathbf{x})). \tag{3.11}$$

This is commonly known as the cost function. The particular $\mathbf{x}$ that minimises this can be found analytically, if the observation operator is linear, giving

$$\mathbf{x}^a = \mathbf{x}^f + \mathbf{P}_n^f\mathbf{H}(\mathbf{H}\mathbf{P}_n^f\mathbf{H}^T+\mathbf{R})^{-1}(\mathbf{y}-\mathbf{H}(\mathbf{x})), \tag{3.12}$$

or

$$\mathbf{x}^a = \mathbf{x}^f + \mathbf{K}_n(\mathbf{y}-\mathbf{H}(\mathbf{x})) \tag{3.13}$$

with

$$\mathbf{P}_n^a = (\mathbf{I}-\mathbf{K}_n\mathbf{H})\mathbf{P}_n^f, \tag{3.14}$$

where $\mathbf{K}_n$ is the Kalman gain. The Kalman gain is given by

$$\mathbf{K}_n = \mathbf{P}_n^f \mathbf{H}^T (\mathbf{H}\mathbf{P}_n^f \mathbf{H}^T + \mathbf{R})^{-1}. \tag{3.15}$$

This is one means of deriving the update equation.

The KF alone is difficult to apply for many practical uses, including climate modelling, because of the size of the covariance matrix $\mathbf{P}_n^f$. The ensemble Kalman filter solves this by instead sampling the mean and covariance from the prior probability density function and updating the ensemble states. Ensemble Kalman filter methods can be broken up into two approaches: stochastic and deterministic. Stochastic ensemble Kalman filters were originally developed to counteract the problem of ensemble collapse by introducing perturbed observations, though later developments of this method have focused on perturbing the model version of the observations with noise from measurements, as the actual observations already contained error and noise. This method however increases computational cost and importantly, was found to introduce additional sampling noise (Whitaker and Hamill, 2002). This problem led to the development of the ensemble square root filters (which are deterministic), such as the Ensemble Transform Kalman Filter (ETKF) and its localised version LETKF, which we use in this thesis (Hunt et al., 2007). Instead of updating each ensemble member separately, the ETKF updates the analysis perturbations so that their covariance is consistent with equation 3.14. This is the idea of the deterministic ETKF (Bishop et al., 2001). The prediction step in the ensemble square root filter method begins by evolving each ensemble member $\mathbf{x}_n^{(i),f}$ forward using the model M_{t_{n-1},t_n}

$$\mathbf{x}_n^{(i),f} = M_{t_{n-1},t_n}(\mathbf{x}_{n-1}^{(i),f}), \tag{3.16}$$

where $\mathbf{x}_n^{(i),f}$ is the forecast ensemble member i at time n. The forecast ensemble mean is then computed

$$\bar{\mathbf{x}}_n^f = \frac{1}{N}\sum_{i=1}^{N} \mathbf{x}_n^{(i),f}, \tag{3.17}$$

where N is ensemble size. The ensemble covariance matrix is given by

$$\mathbf{P}_n^f = \frac{1}{N-1} \sum_{i=1}^{N} \left(\mathbf{x}_n^{(i),f} - \bar{\mathbf{x}}_n^f \right) \left(\mathbf{x}_n^{(i),f} - \bar{\mathbf{x}}_n^f \right)^T, \tag{3.18}$$

and by writing this in terms of the perturbations to the mean

$$\mathbf{X}_n^f = \sum_{i=1}^{N} \left(\mathbf{x}_n^{(i),f} - \bar{\mathbf{x}}_n^f \right), \tag{3.19}$$

we find

$$\mathbf{P}_n^f = \frac{1}{N-1} \mathbf{X}_n^f (\mathbf{X}_n^f)^T, \tag{3.20}$$

and a similar expression can also be written for the analysis error covariance matrix

$$\mathbf{P}_n^a = \frac{1}{N-1} \mathbf{X}_n^a (\mathbf{X}_n^a)^T. \tag{3.21}$$

In the same way the forecast ensemble $\mathbf{y}_n^{(i),f}$, its mean $\bar{\mathbf{y}}_n^f$ and perturbation matrix $\mathbf{Y}_n^f$ in observation space are calculated which are needed for the update step. For the update step, the ensemble mean is updated

$$\bar{\mathbf{x}}_n^a = \bar{\mathbf{x}}_n^f + \mathbf{K}_n (\mathbf{y}_n - \bar{\mathbf{y}}_n^f), \tag{3.22}$$

where

$$\mathbf{K}_n = \mathbf{X}_n^f (\mathbf{Y}_n^f)^T \left(\mathbf{Y}_n^f (\mathbf{Y}_n^f)^T + (N-1)\mathbf{R} \right)^{-1}, \tag{3.23}$$

is the Kalman gain computed from the ensemble, with

$$\mathbf{Y}_n^f = \mathbf{H}\mathbf{X}_n^f. \tag{3.24}$$

To update the ensemble perturbations (from forecast perturbations to analysis perturbations), we use equations 3.20 and 3.21 starting from the ensemble version of equation **??**

$$\mathbf{P}_n^a = \frac{1}{N-1}\mathbf{X}_n^a(\mathbf{X}_n^a)^T, \tag{3.25}$$

and we use an $N \times N$ matrix $\mathbf{T}_n^a$ whereby

$$\mathbf{P}_n^a = \frac{1}{N-1}\mathbf{X}_n^a\mathbf{T}_n^a(\mathbf{X}_n^a\mathbf{T}_n^a)^T \simeq (\mathbf{I}-\mathbf{K}_n\mathbf{H})\mathbf{P}_n^f, \tag{3.26}$$

and so the perturbation matrix is updated via

$$\mathbf{X}_n^a = \mathbf{X}_n^f\mathbf{T}_n, \tag{3.27}$$

by equating $\mathbf{T}$ with the Kalman update, and then solving the equation to find $\mathbf{X}_n^a$ and $\mathbf{K}_n$, $\bar{\mathbf{x}}_n^a$ is then found via equation 3.22.

In this method $\mathbf{T}_n^a$ is not uniquely defined, which has led to the development of a number of different ensemble square root Kalman filters, which have been extensively reviewed in (Tippett et al., 2003) and more specifically for atmospheric data assimilation applications in (Houtekamer and Zhang, 2016). The ensemble transform Kalman filter (ETKF) (Bishop et al., 2001) is one of a number of these square-root Kalman filters. ETKF's use the Sherman-Morrison-Woodbury formula to compute $\mathbf{T}_n^a$ (see Bishop et al. (2001)) and thereby update the perturbation matrix $\mathbf{X}_n^a$.

The ETKF was later expanded upon further in Hunt et al. (2007), particularly focusing on using this assimilation method for spatiotemporally chaotic systems, such as those used in climate models. This method is known as the Local Ensemble Transform Kalman Filter (LETKF) (Hunt et al., 2007), which adds a technique of spatial localisation, for the purposes of avoiding long-range spurious correlations. This is needed to alleviate effects of aforemen-

tioned undersampling which can occur in ensemble Kalman filters with a small number of ensemble members (see end of section 3.3). Localisation was first introduced in Houtekamer and Mitchell (1998), and has been adapted and developed for the LETKF and application to climate models. The basic underlying idea is to restrict the influence that observations can have on grid points depending on the distance between them. This is done via a Gaspari and Cohn function (Gaspari and Cohn, 1999), a piecewise polynomial function that acts as a weighting function for the observation error covariance, which is scaled such that the effects of the observation smoothly reach zero at and beyond a defined localisation radius away from the observation.

The other method that we use in this study to mitigate undersampling is inflation. Ensemble inflation is most commonly applied multiplicatively, whereby each ensemble member is multiplied by an inflation factor r before or after analysis (Anderson and Anderson, 1999). In our study we implement inflation using a forgetting factor (Pham et al., 1998). This is a more computationally efficient way of implementing inflation in many deterministic ensemble Kalman filters because it is applied to TT^T, which is smaller (in terms of size) than the ensemble members that inflation is usually applied to. The forgetting factor ρ is related to r by

$$\rho = r^{-2}. \tag{3.28}$$

In this study we have chosen to use the LETKF formulation of (Hunt et al., 2007) with PDAF, rather than variational methods. We choose this method for a few reasons; because there is no need to linearise the CICE model or develop tangent-linear and adjoint models, PDAF provides an efficient way of implementing the LETKF and the LETKF makes it easy to account for the mean model state error, which is time-dependent. Additionally the covariances between the model variables vary strongly over the year, and within a season close to the ice edge, and so the LETKF provides an estimate of the instantaneous covariances between these variables. The non-static uncertainty of the model is important, as the uncertainty in the estimated sea ice cover varies by season significantly when compared with in-situ or satellite observations of sea ice (Wang et al., 2020). In the next chapter we investigate many of the assimilation parameters discussed here in further detail and conduct further studies to determine the optimal parameters that we should use in our reanalyses. For a more in-depth review of current ensemble data assimilation methods, see Vetra-Carvalho et al. (2018).

3.5 Currently available sea ice reanalyses

3.5.1 PIOMAS

The Pan-Arctic Ice Ocean Modelling and Assimilation System (PIOMAS) (Zhang and Rothrock, 2003) (Lindsay and Zhang, 2006) is the most widely known and extensively validated sea ice reanalysis currently available. It covers the whole Arctic during the satellite era from 1979 to the present day, and is primarily designed to provide estimates of daily Pan-Arctic sea ice volume. PIOMAS uses a thickness and enthalpy distribution (TED) sea ice model with 12 categories, simulating the evolution of the ice, snow and enthalpy by solving a distribution equation for each, based on an Eulerian model developed by Hibler Iii (1980) and then improved by Flato and Hibler III (1995). This sea ice model is broadly similar to the CPOM-CICE sea ice model that we will be using, but does not feature some of the more recent advancements in sea-ice modelling such as melt pond formulation and form drag parametrisation, although it does use more ice and snow thickness categories. The TED model is coupled to the Parallel Ocean Program (POP) ocean model, which is based on the Bryan-Cox model (Cox, 1984). An interesting difference for polar climate studies is in comparisons between the Bryan-Cox and other ocean models is that it differs significantly in its representation of the North Atlantic Current, which has an impact on the subpolar gyre and the Greenland-Iceland-Norway ocean basin, which during Winter is partly covered with sea-ice (Roberts et al., 1996).

PIOMAS assimilates sea ice concentration from the National Snow and Ice Data Center (NSIDC) near-real time product, which is produced using the NASA Team concentration retrieval algorithm (see chapter 2). This is assimilated in PIOMAS using a relatively simple nudging method which works to move the model variables closer to their observed counterparts through a weighting factor. This weighting factor is a strong function of the difference between the model and observed state derived using a least squares method and is found by

$$K = \frac{|C_{obs} - C_{mod}|^{\alpha}}{|C_{obs} - C_{mod}|^{\alpha} + R_{obs}^2}, \tag{3.29}$$

where K is the weighting factor, C_{obs} is the observed sea ice concentration, C_{mod} is the model sea ice concentration, R_{obs} is the observation error and $\alpha = 6$. PIOMAS uses an observation error of 5% (0.05) for all sea ice concentration observations (Lindsay and Zhang, 2006). The model sea ice concentration is nudged daily using

$$\hat{C_{mod}} = C_{mod} + K(C_{obs} - C_{mod}). \tag{3.30}$$

This means that the observations will be weighted more heavily when the discrepancy between the model and the observations is larger. Essentially this means that the nudging will have the biggest impact at the sea ice edge, which also means that the assimilation method will favour the ice extent over the ice concentration, because the difference between modelled and observed ice concentration is likely to be reduced away from the ice edge, and the greatest uncertainties in sea ice concentration lie at the edges of the ice cover (Lindsay and Zhang, 2006). PIOMAS also assimilates sea surface temperatures from the NCEP/NCAR reanalysis in ice free areas, and uses atmospheric forcing in areas with sea ice using information (wind stresses, humidity, surface temperatures) from the same reanalysis. Monthly sea ice volume in April and September estimated by PIOMAS since 1979 (44 years) is shown in figure 3.1. These two months are shown because September shows the greatest decreasing trend and April shows the smallest decreasing trend in sea ice volume over the 44 year reanalysis.

PIOMAS has been extensively validated through satellite (ICESAT) (figure 3.2) (which showed general agreement with PIOMAS, particularly in the spatial distribution) and in-situ (submarine, mooring) observations (figure 3.2). Uncertainty for October sea ice volume estimations is believed to be $1.35 \times 10^3 km^3$ (Schweiger et al., 2011). This includes a mean thickness uncertainty of 0.78 m where biases could be as large 0.4 m. In general it was found that PIOMAS overestimates the thickness of thinner ice and underestimates the thickness of the thickest ice. Further investigation showed that this occurred particularly in the Beaufort Sea, Greenland Sea and the Canadian Archipelago (Wang et al., 2016). In the same study they found that CS2 could suffer from a similar issue. In this study we use the PIOMAS reanalysis as an evaluation and validation tool for comparison with our CICE-PDAF reanalysis.

3.5.2 TOPAZ

Another ocean sea-ice reanalysis available is TOPAZ (Towards an Operational Prediction system for the North Atlantic European coastal Zones), currently on its fourth iteration

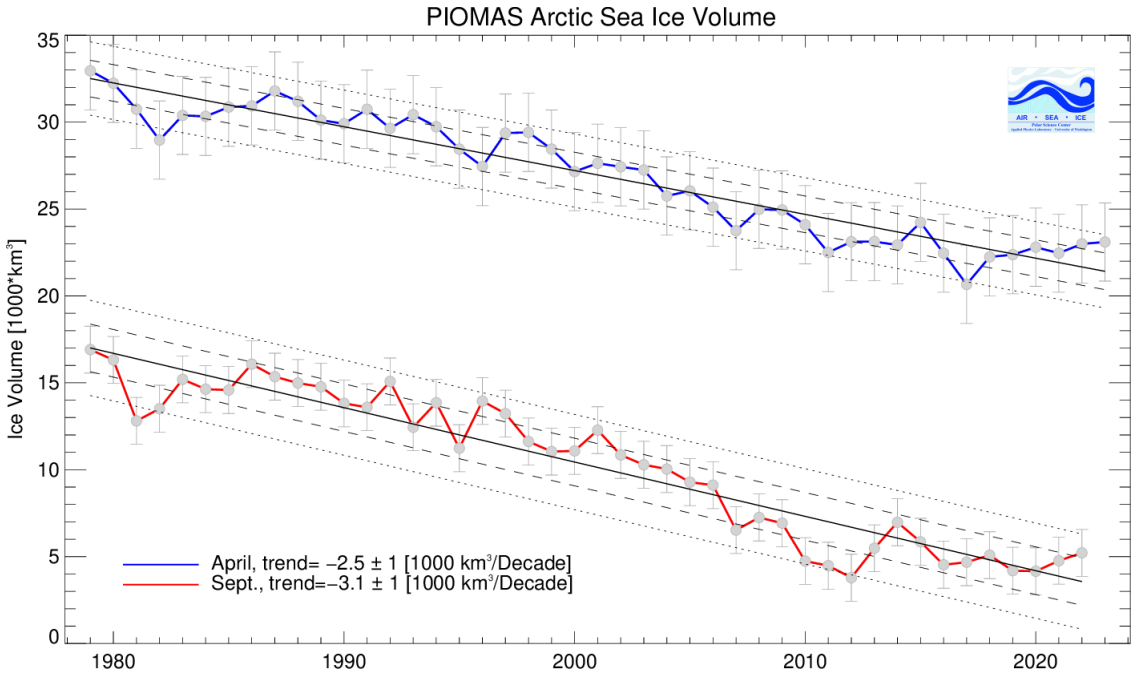

Fig. 3.1 PIOMAS monthly sea ice volume between 1979 and 2023 in April and September. Solid lines show the trend, dashed lines show 1 standard deviation from the trend and dotted lines show 2 standard deviations from the trend. Source: Polar Science Center, University of Washington

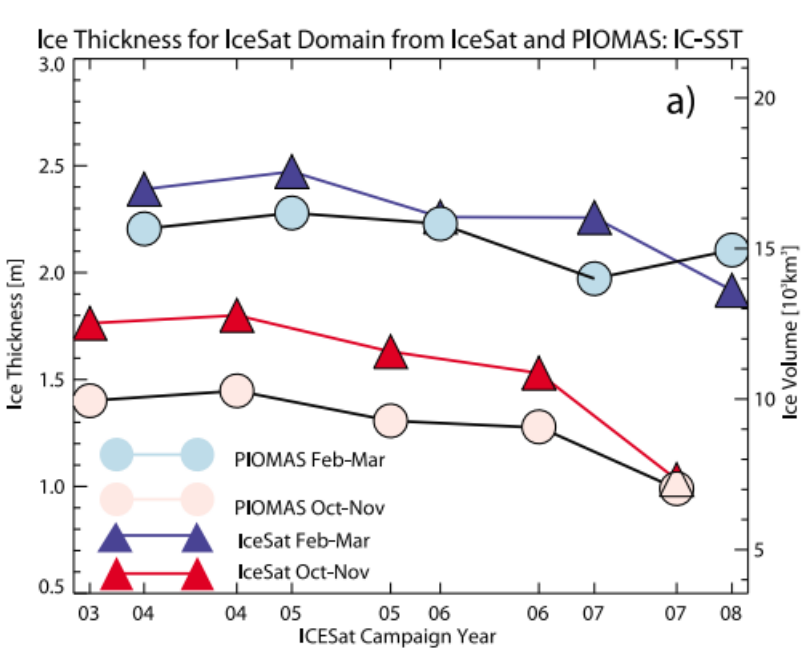

Fig. 3.2 Comparison of ICESat and PIOMAS mean thickness and volume between 2003 and 2007 over the ICESat Domain. (Schweiger et al., 2011)

TOPAZ4 (Sakov et al., 2012). TOPAZ4 is a coupled sea ice-ocean data assimilation system covering the Arctic and North Atlantic for a twenty year period from 1989-2018. The ocean model used in TOPAZ is the HYbrid Co-ordinate Ocean Model (HYCOM) (Chassignet et al., 2007) coupled to an earlier version of the CICE model with a single thickness category. The coupled model is forced using 6-hourly atmospheric fields from the ERA-interim reanalysis. It uses a 100 member ensemble and a deterministic ensemble Kalman filter configuration for assimilation. This system is similar to the ensemble square root filter when increments are small, and is similar to the ensemble transform Kalman filter when increments are larger. They use a Gaspari and Cohn function for the localisation, with a radius of 300 km. To help maintain a robust ensemble spread, a model perturbation system is also used whereby some of the forcing fields are perturbed. The perturbations to the atmospheric fields are implemented by generating a smooth pseudo-random field with a prescribed variance, and a mean of zero (Brusdal et al., 2003). TOPAZ4 assimilates a large number of observation fields and from a number of different sources. This includes sea surface temperature, in-situ temperature and salinity and sea level anomalies for the ocean. Sea ice observations assimilated include sea ice concentration and sea ice drift from the Ocean and Sea Ice Satellite Application Facility (OSISAF). The assimilation of sea ice thickness observations in the TOPAZ4 reanalysis system was tested using the combined CS2 and SMOS sea ice

thickness product (Ricker et al., 2017). Assimilating this product was found to significantly reduce the biased low ice thicknesses in the system and the standard error when compared to the assimilated product (Xie et al., 2017), and when evaluated against independent sea ice thickness estimates from buoys and Operation IceBridge (OIB), it was also found that errors were significantly reduced (Xie et al., 2018). Further evaluation against independent thickness estimates has been undertaken but is difficult to quantify due to the sparseness of the available observational data but in general a good agreement with the spatial distribution of the ice thickness is found with PIOMAS and CS2, with the biggest differences in the Beaufort sea and in September (Xiu et al., 2021). In an evaluation of other important sea ice indicators, it was generally found that TOPAZ4 agrees well with the OSISAF sea ice concentration, with the poorest performance occurring at the ice edge, which included an ice edge which was too sharp. Sea ice drift from TOPAZ4 was comparable to independent observations but there were significant issues such as a misplaced Beaufort Gyre and a fast ice bias (Xie et al., 2017). In general, it seems that TOPAZ4 performs well in moving the model closer to the observations, but there are significant issues, many of which arise due to the use of a simple sea ice model.

3.5.3 Further studies

There have been a number of studies undertaken in the past five years to assess the performance and effectiveness of the assimilation of sea ice thickness within climate models. We will discuss some of the more interesting and relevant studies in this section. The UK Met office has tested the assimilation of CS2 sea ice thickness in its Forecast Ocean Assimilation Model (FOAM) coupled ocean and sea ice analysis and forecast system which uses the Nucleus for European Modelling of the Ocean (NEMO) ocean model coupled to the CICE sea ice model (Blockley and Peterson, 2018). The model is forced with atmospheric data from the ERA-interim reanalysis at 6-hourly time steps. The FOAM system currently assimilates temperature, salinity, sea level anomaly and sea ice concentration daily using a modified 3D-var scheme. Assimilation of both monthly mean (Blockley and Peterson, 2018) and daily (Fiedler et al., 2022) CS2 thicknesses have been performance evaluated in shorter multi-year runs of the system, first using a simple nudging technique and then later using a 3D-var scheme. It was shown in both studies that the assimilation of the CS2 sea ice thickness had a positive effect on the modelled ice thickness, reducing the Root Mean Square Differences (RMSDs) to independent ice thickness observations when compared to a control run. It was also found that the information from the assimilation during winter would still be useful for the model during the melting season, when ice thickness observations from CS2 are not available. They have also recently tested the model with assimilation of the CS2-SMOS

product (Mignac et al., 2022). The assimilation of the CS2-SMOS product counteracted the negative effects of assimilating only CS2 data, which caused thicker ice than independent measurements from moorings in the marginal ice zones.

At the Geophysical Fluid Dynamics Laboratory (GFDL), they have further developed their seasonal prediction system to include the assimilation of sea ice concentration using the ensemble adjustment Kalman filter, which significantly improves seasonal predictions of sea ice extent (Zhang et al., 2021). The assimilation of OSISAF sea ice concentration, OSISAF sea ice drift, CS2-SMOS sea ice thickness and sea surface temperature have been studied in a global climate model at the Alfred Wegener Institute (AWI-CM v1.1). This uses a 1-category thickness distribution, zero-layer thermodynamics scheme and Elastic-Viscous-Plastic (EVP) sea ice rheology and assimilates using a Local Error Subspace Transform Kalman Filter (LESTKF). This has been found to perform well against independently available in-situ data (Mu et al., 2020).

Chevallier et al. (2017) is a good in-depth review and intercomparison of currently available global ocean-sea ice reanalyses, as previously discussed in chapter 1, and further discussed in this thesis. It finds that the Arctic sea ice extent and concentration is generally consistent between the various reanalyses, largely because almost all of them assimilate sea ice concentration and the atmospheric forcing (particularly by the SST) exerts a strong restoring force (Chevallier et al., 2017). Those which do not assimilate concentration tend to overestimate sea ice concentration (as we will see happens in this study in the contrl run). The reanalyses which do assimilate concentration are generally good at capturing the recent trends in extent and area. In terms of the ice velocity (direction and magnitude), the reanalyses tend to all overestimate the magnitude of the drift, though monthly and interannual variability, and the seasonality of the ice velocity fields are reproduced well in the reanalyses in comparison to observations from the NSIDC. In terms of the ice thickness, the paper primarily compared the reanalyses to the ICESat data (as we saw earlier in 3.2 for PIOMAS). It is generally found that the ice is too thick in the Beaufort Sea and too thin near the North Pole and near the Canadian Archipelago. None of the reanalyses compared assimilate ice thickness, and they often use PIOMAS to calibrate the ice thickness, which as previously mentioned, also does not assimilate ice thickness. The ensemble of reanalyses for this paper can find a statistically significant negative trend over a short period (1993-2007), but the reanalyses are very inconsistent in terms of the thickness and volume, so the patterns of interannual variability in the reanalyses and the resulting ensemble trend estimates are judged as not robust by Chevallier et al. (2017). In terms of the ice thickness distribution, there is large disagreement between

the reanalyses (see figure 3.3), because many do not choose to explicitly treat the thickness when assimilating concentration, which has been found to be important from a number of studies (Dulière and Fichefet, 2007, Massonnet et al., 2014). Finally Chevallier et al. (2017) recommends that substantial work is needed on sea ice data assimilation, some of which we hope to address in this thesis, these include

- Better estimation of observation error for sea ice concentration.
- Adjustment of thickness in post-processing.
- Assimilation or validation of thickness, without calibration through PIOMAS.
- Use of advanced data assimilation techniques.
- Assimilation of sea ice velocity to address ice thickness biases (as in TOPAZ4).

3.6 Summary

In this chapter we have presented a detailed background on the model physics of the CPOM version of the CICE model, we have discussed data assimilation in general and the particular assimilation system (LETKF) that we will be using in this study, and our reasons for doing so. We have also conducted a literature review of previously available reanalyses, the two most notable of which are PIOMAS, which assimilates sea ice concentration and sea surface temperature, and TOPAZ4, which assimilates sea ice concentration, sea ice drift, and a large number of ocean observations. We find that although our design for a reanalysis system has some similarities with these systems, there are also important differences in the model used, assimilation systems, observations assimilated and their associated uncertainties. Given the current state of sea ice reanalysis studies, there is clearly a potential for a long-term reanalysis of the sea ice cover in a state-of-the-art sea ice model which assimilates newly available observations from CS2, uses state-of-the-art assimilation techniques and could provide new insight into the sea ice thickness,and its distribution across the Arctic.

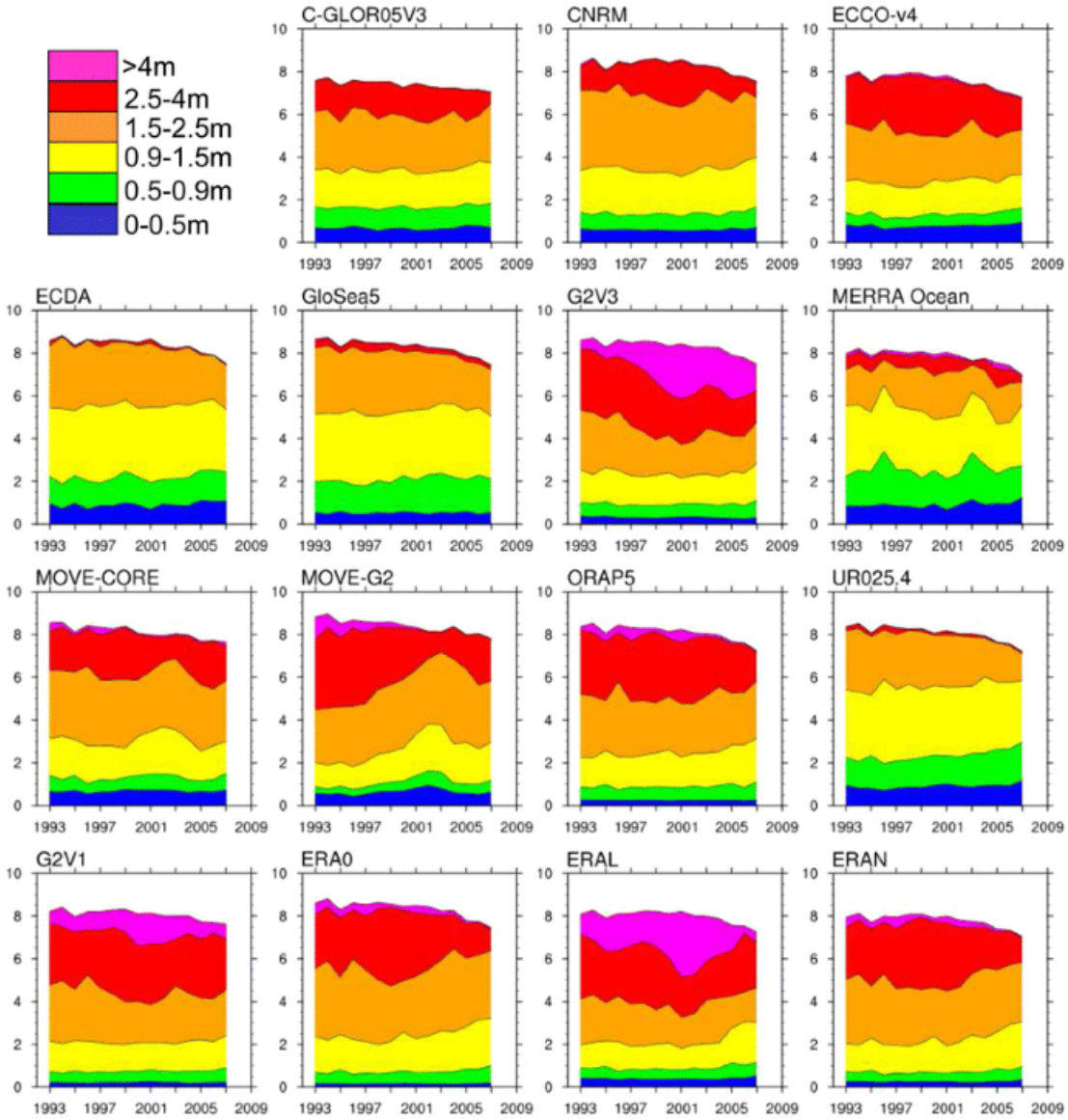

Fig. 3.3 The annually averaged sea ice area (in million km^2) broken down by sea ice in within five different thickness classes (see top left of figure) for 15 ocean-sea ice reanalyses (Chevallier et al., 2017).

Chapter 4

Methodology

4.1 Overview

In this section we discuss the methodology behind the sea ice data assimilation system. This includes discussion about how the ensemble spread was generated in a stand-alone CICE model, and some of the key parameters for a data assimilation system. In section 4.2 we discuss the Parallelised Data Assimilation Framework (PDAF), and its coupling to the CPOM CICE model. In section 4.3 we discuss the post-analysis step processing, which is required to keep the changes made by the data assimilation consistent with the sea ice physics in the model. In section 4.4 we discuss how ensemble spread was generated by perturbing the atmospheric forcing fields. The observation operators for the sea ice observations we have chosen to assimilate are described in section 4.5. The basic experimental setup for all data assimilation and reanalysis studies in this paper is discussed in section 4.6. In section 4.7 a short sea ice data assimilation study is examined to understand how changes in assimilation parameters will affect the system. Finally in section 4.8 we look at how the data assimilation works at a singular grid cell level.

4.2 PDAF and the CICE-PDAF Coupling

The Parallelised Data Assimilation Framework (PDAF) is a software framework designed to enable the use of data assimilation in current state-of-the-art climate models without the need to make significant changes to the model code (Nerger and Hiller, 2013). Known hereinafter as PDAF, it is a software environment designed to provide ensemble based data assimilation algorithms that can be implemented within existing numerical models with only minimal changes to the existing model code. We are using PDAF V1.16, which has

improved observation handling over previous versions of PDAF through the use of a modular implementation. PDAF currently contains the ability to implement many types of ensemble Kalman filters, such as the LETKF, LESTKF and stochastic ensemble Kalman filters. PDAF is designed such that the model source code should be changed as little as possible when coupled. This is achieved by having PDAF collect and operate on the model state vectors, not the physical fields within the model. The ensemble is propagated forward in time by the model and at assimilation time steps the model state vector is collected by PDAF. The assimilation is then computed by PDAF, the analysis state vector is post-processed and then written back into the model fields. This reinitializes the next forecast phase and the number of time steps until the next assimilation is computed. In figure 4.1 the basic concepts of PDAF are shown in a flow chart.

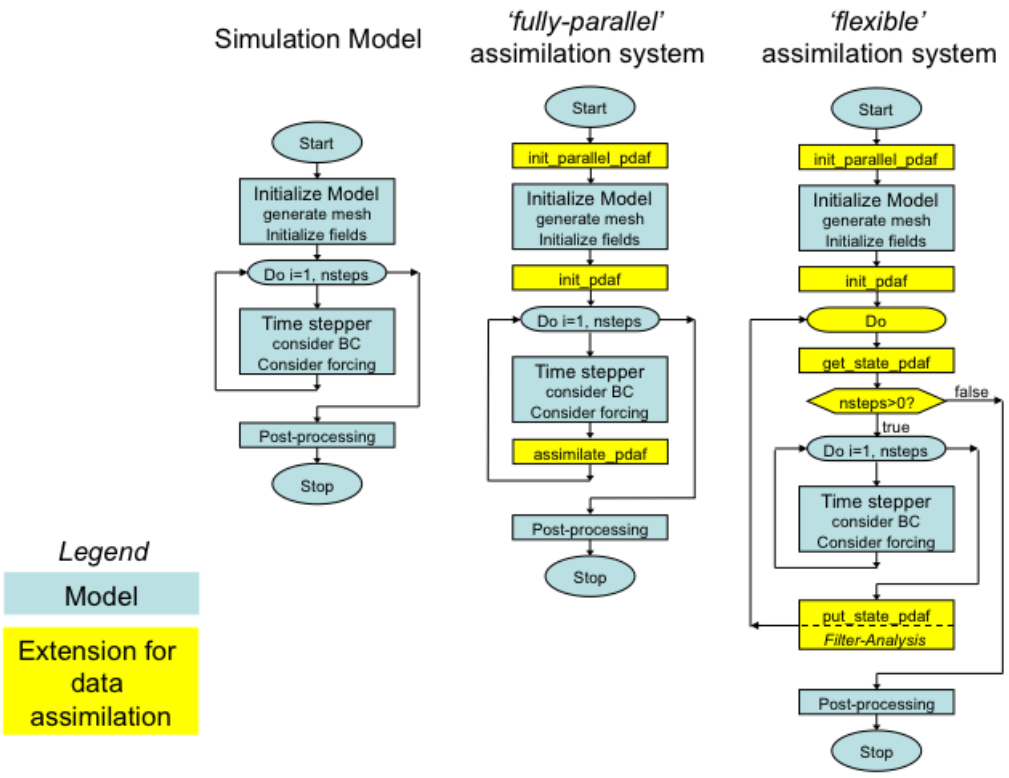

Fig. 4.1 Flow Chart explaining how PDAF assimilation is implemented in models. courtesy, Nerger et al. (2005)

Beyond the implementation of the data assimilation in CICE, PDAF can also schedule ensemble forecasts in parallel. This ability is useful for this study as CICE itself does not have

this ability and to modify the CICE source code for this could have proven difficult. The module-based implementation of assimilation also enables the assimilation to be configured for different types of observations - such as sea ice concentration and sea ice thickness, which is useful for this study.

4.3 Post analysis step processing

In the previous section we explained how PDAF works alongside CICE, collecting the state vector, performing the assimilation and then distributing the state vector back to CICE, with each ensemble member working in parallel. However the assimilation can cause the CICE state variables to become unphysical, due to correlations arising from small sample sizes or bounded variables exceeding their defined limits. The latter problem is particularly significant for CICE because it contains a large number of these variables - such as the ice concentration, thickness, ice drift, enthalpy - most of the variables have bounds, and some of the most important have both upper and lower bounds. Alongside this they are often physically linked to one another - for example the ice concentrations in each category cannot sum to more than 1. As a result of these problems, the analysis state vector must be post-processed before it is redistributed back to CICE, otherwise the model will crash. In this section, we will lay out the necessary checks in post-processing for each state variable carefully, which must be carried out in the correct order to avoid creating new issues.

There are three cases to consider when post-processing the analysis state vector for sea ice in each grid cell

- the case in which sea ice is created in a grid cell where none existed previously
- the case where no sea ice exists in a grid cell where it did exist in the forecast
- the case where the amount of ice in a grid cell has been modified

The first case is the most important because if the analysis creates new ice we must create an enthalpy (temperature) and salinity profile for the ice; the correlations between these variables are not enough for the LETKF to create the correct physical profiles for these properties. We must prescribe the ice enthalpy, snow enthalpy, salinity and surface temperatures in each thickness category and layer. For physical consistency with CICE this is done using the thermodynamic layer model present in CICE, using a linear temperature profile with a predefined salinity profile and melting temperature. This is based on the Bitz and Lipscomb thermodynamic model, with snow enthalpy prescribed as

$$q_s(T) = -\rho_s(-c_O T + L_O), \tag{4.1}$$

where q_s is the enthalpy of the snow (which has one layer in this model), ρ_s is the density of snow, c_O is the specific heat of the ocean, T is the surface temperature and L_O is the latent heat of melting of snow (or fresh ice). We use the surface temperature from the analysis state vector for this calculation. We then need to calculate the sea ice enthalpy in each layer. We first calculate the linear temperature profile using the surface temperature and the temperature of the bottom of the ice (fixed at the freezing temperature of sea water -1.836 C). We then calculate the profile of the melting temperature using the prescribed salinity profile and the ratio between the freezing temperature of sea ice and the brine salinity. The sea ice enthalpy is determined using equation 3.3

After accounting for the creation of completely new ice in a grid cell we now look to assure some variables are within bounds. We check to ensure that if either area or volume of sea ice in a thickness category is zero or negative then sea ice area, volume and snow depth in that thickness category are set to zero. We then check whether the total sea ice concentration in a grid cell (the sum of the ice concentrations in each category) are greater than 1. If this is the case then the ice concentrations in each thickness category in that grid cell are normalised. This is done so that the percentage of ice in each category created through the LETKF by the correlations is preserved. As we have now decreased the total ice concentration we have to be careful about the ice and snow volumes as this normalisation could thicken the ice significantly. To avoid this the ice and snow volumes are also normalised so that we maintain the ice thickness in the Kalman filter analysis.

In the second case, where there is no longer any ice (ice concentration is at zero) within a given thickness category in a grid cell, we must reset a number of state variables to their default (ice-free grid cell) values. This includes concentration, ice and snow volume, snow and ice enthalpy, melt pond variables and surface temperature. This is to avoid any complications which could arise when a future assimilation wants to create ice at the same grid cell - the correlations from the model forecast would be strange and cause strange modifications to some of the state variables.

In the final case, where the amount of ice in a grid cell has only been modified by the assimilation, we only need to conduct some physical checks to ensure again that variables

Table 4.1 Configurations of different CICE-PDAF experiment runs. SIC indicates assimilation of daily sea ice concentration (NASA Bootstrap), SIT indicates assimilation of monthly mean sea ice thickness from CS2, and SID indicates assimilation of monthly mean sea ice thickness distribution from CS2. n_e indicates the number of ensemble members in the run, ff is the forgetting factor ρ, r_l is the localisation radius, α is an amplification factor for the perturbation of the atmospheric forcing fields and t indicates the length of the assimilation run in years.

state variable	**physical meaning**	**checks**
qice(001-007)	sea ice enthalpy	within physical bounds and physically consistent
sice(001-007)	sea ice salinity	within physical bounds and physically consistent
qsno001	snow enthalpy	within physical bounds and physically consistent
aicen	fractional sea ice area	within physical bounds, normalised if total ice concentration above 1
vicen	sea ice volume	within physical bounds, normalised if total ice concentration above 1
vsnon	snow volume	within physical bounds, normalised if total ice concentration above 1
apnd	melt pond area	within physical bounds
hpnd	melt pond depth	within physical bounds
ipnd	melt pond refrozen lid thickness	within physical bounds
Tsfcn	snow/ice surface temperature	must be $> -70°$C

are within bounds. This includes the checks above for ice concentration and snow and ice volumes below or above bounds but some additional checks are required for enthalpy, salinity and surface temperature. Firstly for snow enthalpy, given equation 4.1, the minimum possible snow enthalpy in a grid cell must be smaller than

$$q_s = -\rho_s L_O. \tag{4.2}$$

We also check that it does not get unreasonably low, we use equation 4.1 and use $T = -100°C$. Similarly we use this same check for surface temperature, this minimum temperature is arbitrary, but still 30 degrees lower than the record minimum temperature recorded in the Arctic ($-69.6°C$). Finally, we check that the sea ice enthalpy remains below zero, and that salinities are greater than zero. Additionally it was also found that situations can occur on the ice edge where the LETKF reduces the ice concentration to a very small amount (lower than 10^{-5}) but ice volume is not reduced in the same way, which leads to ice spikes which can cause the CICE model to crash. In these situations ice in these grid cells is removed. The exact variables which may be modified in this post-processing are specified in 4.1 below. The CICE model itself also contains its own routines that check for consistency and correct physical properties within the state vector, however we found the checks detailed in this section were still necessary to avoid model crashes within CICE.

4.4 Generating Ensemble Spread in CICE

CICE is a forced dissipative model, meaning that if the model is run twice under the same atmospheric and oceanic forcing conditions it would produce near-identical results. This being the case, we need a method to induce ensemble spread, as it is a key ingredient for a well functioning ensemble Kalman filter. To achieve this, we use a multivariate empirical orthogonal function (EOF) perturbation method on the atmospheric forcing fields used to drive the model. This is similar to the EOF-based perturbation method first presented in Brusdal et al. (2003). We start with the 6-hourly fields of humidity, 2 m temperature, shortwave and longwave radiation and the u and v components of the wind from the NCEP-2 reanalysis (Kanamitsu et al., 2002). For each month we pick out the 00z time data at each date and convert them into one continuous time series spanning 1979 to the present. We remove the data from grid cells that are on land, and have a 2d matrix, with vectors representing the respective surface fields and the columns representing each field of data (of n, where n is 31 days $\times$ 40 years). For example, for January we now have

$$\mathbf{X}_{\mathbf{January}} = \begin{pmatrix} \mathbf{q}_1 & \mathbf{q}_2 & \cdots & \mathbf{q}_n \\ \mathbf{T}_1 & \mathbf{T}_2 & \cdots & \mathbf{T}_n \\ \mathbf{SW}_1 & \mathbf{SW}_2 & \cdots & \mathbf{SW}_n \\ \mathbf{LW}_1 & \mathbf{LW}_2 & \cdots & \mathbf{LW}_n \\ \mathbf{u}_1 & \mathbf{u}_2 & \cdots & \mathbf{u}_n \\ \mathbf{v}_1 & \mathbf{v}_2 & \cdots & \mathbf{v}_n \end{pmatrix} \tag{4.3}$$

We then detrend the data point by doing a linear least squares fit at each spatial point which we then subtract from the original data. The standard deviation of each of these fields is then found (i.e climatological standard deviation in $\mathbf{X}_{\mathbf{January}}$), and then we divide the data by this standard deviation. This is done to normalize each field because otherwise they will have large differences in their variances, which can cause problems in the singular value decomposition (SVD) analysis. We now have six 40-year-long fields for each month detrended at each spatial point, divided by the standard deviation of the full spatial and temporal field (and divided by $\sqrt{n-1}$). This gives a matrix of the form:

$$\mathbf{Z_{January}} = \frac{1}{\sqrt{n-1}} \begin{pmatrix} \tilde{\mathbf{q}}_1 & \tilde{\mathbf{q}}_2 & \cdots & \tilde{\mathbf{q}}_n \\ \tilde{\mathbf{T}}_1 & \tilde{\mathbf{T}}_2 & \cdots & \tilde{\mathbf{T}}_n \\ \mathbf{S\tilde{W}}_1 & \mathbf{S\tilde{W}}_2 & \cdots & \mathbf{S\tilde{W}}_n \\ \mathbf{L\tilde{W}}_1 & \mathbf{L\tilde{W}}_2 & \cdots & \mathbf{L\tilde{W}}_n \\ \tilde{\mathbf{u}}_1 & \tilde{\mathbf{u}}_2 & \cdots & \tilde{\mathbf{u}}_n \\ \tilde{\mathbf{v}}_1 & \tilde{\mathbf{v}}_2 & \cdots & \tilde{\mathbf{v}}_n \end{pmatrix},$$

where the 'tilde' indicates the detrending and normalisation described above. We then perform an SVD on this matrix X with weights of $\sqrt{\cos(2\phi)}$ to account for the fact that this is a flattened grid on a curved 3D surface. We find the following for each forcing field:

$$\mathbf{Z}_{January} = \mathbf{UDV}^T, \tag{4.4}$$

where **U** is the matrix of left singular vectors (these are the EOFs), **D** is the (diagonal) matrix of singular values (the amplitudes of the EOFs), and **V** is the matrix of right singular vectors. For each month we pick the number of EOF modes that represent the majority (95%) of the variability in each of the forcing fields. In figure 4.2, as an example, we show the percentage of variance explained by each EOF mode for 2 m air temperature from the NCEP-2 reanalysis, where this example shows the variances when doing the EOF analysis only on the air temperature field, not a full multivariate analysis. This shows the standard pattern we see when looking at EOF modes, with the most variance explained by the initial mode and then the variances tail-off thereafter. When looking at an individual field in an EOF analysis we generally see 95% of the variance explained by the first few modes. However because this is a multivariate EOF analysis the number of EOF modes required to explain 95% of the variance in a given field are much higher. The number of EOF modes needed for each month in our analysis varies slightly but is within 160 and 210, being lowest in winter and highest in summer.

We then add perturbations to the original forcing fields for a given month for each ensemble member using

$$\sum_{i=1}^{j} \alpha \sigma N_i U_i D_{ii}, \tag{4.5}$$

with i being the EOF mode and j the total number of EOFs chosen to represent the variance in

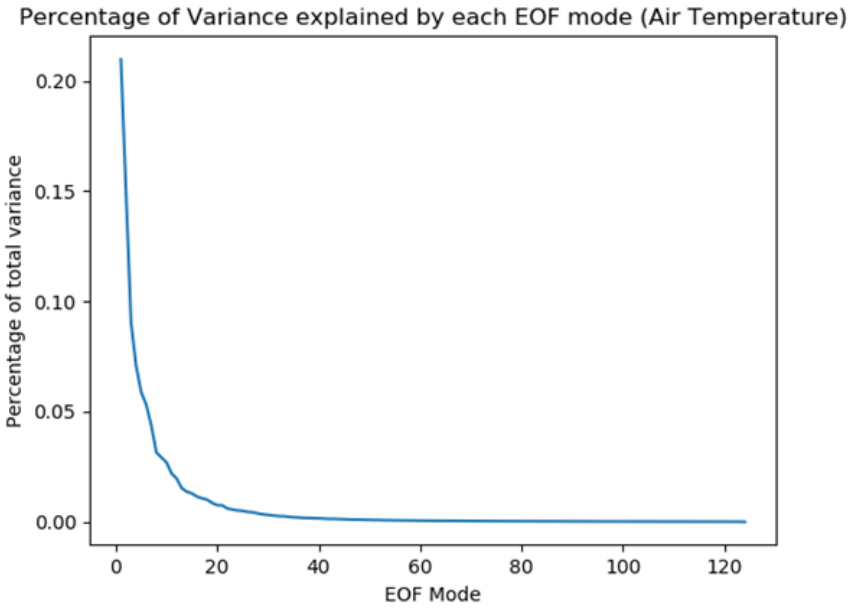

Fig. 4.2 An example showing the percentage of variance in 2m Air temperature explained by each EOF mode after doing an EOF analysis on the NCEP-2 2m air temperature.

the field, N_i random numbers chosen from a normal distribution with mean = 0 and variance of 1, σ are the climatological standard deviations of that forcing field in a given month, and α is a multiplicative factor that we can use to amplify the perturbations on the atmospheric forcing to induce additional ensemble spread.

As part of this study we have looked at how much spread is generated using this method, and whether we have to use an 'amplification factor' a to produce additional ensemble spread. This study, its results and effects on the reanalysis results are discussed in section 4.7. Note that for each month in a particular year, the same random numbers are chosen for each field for perturbing each point for the field to maintain consistency between each field as they were in the original forcing. If this was not done then the correlations between the atmospheric forcing fields would be broken, which would lead to inconsistencies between highly correlated fields, for example, the 2 m temperature and shortwave radiation.

4.5 Observation operators for sea ice observations

For the data assimilation to work, observation operators, **H** in section 3.4 are needed to transform the model into observation space, and using the correct model variables such that we are comparing like-for-like in terms of model and observation. For the sea ice observations that we assimilate, these are relatively simple operators. Before any data assimilation is done all the observations have been regridded and interpolated onto the same NEMO 1 degree (a roughly 40km by 40km grid size) tripolar grid as the model, which makes the observation operators much simpler. For the sea ice concentration, the model equivalent of the observations are found just by summing the ice concentrations a_n in each category n in each grid cell. For the sea ice thickness, we assimilate the observations of grid cell mean ice thickness, which is just the sum of v_n volume of ice per m^2 of grid cell area, in each category n. For the sea ice thickness distribution, we have observations of a_n^*, ice concentration in category n (where the open water fraction a_{i0} is unknown) and observations h_n, ice thickness in category n. These are related to the state variables a_n and v_n by

$$a_n = a_n^* a \tag{4.6}$$

$$h_n = \frac{v_n}{a_n}, \tag{4.7}$$

where a is the total fraction of sea ice in a grid cell. As described in section 2.4, for the assimilation of thickness distribution, we only assimilate the thinnest four categories of ice. Sea ice concentration is assimilated daily, and sea ice thickness and thickness distribution observations are assimilated monthly, using monthly means and assimilated in the middle of the month, with the model equivalent of the observation constructed using the daily mean on the day of assimilation. This assimilation time step is the same for all assimilation studies and reanalyses described in chapters 4, 5, 6 and 7. Assimilating the CS2 data as monthly means does mean that the size of some of the changes in the sea ice model can be significant, with large increments in grid cells where the model has a high degree of ensemble spread and its ensemble mean differs significantly from the observations. Even though there is no assimilation of CPOM CS2 data in summer months (May-September), we find that these updates in preceding months are still extremely useful to the model and can cause significant changes in the sea ice state. For example, at the end of September, when assimilation of CS2 data has not taken place for many months, the thickness and volume will differ significantly from the case when only ice concentration is assimilated. The observation errors used are consistent across all the studies, and are described in sections 2.2, 2.3 and 2.4.

4.6 Model Assimilation Setup

Before any assimilation takes place in CICE-PDAF, we first run CICE in stand-alone mode from 1979 until 2019, using the NCEP-2 atmospheric forcing data and the ocean reanalysis from Ferry et al. (2011) to drive the model. To begin any reanalysis or data assimilation studies we give the model time to spin-up and use restart files from the stand-alone run to begin all 100 ensemble members. With our generated set of perturbed atmospheric forcing fields, we then run CICE-PDAF in coupled mode with no assimilation taking place for one year. This allows a sufficient amount of time for the perturbed forcing fields to generate enough ensemble spread in the state vector such that the data assimilation will be effective and ensemble collapse is avoided. We then restart CICE-PDAF again from the end of this period so that each ensemble member will be initialised differently because of the perturbed forcing. Without taking this step the data assimilation will either take much longer to have an effect on the model (maybe more than the time period of the experiment) or the ensemble spread in the model may never grow sufficiently for any effects from the assimilation to occur. The coupled run without data assimilation begins in 2011 for the experiments described in this chapter. Beginning in 2012 we then perform a significant number of different sea ice data assimilation experiments in order to optimise and fine-tune some of the LETKF assimilation parameters and to assess the performance of the assimilation. These experiments and their parameters are detailed in table 4.2.

Although total sea ice concentration and mean sea ice thickness are not variables in the CICE state vector, their assimilation has a large effect on the CICE state vector through the correlations between each variable. For example, when assimilating sea ice concentration, the ice concentrations in individual categories will be affected by their correlation with the total sea ice concentration calculated by the observation operator. This means that even when not assimilating sea ice thickness, the assimilation can still have an effect on the model estimates of sea ice thickness (and all other variables in the CICE state vector). This is covered in detail in section 4.7.

4.7 Assimilation Parameters

There are four key assimilation parameters that we diagnose and analyse in order to increase the effectiveness of the LETKF before we conduct the reanalysis; these are the amplification factor, ensemble size, forgetting factor and the localisation radius. PDAF provides control of the ensemble size, forgetting factor and localisation radius within its assimilation routines,

Table 4.2 Configurations of different CICE-PDAF experiment runs. SIC indicates assimilation of daily sea ice concentration (NASA Bootstrap), SIT indicates assimilation of monthly mean sea ice thickness from CS2, and SID indicates assimilation of monthly mean sea ice thickness distribution from CS2. n_e indicates the number of ensemble members in the run, ff is the forgetting factor ρ, r_l is the localisation radius, α is an amplification factor for the perturbation of the atmospheric forcing fields and t indicates the length of the assimilation run in years.

run name	SIC	SIT	SID	n_e	ff (ρ)	r_l	α	t
control	N	N	N	100	N/A	N/A	1	4
assim_conc	Y	N	N	100	0.995	100 km	1.5	4
assim_conc_hi	Y	Y	N	100	0.995	100 km	1.5	4
assim_conc_hi_4hd	Y	N	Y	100	0.995	100 km	1.5	4
assim_conc_hi_f100	Y	Y	N	100	1.00	100 km	1.5	1
assim_conc_hi_f99	Y	Y	N	100	0.99	100 km	1.5	1
assim_conc_hi_f98	Y	Y	N	100	0.98	100 km	1.5	1
assim_conc_hi_loc200	Y	Y	N	100	0.995	200 km	1.5	1
assim_conc_hi_loc400	Y	Y	N	100	0.995	200 km	1.5	1
assim_conc_hi_loc50	Y	Y	N	100	0.995	50 km	1.5	1
assim_conc_hi_amp1	Y	Y	N	100	0.995	100 km	1	1
assim_conc_hi_amp125	Y	Y	N	100	0.995	100 km	1.25	1
assim_conc_hi_e10	Y	Y	N	10	0.995	100 km	1.5	1
assim_conc_hi_e10	Y	Y	N	20	0.995	100 km	1.5	1

and the amplification factor is a parameter we have generated ourself through our method of creating an ensemble by perturbing the atmospheric forcing fields. In this section we will show the results and analysis of a study of each of these parameters in order to fine-tune them for the final reanalysis.

4.7.1 The Amplification factor

As discussed in section 4.4, we generate ensemble spread by perturbing the atmospheric forcing fields that are used for each ensemble member by picking random numbers from a normal distribution. This method alone, however, may not be sufficient to create enough ensemble spread for the assimilation to work properly. For this reason, we investigate using an amplification factor in equation 4.5. In figure 4.3 we show the ensemble spread in sea ice volume for four different CICE-PDAF runs; one control and three assimilating concentration and thickness using amplification factors of 1, 1.5 and 2. Interestingly with an amplification factor of 2 we were able to generate a larger ensemble spread when assimilation took place than in the control with no assimilation. This mainly occurred during the melting season but there were a few days at the end of March and November when this also occurred. In figure 4.3 you can also see where the assimilation of monthly mean thickness takes place in many months due to the large increments in the ensemble spread. This is especially clear in January, and also in October, after the summer gap in CS2 thickness observations. The effects of the amplification factor are much more pronounced in summer than winter. The peaks in the sea ice volume ensemble spread in figure 4.3 appear to occur when the peak rate of melting happens, or just prior. We found that using an amplification factor increased ensemble spread significantly, especially during the peak melting period in Summer. However if the amplification factor was increased too much this became detrimental to the sea ice state estimates in the model. Using higher amplification factors than 1.5 often caused so-called ice spikes, grid cells with small concentrations but very large thicknesses (over 10 m) to appear in grid cells at the sea ice edge. We believe the reason for this is likely to be that using a high amplification factor could cause extremes in some of the forcing fields to appear in many places, and if they occurred at or close to the ice edge this would lead to instability in some of the physics in the sea ice model. For this reason, although higher amplification factors leads to a significant increase of spread, we use a factor or 1.5, which does not have the same problems as above but still increases ensemble spread significantly.

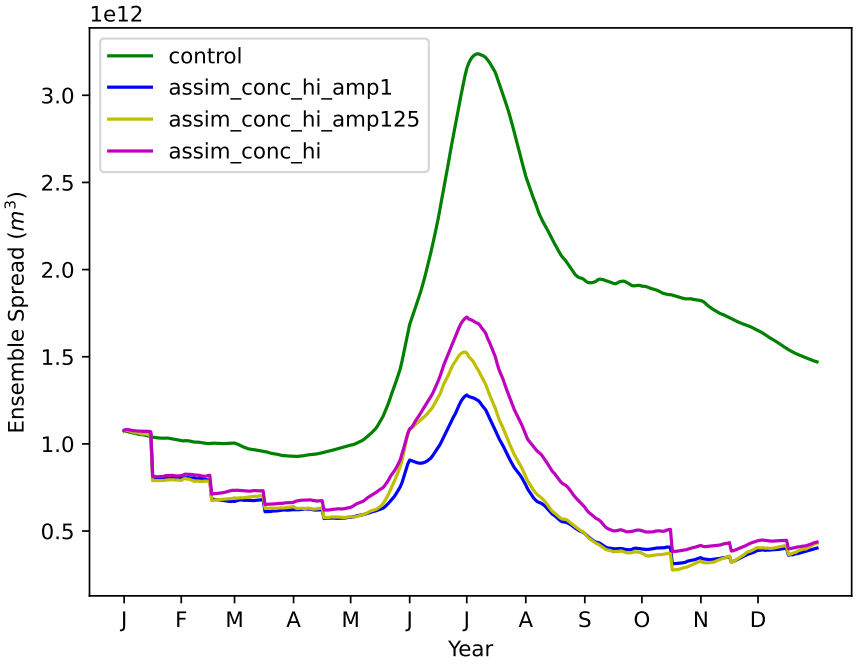

Fig. 4.3 Sea ice volume ensemble spread (one standard deviation) in a control run and three CICE-PDAF runs using atmospheric forcing fields which have been perturbed with different amplification factors (1, 1.25 and 1.5).

4.7.2 Ensemble Size

A sufficient ensemble size is important for mitigating the problem of undersampling in ensemble Kalman filters. However there is the additional problem of computing power needed to run the model in a reasonable time frame. In this project we had use of the Archer-2 supercomputer and have run a maximum ensemble size of 100. However it is still useful to see how exactly a change in ensemble size will effect CICE-PDAF. In this study we look at three different 1-year assimilations runs in 2012 with 10, 20 and 100 ensemble members respectively, all use a forgetting factor of 1.00 and a localisation radius of 100 km. All runs assimilate concentration and CPOM CS2 mean thickness. In figure 4.4 we show the sea ice volume ensemble spread in these runs alongside a control run. As expected we see an increase in the ensemble spread as ensemble size is increased during the majority of the 1-year run, although the effect seems to be reversed during June and in late December. As with the amplification factor, there again may be some interesting effects occurring within the model during the peak melting season. It may be showing that the model is very sensitive to the rapid decrease in sea ice that takes place during this time. There is more uncertainty around why the experiment with 100 ensemble members has the least spread at the end of

the run. It is possible that this is just because of the random nature of the perturbations selected. With 100 ensemble members the model takes just over 23 hours to obtain four years of results. This being the case we chose to limit these experiments at 100 ensemble members as larger ensembles would lead to further increases in running time and additional need for supercomputer time and storage. We believe that 100 ensemble members is sufficient for gaining a representative sample of the model for data assimilation purposes.

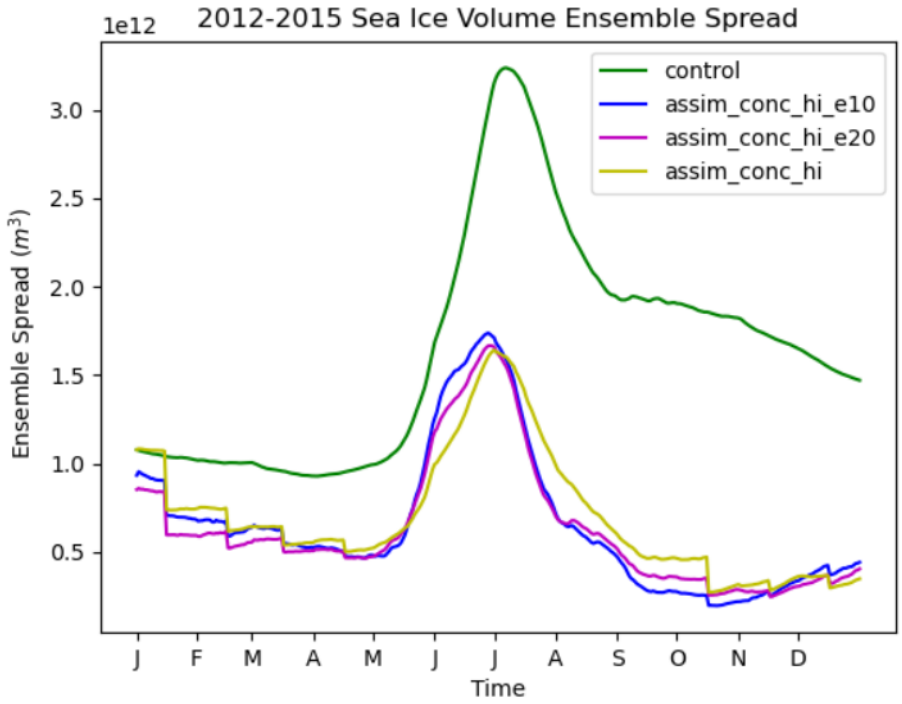

Fig. 4.4 Sea ice volume ensemble spread (one standard deviation) in a control run and three CICE-PDAF runs using different ensemble sizes (10, 20 and 100).

4.7.3 Forgetting Factor

After choosing an amplification factor and 100 member ensembles we now seek to choose an appropriate forgetting factor, if necessary for our reanalyses. The forgetting factor, like ensemble size, will work alongside the atmospheric forcing perturbations to increase ensemble spread and reduce the likelihood of significant undersampling and ensemble collapse. In figure 4.5 we again show sea ice volume ensemble spread this time for a control and three

CICE-PDAF experiments with different choices of forgetting factor. As expected an increase in forgetting factor leads to an increase in ensemble spread. The increase in sea ice volume spread roughly appears to follow a linear relationship with the decrease in forgetting factor in the first three quarters of the year. After September using a forgetting factor of 0.98 had an even more significant effect on the ensemble spread.

In CICE-PDAF we have found that the model is extremely sensitive to forgetting factors below 1. This is particularly true when assimilating CS2 products. We believe this is because the analysis increments when assimilating CS2 observations can be large. This problem often causes the model to crash, and although fixable in post-processing becomes worse as the forgetting factor is lowered. Using forgetting factors below 0.99 led to a large amount of instability in the thermodynamic model in CICE and cause crashes after only a few years of results. For these reasons we have chosen to use a forgetting factor of 0.995 (an inflation factor of 1.003) in our reanalysis runs, this should help maintain ensemble spread while avoiding problems caused by large increments in the model state vector.

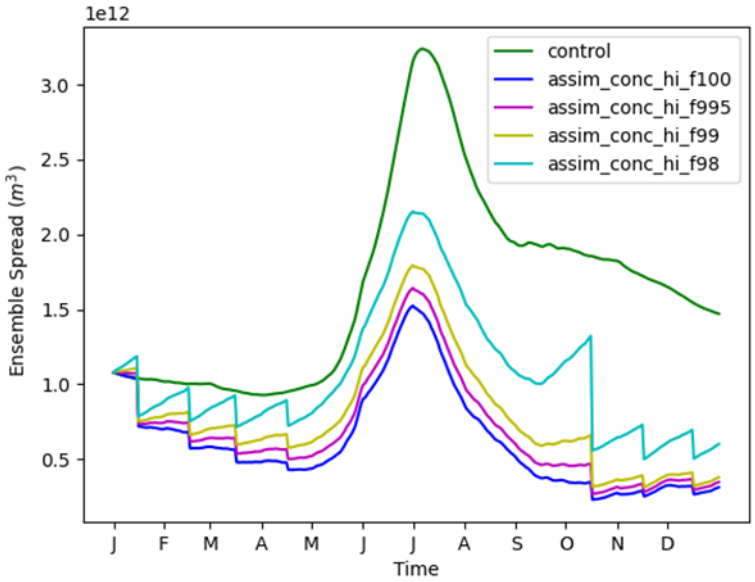

Fig. 4.5 Sea ice volume ensemble spread (one standard deviation) in a control run and four CICE-PDAF runs using forgetting factors of 1.00, 0.995, 0.99 and 0.98.

4.7.4 Localisation Radius

Finally, we look at how changes in the localisation radius can affect the sea ice state in CICE-PDAF. Our choice of model grid gives us grid cell widths of about 40 kilometres. The choice of localisation radius is essentially guided by how changes in one model grid cell could affect or be affected by those around it within a reasonable time frame as determined by the real-world or model physics. Grid cells located at the sea ice edge are most likely to be affected by these changes in localisation. Depending on the correlations, changes in grid cells at the sea ice edge could potentially cause an over or underestimate of the sea ice at these locations. In figure 4.6 we show Pan-Arctic maps of sea ice thickness in March and October for a control and three CICE-PDAF assimilation experiments with different localisation parameters. The changes in the results when using differing localisations only show very slight differences with each other, though there are noticeable changes in the region of thickest ice. For our reanalysis we have chosen a localisation radius of 100 km, using a Gaspari and Cohn function. This means that the correlation effects of assimilation in a grid cell will smoothly reduce until reaching zero at 100 km away.

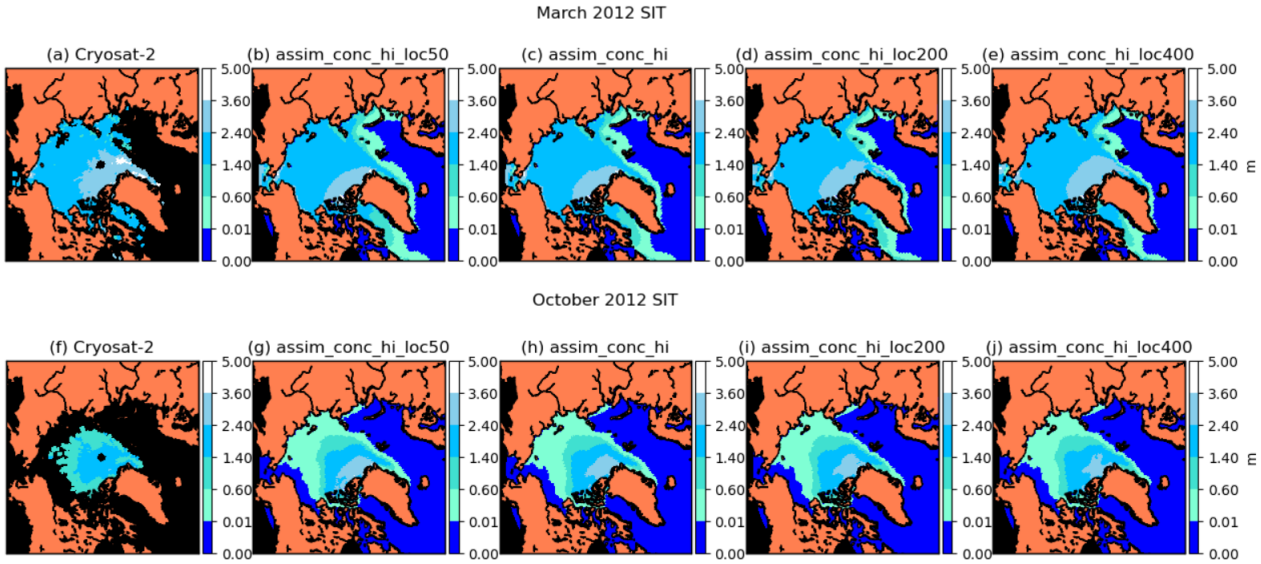

Fig. 4.6 Maps of ensemble mean sea ice thickness in March (top row) and October (bottom row). Columns show Cryosat-2 and three CICE-PDAF runs using localisations of 50 km, 100 km, 200 km and 400 km.

4.8 Grid Cell Level Analysis

Before presenting the reanalysis, we wish to study how the assimilation will effect changes in the model, particularly for the assimilation of the thickness distribution. To do this we will study the correlations between some of the key CICE state variables: sea ice concentration and volumes in each category in a few grid cells in some key areas of the Arctic. We look at the evolution of these variables through a one year period. We pick four grid cells for study, located in the Barents Sea, central Arctic, Lincoln Sea and Beaufort Sea. We pick these locations because they each have different and interesting characteristics for study, the correlations and evolution of the sea ice at these locations will be significantly different because of how the sea ice cover evolves differently in these regions. The Barents Sea is ice free in summer and occupied by thin first year ice in winter. The Central Arctic is ice covered virtually year-round, although the rapid decrease in sea ice in recent years means that it is now ice free in some parts in summer. The Lincoln Sea is covered in thick MYI year-round, with some ice exceeding 10 m thickness in winter. The Beaufort Sea is frozen over for most of the year, except in August and September, with significant loss in MYI since 2000 due to climate change. Between 2005 and 2008 MYI loss in the Beaufort Sea was responsible for 32% of all MYI loss in the Arctic according to ICESat (Kwok and Cunningham, 2010). As an area of rapid change it is interesting for this study. We highlight these four grid cells on a map of the Arctic in figure 4.7.

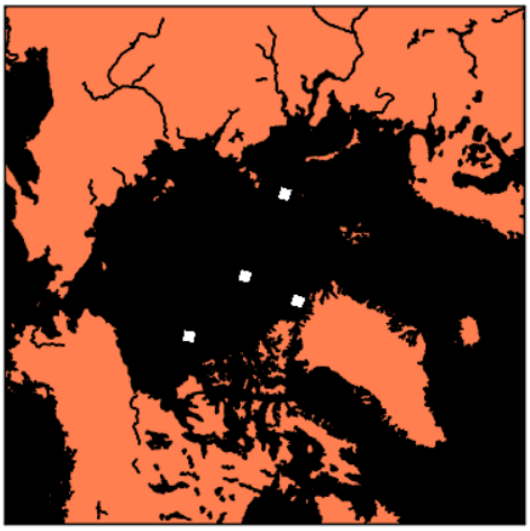

Fig. 4.7 Locations of the four grid cells chosen for this study shown in white. These four grid cells are in the Central Arctic, Beaufort Sea, Barents Sea and the Lincoln Sea.

4.8.1 Correlations

In figure 4.8 we show the correlations between the ice concentration in each category, ice volume in each category, total ice concentration, total ice thickness and total ice volume in each of these four grid cells in January 2012. In the Central Arctic and Beaufort Sea ice thickness and volume are negatively correlated with ice in the thinnest two categories, and positively correlated with the three thicker categories. In winter these grid cells will be fully ice covered (so have an ice concentration very close to 1), which means that ensemble members with ice in thinner categories will have a smaller ice volume. As these two regions have similar ice thickness and volume levels in winter, this is expected. In the marginal ice of the Barents Sea, the ice is thin and will mostly be in category one. This means that any small increase in category two or thicker ice categories will increase ice thickness and volume. Therefore we see negative correlations only between category one and thickness/volume, with positive correlations between these and the thicker four categories. Finally in the Lincoln Sea (which will also have a concentration very close to 1) we see positive correlations between categories four and five and thickness and volume. As this is the region containing the thickest Arctic ice the two thicker ice categories are the determining factor for these correlations. There is a small positive correlation between category one ice and volume, however we believe this to be anomalous because the ice concentration in category one in this grid cell will likely be extremely small (around 10^{-3}) in all ensemble members. In general the correlations (positive or negative) appear to be stronger in grid cells with more ice. In the Lincoln Sea the correlations are generally strongly positive or negative. The correlations are slightly weaker in the Central Arctic and Beaufort Sea and in the marginal ice zone of the Barents Sea the correlations are weaker still.

In figure 4.9 we now show the correlations between the same variables as before but this time in July 2012. For the Central Arctic and Beaufort Sea, the correlations are similar to those in winter, and again similar to each other. In summer the Central Arctic Ocean and Beaufort Sea are covered in thinner ice, with some parts ice free in September. You would also expect some of the thick MYI to survive through the melt season. The negative correlations between volume and the thinner categories have increased. As in winter, these areas have an ice concentration close to 1 so a movement of ice towards the thicker categories leads to an increase in ice thickness and volume. In the Beaufort Sea, the correlations have a very similar pattern, but are slightly weaker. There is a positive instead of a negative correlation between

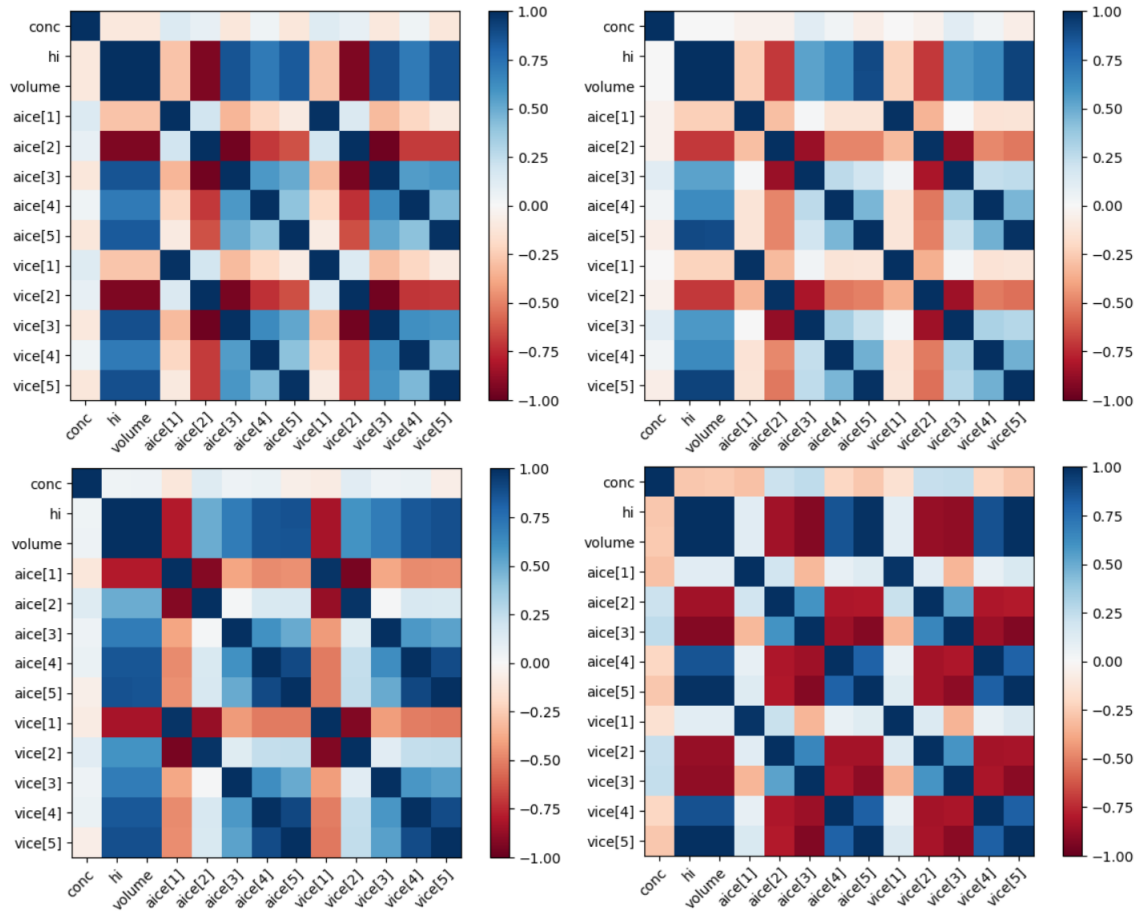

Fig. 4.8 Correlation matrices of CICE state variables: fraction of ice in category n (aice[n]), volume of ice per unit grid cell in category n (vice[n]), as well as the total sea ice concentration (conc), grid cell mean ice thickness (hi) and total grid cell sea ice volume (volume) in January for a grid cell in the Central Arctic Ocean (top left), Beaufort Sea (top right), Barents Sea (bottom left) and Lincoln Sea (bottom left) in January 2012.

ice volume and category 3 in the Beaufort Sea. In the Barents Sea the correlations are also significantly different than those in winter. The correlations in the Beaufort are positive except for category 1 ice. This is because this region is now most likely covered with ice only in the thinnest category, meaning that any small increase of ice in the thicker categories will lead to a higher thickness and volume. As the Barents Sea probably has the highest variability in concentration between ensemble members, the correlations for concentration are the strongest from all the correlations we study. Finally, in the Lincoln Sea, correlations are again similar to those in winter, with positive correlations between volume and the two thickest categories of sea ice. This region remains covered in thick ice throughout the melt season so it is not too surprising that the correlation pattern remains almost identical to those in winter. In general the correlations between concentration and other variables are stronger

in summer due to the reduction in ice coverage, conversely the correlations between volume, thickness and the ice in each category are weaker. Overall the correlations in these grid cells we have studied are plausible and so we would expect the assimilation of concentration, thickness and thickness distribution to be effective.

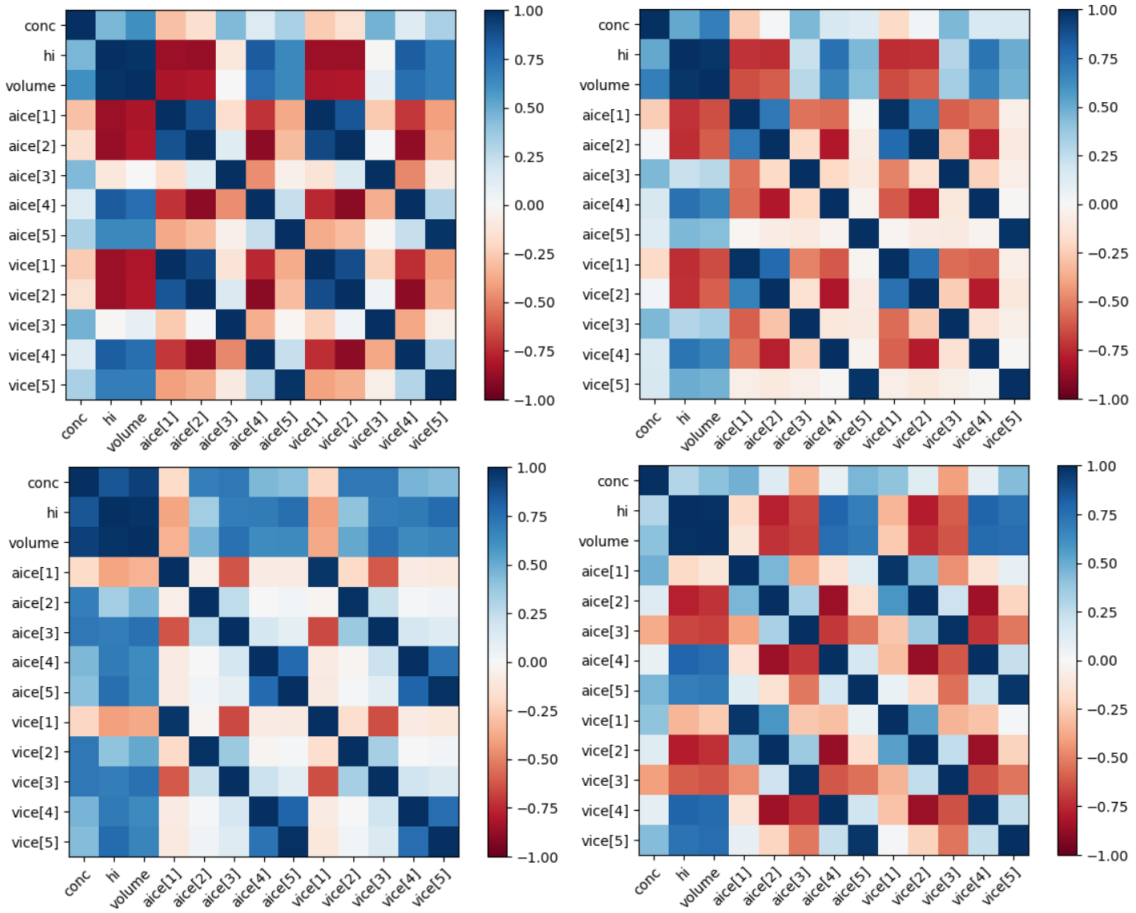

Fig. 4.9 As 4.8, but for July 2012.

4.8.2 Sea Ice Concentration

Now we have studied correlations between some of the most important CICE state variables at a few individual grid cells, we want to see how the assimilation affects them over a reasonable time period. In these short reanalysis studies we study how the assimilation changes the sea ice state and in particular the thickness distribution, in the same grid cells we selected

above. In figure 4.10 we show the evolution of sea ice concentration in our chosen grid cells through one year of the control run, three assimilation runs alongside the assimilated Bootstrap observations.

In the Central Arctic grid cell concentration is above 0.9 year round in Bootstrap, whereas the control has significant ice loss in late August and September. In the Beaufort Sea the control is similar to the observations, with the only difference being that the melt occurs earlier in the control. In this grid cell the assimilation runs tend to stay very close to the observations, though the observations show strong daily variability during the melt season, which is not reproduced in the control run. In the Barents Sea the observations are again similar to the control run but with much more rapid changes in the sea ice cover. In the bootstrap observations there are also rapid changes in observed concentration of up to 0.5 for a few days in early November. In the Lincoln Sea the sea ice concentrations also remain higher in Bootstrap than the control though the effect is not as severe as for the grid cell in the Central Arctic. The assimilation runs again stay close to the observations but there is a compromise between model and observation in the assimilation in August and September due to the differences between the control and Bootstrap.

Relative to the observations the control model performed better in areas of thinner ice in the Beaufort and Barents Seas than in the Central Arctic and Lincoln Sea where the ice melt was exaggerated by the control. In general, in terms of these concentration diagnostics we see that CICE-PDAF with the assimilation of concentration is significantly closer to the observations than the control run. There appears to be no additional benefit to sea ice concentration estimates when assimilating CS2 sea ice thickness or thickness distribution. This is not surprising because we assimilate sea ice concentration daily whereas we only have monthly mean data from CS2, and only for 7 months of the year. We will see in the next sections that sea ice thickness observations do impact other diagnostics

4.8.3 Sea Ice Thickness

After studying the evolution of the concentration we now want to look at the evolution of the sea ice thickness. In figure 4.11 we show the sea ice thickness in the same grid cells over a period of one year for CICE-PDAF experiments and the monthly mean CS2 observations (shown as points on the days they were assimilated). In the central Arctic the assimilation of the thickness distribution actually had a negative effect in comparison to the observations

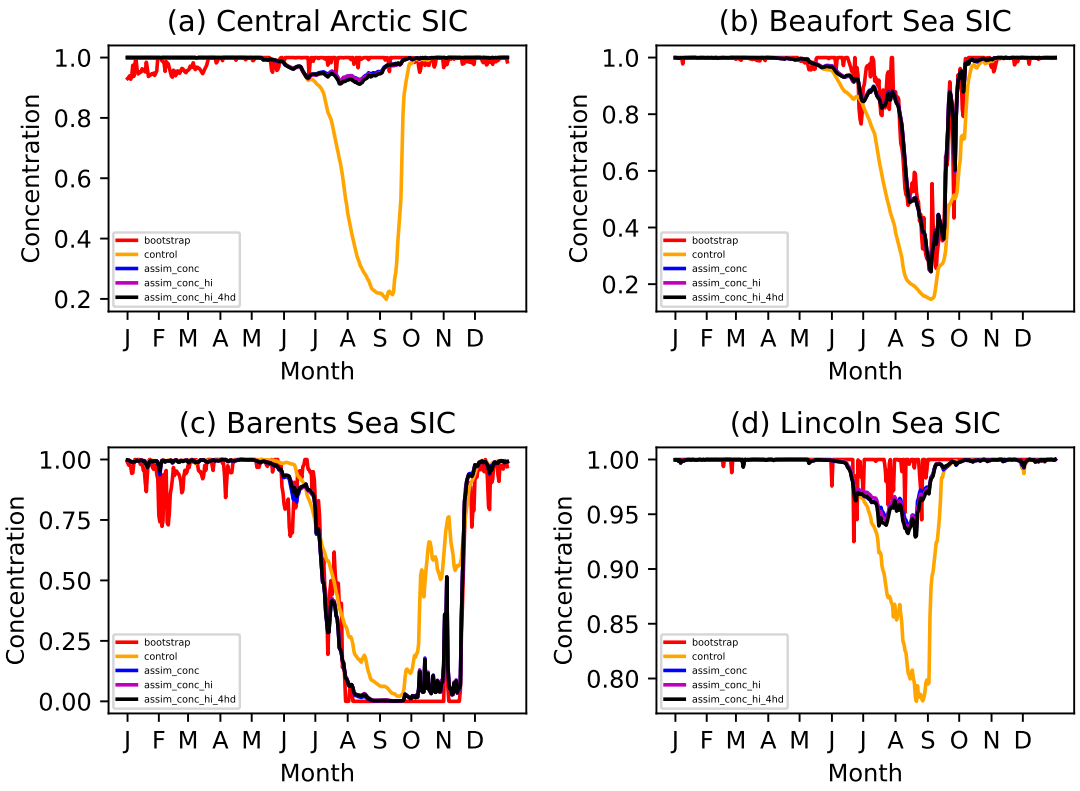

Fig. 4.10 Sea ice concentration (ensemble mean) from Bootstrap observations and CICE-PDAF in 2012 for one grid cell in each of the Central Arctic, Beaufort Sea, Barents Sea and the Lincoln Sea.

between January and April. However the thickness was much better in October and close to the observations in November and December as well. The negative impact of assimilating concentration is clear in November and December, as the melt season begins the assim_conc experiment maintains a much higher thickness than the control through the rest of the year. The sea ice in the control experiment thins dramatically in comparison to the assimilation experiments. In the Beaufort Sea again we see that the assimilation of thickness distribution favours a decrease in thickness that appears to be due to a reduction in category 5 sea ice. The control run and the observations are similar here in the early part of the year so thickness assimilation cannot provide any benefits. Again though, in the latter half of the year, when CS2 observations become available again, the assimilation of thickness distribution appears to work best at points, and is this time quite similar to the assim_conc_hi runs. The thickness in assim_conc appears to be slightly too thin during the last few months.

In the Barents Sea the story is quite different. Given that all of the assimilation exper-

iments are further away from CS2 than the control it seems that the assimilation of the concentration here, occurring daily, has a negative impact. There are only monthly mean observations at this grid cell for three months (instead of the usual seven) here. This is because the sea ice here is very thin year-round, making it more difficult to process and extract thickness observations from the CS2 altimetry data.

Finally, in the Lincoln Sea, we see the fullest benefit of assimilation of the CS2 data. The assimilation of mean thickness and thickness distribution is clearly significantly better than the control and assim_conc, particularly during January-April. The assim_conc experiment is particularly poor in this region and the pattern is similar to the one we see in the Central Arctic whereby the assimilation of concentration maintains substantially thicker sea ice through the melting period. This then has a negative impact on the thickness estimates of assim_conc during October-December.

There are common patterns that are occurring in all four grid cells. In grid cells with thicker ice, assim_conc tends to overestimate the sea ice thickness and undergoes less thinning of the sea ice than the other experiments. On the other hand the control run tends to undergo more melting during the melt season. The assim_conc_hi experiment tended to be closer to the CS2 observations between January and April than assim_conc_hi_4hd, but they were similar in October-December with assim_conc_hi_4hd maybe performing slightly better. The assim_conc_hi_4hd experiment generally had the thinnest ice out of the assimilation experiments and seems to have a good ice thickness distribution estimate before the summer period where no assimilation takes place such that it forecasts the CS2 observations between October-November well.

4.8.4 Category 5 thickness and volume

Finally, we want to look at how the thickness of ice in category 5 evolves throughout the experiment, as this is the thickness category which is not assimilated in the thickness distribution assimilation. In figure 4.12 we show mean ice thickness in category 5 over the whole grid cell (normalised with ice concentration in category 5) again in the same four grid cells. It is clear here that the model is significantly overestimating the thickness of the ice in category 5. The control experiment has much higher ice thickness in this category than the observations. The assim_conc experiment generally has similar thicknesses to the control experiment until the melting season when it is slightly thicker (or in the case of the Central Arctic nearly a

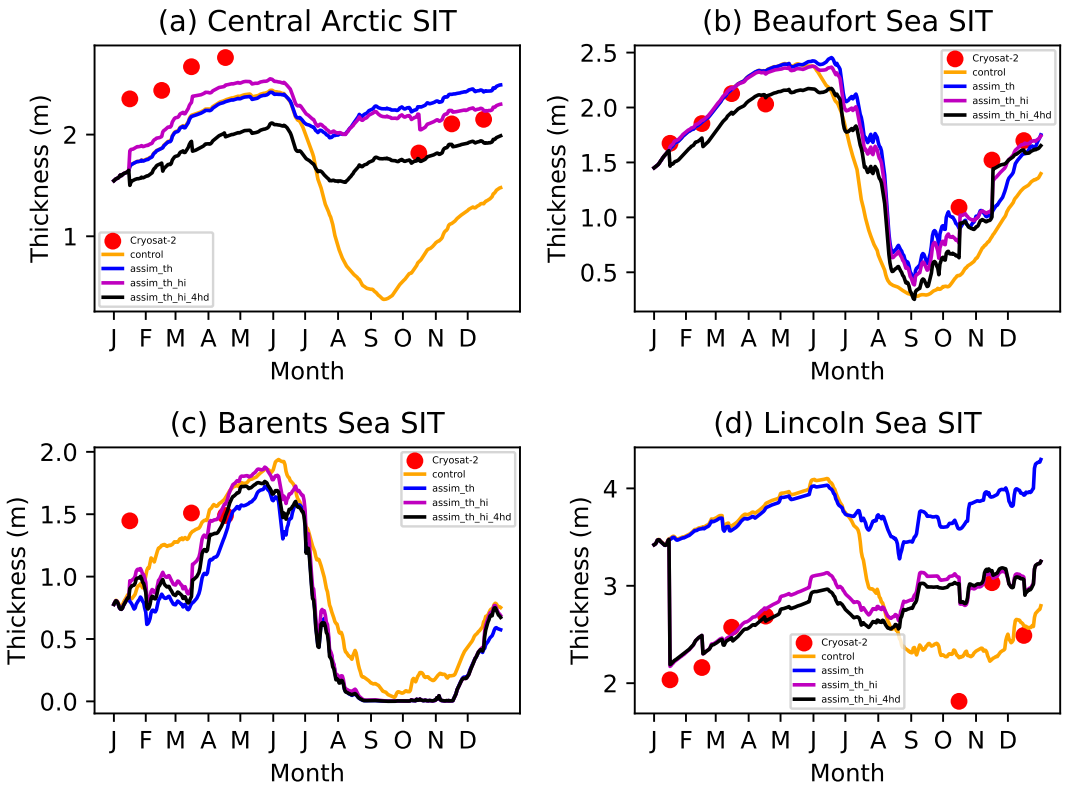

Fig. 4.11 Ensemble mean sea ice thickness (in metres) from Cryosat-2 observations and CICE-PDAF in 2012 for one grid cell in each of the Central Arctic, Beaufort Sea, Barents Sea and the Lincoln Sea. Cryosat-2 monthly mean observations shown at time of assimilation.

metre thicker). The assimilation of mean thickness generally followed a similar pattern but was worse than the control in the Central Arctic and Lincoln Sea, where the ice is thicker. In the Lincoln Sea grid cell the assim_conc_hi experiment is especially poor in comparison to the CS2 observations. The assim_conc_hi_4hd experiment performed significantly better with respect to the CS2 estimates in three of the four grid cells (Central Arctic, Beaufort Sea and Lincoln Sea). Between August and November the thicknesses in the Barents Sea are largely irrelevant because the concentration of ice in this grid cell is so small. This means the volume of ice in category 5 is also very small. There is also only small volumes of category 5 ice in the Beaufort Sea between July and October. The assimilation of thickness distribution is most effective for category 5 estimates in the Beaufort Sea between January and April, and also December. It is not completely clear why this should be, although it could be because it has a smaller concentration of ice in category 5 than the Central Arctic and the Lincoln Sea, but a concentration not completely negligible like that in the Barents Sea. The results in the Lincoln Sea are particularly interesting because they show the potential importance of

assimilating thickness distribution alongside mean thickness (and in likelihood other regions of very thick ice). The assimilation of mean thickness without thickness distribution made the assim_conc_hi estimates of category 5 ice thickness significantly poorer than the control, an effect that was completely reversed by assimilation of thickness distribution as well.

We believe the reason that the assimilation of the ice concentration and mean thickness of the four thinnest categories of sea ice works so well for the thickest sea ice in category 5 is because of the restrictions in the ice concentration. This is because the sum of the ice concentrations in each category must add up to 1, and the model is underestimating the amount of ice in category 5 which leads to it overestimating the thickness. This means that when the concentration of ice in category 5 is increased due to its relationship with the concentration in the other four categories, the thickness of this ice is then decreased so that the increments in the sea ice volume in category 5 are not too large. However the sea ice volume in category 5 is still significantly affected in the regions of very thick ice, for example, in the Lincoln Sea. Overall, it seems clear that assimilation of the thickness distribution of the thinnest four categories significantly improves category 5 ice thickness estimates in regions that are covered in thick ice year-round, or almost year-round.

These changes in category 5 thickness distribution are important because they affect not only the grid cell mean thickness but also the sea ice area and volume budget in the grid cells. In figure 4.12, we show the total sea ice volume in category 5 in each of the grid cells. In the Central Arctic the difference in category 5 ice volume that occurs between assim_conc_hi and assim_conc_hi_4hd is significant, especially in winter, where the assimilation of thickness distribution leads to lower category 5 ice volume than the control, without the thickness distribution assimilation the category 5 ice volume is increased. In winter the control has the lowest volume, this is likely because the control has much thinner ice in this region than the observations. Assimilating only concentration leads to the highest volumes of thick ice. The story in the Beaufort Sea is similar except that the control experiment is very similar to the control between August and November. In the Barents Sea, which is ice free or covered in thin ice for most of the year, the experiments have very little ice volume in category 5 except between March and June. In this case assim_conc actually has the lowest volume of the experiments, with assim_conc_hi_4hd again also having lower volumes of category 5 ice. Finally in the Lincoln Sea the two experiments which assimilate CS2 actually have an analogous volume of category 5 ice for the first three quarters of the year. This is primarily caused by a significant change in the first assimilation time step in January. When we looked at the thickness in category 5 we saw that assim_conc_hi_4hd had a much lower mean thickness

than assim_conc_hi, so their comparable volumes have been caused by assim_conc_hi_4hd having a much larger area of category 5 ice in this grid cell. However after September the two experiments have a difference in category 5 ice volume on the order of 10^9 m^3, which is substantial both in terms of volume and for the mass budget. If assim_conc_hi_4hd has more thicker ice this also makes it less vulnerable during the melting season.

Interestingly, in the Lincoln Sea and the Central Arctic, the only experiment which experiences a rapid decrease in category 5 sea ice volume during the melting season is the control. This either suggests that ice in the thickest category is not as vulnerable during the melting season as the model suggests, or this could be a negative impact that occurs from the assimilation of Bootstrap concentration. In the three grid cells containing MYI (Central Arctic, Beaufort Sea and Lincoln Sea), assim_conc has much larger category 5 ice volumes than other runs. In the Lincoln Sea the excessively high thicknesses caused by only assimilating concentration look to be a result of the assimilation putting too much ice into category 5. In the Central Arctic grid cell the volume of category 5 ice increases in the assim_conc experiment during the melting season, whereas the category 5 thickness stays relatively stable and in late summer is increasing. You would expect the area of category 5 ice to decrease as some of it thins and is moved into a lower category, yet this does not appear to be the case in some regions in the model. Instead the decrease in ice volume is largely a result of changes in the ice area. On the whole the assimilation of the thickness distribution results in lower estimate of category 5 sea ice volume during the freeze-up season than the control and other assimilation experiments. In the melting season the control experiment experiences significant loss of category 5 sea ice volume which leads to lower category 5 volume estimates than seen in assim_conc_hi_4hd. These changes may be what causes the underestimate in Arctic sea ice thickness in 2012 in comparison with CS2 and OIB.

In summary, we can clearly see that the assimilation is working well at grid cell level. The assimilation of the Bootstrap concentration is highly effective and significantly reduces the RMSE sea ice concentration to Bootstrap in comparison to the control. However assimilating concentration alone appears to be detrimental to the ice thickness estimates, particularly during the melt season which has an effect on assim_conc estimates of thickness not alone during the melt season but also the rest of the year. Assimilating ice thickness in tandem with ice concentration negated this effect and reduced RMSE sea ice thickness to the assimilated product successfully. The assimilation of the thickness distribution was similarly successful in the assimilation of mean thickness in terms of both concentration and thickness but also substantially improved estimates in regions of thicker ice because of how well the assimila-

tion of thickness distribution of the thinnest four categories improved estimates of the ice state in the thickest category of ice.

4.9 Summary

In this chapter we have presented an extensive overview of how our sea ice data assimilation functions. We introduced our method of perturbing the atmospheric forcing fields to generate ensemble spread. We found that we are able to generate a good ensemble spread in the sea ice model state vector such that the assimilation system can function well and correctly. We apply a post-analysis step processing that means the sea ice concentration and volume in each category are not updated in an unphysical way to avoid model crashes and more importantly in order to not make the incremental changes to the sea ice state too large or strange, which could upset the model system and potentially cause large biases or other unwanted results. We conducted short studies into four important parameters: amplification factor, ensemble size, forgetting factor and localisation radius, and found appropriate settings for each, although there is significant room for further studies in these parameters whereby calibration of these parameters could improve the sea ice estimates produced by the system, possibly significantly, as Chevallier et al. (2017) found that there was much room for improvement in current sea ice reanalyses by improving and tuning the assimilation system and its parameters. We also tested the assimilation of some sea ice observations at a grid cell level, to ensure that the assimilation is functioning correctly and that it has the desired effect. Now that we have established the feasibility and success of our data assimilation system, CICE-PDAF, on a local level over a reasonable length of time, we will next look to produce a multi-year test of the assimilation of the observations to make a more detailed analysis of the system and to decide which observations we will assimilate in the full reanalysis.

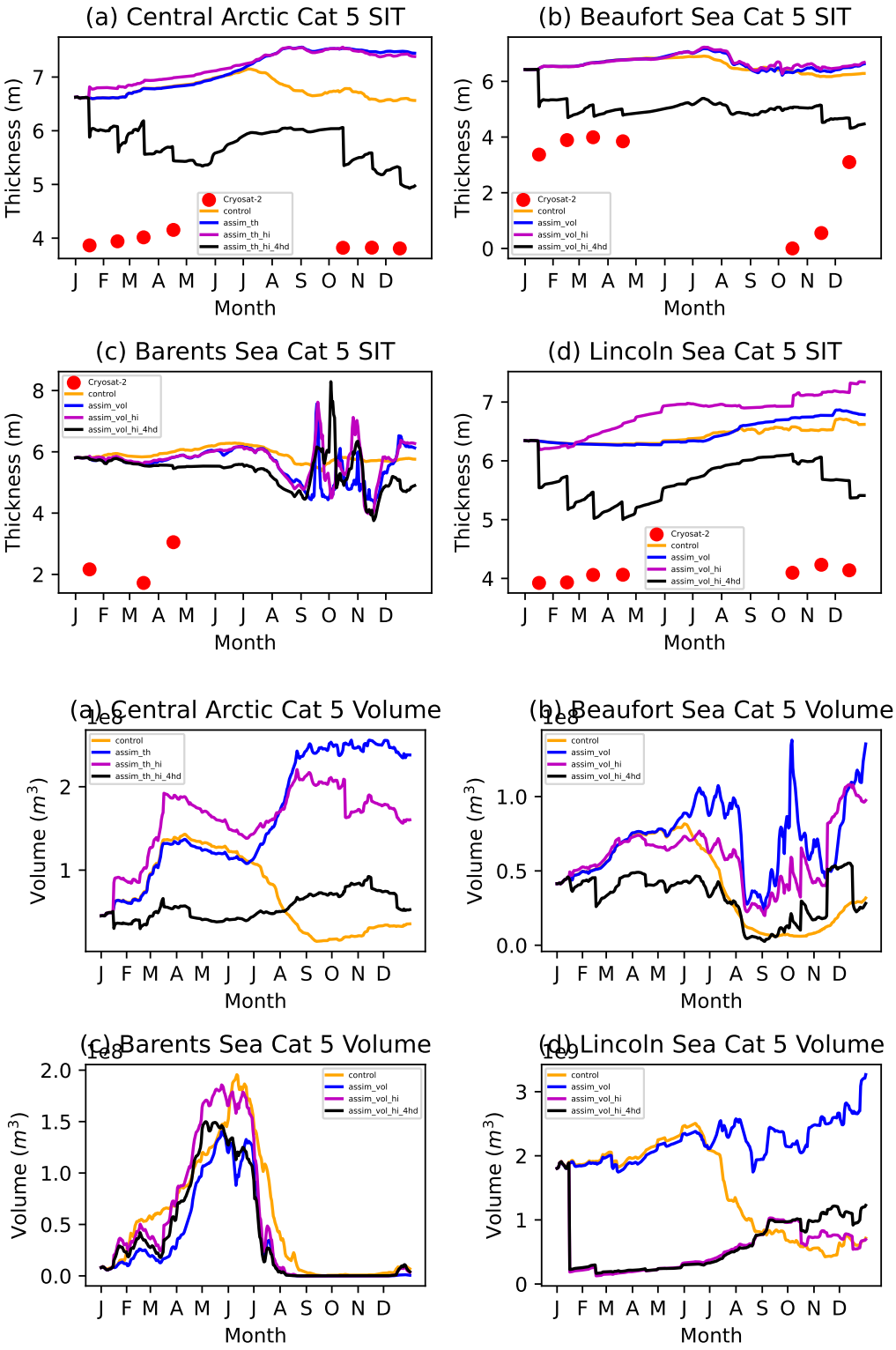

Fig. 4.12 Top four panels: Category 5 sea ice thickness (in metres) from Cryosat-2 observations and CICE-PDAF in 2012 for one grid cell in each of the Central Arctic, Beaufort Sea, Barents Sea and the Lincoln Sea. Note that these are normalised by ice concentration so they are not necessarily within the category bounds. Cryosat-2 monthly mean observations shown at time of assimilation. Bottom four panels: Category 5 ensemble mean sea ice volume (in metres cubed) from CICE-PDAF in 2012 for one grid cell in each of the Central Arctic, Beaufort Sea, Barents Sea and the Lincoln Sea.

Chapter 5

An intercomparison of short term sea ice data assimilations studies investigating the effects of assimilating different sea ice observations

5.1 Overview

In this chapter we present an intercomparison study of a short term (4-year) reanalyses, which assimilate different configurations of the sea ice observations we describe in the literature review. This intercomparison is used to help us decide which observations we should assimilate in the full reanalysis, and in particular to assess the potential contribution of the assimilation of the sub-grid scale sea ice thickness distribution. This chapter also provides an important test as to the feasibility of a long term sea ice reanalysis produced by this system. The usefulness of the data assimilation is assessed using root-mean-square-error (RMSE) tests against both the assimilated data and independent data. The experimental setup is described in section 5.2. The results are evaluated against Bootstrap sea ice concentration and CS2 data in section 5.3. The results for sea ice concentration, area and volume are discussed in section 5.4. The results are discussed in section 5.5 and the chapter is summarised in section 5.6.

Table 5.1 Configurations of different CICE-PDAF experiment runs. SIC indicates assimilation of daily sea ice concentration (NASA Bootstrap), SIT indicates assimilation of monthly mean sea ice thickness from CS2, and SID indicates assimilation of monthly mean sea ice thickness distribution from CS2.

run name	**SIC**	**SIT**	**SID**
control	N	N	N
assim_conc	Y	N	N
assim_conc_hi	Y	Y	N
assim_conc_hi_4hd	Y	Y	Y

5.2 Experimental Setup

Four short-term assimilation studies are conducted, spanning the years 2012-2015. This includes a restart from a stand-alone CICE model run in 2011, and then a further year with the system running in ensemble mode, with no assimilation taking place. All experiments use an ensemble size of 100, a forgetting factor of 0.995 and a localisation radius of 100 km. All experiments use a set of atmospheric forcing data generated using an amplification factor of 1.5. In table 5.1 we describe which observations are assimilated in each experiment. These are the same configurations of observations that we looked at in the previous section except we now look at the effects of this data assimilation on regional and pan-Arctic scales.

5.3 Evaluation of CICE-PDAF against Bootstrap and Cryosat-2 observations

To assess the effectiveness of the DA we look at the root-mean-square-error (RMSE) of the control runs, assimilation runs and observations assimilated, against the Bootstrap data and the CS2 data randomly selected for validation throughout the four years. The CS2 data randomly selected is only used for evaluation and not assimilated. 25% of the data is randomly chosen for each month of data where it exists. In figure 5.1 we show the RMSE in daily sea ice extent for CICE-PDAF against the Bootstrap extent. We see a large reduction in total sea ice extent RMSE when assimilating sea ice concentration (blue, magenta, and gold lines) in comparison to the control run (green line) in all three experiments year-round. Assimilating ice thickness or ice thickness distribution in addition to concentration does not have any visible impact on sea ice concentration.

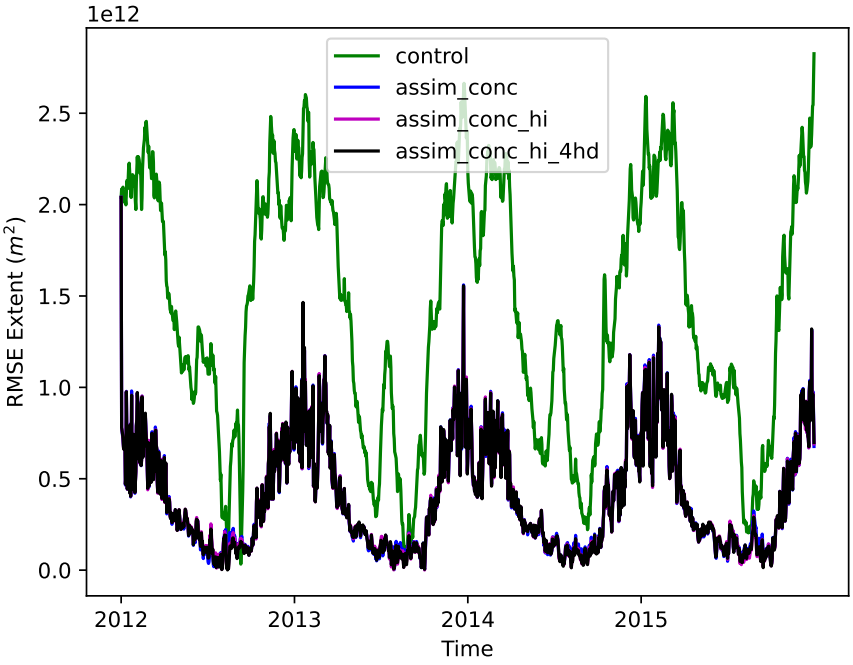

Fig. 5.1 RMSE of daily sea ice extent for the control and three assimilation runs of CICE-PDAF in comparison to the Bootstrap extent from 2012 to 2015. Note that assim_conc, assim_conc_hi and assim_conc_hi_4hd plotted lines overlap.

In figure 5.2 we show mean thickness in CICE-PDAF against CS2 for our four experiments. Assimilating CS2 mean sea ice thickness significantly reduced the RMSE in ice thickness compared to the evaluation data. We can see that the control has a significant number of data points which lie outside the dense central region. For the assim_conc experiment, the ice appears to be much thicker than in Cryosat-2 . With the assimilation of mean thickness included in assim_conc_hi the central region following the linear trend is now more visible. This is also reproduced in assim_conc_hi_4hd, though there is a bulge of slightly thicker ice in CICE-PDAF between 1.5 and 2.5 m. In general it appears that the model is weighted towards slightly thinner ice than the equivalent from Cryosat-2 observations. It seems that most of the improvement in thickness estimates when assimilating Cryosat-2 data comes from removing a substantial quantity of the thickness estimates in the control that are too high. Although the high density of low thickness estimates between 1 and 2 m that appear in the 2d histogram plot for control compared to that in assim_conc_hi and assim_conc_hi_4hd is smaller the assimilation of the products is not able to completely remove this bias.

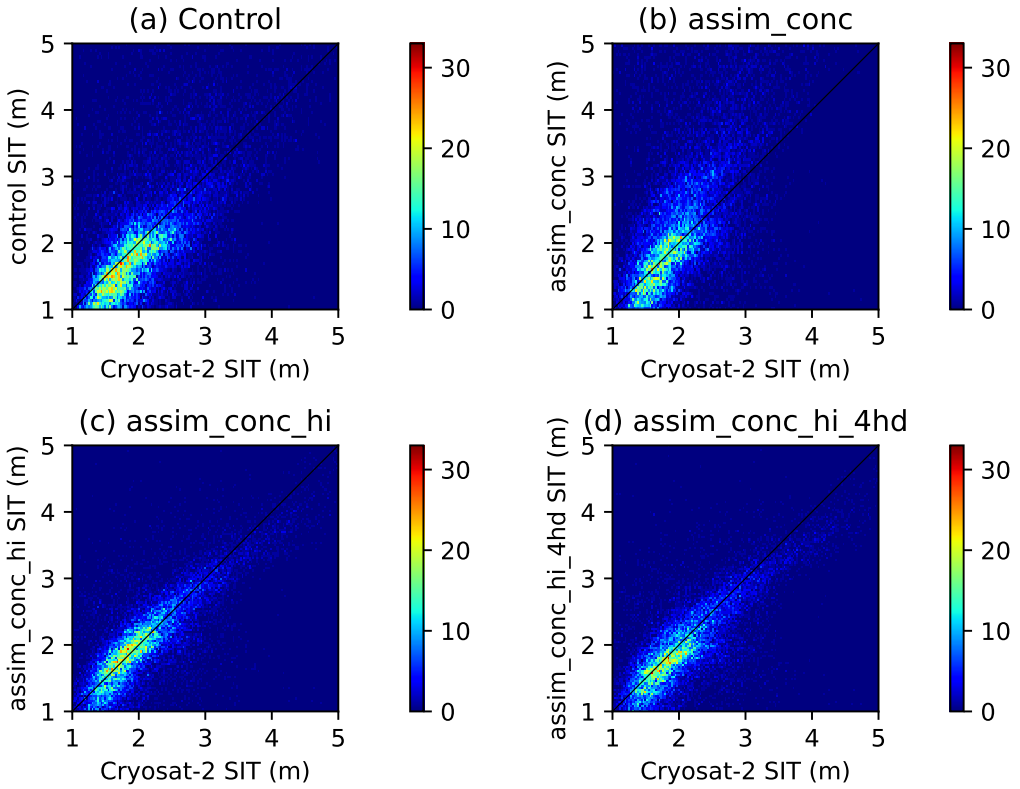

Fig. 5.2 2d histogram plots of sea ice thickness estimates in CICE-PDAF against the Cryosat-2 evaluation data for four CICE-PDAF experiments.

In Table 5.2 we show the RMSE for mean thickness and category 5 thickness compared to CS2. The RMSE in mean thickness was more than halved when assimilating CS2 sea ice thickness in comparison to the control run from 0.63 m to 0.27 m. On the other hand assimilating Bootstrap concentration alone appears to be detrimental to the model estimates of monthly mean thickness, as shown by the assim_conc experiment, which had a higher RMSE (0.88 m) than the control. As shown by the 2d histogram plot in Fig. 7 (top right) this seems to be caused by the assimilation of concentration as the model estimates tend to be much thicker than in CS2. In terms of the mean thickness, assimilating the ice thickness and concentration in the four thinner categories of ice did not improve total mean sea ice thickness estimates. However assim_conc_hi_4hd did lead to significantly improved estimates of the thickness in category 5 (RMSE of 1.7 m vs. 3.2 m), even though information about category 5 was not directly assimilated (see Sect. 5.2). This improvement is not seen in any of the other CICE-PDAF runs. There were no changes to the RMSE in the thickness or concentration in

Table 5.2 RMSE of the domain-averaged monthly mean ice thickness (hi) and ice thickness in category 5 (hice5) to Cryosat-2 evaluation data

RMSE	**hi**	**hice5**
control	0.63	3.2
assim_conc	0.88	3.3
assim_conc_hi	0.27	3.3
assim_conc_4hd	0.27	1.7

the other four categories compared to the CS2 data. This change in thickness in category 5 also has a generally positive effect on the model estimates of volume in this category.

In figure 5.3 we show monthly mean RMSE of ice thickness in category 5 for each experiment, compared to CS2, and snapshots of how this difference in thickness for one month (December 2013) leads to an improvement in the volume in this category (using Bootstrap data to convert CS2 thickness estimates into volume). We found that additionally assimilating thickness distribution leads to a significant decrease in the thickness and volume RMSE of category 5 in the model, because CS2 estimates of thickness in this category are generally much lower. Assimilation of concentration and mean thickness seemed to have a small negative effect on the estimates of category 5 thickness and volume for most of the experiment in comparison to the control. The improvement in category 5 RMSE occurs because the category 5 ice thickness in the control model is 6 to 7 metres in most places year round, whereas CS2 has much thinner estimates around 3.5 to 4 metres. In many areas the thickness and volume of ice of the thickest category is much higher than in CS2, and only assimilating part of the thickness distribution seems to be able to resolve this difference. The assimilation of the concentration and thickness in the lowest four categories then has an important effect on achieving better estimates of the thickness, volume and mass budget distribution in comparison to observations on a pan-Arctic scale.

5.4 CICE-PDAF Assimilation Results

Looking at time series of daily pan-Arctic sea ice area, figure 5.4, we see that in all four years, the sea ice area in the freeze-up season is smaller, and in the melting season is larger

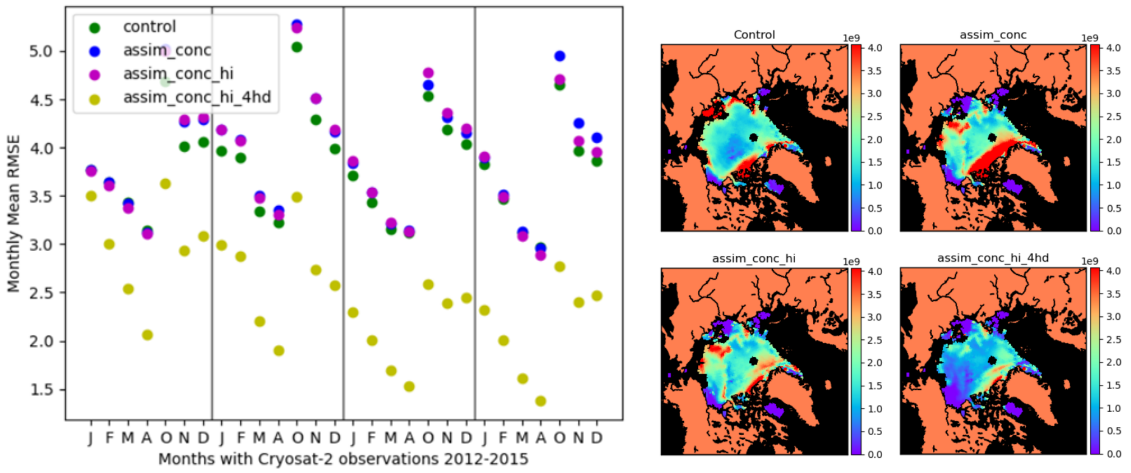

Fig. 5.3 LHS: RMSE of Category 5 sea ice thickness between 2012 and 2015 for January, February, March, April, October, November and December for the control and CICE-PDAF assimilation runs, against Cryosat-2 sea ice thickness evaluation data. RHS: Maps of category 5 sea ice volume RMSE in December 2013 for four CICE-PDAF runs against Cryosat-2 evaluation data. Clockwise from the top left map: control run, assim_conc, assim_conc_hi_4hd and assim_conc_hi.

than the control, leading to a narrower seasonal variation. On a pan-Arctic scale we see again that the assimilation of the concentration is the key factor for this area diagnostic, with the assimilation of CS2 products providing no additional benefits, as expected.

We show pan-Arctic sea ice volume in figure 5.5. We see after the first year that the assimilation of only concentration (blue) increases sea ice volume over the experimental time frame in comparison to the control run (green). The assimilation of monthly mean thickness in addition to this (magenta and gold) appears to mitigate this effect, where assim_conc_hi (magenta) has sea ice volumes in winter comparable to the control run, but on the other hand it has greater sea ice volumes in summer. The assimilation of the sub-grid scale thickness distribution (gold) appears to cause a rebalancing of the ice thicknesses and fractional areas in each category, leading to large swathes of ice being moved into lower thickness categories, which results in lower sea ice volumes. A further analysis (see figure 5.6) shows that this is caused by large differences between the CS2 ice thickness in category 5 and the model ice thickness in category 5. In the first four months of the experiment the increments in sea ice volume caused by the thickness distribution assimilation are significant because of these differences.

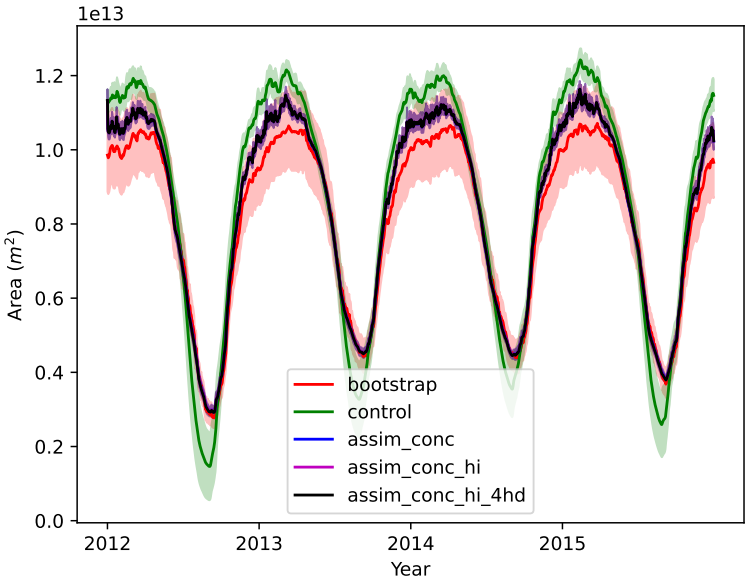

Fig. 5.4 Pan-Arctic sea ice area in m^2 from 2012-2015 from Bootstrap observations and four different CICE-PDAF runs. Solid lines show observations or ensemble mean and the shading shows observation error or ensemble spread (one standard deviation)

In figure 5.6 we show maps of sea ice thickness in October 2012-2015 from CS2, the control run, three CICE-PDAF experiments and PIOMAS. We can see that CS2 has thinner sea ice than all the CICE-PDAF experiments and PIOMAS during this time period. In particular the control and assim_conc experiments show a tendency to pile up thicker and thicker ice against the Canadian Archipelago. If we compare the ice thickness in assim_conc to that in assim_conc_hi we can see that the assimilation of the mean thickness alongside the ice concentration significantly reduces the gradient of sea ice thickness from the sea ice edge towards the Canadian Archipelago. The assim_conc_hi experiment has much thinner ice in these regions, similar to CS2. In assim_conc_hi there is instead a much more homogeneous (in terms of mean thickness) ice cover across the Arctic, with a majority of the ice cover having a mean ice thickness in October between 1.4 and 2.4 metres. The assimilation of the CS2 mean ice thickness appears to be very effective in CICE-PDAF, with the ice thickness of assim_conc_hi looking quite similar to that of the CS2 product, and shown by the reduction in RMSE in Table 5.2. The assimilation of the concentration does however have the effect of significantly reducing the amount of thin ice at the edges of the sea ice pack, with much less ice between 0 and 0.6 metres in the Arctic in October in the CICE-PDAF experiments.

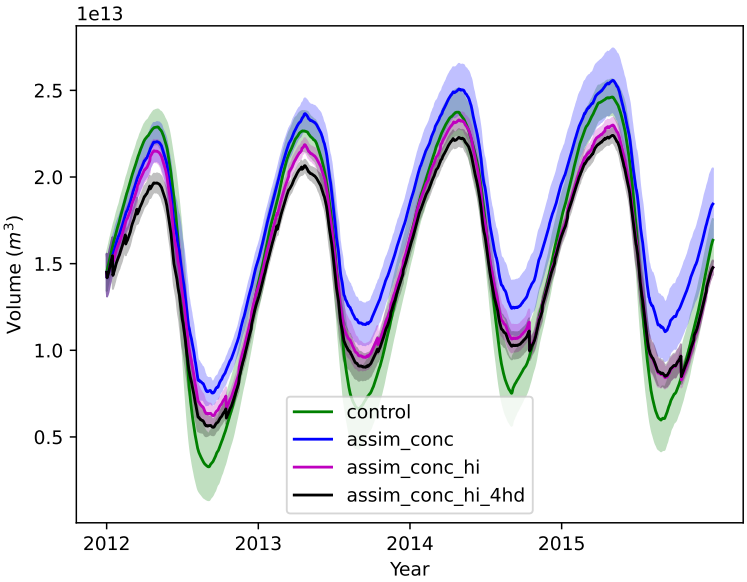

Fig. 5.5 Pan-Arctic sea ice volume from 2012-2015 in four different CICE-PDAF runs. Solid lines show observations or ensemble mean and the shading shows observation error or ensemble spread (one standard deviation).

Additionally assimilating the four thinnest categories of sea ice in the sub-grid scale thickness distribution generally had the effect of slightly increasing the thickness of the thickest ice, however this still has very good agreement with CS2. The assimilation of the sub-grid scale thickness distribution is also most similar to PIOMAS at this time. The assimilation of the CS2 products from October through April causes a thicker sea ice cover to persist throughout the summer period than we see in the control model, with higher sea ice extents and volumes in summer (not shown).

Alongside ice thickness, we also look at sea ice concentration in September 2012-2015 in figure 5.7. Here all runs with assimilation of sea ice concentration showed very similar results, and similar to the Bootstrap sea ice concentration. This shows what the RMSE was telling us from the top panels in figure 5.1 – that the assimilation of sea ice concentration works well, and moves the concentration estimates in the assimilation experiments close to the observations. A significantly smaller marginal ice zone (MIZ, the area of ice containing between 0.15 and 0.8 sea ice concentration), which is present in the Bootstrap sea ice concentration, is also seen in the assimilation runs. The Bootstrap concentration tends to feature ice concentrations close to 1 inside the ice pack, which could also lead to thicker ice within the ice pack because

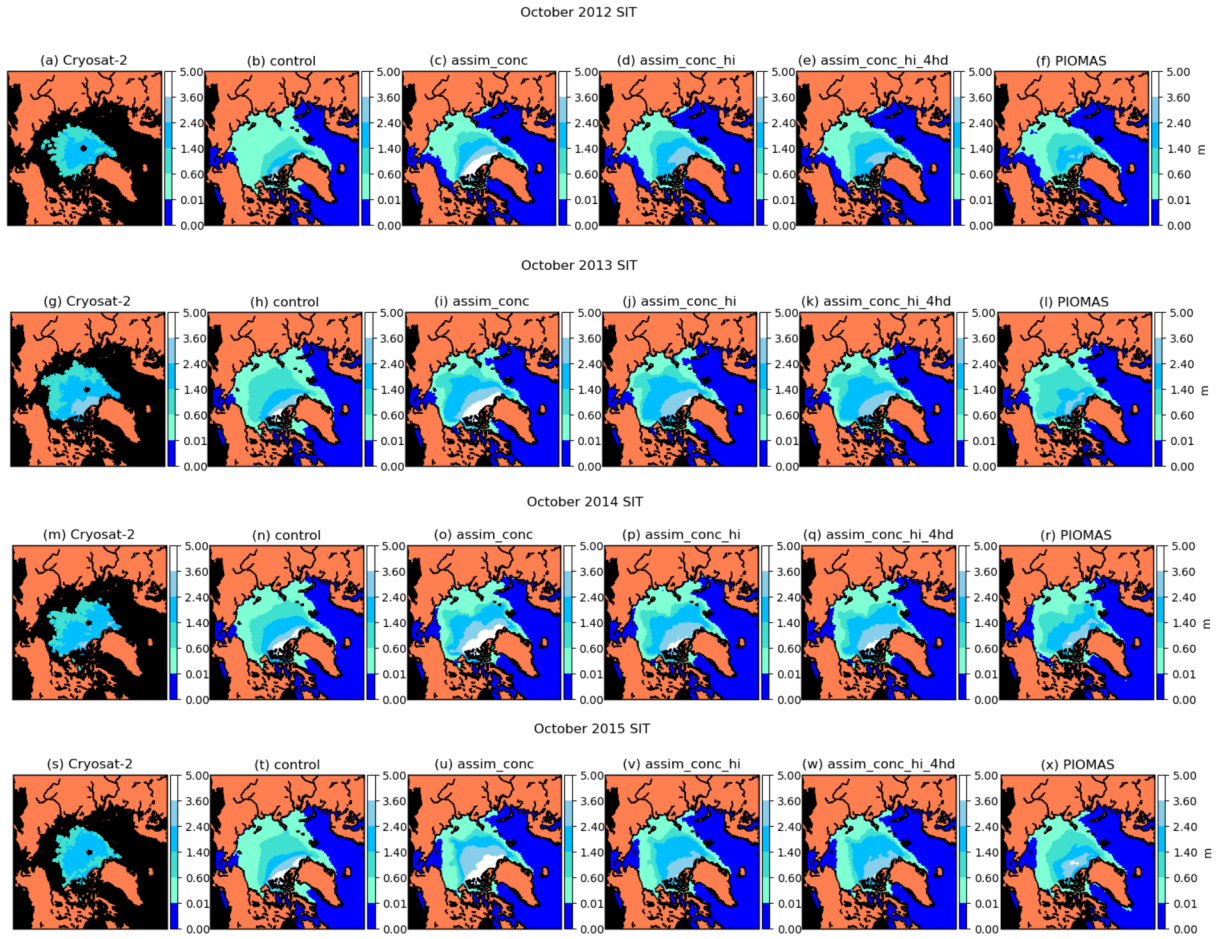

Fig. 5.6 Monthly mean sea ice thickness (in metres) in October 2012, 2013, 2014 and 2015 in Cryosat-2 and our CICE-PDAF experiments (ensemble mean) and PIOMAS.

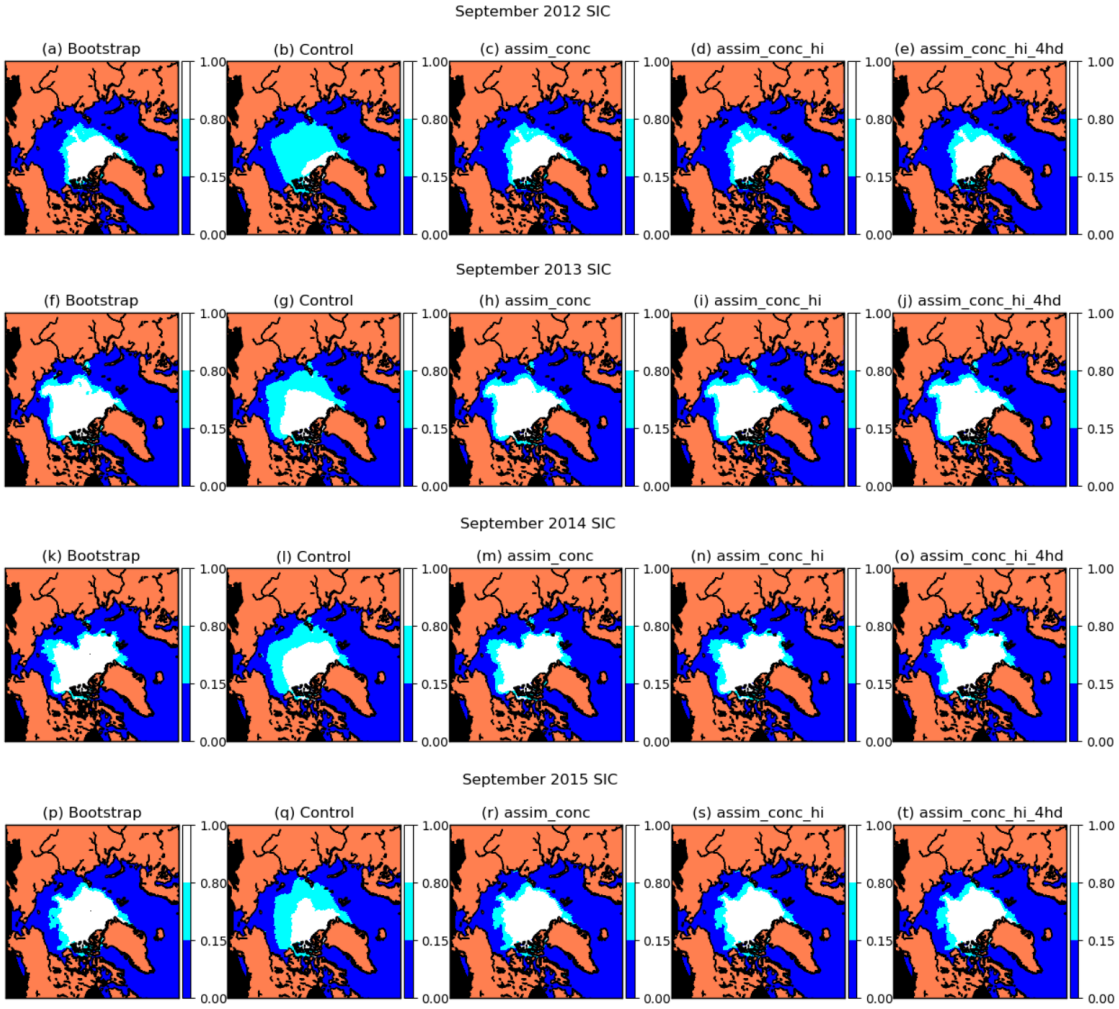

Fig. 5.7 Monthly mean sea ice concentration in September 2012, 2013, 2014 and 2015 in the Bootstrap observations, the control and three CICE-PDAF experiments (ensemble mean).

higher ice concentrations are expected to correlate with higher ice thicknesses – in Fig. 4 strong correlations are shown between concentration and thickness except for the Fram Strait in Summer. These wide areas of high concentrations in the ice pack are not present in other sea ice concentration observation products such as the NASA team product. For this reason it would be interesting to compare the assimilation of different sea ice concentration products.

In figure 5.8 we show sea ice volume in each thickness category and the total Arctic sea ice volume for 2012-2015. Large differences occur in the three largest categories, which we expect because smaller changes in the fraction of ice in these categories would lead to

bigger differences in their volume. In the thinnest category (ice 0.6 m and thinner), there are small decreases in the fraction of ice in this category when compared to the control, but the three assimilation runs are generally similar to one another. The largest differences seem to occur at the end of each melting season, with the control run having significantly more ice in the thinner categories than the assimilation experiments. In category 2 (0.6-1.4 m) the same pattern occurs, but shifted slightly (with the maximum ice volume in this category occurring around late December and early January), and again with significantly more ice at this time in the control run.

In category 3 (ice thickness between 1.4-2.4 m) we first see larger differences between the assimilation runs. Most notably the assimilation of the thickness distribution (assim_conc_hi_4hd) has caused a significant decrease in ice in this category compared to assim_conc_hi at the end of the freezing-up season (March-April) in 2013. This decrease persists throughout the rest of the run. The ice in this category in the control run tends to experience the greatest variation between the minimum and the maximum, generally having the lowest fraction of ice in this category at the end of summer but the most at the end of winter. In assim_conc the reverse is true. The assimilation of thickness alongside concentration has a substantial effect on the volume of ice in this category, particularly during the minimum, with assim_conc_hi having much larger ice volume estimates in this category than assim_conc. Additionally assimilating sub-grid scale thickness distribution seemed to remove this category 3 ice created by the mean thickness assimilation, with assim_conc_hi_4hd having similar category 3 volume estimates to assim_conc. In category 4 (2.4-3.6 m), assimilation leads to more ice in this category, particularly when assimilating the sub-grid scale thickness distribution, where the analysis increments are quite large. This increase of ice volume in category 4 seems to counteract the decrease in categories 3 and 5 in this run.

Looking at the thickest ice (3.6 m and thicker), the assimilation of concentration alone causes a large increase in category 5 volume. The assimilation of mean thickness tends to decrease the volume of the thickest ice compared to the control. The addition of sub-grid scale thickness distribution assimilation does not seem to significantly affect the total volume of ice in this category, however regional differences could be significant. It seems that the primary reason for the decrease in sea ice volume when assimilating thickness distribution is that a decrease in ice in categories 3 and 5 is partially (but not fully) counteracted by an increase in category 4 ice volume. Overall we see that assimilation of the thickness distribution product can have wide-reaching impacts on the distribution of the sea ice in the

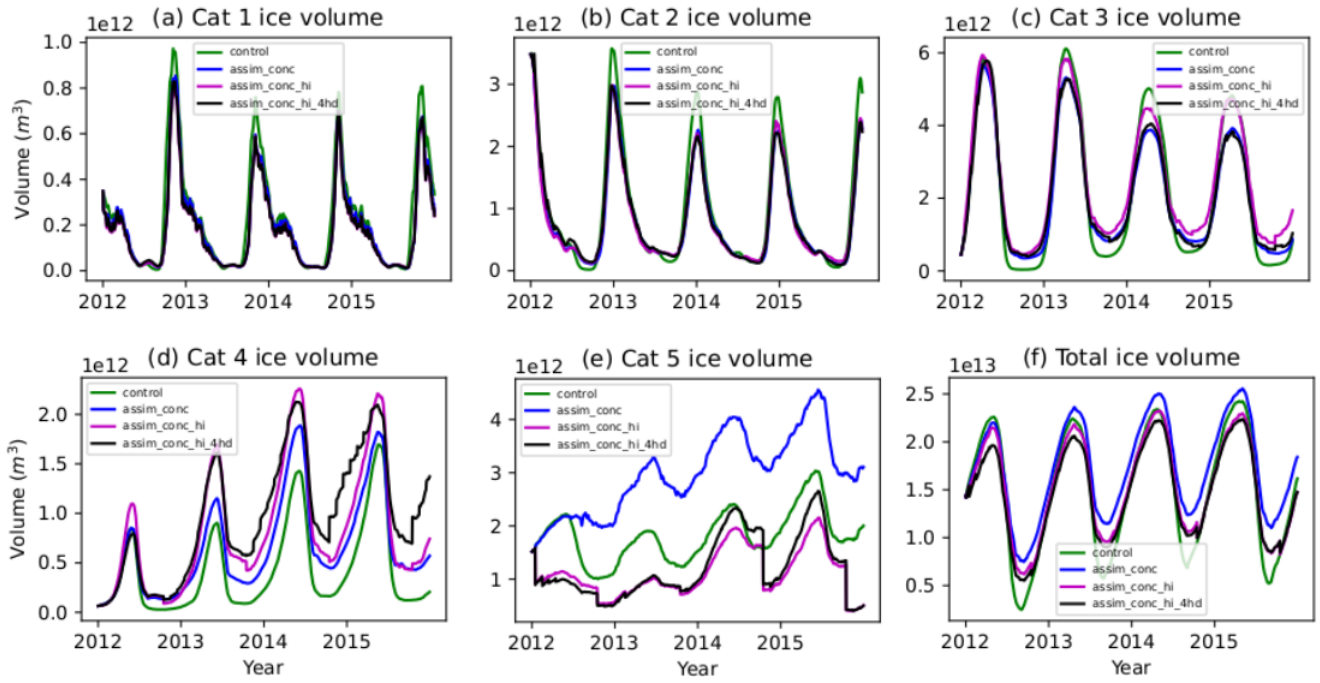

Fig. 5.8 Volume of ice in each thickness category and the total volume for each of the CICE-PDAF experiments (ensemble mean).

Arctic.

5.5 Discussion of Short-Term Reanalysis Study

Overall, the assimilation of sea ice observations decreased the seasonal variation of both sea ice extent and sea ice volume in the freeze-up and melting periods in comparison to the control run. The assimilation of the CS2 observations resulted in an increase in the area of thicker ice extending outwards to the North pole from the Canadian Archipelago, but was compensated by a reduction in the thickness in the regions of the thickest ice. The sea ice in the control experiment was generally too thin throughout most of the year, except in the Canadian Archipelago region. As a lot of thin first year ice is being formed in the control model this will make it more susceptible to subsequent melting during the melting season, and hence increase the seasonal variation. The model generally appears to overestimate both summer ice melt and the winter freeze up, except in the Canadian Archipelago where the ice gets much thicker than observations from CS2. This may be caused by too much ice

advecting into this region in the model or the ridging formulation in the model favouring the formation of too much thick ice. This problem could be being exacerbated by possible issues with the climatology we use to simulate the oceans, which may cause too much congelation growth in this region.

Apart from in assim_conc_hi_4hd, the estimates of ice in the thickest category are poor (see 5.3), so the model appears to have significant difficulties in simulating the thickest sea ice. In assim_conc the ice thickness and volumes are substantially larger than in the control, particularly in the regions of the thickest ice (ice thickness > 3.6 m). This could indicate issues with the open water fraction in the CICE model as CICE generally has lower sea ice concentrations within the ice pack than Bootstrap (which has concentrations generally close to 1 away from the ice edge) and the correlations between concentration and thickness within the model could cause new ice created to be thicker than it should be. The marginal ice zone (MIZ) which is defined as the area of ice between 15% and 80% concentration, forms a boundary region of small sized ice floes between the open ocean and the central ice pack which are strongly affected by ocean waves (Sundfjord et al., 2007). The interactions between the atmosphere, ocean and sea ice are particularly strong in the MIZ, and a reduction in MIZ could also have strong impacts on Arctic sea ice ecosystems (Barber et al., 2015). The assimilation of Bootstrap sea ice concentration also appears to decrease the marginal ice zone (MIZ) area, which is again an artefact of the characteristics of the Bootstrap sea ice concentration. A wholesale change in the mean thickness across the Arctic will change how a lot of this ice behaves because the dominant physical processes on the sea ice change depending on its thickness. As the ice is much thicker the ocean waves have a much smaller effect on it. Thicker ice created by the assimilation can also advect into the Beaufort and Lincoln seas causing higher than expected ice thickness and volume in these regions.

The areas of thickest ice (> 3.6 m) and thinnest ice (< 0.6 m) narrowed rather than broadened when ice thickness products from CS2 were additionally assimilated. This resulted in a significant increase in the area of ice between 0.6 and 3.6 m thick. In addition to the effects of the sea ice concentration assimilation, this could partially explain why the sea ice extent minima in September were larger in the assimilation runs than the control model every year, because the thicker ice would be more resilient to being fully melted during the melt season than the thinner ice. This study highlights significant benefits of observations of sea ice thickness and sub-grid scale thickness distribution for estimation of sea ice thickness and volume using data assimilation. It shows that there should be further emphasis put on making future observations of sea ice thickness in order to establish a more accurate long term record

of ice thickness and volume in a reanalysis, and also in making use of different types of observations in sea ice data assimilation studies to ascertain a clearer picture of the Arctic sea ice.

One shortcoming of this study is that the observation errors of ice thickness, and the sub-grid scale thickness distribution (ice concentration and ice thickness in each category) are highly correlated, but for simplicity we do not account for observation error correlations. The observation error statistics on the sub-grid scale thickness distribution and the mean thickness are both highly uncertain and are assimilated only once a month and only outside of the Arctic melting season. Assimilating only once a month can cause large increments in some of the CICE state variables especially in October, after the 5 month Summer period without assimilation. The assim_conc experiment differs significantly from assim_conc_hi and assim_conc_hi_4hd so the thickness assimilation is not only highly effective in reducing the RMSE in mean ice thickness but has a significant effect in September, 5 months after any thickness or thickness distribution assimilation has taken place. A more accurate assessment of the uncertainties in the Cryosat-2 products assimilated in this study would likely lead to significant improvement in the system and estimated sea ice state.

Another important factor to consider is that many of the variables in the CICE state vector are assumed to be Gaussian are bounded, for example sea ice concentration, as well as many other state variables which have upper or lower bounds. This means that we need to account for the correlations in the LETKF leading to unphysical sea ice states, so some variables need to be altered after the assimilation to avoid model crashes. Of the observations we assimilate, sea ice concentration and sub-grid scale thickness distribution have upper and lower bounds, and sea ice thickness has only a lower bound, therefore the observation error covariances for our observations should approach zero as the bounds are reached (Bishop, 2019). For simplicity we have not applied this in our study. The observation error variances we have used for sea ice concentration and sea ice thickness do depend on the measured state, and in the case of sea ice concentration do get smaller as some bounds are approached, but this is done to account for uncertainties in the observational method. To evaluate the ice thickness from the studies in this chapter, we used randomly selected Cryosat-2 data held back for evaluation. When evaluating the studies with the Cryosat-2 we have to recognise that although the data held back for evaluation was randomly selected, it is not completely independent and so the evaluation data will be correlated in some way with the observations chosen for assimilation.

Assimilating Bootstrap sea ice concentration alone resulted in an increase in sea ice thickness and volume in comparison to the control experiment, and it performed worse against our evaluation CS2 dataset. This effect has not been seen seen in other studies assimilating only ice concentration and evaluating modelled ice thickness. In Fritzner et al. (2019) when only OSISAF sea ice concentration was assimilated estimates of thickness generally improved in comparison to independent observations, only performing worse in May, and unlike in our experiment the ice thickness and volume were generally reduced. It appears to be caused by the assimilation of Bootstrap sea ice concentrations in the summer months. There are a few months in summer when Bootstrap sea ice concentrations are higher than the control model, which would lead to positive increments in sea ice concentrations. This may be causing unrealistic thickening of the sea ice through positive correlations between sea ice concentration and sea ice thickness within the data assimilation. It seems that further care is required when assimilating sea ice concentration alone when using assimilation schemes like we have used in this study. This is not an issue for other reanalyses like PIOMAS, which uses a highly tuned optimal interpolation technique which only affects ice concentration close to the ice edge, and assimilates a different dataset of sea ice concentration observations (NASA Team). It is likely a result of some unique characteristic of the Bootstrap sea ice concentration in combination with the physics of the CPOM-CICE model and the data assimilation scheme we use. It does show that care should be taken in the interpretation of sea ice volume estimates when assimilating sea ice concentration alone in any reanalysis study.

In this study we attempted to tune a number of important assimilation parameters - forgetting factor, localisation radius and an amplification factor. We attempted to do this using a short 1-year assimilation study, which we assumed is a reasonable length with which to determine their long term effects. However we showed that changing any of these parameters could in some cases result in a considerably changed estimate of the sea ice state, without altering any part of the model or observations assimilated. We have used the results of this study to fine-tune parameters selected for the satellite era reanalysis presented in chapters 6 and 7. There is a significant amount of room for additional fine-tuning which could result in further improvements in estimates of the sea ice state, but this is outside the scope of this study. The localisation radius study did show that larger radii may slightly improve the model estimates, but these larger radii are probably physically unrealistic for the range of the effects of the CPOM-CICE model sea ice dynamics. In the future a location-dependent localisation radius would be beneficial, especially near the sea ice edge. However they would not likely change any of the outcomes of the study with regards to the intercomparison between each

assimilation experiment. With regards to ensemble size, more is generally better for the health of a data assimilation system, though 100 is on par with, for example, TOPAZ4, and much larger than in Fritzner et al. (2019).

In this study we have assimilated a sub-grid scale thickness distribution for the first time. When this is additionally assimilated alongside the mean thickness there are benefits to the estimates of ice in category 5. The model appears to overestimate the thickness of the thickest ice substantially. However it could be argued that this region where category 5 sea ice is present in large quantities is the least important because the ice cover has not changed as drastically here as it has in any other region of the Arctic. The ice is so thick in this region that even under increased Arctic warming the ice concentration here is close to or is 1, and has been throughout the satellite era. However a more accurate sub-grid scale thickness distribution could lead to medium and longer term benefits to sea ice estimates in the rest of the Arctic.

5.6 Summary

In this chapter we have conducted an intercomparison study of three short-term reanalyses from 2012-2015. This was done in order to ascertain the most useful observations for assimilation, and to better understand how the model reacts to the assimilation of these observations, before we produce the satellite era reanalysis in the next chapter. Importantly, we have seen that the sub-grid scale thickness distribution significantly improves the estimates of sea ice concentration, thickness and volume in category 5, though only in comparison to the assimilated observations, which have not been fully validated themselves due to a lack of independent ice thickness distribution observations. Therefore it is difficult to say with complete confidence that the estimates of ice thickness distribution have been improved. The assimilation of Bootstrap sea ice concentration was less successful, so we will produce two separate reanalyses assimilating Bootstrap and NASA Team sea ice concentration separately. The information from the CS2 observations of mean thickness are also very important for the thicker ($>$ 1 m) sea ice in the ice pack, as the mean thickness in the control was either too thin in the central Arctic, or too thick north of Greenland and in the Canadian Archipelago. In this chapter we show that the assimilation of the CPOM Cryosat-2 observations can provide important benefits in sea ice data assimilation. We find that the system seems to work well over the 4-year experimental period when ice concentration is assimilated alongside observations of thickness, thus in the next chapters we will now look at repeating this experiment and producing the full 40-year reanalysis. As a result of this study we choose

to assimilate sea ice concentration, CS2 sea ice thickness and the CS2 sub-grid scale sea ice thickness distribution observations in our satellite era reanalysis.

Chapter 6

A Satellite Era Arctic Sea Ice Reanalysis: Part I

6.1 Overview

The presentation and analysis of the nearly 40-year satellite era Arctic sea ice reanalyses is split between two chapters. Part I (this chapter) concerns the set-up and evaluation and Part II (chapter 7) concerns analysis of the sea ice processes. In this chapter we will present three newly produced satellite era Arctic sea ice reanalyses between 1981 and 2019. This includes a comparison to a free run of the CPOM-CICE model as well as evaluation against independent data and comparisons with currently available sea ice reanalyses. In this chapter we will examine the differences between the model and reanalyses, and importantly, look at the long-term trends in the reanalyses and their similarities and differences with observations and PIOMAS. We discuss the reanalysis setup in section 6.2. In section 6.3 we evaluate the reanalysed sea ice concentration, extent and thickness against assimilated and independent observations. In section 6.4 the simulated sea ice extent in the reanalyses are evaluated and compared with a control and observations. The regional changes in ice concentration are studied in section 6.5. The same is done for the sea ice volume in section 6.6, and for the thickness in section 6.7. The changes to the Pan-Arctic thickness distribution are investigated in section 6.8. Finally, the chapter is summarised in section 6.9.

6.2 Reanalysis Setup

The reanalysis setup is similar to that of our short-term reanalysis studies. There is a four year spin-up phase beginning in 1977, with the CPOM-CICE model running in ensemble

Table 6.1 Configurations of three different reanalyses produced in this chapter. SIC is sea ice concentration, SIT is sea ice thickness and SID is sea ice thickness distribution. N indicates no assimilation of this product takes place.

Experiment	**SIC**	**SIT**	**SID**
CPOM-CICE	N	N	N
reana_bt	Bootstrap	CPOM CS2	CPOM CS2
reana_nt	NASA Team	CPOM CS2	CPOM CS2
reana_landy	Bootstrap	Landy CS2	N

mode to allow for the spinning up of the CICE model and for the generation of an ensemble spread that will be sufficient for the Kalman filter to reasonably account for the model error. All reanalyses are run with 100 ensemble members using a newly generated set of atmospheric forcing fields, with an amplification factor α of 1.25. The forgetting factor is 0.995 and the localisation radius is 100 km as was used in the shorter studies. The reanalysis period spans 1981-2019 with sea ice concentration assimilated bi-daily from 1981 to 1989, and daily thereafter. CS2 mean sea ice thickness and sub-grid scale sea ice thickness distribution are assimilated monthly in the middle of the month from October 2010. We run three configurations of the reanalysis in this thesis, assimilating different combinations of Bootstrap sea ice concentration observations, NASA Team sea ice concentration observations, CPOM CS2 sea ice thickness, CPOM CS2 sea ice thickness distribution and Landy CS2 sea ice thickness. The control run is known as CPOM-CICE. As the errors in the NASA Team and Bootstrap products are believed to be similar we use the same observation errors when assimilating the two products (see section 2.2). All other parameters in the assimilation system are also the same. The configurations of these reanalyses are detailed in table 6.1.

6.3 Evaluation of sea ice reanalyses

In order to evaluate our reanalyses, we will use data from both assimilated observations, semi-independent data from CS2 and NASA Team, and some independent data from OIB. We will use the concentration and extent using the Bootstrap and the NASA Team sea ice concentration data, which although they are separate data sets are not truly independent, as they both use some of the same raw data from the same satellites, and are processed in a similar way (see section 2.2). To evaluate the grid cell mean ice thickness and ice thickness distribution assimilation we will use the randomly selected 25% of CS2 data held back from assimilation, and we will also use ice thickness data from OIB to evaluate the mean ice thickness.

6.3.1 Evaluation of sea ice extent and concentration

To assess the reanalysis estimates of sea ice extent we evaluate the monthly mean sea ice extent in March, June, September and December using the RMSE in comparison to both the Bootstrap and NASA Team observations, which is shown in figure 6.1. In all four months the RMSE is greatly reduced by the assimilation throughout the reanalysis period. In March the reduction in RMSE for reana_bt to both Bootstrap and NASA Team is on average $0.716 \times 10^{12}\ m^2$ in comparison to the CPOM-CICE model. The RMSE to the NASA Team extent in reana_bt increased in the last decade of the reanalysis, though this is probably more a result of NASA Team and Bootstrap having greater differences at this time. There is a small increasing trend in the RMSE of CPOM-CICE in March over the whole period, which may indicate the model does a poor job of simulating the trend in sea ice extent that occurs over the satellite period in winter, this is also seen in Schröder et al. (2019). In June the reduction in RMSE in reana_bt is much smaller between 1981 and 2000 compared to March, but after 2000 the differences become much larger and there is a strong increase in the CPOM-CICE RMSE to both Bootstrap and NASA Team observations. As we also saw in March, the difference in RMSE to Bootstrap and NASA Team increased later in the reanalysis period, showing again that there is stronger disagreement between Bootstrap and NASA Team later in the satellite period.

In September the differences between NASA Team and Bootstrap sea ice concentrations are at their highest because of the different methods used to estimate summer sea ice cover, so the RMSEs to Bootstrap and NASA Team differ the most here. Interestingly, after 2005 the RMSEs of CPOM-CICE improve substantially and are better than the RMSE of reana_bt to NASA Team. The stand-alone model does a much better job of estimating sea ice extent after 2006 in September, particularly in comparison to the NASA Team data. We saw that the CPOM-CICE model estimates very low September sea ice extent (see section 6.4) throughout the satellite period, whereas it seems that the observations show that a more dramatic decline occurs around 2005 such that the model and observation estimates are now much closer. In December we see RMSEs in CPOM-CICE and reana_bt similar to what we see in March, with the exception of 1987. There are no observations of sea ice concentration in December 1987 after December 3rd, though it is surprising to see that the RMSE of reana_bt could be higher than CPOM-CICE, given that the estimate of reana_bt before the period without observations has a much lower RMSE. We have already seen that the model performs

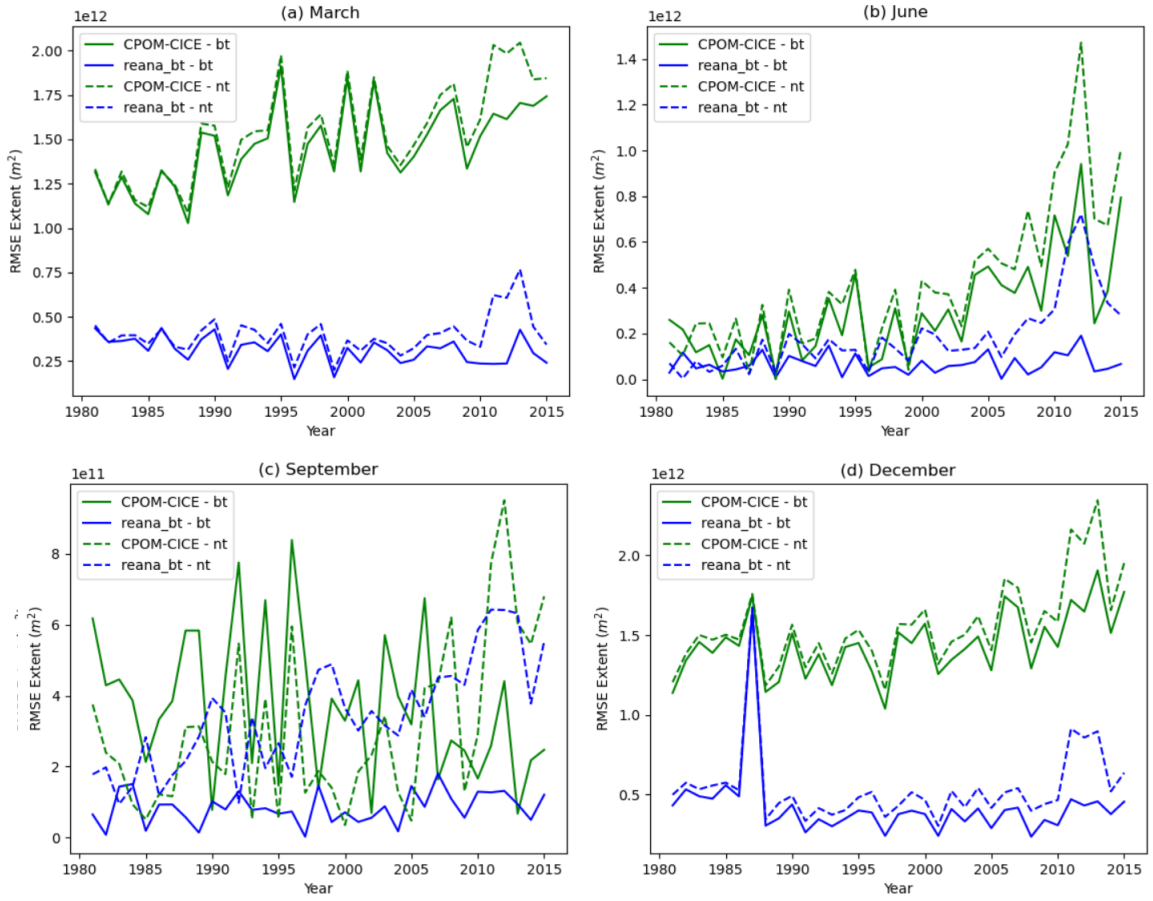

Fig. 6.1 Root mean square error of monthly mean Arctic sea ice extent in March, June, September and December in reana_bt. 'bt' indicates comparison with Bootstrap sea ice concentration and 'nt' indicates comparison with NASA Team sea ice concentration.

poorly in the freeze-up season and this may be evidence of just how poorly it performs without assimilation, even when it is initialised from a sea ice cover that compares well to the observations.

Overall the RMSE is reduced to both NASA Team and Bootstrap when Bootstrap sea ice concentration is assimilated, and for March, September and December the improvement is substantial. In September the RMSE reduction in comparison to Bootstrap is large but because of the uncertainty in sea ice concentration observations at this time it is difficult to fully ascertain how useful the changes made by the assimilation in reana_bt are in relative terms. This RMSE analysis has also shown us some detrimental aspects of the CPOM-CICE model. It does a poor job of capturing the overall trend compared with observations in all four months we studied, especially for June and September trends in the 21st century. The

estimates of the sea ice extent in winter appear to be particularly poor at a time when different sea ice concentration observations generally have good agreement. Given that the differences between NASA Team and Bootstrap ice concentration observations are much more different in the 21st century in June, there may be changes in the melting season in the Arctic sea ice that are not currently reflected in the CPOM-CICE model, given how the RMSE at this time is increasing at a high rate in the 21st century.

6.3.2 Evaluation of Ice Thickness using Cryosat-2

We evaluate the CPOM-CICE model, reana_bt, reana_nt and reana_landy using a 2d histogram plot, which is shown in figure 6.2. CS2 data from all months possible (October-April) between October 2010 and April 2020 is used in this evaluation We only show this for ice thicker than 1 m and thinner than 5 m, because we do not use CS2 ice thickness data thinner than 1 m and because of large uncertainties in CS2 data outside this range, and there is only a very small number of data above 5 m thickness. We use 200 bins, so each bin covers a range of 2 cm of thickness. For ice between 1 and 3 m measured by CS2, CPOM-CICE appears to underestimate the thickness of the ice. If more grid cells are covered in thinner ice between October and April (when we have the CS2 observations), then they are more likely to become completely open water throughout the summer melting season, so CPOM-CICE has a minimum extent which is too low in September. Conversely for regions of the ice cover above 3 m in CS2 the ice appears to be too thick in CPOM-CICE. The distribution of the ice thickness in CPOM-CICE is too heterogeneous, with thin ice too thin, and thick ice too thick, in comparison to the observations. In comparison, when we compare reana_bt to the CS2 observations, reana_bt ice thickness is much closer to the required linear fit, with the majority of grid cells close to a dense control core between 1 and 3 m (though still a slight underfit). The assimilation has improved the ice thickness estimates of the thicker ice (above 3 m) by a lot. In the comparison with CPOM-CICE there were some bins well above the linear fit, but these have almost completely disappeared in the comparison with reana_bt. The reana_nt experiment (c) in figure 6.2 is very similar to reana_bt (b), which shows that the assimilation of the CS2 observations has the dominant impact on changes to the thickness, not the assimilation of different concentration products. The comparison of reana_landy shows the ice thickness in this experiment more closely packed in a thinner arrangement just underneath the linear fit, following a very linear trend, but with an offset to the best fit. As the Landy CS2 data are generally thinner than the CPOM CS2 data this is expected, and we should treat the comparison between reana_landy and the CPOM CS2 data with caution.

Alongside the histogram plots, we also show RMSE and the Pearson linear correlation coef-

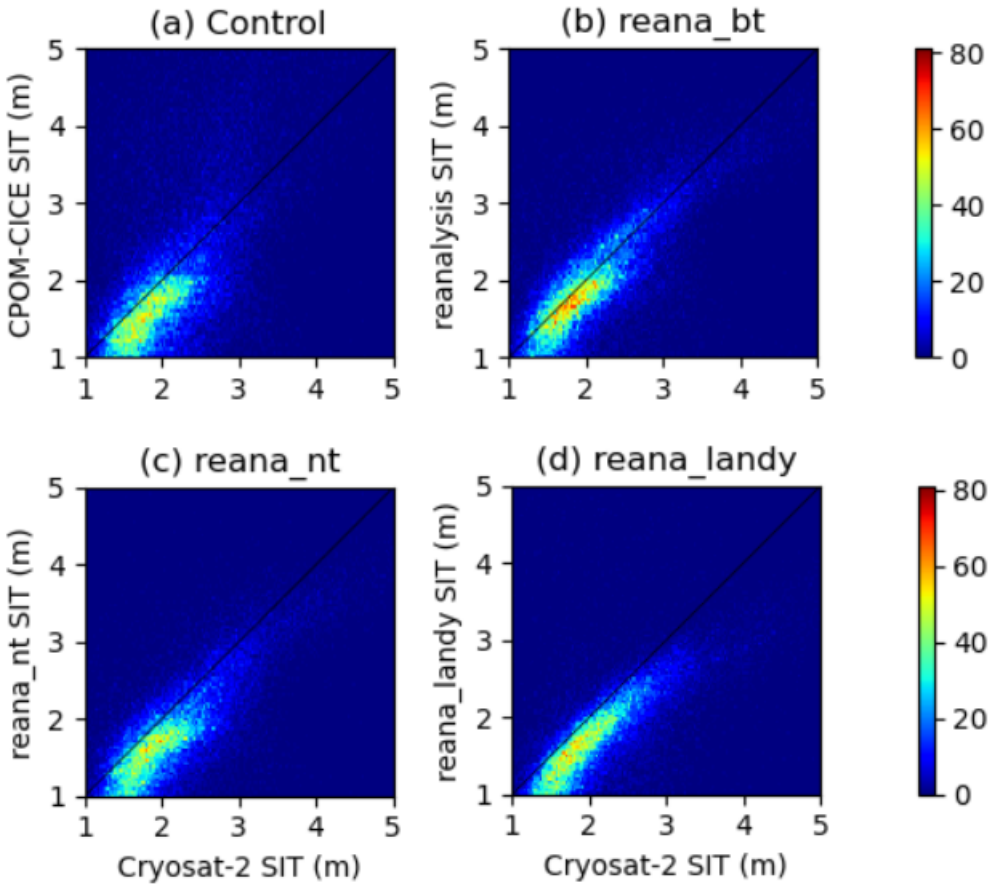

Fig. 6.2 2d histogram plots of CPOM-CICE, reana_bt, reana_nt and reana_landy (ensemble mean) ice thickness against the Cryosat-2 evaluation data. There are 200 bins with a bin size of 2 cm each.

ficient for CPOM-CICE and reana_bt, reana_nt and reana_bt_landy against the evaluation data in table 6.2. The RMSEs in reana_bt and reana_nt are reduced significantly, with ice thickness RMSE 0.72 m lower in reana_bt than CPOM-CICE. The RMSE in reana_nt is slightly lower at 0.27 m, so there are only minimal benefits to estimates of sea ice thickness depending on which ice concentration product you choose to assimilate. The correlation coefficient is higher in reana_bt at 0.64, compared to 0.51 for CPOM-CICE. This further reinforces what we saw in figure 6.2. For reana_nt the correlation coefficient is marginally better, which coincides with what we found for the RMSEs in the two reanalyses. Due to the differences seen when looking at ice below and above 3 m, we also looked at the RMSE in these two different categories. The RMSEs for reana_bt for ice both thicker and thinner than 3 m is similar but the differences in the CPOM-CICE RMSE are larger. We found that the RMSE in ice thicker than 3 m was 1.47 m for CPOM-CICE, but only 0.28 m in reana_bt. The improvement in RMSE for the thickest ice in the Arctic is substantial in reana_bt, and shows how poor the model performs in the regions of the thickest ice. Despite the reduction in RMSE we find that the correlation coefficient for ice thicker than 3 m is almost identical in both CPOM-CICE and reana_bt, which is surprising. We do however see a clear increase in correlation coefficient in reana_bt for ice thinner than 3 m. There are a lot more grid cells with ice thickness below 3 m than above, especially in reana_bt and CS2 data, so there is more uncertainty attached to the RMSE and correlation coefficients on ice thicker than 3 m. Overall we see there are clearly important benefits to the model estimates of sea ice thickness when we assimilate randomly chosen 75% of CPOM CS2 monthly mean ice thickness and thickness distribution in comparison with the 25% of data kept back for evaluation. It is also clear that either choice of sea ice concentration product you assimilate alongside the CPOM CS2 sea ice thickness does not provide any clear benefit to the reanalysis against the CS2 evaluation data.

6.3.3 Evaluation of Ice Thickness using Operation IceBridge

For further evaluation of the reanalyses we also use OIB sea ice thickness data. We use data from 2012-2015 which uses the OIB Quicklook version 1 dataset (Kurtz et al., 2016) and the more reliable Level 4 product (Kurtz et al., 2015) are used. In table 6.3 we show the RMSE for the CPOM-CICE model and the reanalyses. All three reanalyses have better RMSE values to OIB than CPOM-CICE, with the largest reduction in RMSE seen in the reana_landy experiment. Assimilating the Landy CS2 observations then shows a big improvement in sea ice thickness estimates in comparison with independent observations. Given that reana_nt has a lower RMSE than reana_bt and assimilates NASA Team instead of Bootstrap sea ice concentration, it may be possible to find further reductions in RMSE if NASA Team sea ice

Table 6.2 Root-Mean-Square-Error of domain-averaged monthly mean ice thickness (m) and the correlation coefficient for the CPOM-CICE model and our reanalyses (ensemble mean). This analysis is also done separately for ice below and above 3 m thickness.

Experiment	**RMSE (m)**	**Correlation Coefficient**
CPOM-CICE	1.01	0.51
reana_bt	0.30	0.64
reana_nt	0.28	0.65
reana_landy	0.38	0.62
CPOM-CICE ($<$ 3 m)	0.94	0.38
reana_bt ($<$ 3 m)	0.30	0.57
CPOM-CICE ($>$ 3 m)	1.47	0.27
reana_bt ($>$ 3 m)	0.28	0.26

Table 6.3 Root-Mean-Square-Error of domain-averaged monthly mean ice thickness (m) and the correlation coefficient for the CPOM-CICE model and our reanalyses (ensemble mean) against Operation IceBridge observations.

Experiment	**RMSE (m)**
CPOM-CICE	0.54
reana_bt	0.46
reana_nt	0.40
reana_landy	0.29

concentration is assimilated alongside the Landy CS2 thickness data.

6.4 Sea Ice Extent and Area

Firstly, we will investigate the sea ice extent in the reanalyses. In figure 6.3 we show the daily sea ice extent between 1981 and 1987. We look at this early period of the reanalyses to investigate how assimilation of concentration is working. As we would expect, the sea ice extent is affected substantially by the assimilation of sea ice concentration. During the freeze-up season the sea ice extent in reana_bt and reana_nt is decreased when compared to the CPOM-CICE model, with the sea ice extent reduced in both reanalyses at this time. In winter the sea ice extent in both reanalyses is extremely similar, to the point that they can be difficult to distinguish during this time of the year in figure 6.3. Both reana_bt and reana_nt have similar sea ice extent throughout the majority of the assimilation period shown. The only exception being that the melting period begins slightly earlier in reana_nt and it has a

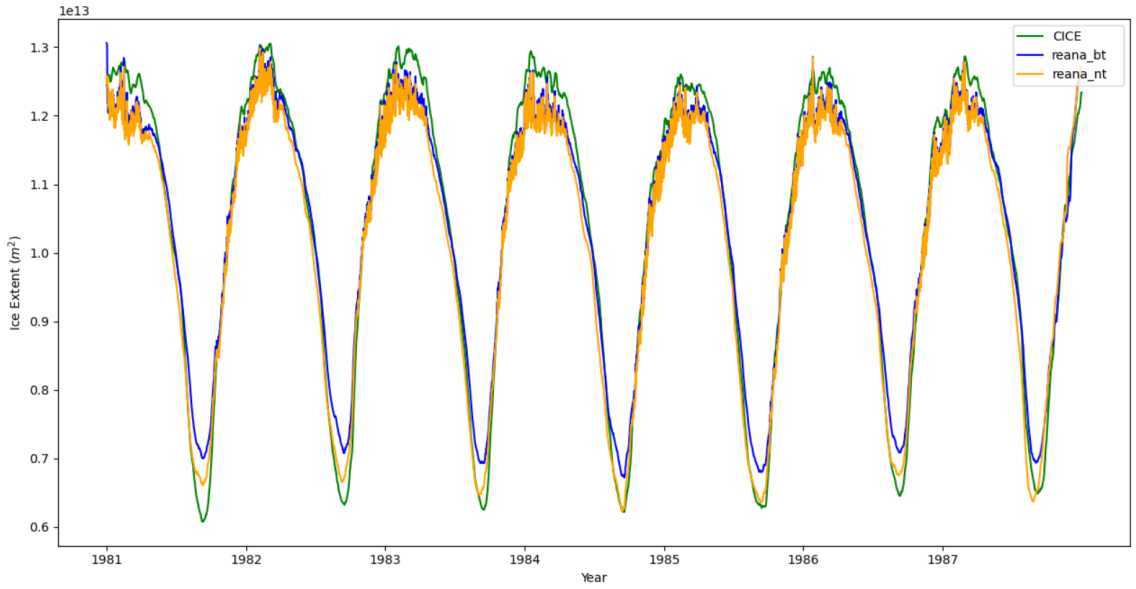

Fig. 6.3 Daily sea ice extent between 1981 and 1987 in the control CPOM-CICE model, reana_bt and reana_nt (ensemble mean).

lower minima in sea ice extent in September - closer to the minimum seen in CPOM-CICE. In comparison to the CPOM-CICE model, the same trend occurs that we saw in the shorter studies in chapter 5, with the interseasonal variation of the ice extent diminished by the sea ice concentration assimilation. If the assimilation of Bootstrap ice concentration is causing a thickening of the central ice pack, this would mean that the number of grid cells that could become completely ice free would decrease because a similar amount of ice loss through thermodynamic effects caused by the atmospheric forcing would not be enough for these grid cells to become ice free. This would cause a higher sea ice extent minima than seen in CPOM-CICE, so therefore, interseasonal variation is reduced. Winter ice growth is larger in CPOM-CICE than seen in Bootstrap, and so both reanalyses moves closer towards CPOM-CICE - with winter ice extent decreased and summer ice extent increased, seasonal variation is much smaller, which is shown in figure 6.3.

In figure 6.4 we show the monthly mean sea ice extents for CPOM-CICE, Bootstrap, reana_bt and reana_nt for March, June, September and December between 1981 and 2019. Note that in March and December the sea ice extents in reana_bt and reana_nt are virtually identical, and the differences are only slightly larger in June and September. This is because NASA Team and Bootstrap generally have strong agreement in terms of extent, but not so much in

terms of ice concentration in summer (Ivanova et al., 2015). In section 6.5, we will see that the main differences, albeit still small, occur at the ice edge. We see that the assimilation is highly effective in moving the sea ice extent estimates closer to Bootstrap observations in both reanalyses, particularly in September. We can also see that both reanalyses follow the trends much closer in the Bootstrap extent than the CPOM-CICE model does. Between 1981 and 2000, sea ice extents in June were similar for Bootstrap, CPOM-CICE and both reanalyses. However since 2000 the June sea ice extent in Bootstrap and the reanalyses are lower than CPOM-CICE, showing that the increasing June ice melt seen in the observations has been reproduced in the reanalyses. This is interesting because it occurs around the same time as sea ice extent in September began to decrease a lot, it may show that the intensive period of the sea ice melt season began earlier than the CPOM-CICE model simulates. On the other hand, the September sea ice extent is lower in CPOM-CICE, so it seems that the melting season overall is too intense in the model. In December and March both Bootstrap and both reanalyses are substantially lower than the model, so the assimilation of ice concentration appears to not be as highly effective as it is in September and June, but there are still large changes.

In figure 6.5 we show the daily sea ice area and marginal ice zone (MIZ) area between 2009 and 2016 in CPOM-CICE, Bootstrap, reana_bt and reana_nt. As ice area is closely related to the extent, some of the interseasonal patterns look similar to the daily extent we saw in figure 6.3. The reason we also look at this plot is to show the MIZ, an important region of the sea ice, where ice is primarily affected by interactions with ocean waves. The MIZ area is defined here as grid cells with ice concentration between 15% and 80%. The MIZ areas in the reanalyses, Bootstrap observations and the CPOM-CICE model are very comparable for most of the year except during the peak melting season. In some years the CPOM-CICE and reana_nt MIZ become larger during the melting period than both Bootstrap and reana_bt, and it is very likely that this increased MIZ area then undergoes further melting and becomes ice free. In fact the additional MIZ area seen in the CPOM-CICE model appears to directly correlate to the decreased sea ice extent in CPOM-CICE. For this reason the ice area in CPOM-CICE is smaller in summer than in the Bootstrap observations and reana_bt. The increased MIZ appears in reana_nt but not reana_bt, so the observations you choose to assimilate are important for estimates of the MIZ. The NASA Team dataset is believed to underestimate concentration when the ice is thin (see section 2.2), so this could be the cause of the increased size of the MIZ in reana_nt.

Our discussion about both the sea ice area and the extent so far appears to suggest that

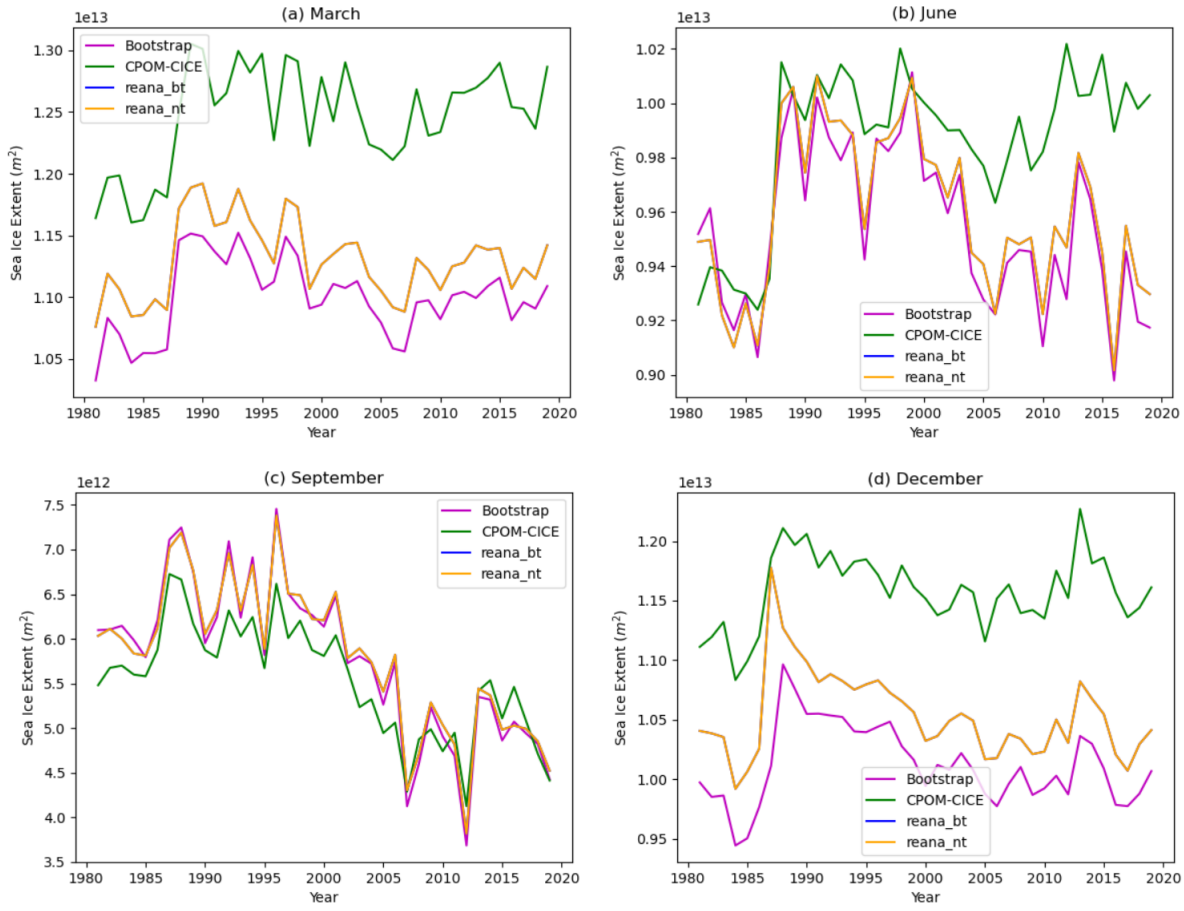

Fig. 6.4 Monthly mean sea ice extent in m^2 between 1981 and 2019 in the control CPOM-CICE model and the ensemble mean of reana_bt and reana_nt in March, June, September and December. Note that the lines for reana_bt and reana_nt are coincident in these figures.

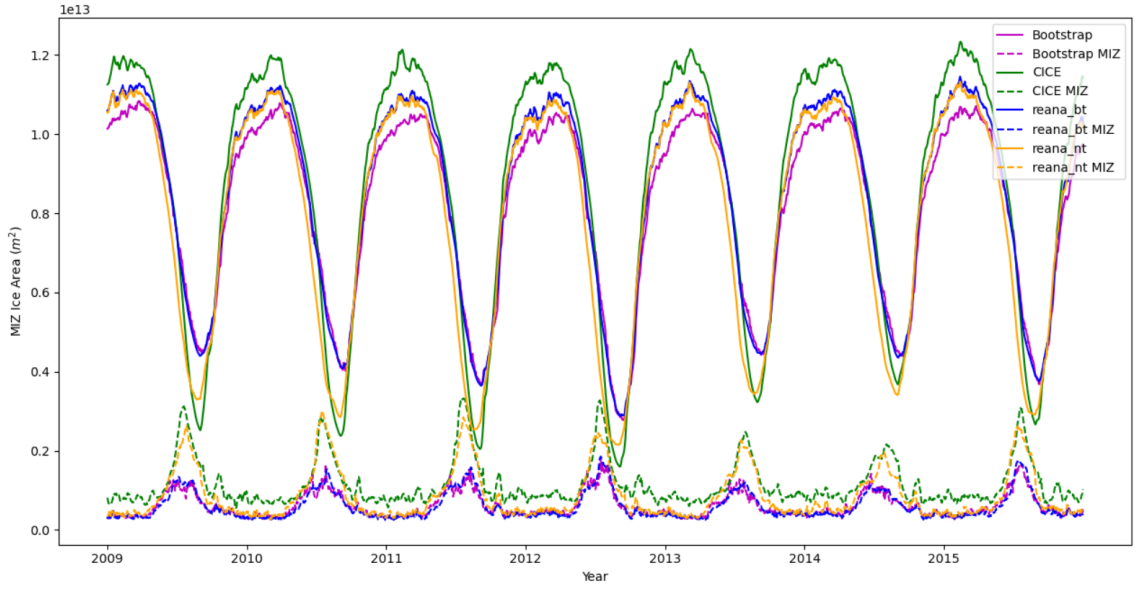

Fig. 6.5 Daily sea ice area and marginal ice zone area in m^2 between 2009 and 2016 in the control CPOM-CICE model, reana_bt and reana_nt (ensemble mean).

the CPOM-CICE model melts thin ice too strongly, whereas thicker ice is less affected thermodynamically by the atmospheric forcing than perhaps it should be in the model during the melting season. An excess of melting and creation of thinner ice in CPOM-CICE would mean that it has a much larger seasonal variation in ice concentration and area than the observations and the reanalyses, which is what seems to occur. However the MIZ areas outside of the July-August period are similar, so the ice growth caused by the forcing is not completely realistic. This could be an issue with the use of the 1D mixed layer ocean model in CICE, the sea surface temperatures are restored to a climatology after 20 days but this restoring is slower than the true process, so more ocean could be frozen than in truth in the CPOM-CICE model. The sea surface temperatures are highly important for modelling changes in the ice cover in the MIZ so it is possible this problem could be reduced by considering the use of an ocean reanalysis to provide forcing data or to couple the system to an ocean model. If we were to use a reanalysis, this could not only improve the sea surface temperatures used to force the model but also provide information about the trends in the sea surface temperature over the reanalysis period. If this sea ice data assimilation system was coupled to an ocean model it would then also be possible to assimilate sea surface temperatures (as is done in PIOMAS over open ocean), to further improve the ice estimates in the MIZ in the system.

The monthly mean MIZ area in March and September over the whole reanalysis period for the

Bootstrap observations, the CPOM-CICE model, reana_bt and reana_nt is shown in figure 6.6. In March the MIZ is relatively stable throughout most of the period in observations, models and reanalyses. There is a large amount of variation in MIZ area seen in the late 90s, with minimum MIZ area in both Bootstrap and reana_bt occurring in 1999. There appears to have been another low point in MIZ area in March during the late 2000s but then a recovery to a slightly higher stable point in the last decade. There is no clear overall trend in MIZ in March over the reanalysis period. The March MIZ area is much larger in CPOM-CICE than our reanalyses and observations in March, double the area in some cases. The model clearly fails to represent the size of the MIZ correctly at this time of the year, though the trend in the MIZ is comparable between CPOM-CICE, Bootstrap observations and reanalyses. The reduction of MIZ area in winter is largest in the reanalyses. However without knowing where the MIZ is each year, this could mean that the central ice pack region is relatively stable, and that only the MIZ is becoming more volatile. In September there is a clear positive trend in MIZ area in the CPOM-CICE model, which as we saw in figure 6.5, seems to happen because of accelerated ice melt in August and September in CPOM-CICE, and the ice in the MIZ is then further melted and later become ice-free. In reana_nt the MIZ area in September is initially similar to that from CPOM-CICE, but in the mid-2000s and thereafter is slightly decreasing, though it varies significantly year on year. It appears that CPOM-CICE is melting too much ice in the Central Arctic (see section 6.7), which is why the sea ice concentrations in this region in CPOM-CICE are lower than in Bootstrap and reana_bt. This could be because the ice is not thick enough in the Central Arctic, so it becomes MIZ and eventually is fully melted, and this ice is thicker in reality which means it remains throughout summer. The increasing trend in CPOM-CICE over the whole period in September MIZ area is $15.1 \times 10^9 m^2$ per year, which given the relative stability of the MIZ in CPOM-CICE in March is significant. For comparison it is around 2.5% of the average MIZ area over the same period per decade. The MIZ in Bootstrap and reana_bt are stable in comparison with CPOM-CICE and reana_nt. The MIZ is too large in CPOM-CICE in March and September over the last twenty years, and there is a trend occurring in the model which does not appear in observations or the reanalyses.

Note that in figures 6.3, 6.4 and 6.5 we account for the hole in the satellite observations that occurs at the pole by interpolating over this region. Although doing this is imperfect, it allows us to make better use of the data for analysing the trends, as the pole hole is much bigger in the early data between 1981 and 1988. Without doing this we would also need to mask the pole hole in our model results and we see an unrealistic increase in ice between 1987 and 1988 as the size of the pole hole reduces. Additionally note that between December

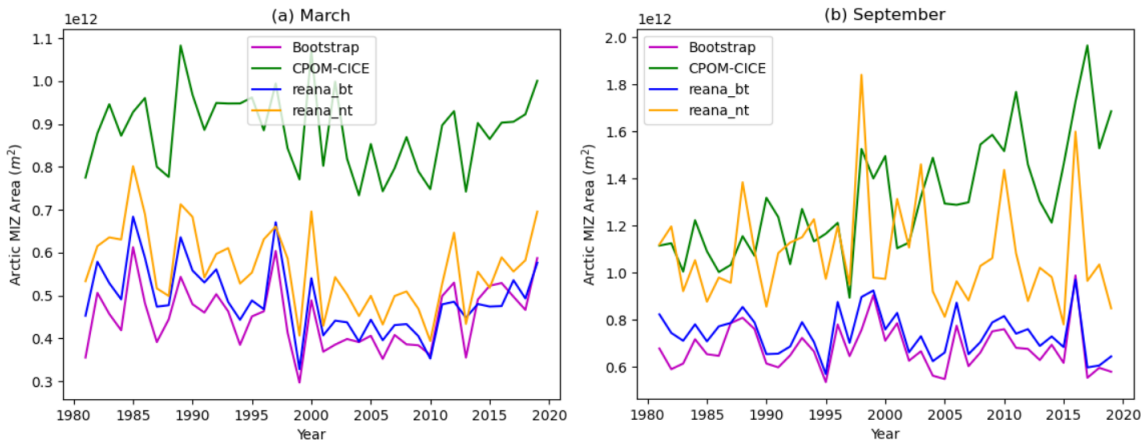

Fig. 6.6 Monthly mean marginal ice zone area in m^2 between 1981 and 2019 in March and September in the Bootstrap observations, the control CPOM-CICE model, reana_bt and reana_nt (ensemble mean).

3rd 1987 and January 13th 1988 there are no Bootstrap sea ice concentration data available, due to a gap in the SSMI brightness temperature observations.

6.5 Regional changes in sea ice concentration

In section 6.4 we saw differences in the sea ice extent and area between CPOM-CICE and the reanalyses. It is important to also try and understand the changes in sea ice concentration on a regional scale. In figure 6.7 we look at maps of mean sea ice concentration for March, June, September and December between 2011 and 2019, the last decade of our reanalysis.

In March the sea ice concentration in CPOM-CICE is greater in Baffin Bay, the Greenland Sea and the Barents Sea, particularly near Novaya Zemlya, which is surrounded by ice in CPOM-CICE but not in either reanalysis. The MIZs are roughly similar, but displaced wherever the ice edge has changed.

There are some very interesting changes in June, where we saw a lot of changes in reana_bt and reana_nt in section 6.4. There are many large areas close to the ice edge which have become devoid of ice in June in comparison to CPOM-CICE. This is particularly noticeable in the north of Baffin Bay, the western Beaufort Sea and the Barents Sea. The ice has retreated much further in the Barents Sea in both reanalyses than it has in CPOM-CICE. In the Chukchi Sea the ice has also receded more in our reanalyses than in CPOM-CICE.

There are, however, larger ice concentrations seen in the Fram Strait and the Greenland Sea, which is a region where ice is exported south from the Arctic Ocean and eventually melts. This could indicate increased melting is occurring in the model from sea ice dynamics, which we will look at in greater detail in section 7.2. The two reanalyses have similar comparisons to CPOM-CICE, but reana_nt has lower ice concentration than reana_bt in many places.

At the nadir of the sea ice extent in September, the mean sea ice concentrations are substantially lower in the Central Arctic in the CPOM-CICE model than they are in either reanalysis, which are highly comparable at this time. CPOM-CICE has a much smaller defined region where the mean sea ice concentration is (or very close to) 1. This decrease in concentration in the Central Arctic is important for when we look at volume in section 6.6 and thickness in section 6.7 later, because the decreases in concentration are seen alongside decreases in thickness and volume, as we would expect.

Finally, in December CPOM-CICE now has greater ice concentrations than either reanalysis in some of the same regions which were noted in March and June. As in March and September, the two reanalyses have very similar ice concentrations. The primary regions in which there are substantial differences in ice concentration between CPOM-CICE and the reanalyses are the Beaufort Sea, Greenland Sea, Baffin Bay and the Chukchi Sea, with the Barents Sea also seeing surprisingly large decreases in sea ice concentration in June and September in both reanalyses. The changes in the Greenland Sea and Baffin Bay are interesting due to the export of ice that happens in those regions. The changes in the Beaufort Sea are also interesting because the differences between CPOM-CICE and both reanalyses are very large, and we see in section 6.7 that PIOMAS estimates ice thickness closer to CPOM-CICE, whereas the reanalyses estimates thicker ice more comparable to CS2.

6.6 Sea Ice Volume in a Satellite era sea ice reanalysis

In figure 6.8 we show the daily sea ice volume in the stand-alone CPOM-CICE model, reana_bt and reana_nt between 1981 and 1987. We are interested in looking at the daily volume for the first few years of the reanalysis period to see how the sea ice concentration assimilation affects the sea ice state when it is the only observation assimilated, because this resulted in higher volume estimates in our intercomparison study (though there are no

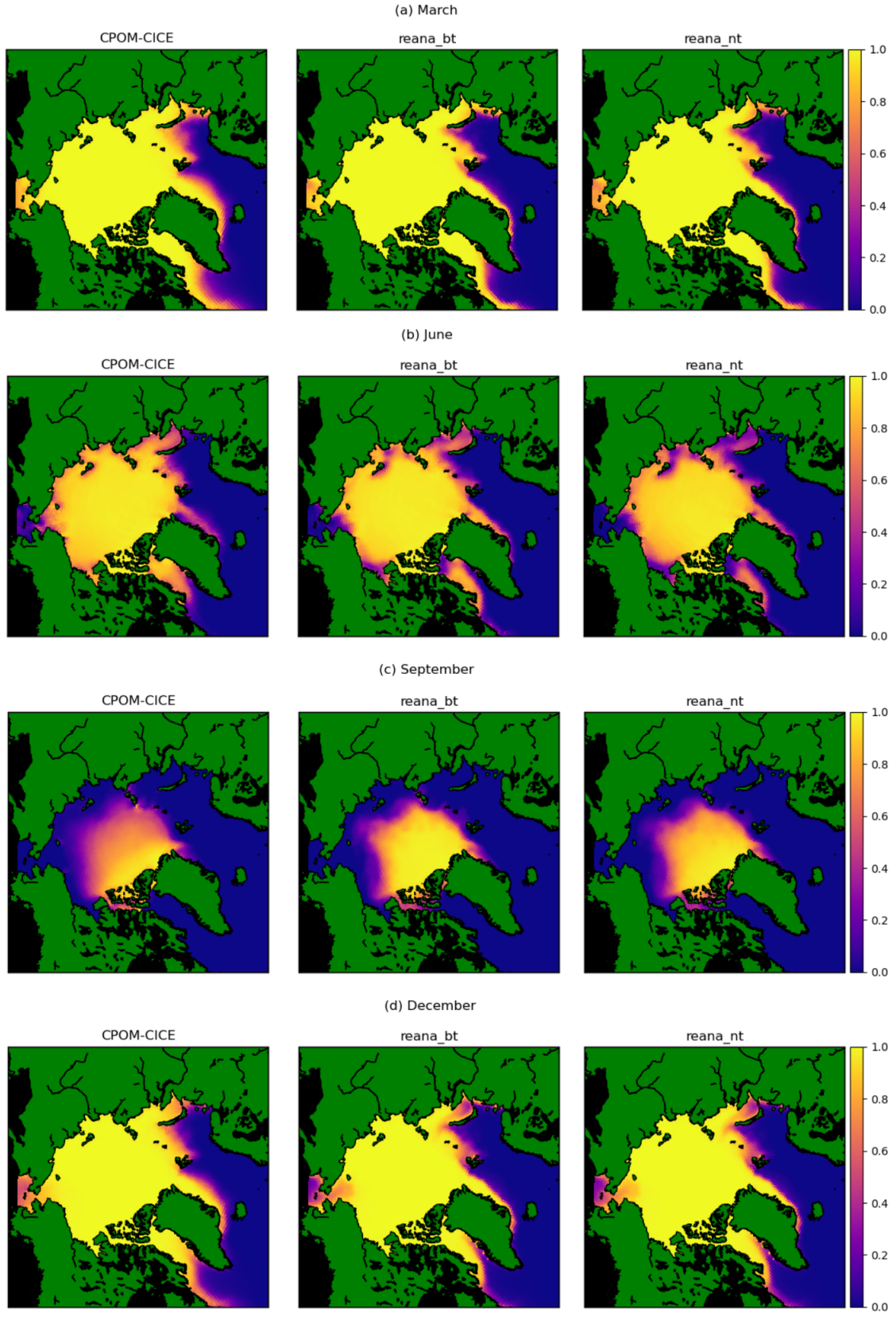

Fig. 6.7 Monthly mean sea ice concentration between 2011 and 2019 in March, June, September and December for CPOM-CICE, reana_bt and reana_nt.

thickness observations in this period). Figure 6.8 shows this happening in reana_bt, and at an increasing trend for this time period. This increasing trend is also shown in the CPOM-CICE model so this is not unsurprising, though the increasing trend in reana_bt is bigger than the CPOM-CICE model. Interestingly the effects of assimilating Bootstrap concentration alone on the sea ice volume are not seen immediately but appear to take place gradually, as reana_bt initially has a lower volume than the CPOM-CICE model until the end of the melting season of 1981. As we saw in the previous section, assimilation of concentration reduces the extent in winter, so we would expect this to reduce the volume as the concentration assimilation should not have an immediate effect on the ice pack, as the ensemble spread will be too small away from the ice edge. What seems to be happening is that the ice concentration assimilation thickens the inner ice pack during the freeze-up season in comparison to the CPOM-CICE model. This would make the ice pack more resilient to melting by the time the melting season begins. It seems that the minimum extent happens slightly earlier in the Bootstrap observations, and when the assimilation creates sea ice during this period it makes the new ice thicker during the initial freeze-up period than the model does when the freeze-up period begins. Some of this ice advects into the Canadian Archipelago, making the thickest sea ice even thicker. Both of these arguments correlate with what we saw happening in the sea ice extent. In this reanalysis we used a spin-up period of two years. While this is sufficient for the ice concentration and most diagnostic variables in the model, this is probably not true for the volume, because it takes time for the ice in the Canadian Archipelago to thicken from the ridging processes in the model.

The most striking result in figure 6.8 is the difference between the two reanalyses. The assimilation of ice concentration in reana_bt and reana_nt has had a similar effect in the first day, with both two volumes beginning from nearly identical points. However they diverge already in the freeze-up season between January and its peak in April. After this, reana_nt sea ice volume estimates are much lower than in CPOM-CICE, while in reana_bt they are much higher. This is expected to some extent, because Bootstrap concentrations are higher closer to the ice edge than NASA Team, and the positive correlations between concentration and thickness would therefore lead to thicker ice covering a larger area in Bootstrap in MIZ regions (see correlation plots in section 4.8.1). However during the melting season the loss of ice volume is much stronger in reana_nt than it is in reana_bt, and there is also less ice growth in the months succeeding the sea ice volume minima. The modelled sea ice volume in reana_nt is on average $0.47 \times 10^{13} m^3$ smaller than in reana_nt, a significantly different estimate.

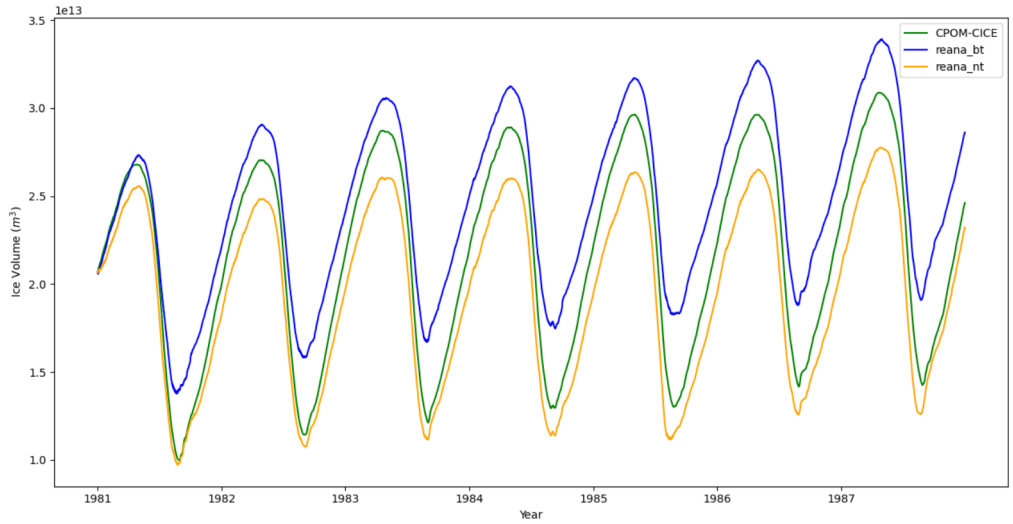

Fig. 6.8 Daily sea ice volume between 1981 and 1987 in the CPOM-CICE model and the ensemble mean of reana_bt and reana_nt.

The daily sea ice volume results show interesting changes occurring when we assimilate sea ice concentration alone, but we should also look at a more recent time period, during which sea ice thickness and sub-grid scale thickness distribution observations are assimilated. In figure 6.9 we show daily sea ice volume from CPOM-CICE and the ensemble mean in our reanalyses. The increments to the volume estimates in reana_bt are substantial after October 2010, the first assimilation time step for CS2 mean thickness and sub-grid scale thickness distribution. Before October 2010 the volume estimates are $5 \times 10^{12} m^3$ larger during the summer minimum and $2 \times 10^{12} m^3$ larger at the winter peak in reana_bt than in reana_nt. In reana_bt there is a big increment in daily sea ice volume in October 2010 and smaller but noticeable increments occur through the first year of assimilation of CS2 observations. The assimilation of CS2 data greatly reduces the ice volume estimates when compared to pre October 2010, with the reana_bt ensemble mean ice volume estimates now lower in winter than in CPOM-CICE. In summer reana_bt still has higher (but not as high as pre October 2010) ice volume estimates than CPOM-CICE. This means that the seasonal variation in the volume, like it was in the extent, has been diminished, an effect we also saw in the much shorter intercomparison study in chapter 5. The lack of observations of mean thickness and sub-grid scale thickness distribution through May to September is affecting the thickness estimates during the latter stages of this period in the reanalyses, as we can see a clear increment in total volume in October 2014. When we assimilate the year-round CS2 thickness observations from Landy et al. (2022), we may find that the volume estimates in CPOM-CICE and the reanalyses are more comparable, because there

are visible volume increments that happen in October which are negative (2011 and 2014 are visible in figure 6.9). Therefore the seasonal variation within the model may not be quite as bad as estimated by the reanalyses, it may just be that winter estimates of sea ice thickness and volume are biased high in comparison with information from observations and reanalyses.

If you compare the volume increments in October 2010 in reana_nt with those in reana_bt, they are much smaller, and less visible in figure 6.9 throughout the period when ice thickness is being assimilated. In reana_nt the ice volume is decreased year-round in comparison with CPOM-CICE and reana_bt, and in winter there is a remarkable decrease in sea ice volume, even though both reana_bt and reana_nt are assimilating the same ice thickness observations, though much smaller than they were before 2010. The only time when any of the experiments are comparable is during September, where reana_nt and CPOM-CICE tend to converge toward similar sea ice volume minima.

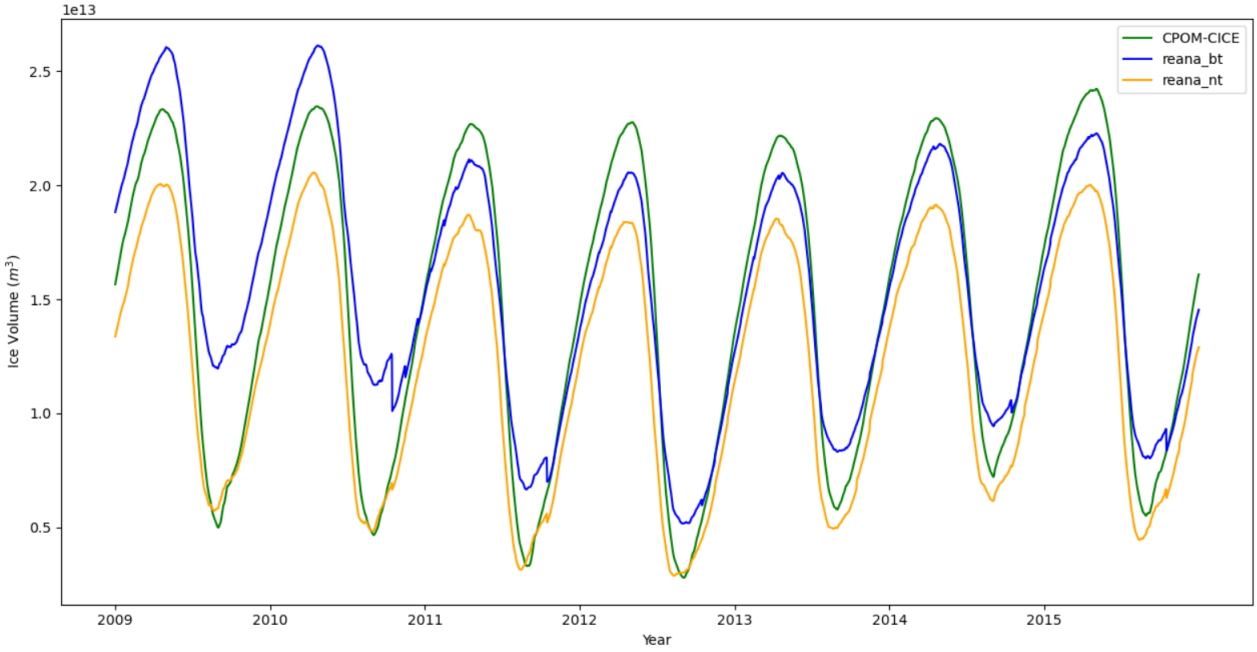

Fig. 6.9 Daily sea ice volume between 2009 and 2015 in CPOM-CICE, reana_bt and reana_nt (ensemble mean).

To further try and understand how the assimilation of the different observations are affecting the reanalyses, we need to look at sea ice volume covering a longer time period. In figure 6.10 we show monthly mean sea ice volumes in March, June, September and December between 1981 and 2020 for the CPOM-CICE, reana_bt, reana_nt and PIOMAS. We see that the

monthly mean volumes are higher between 1982 and 2010 in reana_bt for all months when compared to both CPOM-CICE and PIOMAS, and much higher in March and December. Perhaps unsurprisingly, given that we are now assimilating NASA Team concentration as PIOMAS does, reana_nt is strikingly similar to PIOMAS in both March and December. The reana_nt experiment is less comparable to PIOMAS in June and September, having lower ice volumes during these months. However in some ways it is interesting that PIOMAS and reana_nt are so close, as PIOMAS also assimilates sea surface temperatures in ice-free grid cells, and is a coupled ice-ocean model. It may be that sea surface temperature assimilation is more effective during the melting season, which is why PIOMAS and reana_nt differ in June, or that some sea ice model physics in CPOM-CICE that are not present in PIOMAS (or vice-versa) lead to differences in summer. Perhaps a superposition of these two differences cause the similarities during the growth season and the differences during the melting season. The choice of which sea ice concentration observational dataset you assimilate is very important for the reanalysis estimates of sea ice volume, possibly more important than has been previously understood.

In figure 6.10 there is a substantial change in sea ice volume estimates in reana_bt in 2011 (or for 2010 in the case of December), as the assimilation of ice thickness and sub-grid scale ice thickness distribution begins in October 2010. The sea ice volume estimates for all months are decreased by a lot, showing the strength of the sea ice thickness assimilation, and the drawbacks of assimilating sea ice concentration alone. The effects of ice thickness assimilation on reana_nt are much smaller, but still visible. At the height of the sea ice extent in March, the sea ice volume in reana_bt after 2010 is very comparable to CPOM-CICE, though still higher than PIOMAS and reana_bt. The sea ice volume patterns are similar in December. In June the sea ice volumes after 2010 are lower in reana_bt than CPOM-CICE, and very similar to those from PIOMAS, with reana_nt lower still. June is the month where most disagreement occurs between models, observations and reanalyses. In September the volume estimates split into two groups, CPOM-CICE and reana_bt agree on higher ice volumes, while PIOMAS and reana_nt agree on a lower ice volume estimate. Knowing that CPOM-CICE has a much lower extent in September than reana_bt does we can conclude that the control run has thicker ice within this smaller region than reana_bt does. PIOMAS is most trustworthy during the later decades, as more sea ice thickness data has become available for validating its ice thickness estimates during this period. It seems likely then that the CPOM-CICE model sea ice volume are too high for this period, but the extent is too small according to observations of ice concentration. We will next look at how the thickness compares between the CPOM-CICE model, our reanalyses, PIOMAS and CS2.

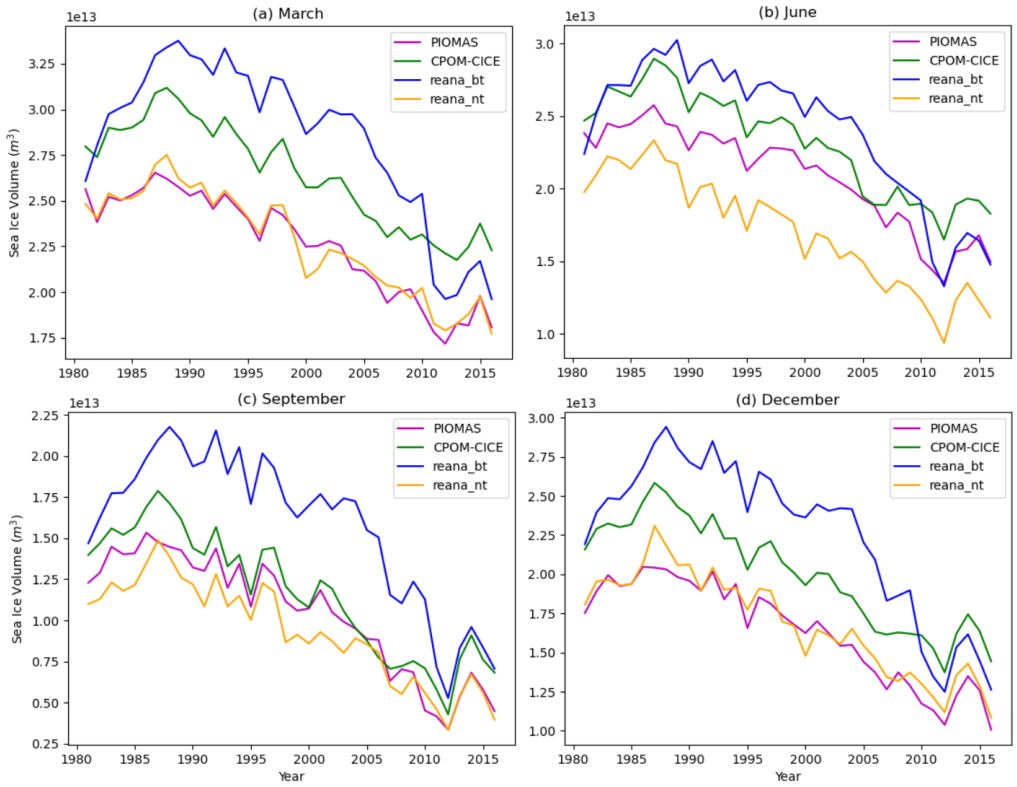

Fig. 6.10 Monthly mean sea ice volume between 1981 and 2018 in March (top left), June (top right), September (bottom right) and December (bottom right) for CPOM-CICE, reana_bt and reana_nt (ensemble mean) and the PIOMAS reanalysis.

6.7 Sea Ice Thickness

We have found that in many cases we have comparable sea ice volumes between our reanalyses and CPOM-CICE, despite very differing estimates of ice extent. This means that the ice thickness in the Arctic must be distributed in different ways. In figure 6.11 we show the daily mean sea ice thicknesses over sea ice covered grid cells for the years 1981, 1982, 2010 and 2011. This helps give us more understanding of how the assimilation of concentration affects the sea ice thickness and how the assimilation of the CS2 products affects the thickness in the first few months that it becomes available. In 1981 both reanalyses initially have higher mean thicknesses than CPOM-CICE, because the assimilation of concentration is removing regions of thinner ice at the edges of the model. Between June and September, the three

models diverge, with reana_nt thinning much more than reana_bt, and by the end of 1981, reana_bt is 34 cm thicker on average than reana_nt and 28 cm thicker than CPOM-CICE. In 1982 the same effect again occurs during this time of the year. This seems to show that a lot of ice forming in reana_bt is thicker than in CPOM-CICE, which might occur because the Bootstrap observations at this point have a greater ice extent than CPOM-CICE does, so when assimilation of Bootstrap concentration occurs, the ice added due to the assimilation is too thick. This concurs with what we saw in the sea ice volume. By 2010, the assimilation of Bootstrap ice concentration has resulted in ice which is 30-40 cm thicker during some parts of the year than in the control. CPOM-CICE and reana_nt on the other hand remain much more comparable even at this time. In the middle of October 2010, the first assimilation of mean ice thickness and sub-grid scale thickness distribution takes place, and there are effects on the mean thickness of the sea ice area, reducing it in reana_bt by 40 cm, a significant amount. The effect on reana_nt is much smaller, only about 10 cm. Subsequent increments in the next 6 months have a noticeable but substantially smaller impact in reana_bt, with mean thickness only reducing a few cm at assimilation time steps. In October 2011 the changes caused by the assimilation are not as drastic in reana_bt as the year before, with around a 20 cm decrease, but this can still have substantial effects on the model state, and make the post analysis step processing necessary. Interestingly the increment in October 2011 in reana_nt is still around 10 cm, but the rest of the time is still unnoticeable in figure 6.11.

We show maps of mean ice thickness in June, August, October and December 1981 in CPOM-CICE, the reanalyses (ensemble mean) and PIOMAS in figure 6.12. It is notable that PIOMAS has smaller regions of thicker ice, especially in August, October and December where there are only a few grid cells with mean thicknesses above 3.6 m. PIOMAS appears to have a much larger seasonal variation in the ice thickness in the Lincoln Sea and the Canadian Archipelago than CPOM-CICE and both reanalyses, because the region of ice between 3.6 m and 5 m disappears almost completely in October but is very large in June. In June the only noticeable difference is that this region of the thickest ice is slightly smaller, otherwise all four maps look relatively similar, though PIOMAS has some thick ice in the East Siberian Sea. In June and August, the thinnest ice in CPOM-CICE, PIOMAS, reana_bt and reana_nt cover a very similar area. However in August CPOM-CICE has a region of ice thicker than 2.4 m that is much larger than both the reanalyses and PIOMAS. In October the same situation occurs with the thicker ice comparison between CPOM-CICE and our reanalyses, however the area of ice between 1.4 and 2.4 m thick is substantially larger in reana_bt than it is in CPOM-CICE. October is where this area of ice in reana_bt was larger

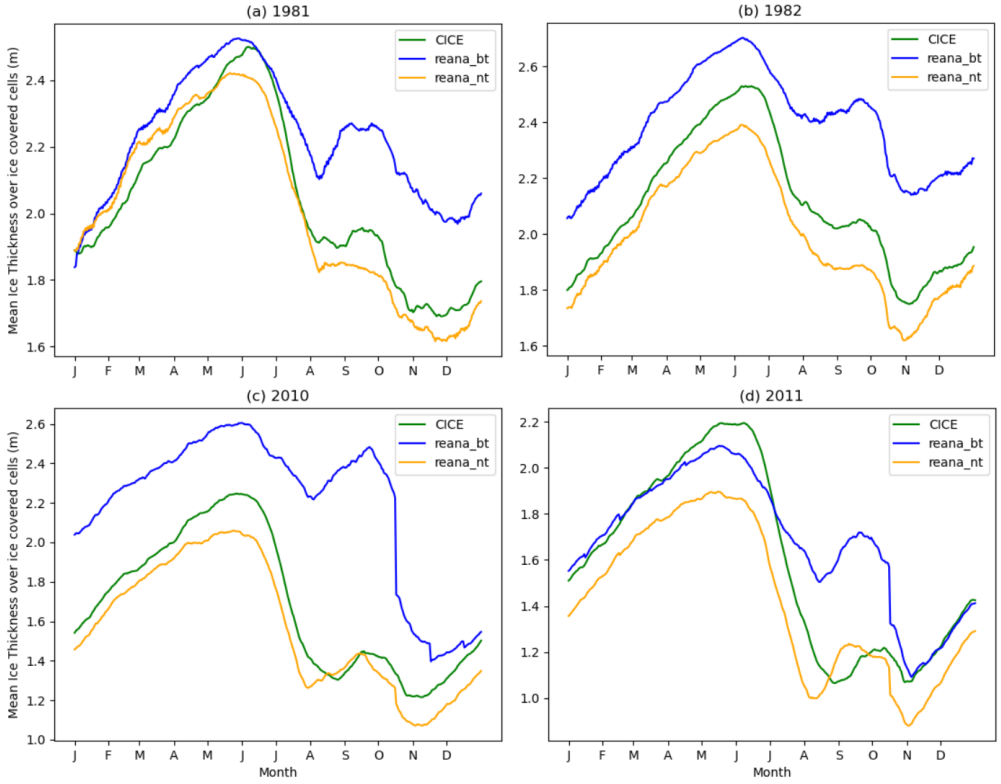

Fig. 6.11 Daily mean sea ice thickness in CPOM-CICE and reana_nt and reana_bt (ensemble means) where ice thickness is greater than 0.15 m in 1981, 1982, 2010 and 2011.

than that in the CPOM-CICE model for the first time in figure 6.12. It may be then that the cause of this issue is open water areas that are close to the ice edge during the early freeze-up season, where there is more likely to be higher open water fractions in the model. As concentration is positively correlated to thickness, increases in concentration caused by the assimilation may also thicken the ice too much. There is enough ensemble spread in these regions at this time such that the assimilation can have an effect on the model, which is not possible at any other time because ensemble spread will be low in the ice pack in winter. In summer the observed concentrations and extent are lower than in CPOM-CICE, so the assimilation is usually removing ice instead of adding it. In December there is a large region of ice between 2.4 and 3.6 m in the Beaufort and Chukchi seas which occurs in reana_bt but not to the same extent in the other models. The ice in the Barents Sea is also thicker in reana_bt than in the other models, the increase in ice thickness in these regions probably explains the overall increase in mean ice thickness we saw in figure 6.11.

Now we have looked at the ice thickness in the early period of the reanalysis, we want to look at how the assimilation of the CS2 products affects the mean ice thickness after 2010 and how

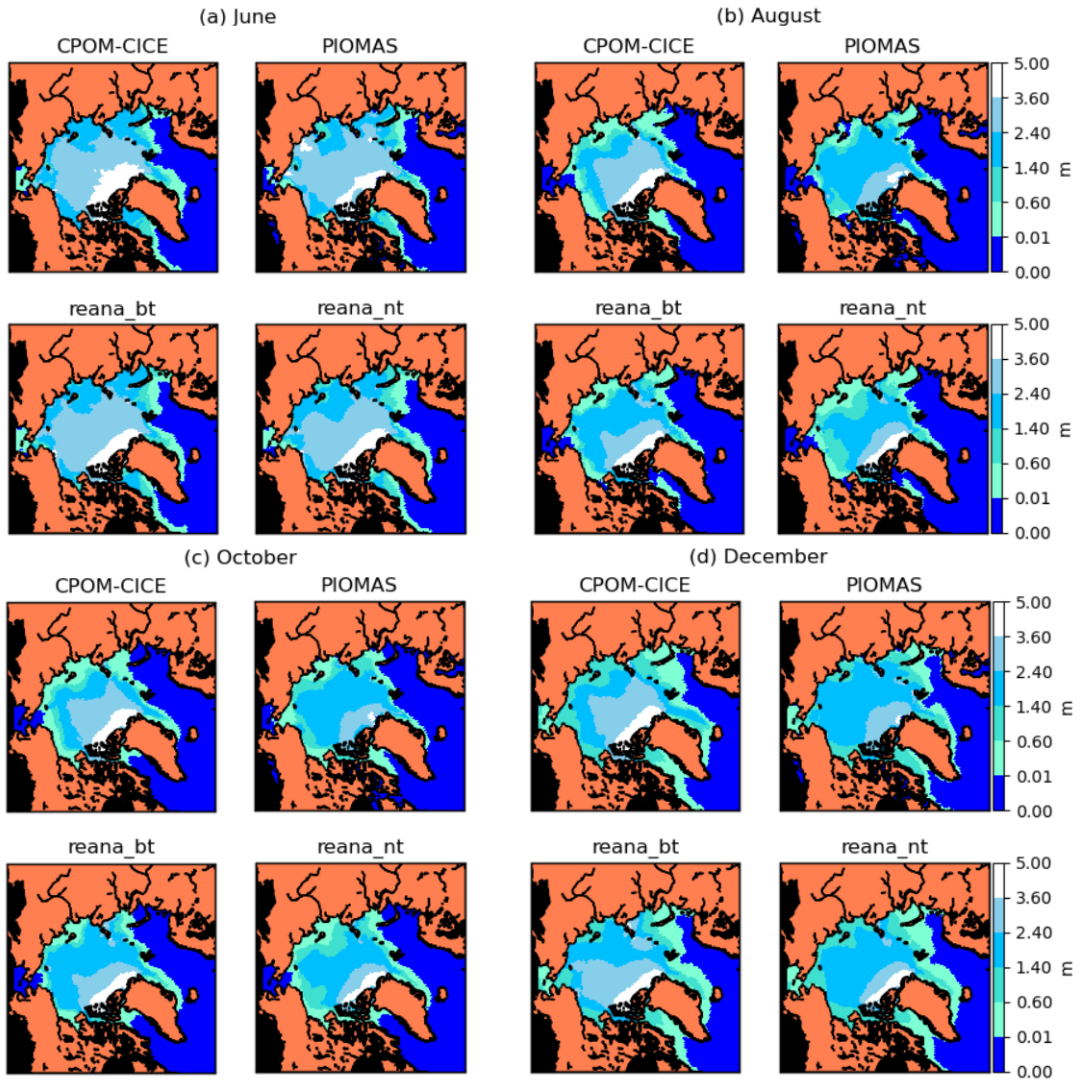

Fig. 6.12 Monthly mean sea ice thickness in June, August, October and December 1981 for CPOM-CICE, reana_bt, reana_nt (ensemble mean) and PIOMAS.

it compares with CS2 and PIOMAS. In figure 6.13 we show the March and October monthly mean sea ice thickness in CPOM-CICE, reana_bt, reana_nt, CS2 and PIOMAS in 2012 and 2017. In March 2012 it is striking how similar the reana_bt and PIOMAS thicknesses are, especially with the region of ice thicker than 3.6 m looking very comparable in broad terms. At the same time, reana_nt is also similar, but with a smaller region of ice thicker than 3.6 m. The only notable difference between PIOMAS and the two reanalyses in March 2012 occurs in the Barents Sea, with PIOMAS ice thinner in this region. In October 2012 reana_bt has thicker ice than in PIOMAS in the Central Arctic and Canadian Archipelago, but the regions of thin ice are now very similar, reana_nt matches PIOMAS even in the region of thick ice at this time. We previously looked at comparing data assimilation results with those from CS2 for ice thickness in 2012 in chapter 5, so for the reanalyses we also look at a later year, 2017. The mean ice thicknesses in March and October 2017 for the most part tell the same story as the 2012 results, though PIOMAS and both reanalyses are slightly more different than they were in 2012. In October 2017 both reanalyses have ice thicknesses much closer to that of CS2 than PIOMAS, as PIOMAS ice in the central pack is too thin relative to CS2. In general PIOMAS ice thickness is slightly thinner than CS2 especially on the outer regions of the ice pack. Conversely both reana_bt and reana_nt tend to do well in these regions, but the ice thickness close to the North Greenland Coast and the Canadian Archipelago is too thick. CPOM-CICE ice thickness is too thick in the Canadian Archipelago and North Greenland Coast in both March and October in comparison to both the CS2 observations, PIOMAS and our reanalyses. CPOM-CICE has ice that is much too thin in the Central Arctic, but the ice that piles up against the Canadian Archipelago in the model is much thicker than seen in CS2, PIOMAS or the reanalyses. In March CPOM-CICE has a much greater extent than PIOMAS, reana_bt and reana_nt, but the regions of thin ice (thinner than 1.4 m), are too large. This clearly identifies a problem in the CPOM-CICE model whereby too much ice gets packed into a small region against the Canadian Archipelago, and this ice is not undergoing the same rate of melting as in PIOMAS or observations. There is also too much thin ice in CPOM-CICE in March.

In the previous section, we saw how monthly sea ice volume estimates in CPOM-CICE and PIOMAS in September were similar, however, by looking at maps of the mean thickness, we have seen a significant difference in how this is distributed across the Arctic. Although CPOM-CICE estimates of volume appeared to be similar to PIOMAS, the distribution of the ice thickness in each model is very different, PIOMAS has a much higher sea ice extent in summer and autumn than CPOM-CICE, and in PIOMAS and CS2 the thickness of the ice is

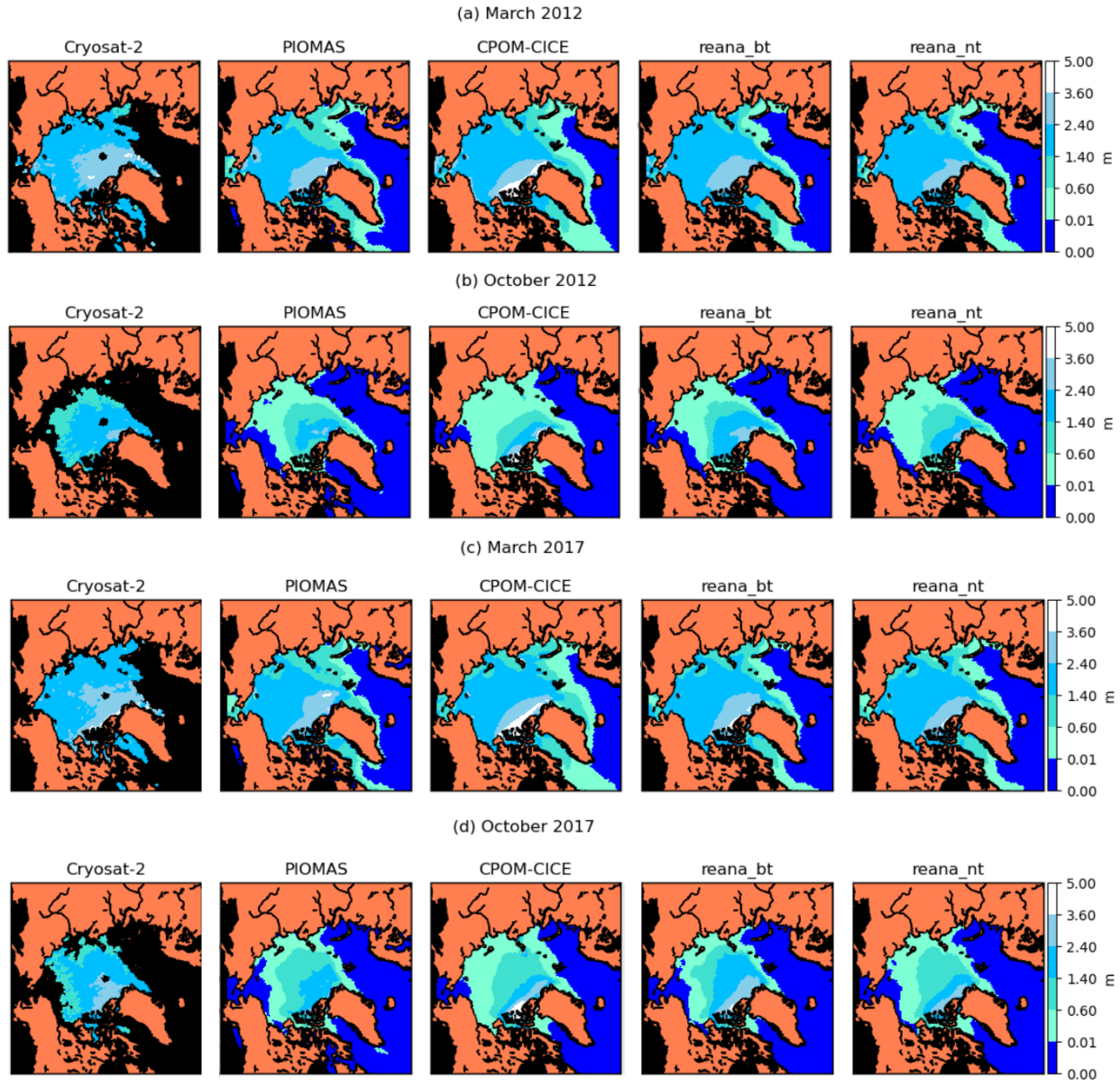

Fig. 6.13 Monthly mean sea ice thickness in March and October for CPOM-CICE, reana_bt, reana_nt (ensemble mean) PIOMAS and Cryosat-2 in 2012 and 2017.

more homogeneous. In CPOM-CICE there is an increasing gradient in the thickness of the sea ice as you move away from the ice edge. This shows the importance of looking at changes in the sea ice state on different scales, and the importance of assimilating thickness products for extending our knowledge of the sea ice state at smaller resolutions. We saw decreases in both concentration and thickness between October and July in the Chukchi Sea, Barents Sea, Greenland Sea and Baffin Bay in the last decades of both reanalyses. Conversely the ice concentration and thickness was increased in the Central Arctic because of the assimilation, which is particularly notable during summer as the increase in ice thickness means more of this ice cover is able to survive in the reanalyses, and this means that both reanalyses have a greater ice extent in summer than CPOM-CICE. The reana_bt reanalysis generally has slightly more thicker ice than reana_nt after 2010, and substantially (likely too much) more beforehand.

6.8 Changes in Pan-Arctic Thickness Distribution

In section 6.7 we saw wide scale changes in the mean ice thickness across the Arctic throughout the year, with big differences between CPOM-CICE and the reanalyses in the Canadian Archipelago, Central Arctic and the Barents and Kara Seas in the past decade. Overall it seemed as though the distribution of thickness in reana_bt and reana_bt was becoming more homogeneous, with the thickest ice thinning and the thinner ice getting thicker. To see whether this assessment is true we look at the distribution of the mean thickness across the Arctic in four different months over the 2011-2019 climatological mean, which are shown in figure 6.14. In general, we see that the sea ice thickness did become more homogeneous in reana_bt, with the distribution in CPOM-CICE covering a much wider range than in reana_bt. In all months there is also very little ice above 4 m thick in reana_bt, whereas in CPOM-CICE there is ice between 4 and 5 m in a non-negligible number of grid cells. In March reana_bt has much less ice between 0 and 2 m thick (some of which is explained by the greater sea ice extent in CPOM-CICE), but more grid cells with ice between 2 and 4 m thick. This will mean that some regions should be less vulnerable to summer melting when the melt season begins. In June, the ice cover is simply more homogeneous in reana_bt, with most ice cover between 0 and 2 m thick.

In September there are a lot of grid cells with less than 1 m ice in CPOM-CICE, but this distribution tails off rapidly to about 3 m thickness, and then much more slowly so that there are still many grid cells with ice thicker than 4 m. In reana_bt the peak of ice thickness is still at the thinnest ice, but the distribution tails off at a more constant rate, with very few

grid cells of a mean thickness above 4 m. This echoes what we saw in 6.13, with a decreased area of very thick ice in reana_bt in comparison to CPOM-CICE, but a wider area of ice over 1 m thick. In December the thickness distribution in reana_bt is very interesting, with the ice cover evenly distributed between 0 and 3 m thick, but with almost no grid cells with ice thicker than 3 m, and in fact, fewer grid cells with ice over 3 m thick than there were in September. This is interesting because it is further evidence that points toward the ice growth of very thick ice being overestimated in the early freeze-up season, but there is also less area covered by ice 1.5 and 3 m thick in CPOM-CICE. CPOM-CICE appears to grow thin ice (less than 1 m thick) too rapidly in the freeze-up season but some of this ice does not thicken enough in comparison to reana_bt or the CS2 observations. This underestimation of ice over 1 m thick was also seen in Schröder et al. (2019).

It has been shown that the sea ice dynamics and Fram Strait export have a strong impact on the winter ice thickness (Ricker et al., 2018), and also that winter atmospheric conditions only play a small role in Arctic sea ice growth and the ice thickness in the late freeze-up season (Schröder et al., 2019). In both reanalyses the ice is thicker at the end of the freeze-up season in March, but occurrence of mean ice thicknesses of 4 m and above are very few or non-existent, so there is a need for additional melting in regions of very thick ice not captured in the CPOM-CICE model. Using these reanalyses we can see that the ice growth in CPOM-CICE is overestimated at the ice edge, but also underestimated in the Central Arctic. We see that the difference between the CPOM-CICE thickness distribution and the thickness distributions in the reanalyses were much larger than the differences between reana_bt and reana_nt, also seen in figure 6.14. The thickness distribution is more strongly weighted towards lower thicknesses in reana_nt, particularly for June and September. In September reana_nt is even more strongly weighted towards grid cells with thin ice than we see in reana_bt, with very few cells containing ice of a mean thickness above 3 m. The reana_nt reanalysis is more strongly peaked throughout most of the year, closer to the distribution shape of CPOM-CICE, but with a smaller distribution overall. There seems to be most agreement between models and observations in terms of both concentration and thickness in late winter, between February and April. These results agree with our analysis of the sea ice thickness and volume, with reana_nt showing thinner ice and a decrease in Pan-Arctic volume in comparison to reana_bt.

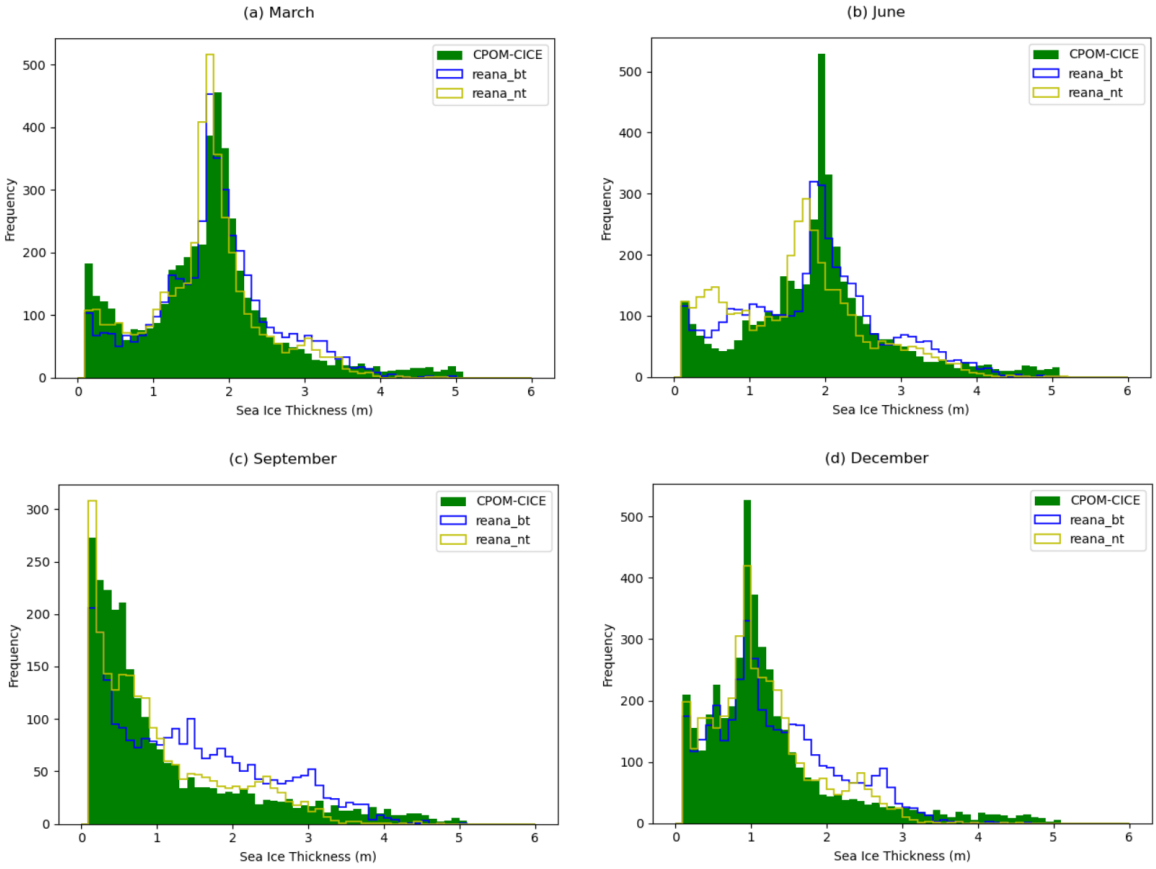

Fig. 6.14 The distribution of grid cell mean thickness across the Arctic in CPOM-CICE, reana_bt and reana_nt in March, June, September and December between 2011 and 2019. Only grid cells with a mean thickness greater than 10 cm are included, bin width is 10 cm.

6.9 Summary

In the first part of this chapter we presented the first results from new Arctic sea ice reanalyses using a stand-alone sea ice model, for the first time assimilating observations of the sub-grid scale thickness distribution from the CPOM CS2 data. We have investigated the reanalyses in three different ways in this chapter. We looked at the differences between the reanalyses and the control model, the long-term trends in extent, thickness and volume in the reanalyses, and the changes in the thickness distribution in the reanalyses. The record of long-term decline in sea ice extent is clearly reproduced in the reanalyses, as is present in the control model, though the assimilation of the Bootstrap ice concentration does severely impact thickness and volume estimates. We would recommend that a lot of care should be used when assimilating the Bootstrap sea ice concentration dataset. We have found that assimilation of sea ice concentration, thickness and thickness distribution can produce reliable estimates of concentration, thickness and therefore volume in the Arctic in a long-term reanalysis, though in this case the results have only been verified when all three were assimilated together, post-2010. It was found that the reanalysis estimates are much closer to both sets of observations than the control. All three reanalyses are evaluated in comparison with sea ice thickness data from the CPOM CS2 data held back for evaluation and independent Operation IceBridge sea ice thickness measurements. In comparison with the CPOM CS2 data reana_nt has an RMSE 2 cm lower than reana_bt, with a similar correlation coefficient. There may be a possibility to reduce RMSE further by assimilating Landy CS2 observations alongside NASA Team sea ice concentration. We found that both reana_nt and reana_bt have a lower sea ice extent than CPOM-CICE throughout most of the year except in August-September, as the CPOM-CICE model creates a lot of thin ice cover during the freeze-up season but this does not thicken enough during the freeze-up, so more of the sea ice cover is melted away in CPOM-CICE by the end of the melting season. As the thin ice in sea ice models is primarily thermodynamically driven, this indicates issues in the modelling in the thermodynamics.

We found that the long term trends in the Arctic sea ice cover were reproduced well by the reanalyses in comparison to observations of the extent and the PIOMAS reconstruction of Arctic sea ice volume. Our reanalyses show a clear decreasing trend in both extent and thickness, and subsequently volume, as a result of the increased warming in the Arctic, though there is substantial uncertainty before 2010 due to the availability of thickness observations. There are relatively few long term records of the Arctic sea ice state which go further than assimilating only sea ice concentration in terms of sea ice model variables (even PIOMAS does not), so this is further evidence of the loss in Arctic sea ice volume seen in previous studies, as mentioned in chapter 3. We found that the thickness distribution of the

reanalyses was much different to that of the control CPOM-CICE model, with a smaller range of thicknesses in the reanalyses due to a lack of grid cells with very thick ice. Many more grid cells in reana_bt and reana_nt are covered in ice with a mean ice thickness of 2 - 4 m, but with comparatively little above this, in comparison with the control run. Our reanalyses appear to estimate that the Arctic sea ice cover has become more homogeneous over the 40-year reanalysis period, and more homogeneous overall than previously estimated. However as the grid cell resolution is quite large, so we should be careful as small scale features could still feature heavily in regions of multi-year ice.

Chapter 7

A Satellite Era Arctic Sea Ice Reanalysis: Part II

7.1 Overview

This chapter represents Part II of the analysis of our newly produced satellite era Arctic sea ice reanalyses between 1981 and 2019. In section 7.2 we discuss changes in the volume fluxes in the reanalyses and compare them with CPOM-CICE. In section 7.3 we investigate the long term trends in the reanalyses in much greater detail. The ensemble spread in the reanalyses is studied in section 7.4. In section 7.5 we assimilate the recently produced Landy CS2 observations of sea ice thickness, which include observations of summer sea ice. The Landy CS2 observations are assimilated in place of CPOM CS2 observations, and we compare the results with our other reanalyses. The results are discussed in further depth in sections 7.6 and 7.7, including identified ways of improving both the CPOM-CICE model and the reanalysis. The chapter is summarised in section 7.8.

7.2 Volume Budget Changes

Ensemble-based data assimilation allows quantities other than those directly observed to be updated, in a way that is consistent with the ensemble's statistics. This means that changes in the state vector of the model made by the assimilation should lead to improved modelling of the sea ice at future time steps, and hence better attribution of the changes that are occurring in the sea ice. One of the reasons we have undertaken this reanalysis is to create a better understanding of why the sea ice cover is changing rapidly with climate change. We can do this by looking at what processes are driving changes in sea ice area and volume in the

model, and how these change between the control CPOM-CICE model and our reanalyses. The processes driving area and volume changes are split into to main categories in the model: dynamical and thermodynamical. The dynamical processes describe changes due to ice drift, ridging and other mechanical processes. The thermodynamical processes are split into congelation, the formation of ice at the bottom of existing ice cover; snow-ice formation, ice forming from snow and seawater on the surface of floes; frazil, the formation of ice crystals on the sea surface; sublimation, the process by which ice turns directly into water vapour; and then melting processes, which are subdivided into top, lateral and basal. We also look at these changes and compare them with area and volume changes made by the LETKF. We will only look at the area and volume fluxes for the last decade of the reanalysis period (2010+) because this is the period of the CS2 observations.

7.2.1 Total annual ice volume changes

In figure 7.1 we show the Pan Arctic sum of the volume fluxes between 2011 and 2020 (in grid cells with ice concentration above 0.15) for each of the processes described above, and the volume changes made by the assimilation. In the reanalyses, the contribution from the assimilation increment is larger than many of the sea ice model processes, but the congelation growth dominates as the source of ice volume change over the period, with a smaller contribution from frazil ice formation. Snow-ice formation contributes very little. There is a decrease in congelation in reana_bt in comparison to CPOM-CICE which is compensated by an increase in frazil ice formation. This happens because the assimilation tends to decrease the ice cover in the Arctic when compared to CPOM-CICE (see section 6.4), so there is less ice area available for ice congelation growth to occur. As a result of this, open water area has increased, and as we do not change the ocean forcing between CPOM-CICE and our reanalyses, this means that frazil ice formation will be possible in these areas as the ocean will still be (or become) cold enough for this to happen. In reana_nt there is higher congelation growth and frazil ice formation, as reana_nt removes even more ice concentration than reana_bt, this could be the model trying to counteract the effects of the assimilation. This could also be a positive effect from the assimilation which results in thicker ice in the Central Arctic, which does not occur in the the CPOM-CICE model.

Snow-ice formation has decreased in both reanalyses but it only contributes relatively little to the overall ice formation in either experiment. Overall, the relative changes in ice formation between CPOM-CICE, reana_nt and reana_bt are small. Conversely, there are substantial

changes to processes contributing to a decrease in the ice volume. Contributions from dynamical processes have tripled towards a decrease in sea ice volume in reana_bt and doubled in reana_nt compared to CPOM-CICE. This may be a sign of the changes to the ice cover we saw in the Fram Strait export region, which we saw in section 6.7 and section 6.5. Basal melt has decreased in both reanalyses in comparison to CPOM-CICE, and this seems another positive effect from the assimilation of ice thickness, as this ice should be thicker according to observations. The changes in top melt are interesting, with reana_bt seeing an increase in top melt, but reana_nt seeing a reduction in comparison to CPOM-CICE. This difference is small in relative terms but intriguing, and would have to be the result of changes to the temperature or enthalpy of the sea ice made by the correlations. The differences in volume due to the assimilation are very different in reana_bt and reana_nt, and primarily the cause of the differences between the two reanalyses. Besides the assimilation, the main reasons for the volume difference between the reanalyses and CPOM-CICE are congelation growth, top melt, basal melt and dynamics. In reana_bt the differences in the melting processes are responsible for 45% of the difference in volume flux in comparison with CPOM-CICE between 2011 and 2020, if you do not include the contribution from the assimilation the melting processes are responsible for 81% of the difference. For reana_nt the difference in congelation to CPOM-CICE is larger, the changes due to the assimilation are greater, and thus the melting processes are less responsible (29%). As this is looking over the whole period, there could likely be seasonal changes in these processes which are important. In order to understand these changes further we will look at volume fluxes in this period in four different months of the year.

7.2.2 Monthly resolved ice volume changes

The Pan Arctic volume fluxes from each process in each month between 2011 and 2019 in grid cells with ice concentration above 0.15 for CPOM-CICE, reana_bt and reana_nt are shown in figure 7.2. In the first three months of the year (the second half of the freeze-up season) congelation growth is by far the dominant process driving sea ice volume changes, as would be expected. Frazil ice formation is stronger in both reanalyses, meanwhile dynamic processes and changes from the assimilation represent stronger decreases in ice volume in reana_bt and reana_nt. The effects of basal melt though are strongly reduced in both reanalyses. In reana_nt there is increased congelation between January-March, which is counteracted by an additional decrease in volume caused by the assimilation. There are some

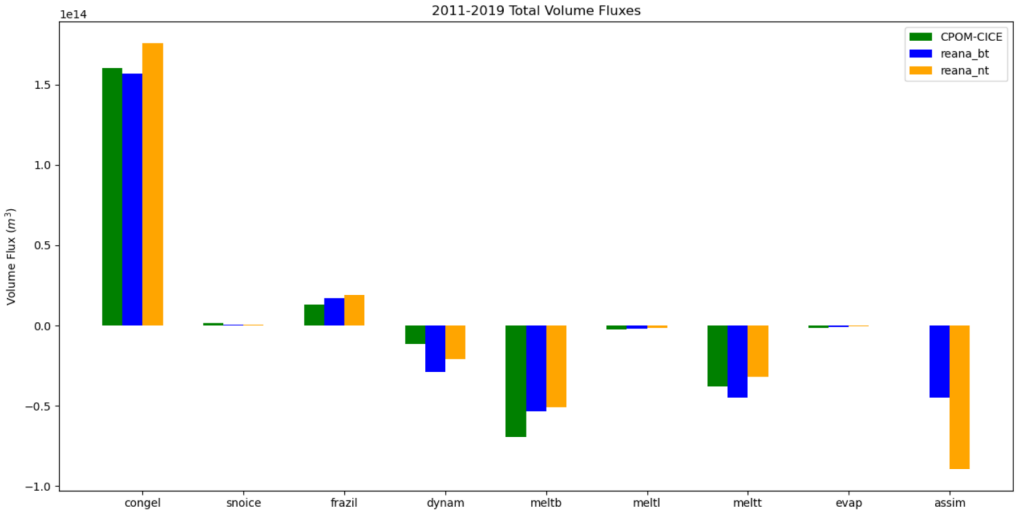

Fig. 7.1 Pan Arctic contribution to sea ice volume fluxes between 2011 and 2019 by each of the different physical processes in the model, volume changes made by the data assimilation, and the total volume flux in CPOM-CICE, reana_bt and reana_nt (ensemble means). Note that 'congel' refers to congelation, 'snoice' refers to snow-ice formation, 'dynam' refers to volume changes due to dynamics, 'meltt' refers to top melt, 'meltl' refers to lateral melt, 'meltb' refers to basal melt, 'evap' refers to sublimation and 'assim' refers to assimilation.

minor changes in some of the other processes but these are negligible in terms of the total volume flux. As we expect there is an increase in sea ice volume during January-March in all runs, but both assimilations lead to a reduction in sea ice volume. The net decrease in ice volume fluxes is relatively small in comparison to total sea ice volume in this period. In April, the assimilation strongly reduces the ice volume added in the reanalyses, reana_bt has just over half the volume increase seen in CPOM-CICE, and reana_nt has a small fraction of CPOM-CICE.

May is a very interesting month in terms of volume flux, in CPOM-CICE the volume flux is small compared to other months, with ice formation and melting mostly cancelling one another out. The assimilation removes a huge amount of ice in both reanalyses and particularly in reana_nt. The beginning of the melting season in May (and June) are much stronger in the reanalyses than in CPOM-CICE. We see again that the dynamical processes in the reanalyses cause a stronger decrease in volume than in the control. Relative to the changes made by the assimilation, the changes in the other contributions are minimal. The ice volume reduction in June in reana_bt is $1.5 \times 10^{13} m^3$ greater than CPOM-CICE over the 2011-2019 period, while for reana_nt it is $2.4 \times 10^{13} m^3$ greater, a reduction in sea ice

volume of almost double than that seen in CPOM-CICE. Some of this difference is likely explained by how the sea ice concentration in both observational datasets in comparison to CPOM-CICE is much smaller, so we expect that some of this change is accounted for by a decrease in ice area. In July the differences in the volume fluxes are smaller, though the melting in reana_bt and reana_nt is still stronger. In August we see for the first time that the assimilation is adding ice, which is again stronger in reana_nt. This results in a much smaller loss in ice volume for reana_nt, however for reana_bt an increase in basal melt and top melt mean that more ice volume is lost in August than in CPOM-CICE. The choice of assimilating Bootstrap or NASA Team sea ice concentration lead to very different sea ice volume changes over the melting season.

In September we see the most striking differences between the CPOM-CICE and the reanalyses, ice formation is substantially decreased in both reana_bt and reana_nt, and melting is increased. This melting effect is stronger in reana_bt. This is interesting because neither reanalysis has assimilated thickness observations for five months, yet the difference between the model and reanalyses are largest at this time of the year. The possibility of introducing thickness observations in summer could then be very important for constraining the volume. In all three models the minimum sea ice volume occurs at this time of the year, but is greater in reana_bt (see section 6.6). The melting season is either stronger or lasting further into September in both reanalyses than in CPOM-CICE, because ice growth is weaker and melting is stronger. However the assimilation is adding huge amounts of ice volume in September with concentration observations alone. In fact, without the assimilation of the ice concentration, the total ice volume would have decreased in both reanalyses in this month. A lot of ice volume is added in reana_nt, but more ice volume is removed in reana_nt during the melting season which negates this effect.

In October the freeze-up season is much stronger in CPOM-CICE than in reana_bt, which is caused by differences in congelation, with the assimilation only accounting for around 25% of the differences between reana_bt and CPOM-CICE. The ice volume flux in reana_nt is much closer to the CPOM-CICE estimates, and the assimilation in reana_nt only contributes to a small decrease in the total volume flux. This seems to show that the ice growth in October is too strong in the model, though this could be balancing out the lower volume flux in CPOM-CICE in September. The ice area in both reanalyses is smaller at this time, but not enough to account for the total congelation difference. The high congelation growth in the CPOM-CICE model in this month could be responsible for the ice being too thick in the area close to North Greenland and the Canadian Archipelago, which is an important

difference between the model compared with reanalyses and observations. In November and December, as we saw in January, February and March, congelation growth is the dominant process driving changes in ice volume, with only relatively small decreases in the reanalyses in comparison to CPOM-CICE. As the ice cover is smaller in winter in the reanalyses (see section 6.4), this means that a smaller area of ice has increased in thickness in comparison to CPOM-CICE. Frazil ice formation is increased at the same time, which is probably because there is an increase in ice-free areas where the ocean is cold enough for this to occur. There are also changes to the dynamics and basal melt, similar to those we saw in March. The assimilation only accounts for a relatively small change in the sea ice volume between CPOM-CICE and the reanalyses during these months, the differences are comparable with those in the basal melt and the dynamics between the two systems.

Somewhat surprisingly the largest changes in volume fluxes appear to be occurring in months where ice thickness and sub-grid scale ice thickness distribution is not being assimilated. This could be caused by spurious correlations between ice concentration and ice thickness during the melting season which have unwanted effects on ice volume when only ice concentration is assimilated. This demonstrates that the CS2 products are having important year-round impacts not only on the modelled sea ice state but on the processes occurring within the model, even though they are assimilated as a monthly mean for only seven months of the year. Here we have identified some processes which have undergone significant changes in both reanalyses either throughout the year or at important times of the year, therefore we would now like to try and understand where and then why these changes have occurred.

7.2.3 Changes to Congelation Growth

Congelation growth was reduced by almost half in September and by about a quarter in October in reana_bt in comparison to CPOM-CICE, which has important consequences for the early freeze-up season. In figure 7.3 we show the differences in congelation between CPOM-CICE and the reanalysis ensemble mean over 2011-2019 for these months. In September there are differences over a large region covering most of the Central Arctic where the reanalysis has much lower congelation than CPOM-CICE. This area of lower congelation growth has increased in October and covers much of the Arctic sea ice cover at this time of year. Interestingly the one region of ice cover where there are no changes is the region which packs up against the Canadian Archipelago and North Greenland (at least in CPOM-CICE). We know the assimilation of CS2 observations reduces the ice thickness a lot in both reanalyses in this region (see section 6.7), but there are very few differences in ice concentration between model and observations. It is positive that the changes made

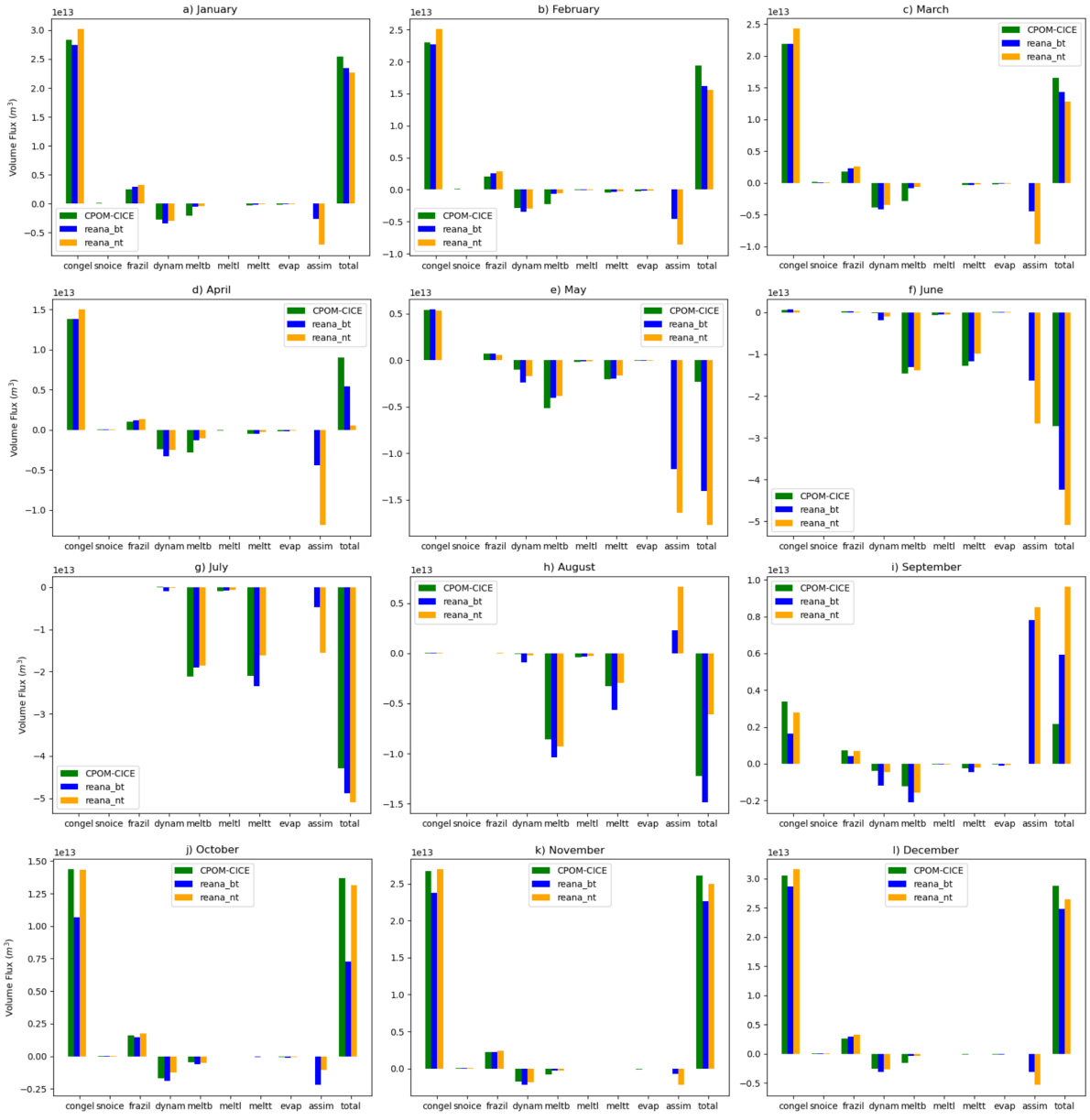

Fig. 7.2 As Fig. 7.1, but separated into months for the period 2011 to 2019.

to the thickness in the Canadian Archipelago by the thickness assimilation do not affect congelation growth in this area - the changes made to the temperature and possibly other thermal properties of the sea ice by the correlations are stopping the model trying to thicken the ice to the level seen before assimilation.

We also saw differences in congelation growth between reana_nt and CPOM-CICE in the latter freeze-up period, and we show the February and March differences in figure 7.3. The reason for the increased congelation growth in reana_nt at this time is because of increasing congelation growth at the sea ice edge. This is not surprising because the assimilation of sea ice concentration reduces the concentration in this area during the freeze-up season, but the model attempts to regrow the ice here because of the ocean forcing used. This shows that care is required in interpreting the volume flux changes because they may be a result of the model attempting to counter the changes made by the assimilation. The differences in the congelation growth between CPOM-CICE and both reanalyses are a result of correlations in the LETKF with the temperature and/or enthalpy of the sea ice in the CICE state vector, as our reanalysis setup does not make any changes to the ocean forcing setup from the CPOM-CICE model. This shows how useful the LETKF and more modern data assimilation techniques can be in comparison to optimal interpolation and nudging methods.

7.2.4 Changes to Dynamical Processes

We have seen that the dynamical processes of the sea ice have caused additional ice volume loss in both reana_bt and reana_nt, this occurs year-round, but is strong (particularly for reana_bt) between June and September. In figure 7.4 we show sea ice volume flux in cm/day (cm^3 of ice per cm^2 of grid cell area) between 2011 and 2019 in June and September in CPOM-CICE and its differences with reana_bt and reana_nt for June and September. In June both reanalyses appear to have more sea ice volume being advected due to dynamics to within a certain area, which also results in a decrease in the area surrounding this. This effect is stronger in reana_bt than in reana_nt but both have similar patterns in comparison to CPOM-CICE. There is stronger ice loss due to dynamics in the Western Fram Strait, and ice volume gain in the Eastern Fram Strait, so both reanalyses appear to be shifting the export pattern of the sea ice further away from the east coast of Greenland. There is also an arc pattern in Baffin Bay occurring in both reanalyses in comparison to CPOM-CICE, with sea ice being shifted from the west of Baffin Bay to an arch pattern surrounding Western Baffin Bay. In September the story is not so clear, reana_bt has stronger differences with

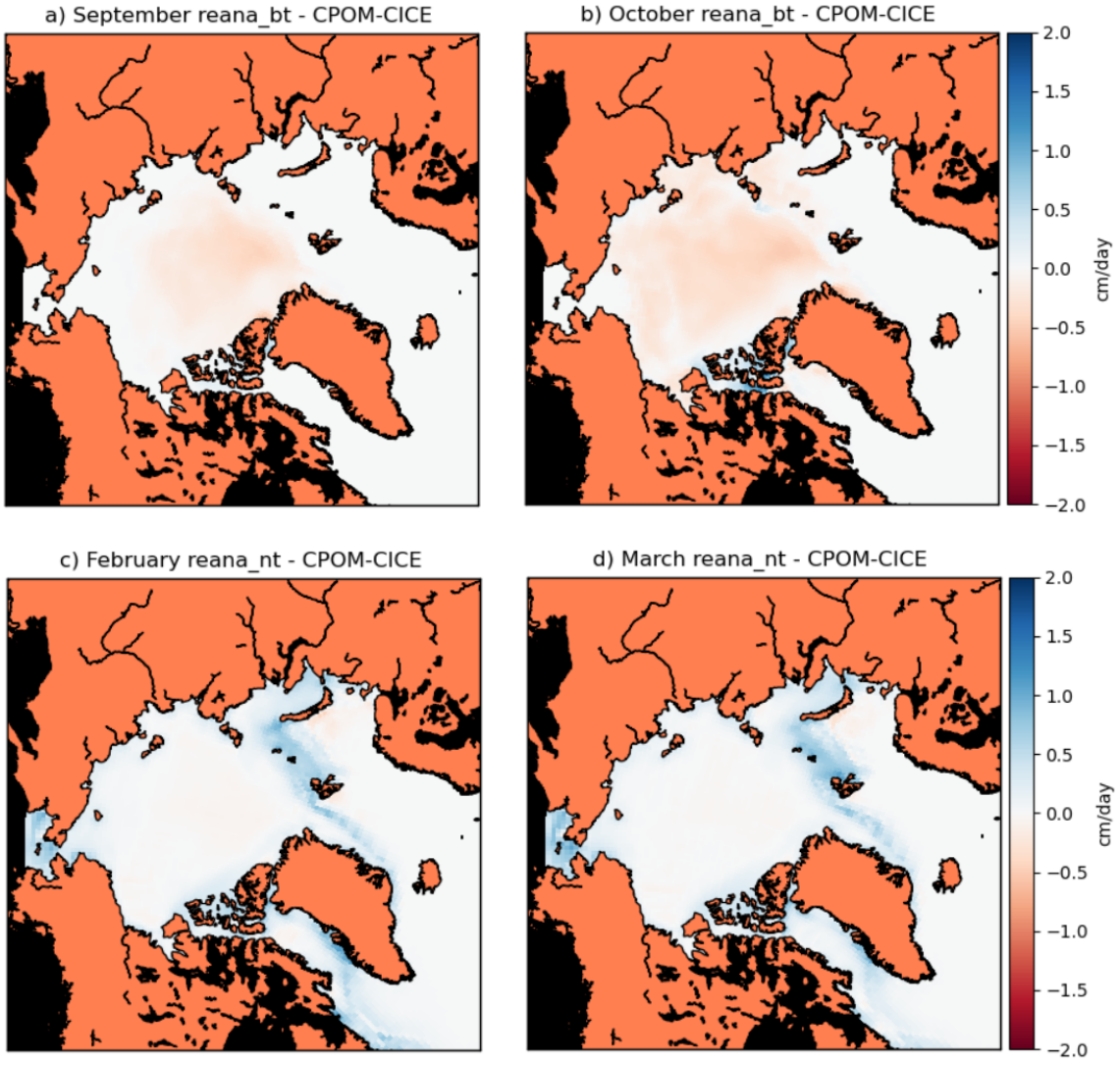

Fig. 7.3 Plotted are differences between reanalyses and CPOM-CICE, reana_bt minus CPOM-CICE is plotted for (a) September and (b) October, and reana_nt minus CPOM-CICE is plotted for (c) February and (d) March

CPOM-CICE than reana_nt does, but there is less of a pattern. There appears to be a region which is close to the ice edge at this time of the year where there is more ice volume loss due to dynamics, with the surrounding areas again compensating. The additional sea ice volume loss in the outer regions of the thicker ice pack could be caused by additional divergence of sea ice floes in these areas. In June this could occur because these regions are now closer to the marginal ice zone, where there is more open water and hence there is more possibility of these regions being influenced by ocean currents. However the key pattern that has carried through from June are the changes in both reanalyses in the export region of the Fram Strait. Both reanalyses clearly agree on a change in ice advection in the Fram Strait, though they disagree as to the strength of these changes. In some areas where additional ice is lost from dynamical processes in the reanalysis, we also see additional loss from basal melting (see section 7.2.5), so it seems likely that increased open water fraction is playing some role in the elevated sea ice loss we see in the reanalysis.

7.2.5 Changes to Basal Melting

For most of the year, Basal melting was reduced in both reanalyses (November-July) in comparison with CPOM-CICE, and increased between August and October, with reana_bt seeing a greater increase in comparison to CPOM-CICE than reana_nt. We will look at the differences in March and September, which have two clearly contrasting patterns. September was also interesting because in both reanalyses it was the most impactful process driving changes in the sea ice volume, whereas congelation growth was more important in CPOM-CICE. In figure 7.5 we show the basal melting (in cm/day) in March and September in CPOM-CICE and its differences with both reana_bt and reana_nt. In March the reduction in basal melt clearly occurs because of the reduced sea ice extent in both reanalyses, which have similar sea ice extents at this time. There is a small increase in basal melt in some grid cells close to the ice edge, which is probably negligible. In September, there is a strong increase in basal melt in both reanalyses in the Fram Strait, which could be due to increased ice cover here as the ice export in this region has increased in both reanalyses. In reana_bt there is increased basal melt in the East Siberian Sea, Beaufort Sea and the Northern Chukchi Sea, which is balanced out by some weaker basal melting in the Southern Chukchi Sea. In reana_nt the increases in basal melt in these regions are not as strong, but the reduction in basal melt in the Southern Chukchi Sea is of a similar amplitude, so Basal melt is not as strong in reana_nt as in reana_bt. As we have seen with the volume fluxes due to the

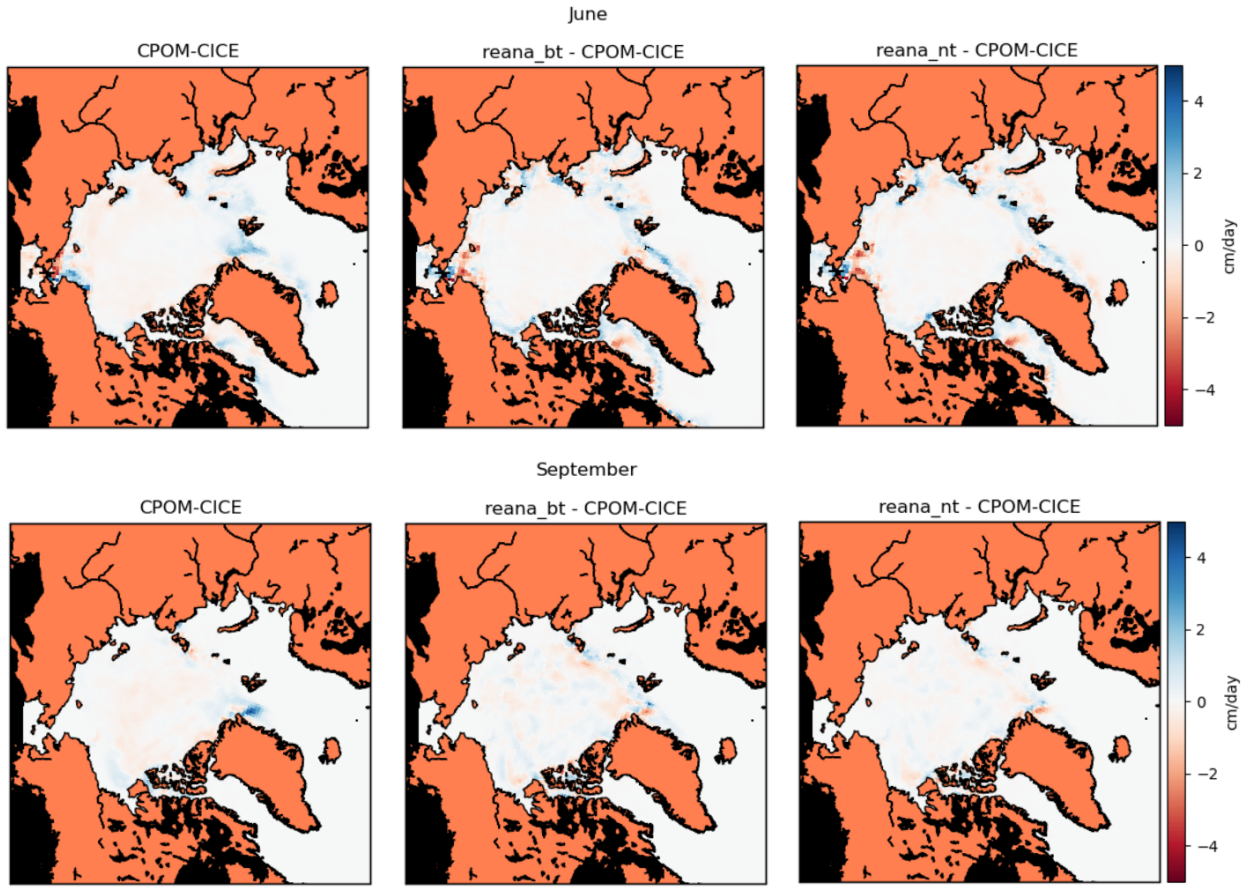

Fig. 7.4 Volume Flux Tendency due to dynamical processes (advection, ridging, convergence) in cm/day in June (top) and September (bottom) between 2011 and 2019 for the reanalyses ensemble means (left), CPOM-CICE (middle) and their difference (right)

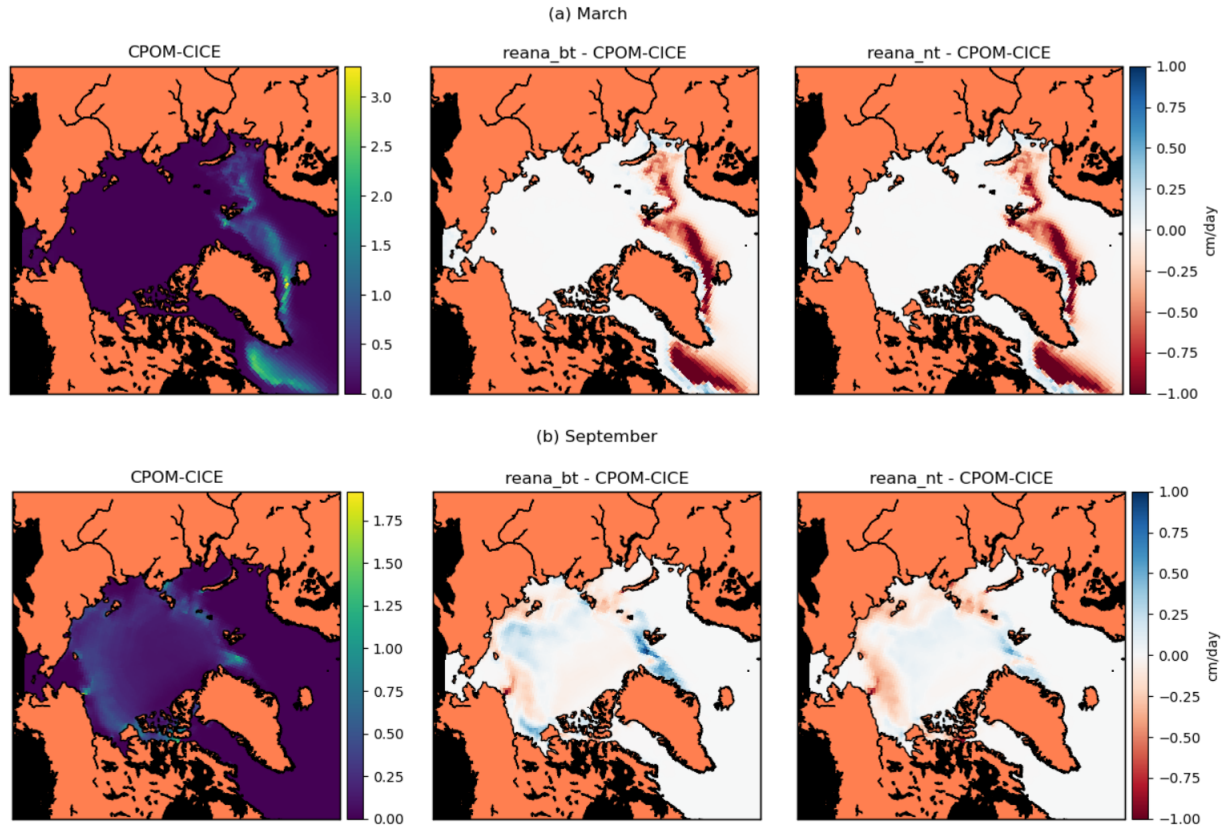

Fig. 7.5 As for Fig 7.4 but for March and September basal melting

dynamical processes, reana_bt and reana_nt agree for the most part on the patterns of the changes with CPOM-CICE, but not on their amplitudes, with changes in the East Siberian Sea and the Fram Strait standing out for the basal melt.

7.2.6 Changes to Top Melting

In July and August there are stark differences between the top melt seen in CPOM-CICE, reana_bt and reana_nt. In general throughout summer reana_nt had lower top melt than the other model runs, whereas reana_bt had comparable or higher top melt in comparison to CPOM-CICE. In figure 7.6 we show top melt in July and August in CPOM-CICE and the difference between each reanalysis and CPO-CICE. In July, top melt is much stronger

in reana_bt in a large region covering a lot of the Central Arctic, though there are some areas of decreased top melt covering a smaller region in the central pack, and the Fram Strait, Baffin Bay, Beaufort Sea and the Barents Sea, which are covered by thinner ice at this time of the year. Conversely, in reana_nt there is a strong decrease in top melt in most regions, with only the innermost ice pack seeing a comparable or slightly increased top melt in comparison with CPOM-CICE. As only concentration is assimilated at this time of the year these effects are occurring either directly from correlations between ice concentration and the thermodynamical properties of the sea ice within the assimilation scheme, or indirectly because of the changes to the sea ice concentration. Thickness observations though have been assimilated in previous winter months, which results in significantly thinner ice, which is likely to be more strongly correlated with an increase in the surface temperature, which will cause an additional top melting to occur. There could also be correlations between other variables and thinner ice that contribute to the increased top melt in reana_bt, but decreased top melt in reana_nt, such as in the presence of melt ponds.

7.2.7 Contribution of the assimilation to volume flux in the reanalysis

We have seen that reana_bt adds more sea ice volume in September than CPOM-CICE and PIOMAS, and this appears to occur in September-October, around and just after the sea ice minima (figure 6.9). In September, reana_nt has more comparable ice volumes with PIOMAS in the last decade of the reanalysis period. In figure 7.2 we saw that a lot of ice volume was added in September through the assimilation. We reasoned that this probably occurs because this is the only time of the year when the observational sea ice extent is higher than in CPOM-CICE. As Bootstrap sea ice concentrations are particularly high in the ice pack throughout the year (unlike NASA Team) it could result in positive correlations between concentration and thickness leading to increased sea ice volume in reana_bt. For this reason we want to see how the changes to the volume made by the assimilation are distributed across the Arctic during this time and at other months of the year, because this should help locate areas of issue within the model. For example the assimilation causes a large decrease in volume in May and June, and total volume flux in other months could overall be small but be balanced out by strong positive and negative changes in different regions. To verify this we show maps of the mean thickness change between 2011 and 2019 for six months in figure 7.7.

In January and March the only substantial changes take place on the ice edge. There

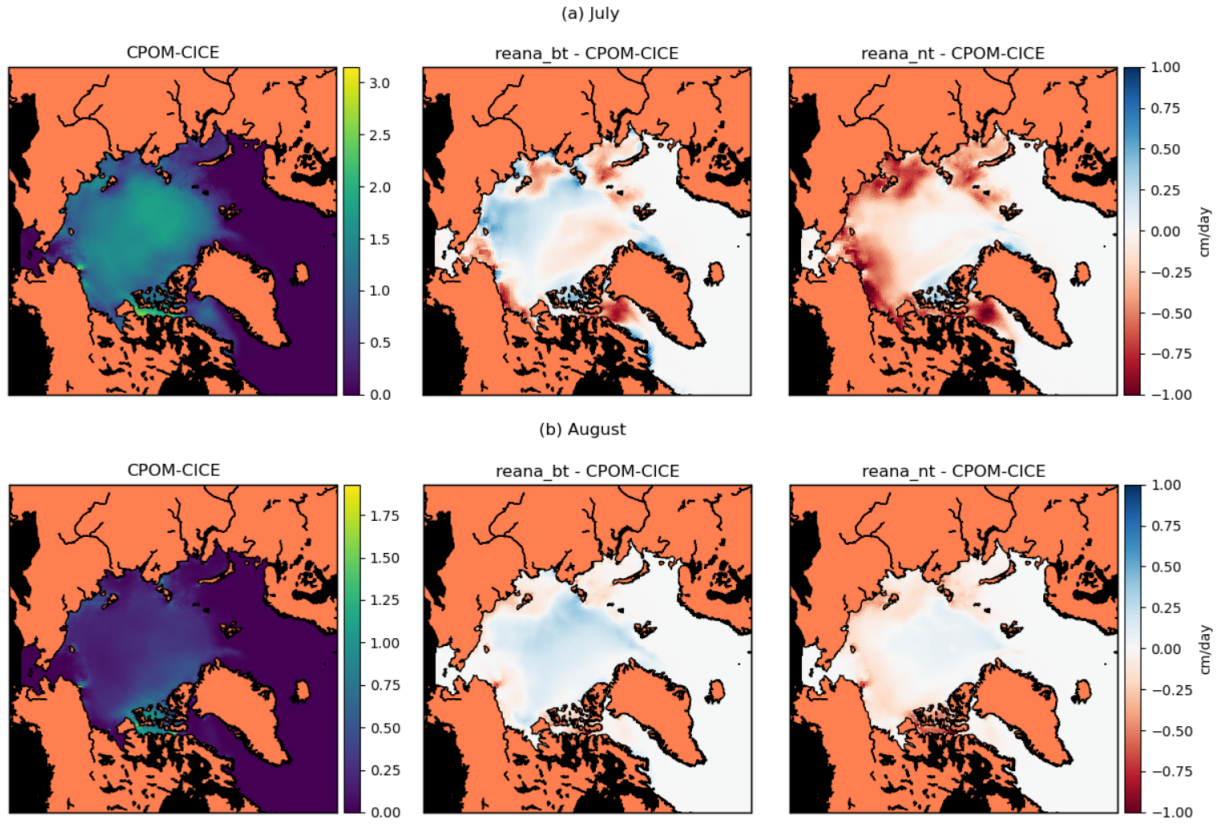

Fig. 7.6 Top melt in July and August for CPOM-CICE and its differences with reana_bt and reana_nt between 2011 and 2019 in cm/day (m^3 of ice per m^2 of grid cell area).

is a decrease in thickness at the ice edge because sea ice concentration observations have a smaller sea ice extent than CPOM-CICE does in these months, and the observations do not have ice in these areas. This means that the decrease in thickness is a result of a decrease in ice concentration. In some cases these grid cells at the edge become completely ice free. Interestingly the biggest changes to the volume made by the assimilation in these months are in the Fram Strait. The assimilation here causes a large decrease in volume lost in the eastern Fram Strait but there is a large volume gain on the western side near the eastern coast of Greenland. The Fram Strait is the primary export region of sea ice in the Arctic, and it appears that the angle of this export out of the Fram Strait is quite different in both reanalyses, much closer to the eastern coast of Greenland. There is very little difference between changes made by the assimilation in reana_bt and reana_nt during these months.

In May there is an increasing area of decreased thickness caused by the assimilation, though still occurring mostly around the ice edge. In the Beaufort and Chukchi seas the ice thickness removed by the assimilation is very strong, particularly in reana_nt. The melting of ice in the Beaufort Sea does not appear to be strong enough in the model at this time, so the ice in the Beaufort sea is thicker in CPOM-CICE than in the reanalysis. The sea ice in the Beaufort Sea is much more seasonal in both reanalyses than in CPOM-CICE for this reason. In reana_nt there is also more loss of ice thickness in the Barents and Kara Seas, this is probably because the NASA Team observations tend to have lower ice concentrations than the Bootstrap observations in summer at the ice edge.

In July, the thickness changes caused by each reanalysis are almost directly opposed. The sole region where the reanalyses agree is the Beaufort Sea. In reana_bt, ice thickness is being increased in the thick ice pack, but at the ice edge thickness is being decreased. On the other hand, in reana_nt the assimilation caused a decrease in the thickness of the central ice pack, but an increase of thickness in the ice edge. This is almost certainly the cause of the higher ice volumes in reana_bt, and it is probably the result of the high ice concentrations in the Bootstrap observations of sea ice concentration in the central ice pack, which are close to 1. In NASA Team observations and the CPOM-CICE model, the ice concentrations are not as high, and so the assimilation of Bootstrap increases concentration at this time in comparison. Due to positive correlations between concentration and thickness, ice thickness is then increased in reana_bt. The Bootstrap sea ice concentrations are believed to be more accurate than NASA Team at this time (see section 2.2), but the correlations are having a potentially detrimental effect on the ice thickness estimates. This is an important result when considering future assimilation of sea ice concentration.

For September, unlike July, there is very good agreement between both reanalyses, both showing an increase in ice thickness due to the assimilation at this time. The increases in ice thickness in reana_nt are perhaps slightly stronger, and in reana_bt there are a few areas on the ice edge where the assimilation is causing a decrease in ice thickness. reana_bt also has a stronger increase in ice thickness close to the Canadian Archipelago.

In November, reana_nt shows a small increase in ice thickness due to the assimilation across most of the Arctic, though the Fram Strait is again an area of significant change. There is a large band of sea ice removed by the assimilation between Franz Josef Land and the eastern coast of Greenland, with ice added to the west against the eastern coast of Greenland, which we also saw in the January-April period. The changes in the Fram Strait also occur in reana_bt, however there are very little changes to the ice thickness made by the assimilation in the Central Arctic in reana_bt. Unlike in reana_nt, there is also a reduction to the ice thickness in the Canadian Archipelago, which may be a result of the thicker ice here caused by the assimilation in July. As we have seen in other months, there is agreement in the Beaufort Sea between the two reanalyses, so the Beaufort Sea seems to be an area in which the CPOM-CICE model performs very poorly.
Overall we have seen that the volume changes made by the assimilation throughout most of the year occur to seasonal ice (regions which are seasonal since 2011). Changes here would not affect the thickness of the thickest ice, but we do see ice thickness increasing due to the assimilation in July in reana_bt, which is the cause of the increased ice volume in this reanalysis. Without the assimilation of the thickness in October, this ice would remain thicker than in reality, and grow throughout the winter freeze-up season, and this is the reason why the sea ice volume increases when only Bootstrap sea ice concentration is assimilated between 1981 and October 2010. We have also identified that the Fram Strait and the Beaufort Sea are two regions with a need for improvement in CPOM-CICE, as there is good agreement in these regions in both reanalyses. In particular the export area is quite different when comparing the reanalyses and CPOM-CICE. The Beaufort Sea requires closer inspection because the ice here varies much more seasonally in the reanalysis than it does in CPOM-CICE, and the assimilation shows that the reanalysis and observations strongly disagree with the model.

Fig. 7.7 Mean change in sea ice thickness (in metres) due to the assimilation between 2011 and 2019 for six months of the year in reana_bt and reana_nt (ensemble mean).

7.3 Changes in the Sea Ice Cover over the Reanalysis Period

7.3.1 Trends in the Sea Ice Extent

One of the primary reasons for doing a reanalysis is to study and improve our understanding of climate trends over a long term period. For reana_bt this is somewhat difficult because of the significant impact of the assimilation of CS2 products in 2010 on the thickness of the sea ice (for reana_nt there is an impact but it is much smaller). However concentration is assimilated almost consistently over the whole time period of the reanalyses and we have shown (see e.g. section 5.4 and section 6.4) that additionally assimilating thickness and sub-grid scale thickness distribution has a very limited (if any) effect on the modelled sea ice extent. Therefore we believe it is still valid to look at trends in the sea ice extent over the whole reanalysis period, and compare these with trends from the control model and other observations. In figure 7.8 we show the reana_bt and reana_nt ensemble mean sea ice extent for each year from 1981-2019, and include the climatological means between 1981-2010. In general the extents and its trends are very comparable in reana_nt and reana_bt, with very few differences in each plot. In the years 1981 and 1988 there are large increments reducing the sea ice extent. In 1981 this increment occurs because it is the second assimilation time step, and the differences between the model and the observations is still substantial. The second occurs on January 13th 1988 and is a result of a gap in the sea ice concentration observations between 3rd December 1987 and 13th January 1988. The size of these increments shows a significant difference in winter sea ice growth between the model with and without constraints from sea ice concentration observations, which appears to be severely overestimated in the model. As we know, the past decade has clearly seen sea ice extents well below the 1981-2010 climatological mean, and both reanalyses follow this trend. The minimum extent occurs in 2012, and in 2016 the sea ice extent was lowest between May and July and in the early freeze-up period between October and November.

7.3.2 Trends in the Sea Ice Volume

As with the sea ice extent, for the sea ice volume we will first look at the whole reanalysis period. We note that due to the substantial reduction in sea ice volume that occurs when ice thickness is assimilated for the first time in reana_bt in 2010 these results should be viewed with some caution. In figure 7.9 we show ensemble mean sea ice volume between 1981 and 2019 for reana_bt and reana_nt and their climatological means between 1981 and 2010. As

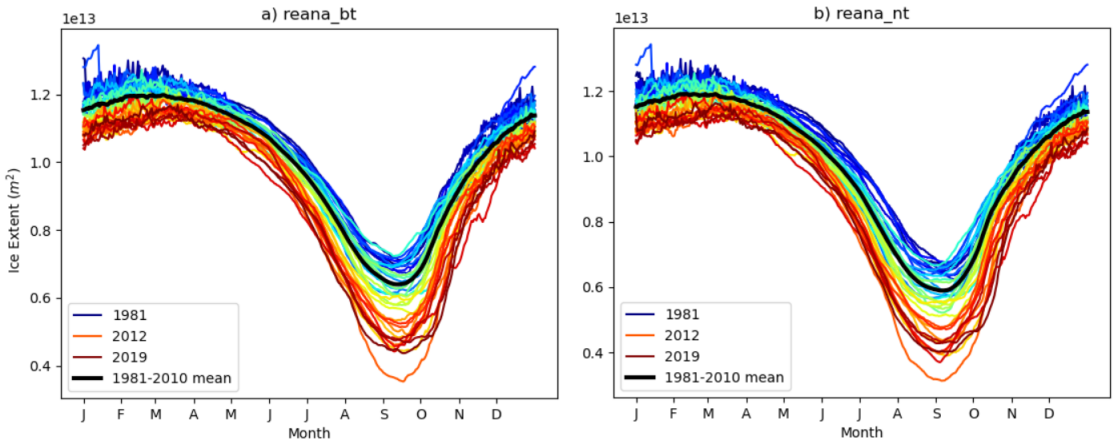

Fig. 7.8 Ensemble mean Arctic sea ice extent in reana_bt and reana_nt between 1981 and 2019 and including a climatological mean between 1981 and 2010.

with the extent there is a clear downward trend in sea ice volume estimates in both reanalyses. In reana_bt there appear to be three distinct groupings. Between 1981 and 2006 ice volume is relatively high, with a few anomalous years of lower sea ice volume in the 80s. Between 2007 and 2009 ice volume is lower than in the previous group. 2010 is also part of this group but only until September, as in October the first thickness observations are assimilated. The final group includes 2010 and subsequent years which all have much lower ice volumes than the 1981-2010 climatological mean. There are clear increments in every year after 2010 when ice thickness assimilation begins after the summer period in which CS2 observations are not available. These are all negative increments, showing again that assimilating Bootstrap concentration alone (in the summer months) anomalously enhances ice thickness and volume. In reana_nt, the ice volumes are lower than in reana_bt, and the groupings are less clear. The increments which take place post-2010 are less obvious, though still visible, and are positive. The climatological mean of 1981-2010 is between $0.6 \times 10^{13} m^3$ and $0.9 \times 10^{13} m^3$ greater in reana_bt than reana_nt, a huge difference. In winter there is never a year with greater than $3 \times 10^{13} m^3$ in reana_nt, whereas in reana_bt many of the winters in the 1980s see an ice volume estimate this high. Both reanalyses however do agree that all years post-2010 are well below the 1981-2010 climatological mean, substantially in the case of reana_bt, where the assimilation of CS2 ice thickness was more effective and the effects of assimilating Bootstrap ice concentration alone caused very high estimates of sea ice volume.

To see how the long term trends in each reanalysis fare over the satellite era, we compare

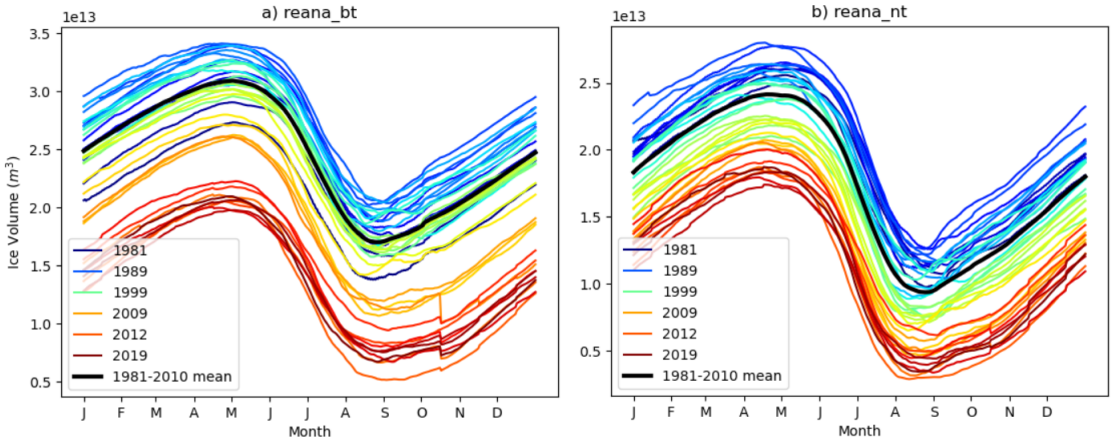

Fig. 7.9 Ensemble mean Arctic sea ice volume in reana_bt and reana_nt between 1981 and 2019 and including a climatological mean between 1981 and 2010. In the past decade sea ice extent has been significantly below 1981-2010 mean.

the linear trends in sea ice volume in CPOM-CICE, reana_bt, reana_nt and PIOMAS in table 7.1. CPOM-CICE and PIOMAS generally have similar trends over all four months we analysed, which peaked in September. On the other hand, reana_bt and reana_nt had larger ice losses which were higher in June and December. The trends in reana_bt are particularly high, and may be biased because of the very large increment in the sea ice volume which take place in October 2010. This does not happen in reana_nt, yet there are still stronger trends in June and December. Meanwhile the downward trend in September was very low in reana_nt in comparison to CPOM-CICE, PIOMAS and reana_bt. This appears to be logically consistent with the ice volume estimates we saw in section 6.6, as reana_nt had lower ice volume estimates than the other models between 1981 and the mid-2000s, whereas estimates afterwards were more comparable. This is a surprising result, as reana_nt seems to disagree strongly with the strong trends in September seen in models, observations and other reanalyses.

7.4 Ensemble spread in the reanalyses

In this study we generated ensemble spread by perturbing the atmospheric forcing fields using EOFs and numbers randomly selected from a normal distribution, this means that the relationship between the different atmospheric forcings - for example 2 m air temperature

Table 7.1 Monthly mean sea ice volume trends for March, June, September and December in CPOM-CICE, reana_bt, reana_nt and PIOMAS between 1981 and 2017 (in $km^3/month$).

Model	**Mar**	**Jun**	**Sep**	**Dec**
CPOM-CICE	-246	-304	-322	-295
reana_bt	-308	-371	-346	-381
reana_nt	-246	-345	-262	-274
PIOMAS	-249	-306	-312	-279

and shortwave radiation - should be kept relatively intact. We found that this generates a significant amount of spread in the model, and thus this procedure may be useful for future data assimilation studies using dissipative models. We also amplified these perturbations in order to create additional spread (see section 4.4) because we felt this might be necessary in the dissipative CPOM-CICE model. The amount of spread that was generated in our data assimilation system meant that although we assimilated sea ice concentration daily with relatively low errors, the reanalyses were able to move significantly closer to the observations, especially the extent. This was the case not only during the early assimilation time steps but throughout the reanalysis period. This means that there was enough ensemble spread throughout the reanalysis period for the assimilation to remain effective. Amplifying the perturbations could have the effect of removing some of the relationship between the atmospheric forcing variables that would have been preserved if we had not done this, because inflating the ensemble could remove the relationship. The ensemble spread appears to be high in our reanalyses compared to the total extent or volume, but this may reasonably reflect that sea ice modelling still has substantial uncertainties, and there are large differences between different models and reanalyses (as we saw in section 3.5). In our reanalyses we begin assimilating new observations from CS2 in October 2010, 29 years after the reanalyses begin and after 29 years of daily sea ice concentration assimilation. We now know (see section 6.3) that the assimilation of CS2 products is effective even after a long period of sea ice concentration assimilation. It appears that the sea ice concentration assimilation largely affects the spread in sea ice concentration (and related diagnostics such as area and extent).

The mean ensemble spread in sea ice concentration for four months over the reanalysis period in reana_bt and reana_nt are shown in 7.10. The regions of the Arctic in each of these months where the assimilation of sea ice concentration will have a strong effect can be seen in purple, as these areas show ensemble spread which is around equal or greater than the observation error of the concentration observations. The ensemble spreads are similar for reana_bt and reana_nt. The region of higher ensemble spread covers the largest area in June and September, with even some inner ice pack areas in the Canadian Archipelago showing

large concentration spread in September. In June and September however, the ensemble spread peaks are generally not as high as in March or December, where there are significant differences at the ice edge. During much of the year the sea ice concentration assimilation will only have noticeable effect at the ice edge. The main exception to this is Baffin Bay in summer where there is a lot of spread throughout the whole region, and as such the reanalyses and CPOM-CICE are quite different at this time which we saw in 6.5 and 6.7.

The sea ice concentration ensemble spread appears to be reasonable and behaving correctly with the observations influential at the ice edge for the majority of the year, as one would expect. The ensemble spread also stays reasonably high throughout the period so that the mean of the ensemble spread over the whole period is still relatively high in the correct places for the assimilation to be effective. To see more clearly whether there are any trends in the ensemble spread, we look at the monthly mean spread in sea ice extent between 1981 and 2019 in the same four months in figure 7.11. There is a reduction in spread that occurs before and after 1987 in the reanalysis, and this is because ice concentration is assimilated once every two days before January 1987 and daily afterwards. There is anomalously high ensemble spread in December 1986 due to the gap in ice concentration observations at this time. In both reanalyses, spread in the sea ice extent is higher in March and December, because ensemble spread at the ice edge is high at this time of the year. March and December have similar ensemble spreads throughout the reanalysis period, as do June and September, so there appears to be a consistency in spread in both the freeze-up and melting seasons for the extent. The ensemble spread in sea ice concentration and extent is not reduced by the additional assimilation of the CS2 products after October 2010. In reana_nt (dashed lines) there tends to be higher ensemble spread than the equivalent month in reana_bt.

Although there is no reduction in the ensemble spread of sea ice concentration or extent when CS2 products begin to be assimilated, we do expect the ensemble spread of ice thickness will be reduced once we begin assimilating CS2 observations. In figure 7.12 we show a comparison of ice thickness ensemble spread between 2000-2009 and between 2010-2019 in reana_bt in March and September. We see that ensemble spread is reduced after 2010, though the patterns in the uncertainty remain similar. The places with the most uncertainty in the model are the Beaufort Gyre, the region of thick ice packed against Greenland and the Canadian Archipelago, and also grid cells next to coasts. There is a ring of higher ensemble spread which surrounds a region of low ensemble spread in the thick ice pack in the Central Arctic. There is a lot of uncertainty in the CPOM-CICE model regarding the existence

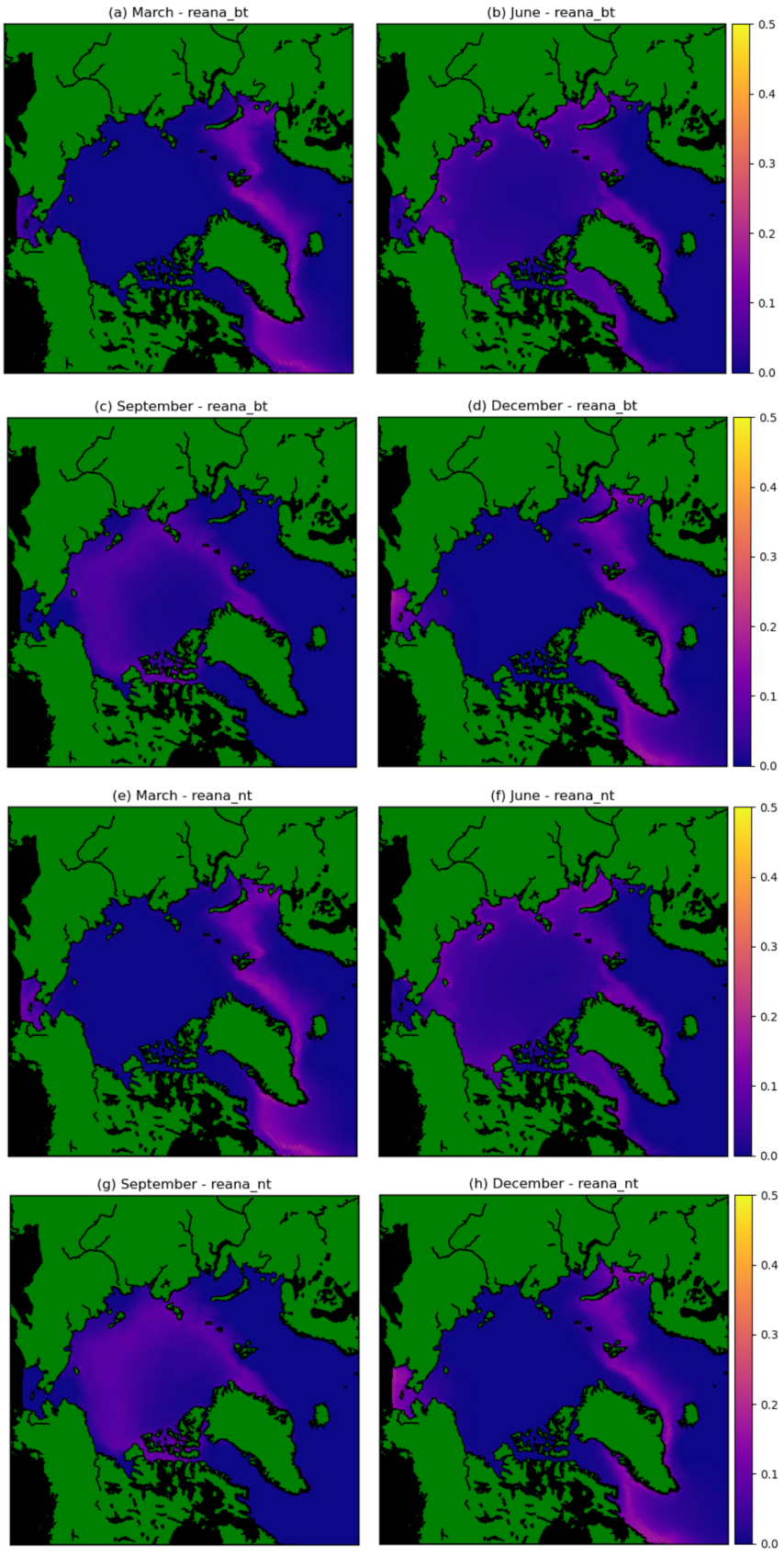

Fig. 7.10 1981-2019 mean ensemble spread in sea ice concentration in March, June, September and December in reana_bt and reana_nt.

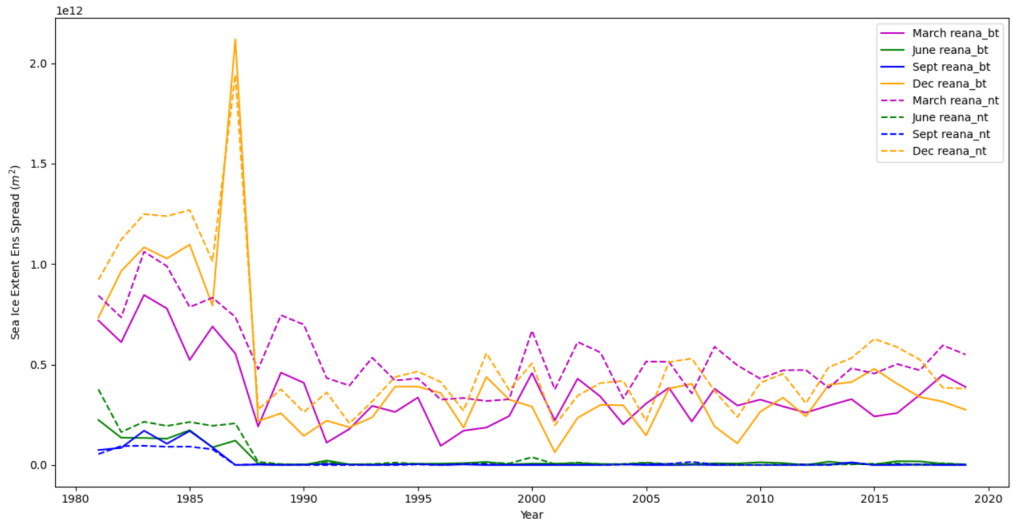

Fig. 7.11 1981-2019 monthly mean ensemble spread in sea ice extent in March, June, September and December in reana_bt and reana_nt.

and size of this region of very thick ice, and we actually see in reana_bt that this thick ice mostly disappears (see section 6.7). High uncertainties in grid cells adjacent to coastlines are unsurprising given the uncertainties of sea ice and ocean dynamics in these regions. In September the ensemble spread in the middle of the ice pack (Central Arctic) is higher than in March. The melting and build-up of ice in the Central Arctic is uncertain, and we have already seen that the early period of the freeze-up season and melting season are not modelled well in CPOM-CICE, which will affect the regions where ice is present year-round or almost year-round the most. The increased uncertainty in the Central Arctic also means that the assimilation of ice thickness products will be more effective in the Central Arctic, which is important for improving the model in this region. As with the concentration, the ensemble spread in the ice thickness looks like it is reasonable and will mean that the assimilation of the thickness observations will be influential in the regions we want and expect.

In terms of the longer term changes in the ensemble spread over the reanalysis period and the effects on the volume, we can look at the monthly mean volume spread between 1981 and 2020 for the same four months, which is shown in figure 7.13. We actually see, as we did for the extent, that the lack of concentration observations in December 1987 had a significant impact on the volume spread in December, the spread in this month (the spread in December 1987 is over three times higher than in December 1986 or 1988 and the ensemble

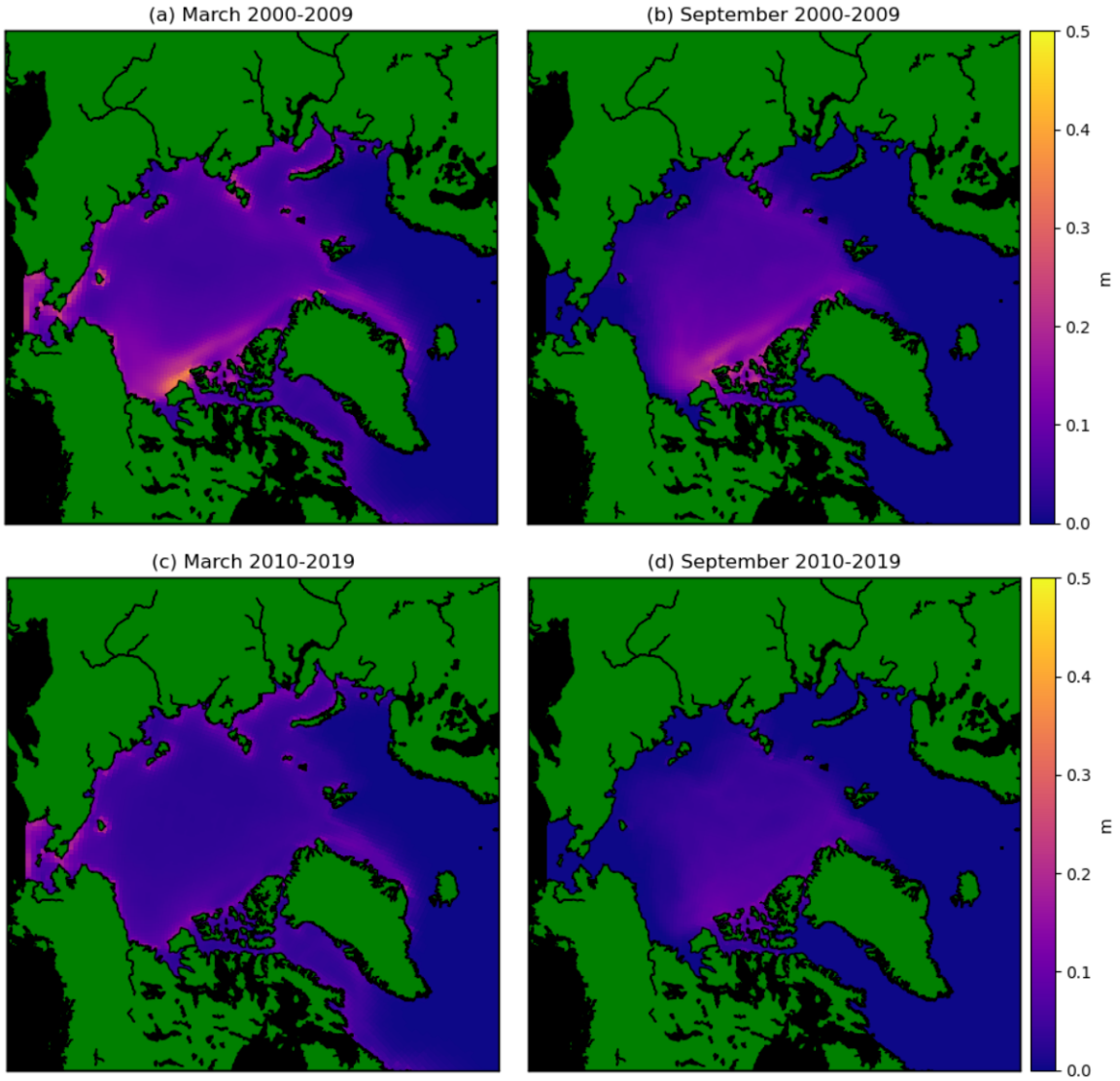

Fig. 7.12 Mean ensemble spread in reana_bt in thickness (m) for the 2000s for March (a) and September (b) and in the 2010s for March (c) and September (d).

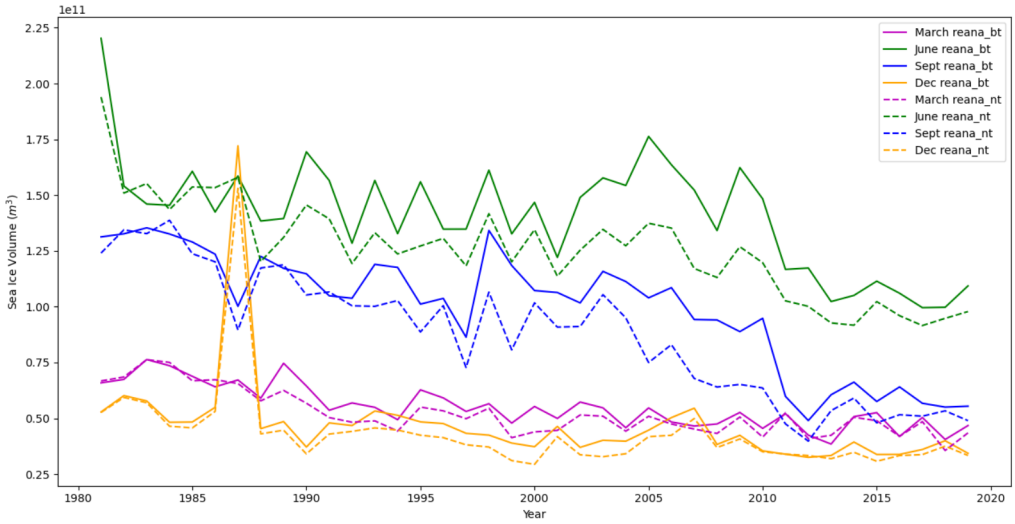

Fig. 7.13 1981-2019 monthly mean ensemble spread in sea ice volume in March, June, September and December in reana_bt and reana_nt.

spread in December is the lowest from all the months we look at, for all years except 1987, when it is the highest). In contrast with the sea ice extent ensemble spread, the pattern is reversed, with June and September having the highest volume ensemble spread, and December and March ensemble spread now lower. The ensemble spread is highest in June, which is further evidence that the modelling of the melting season in June is not particularly great. Surprisingly the sea ice volume ensemble spread is only reduced relatively slightly in December and March with the assimilation of CS2 ice thickness, and conversely the volume ensemble spread is reduced by relatively a lot in June and September, when sea ice thickness is not assimilated. The primary source of ensemble spread in December and March will probably be in the concentration, not in the thickness, so a reduction in the ensemble spread of the thickness does not affect the ensemble spread in the volume much. In June and September however there is a lot more ensemble spread in the thickness, and we saw that the ensemble spread in sea ice concentration (and extent) was much smaller. This means that the uncertainty in thickness plays the important role in determining the ensemble spread of the volume in June and September.

Overall, it does not look like either reanalysis is suffering from continual reduction in ensemble spread for any of the assimilated variables during the reanalysis period, though there are

expected reductions in sea ice thickness and volume ensemble spread when the assimilation of sea ice thickness begins. We do not see any signs of ensemble collapse in the ensemble spread, nor did we see anything in any other results from the reanalysis. The ensemble spread in both reanalyses looks to be relatively healthy and stable throughout the reanalysis period. There is higher spread in sea ice concentration and extent in reana_nt than reana_bt, but there is lower spread in sea ice thickness and volume.

7.5 Assimilation of Landy Cryosat-2 sea ice thickness data

Within the last year, new research in machine learning using CS2 observations has led to the development of a new sea ice thickness observational record (Landy et al., 2022). These observations use the same raw data as the CPOM CS2 observations used above, but are processed in a very different way (see section 2.3.3). The Landy sea ice thickness product has two important features that may make it more useful for assimilation than the CS2 product. Firstly it provides sea ice thickness data between May and August, which the CPOM CS2 data does not and we have seen that the assimilation of sea ice concentration observations alone in this period can negatively affect the sea ice estimates in this period (see sections 5.3 and 6.3). Secondly the Landy CS2 thickness data also provide a quantified error for each observation, which the CPOM CS2 data does not. This is vital for achieving a better analysis state from the LETKF. For this reason we run a new experiment which assimilates the Landy monthly mean sea ice thickness product between 2010 and 2020 instead of the CPOM CS2 mean thickness and sub-grid scale thickness distribution. This experiment (reana_landy - see table 6.1) is restarted from the original reanalysis at the beginning of 2010, and uses the same forgetting factor, localisation radius and ensemble size as our previous reanalyses. The observation errors provided with the Landy thickness data are used in the observation error covariance matrix. Bootstrap sea ice concentration observations are assimilated. Sub-grid scale thickness distribution is not assimilated in this experiment because this is processed using the CPOM CS2 data.

The sea ice thicknesses in the Landy product are generally thinner than those in the CPOM product (compare (Landy et al., 2022) with(Laxon et al., 2013)), and so we find that the reana_landy experiment estimates decreased sea ice volume in comparison to reana_bt, as seen in figure 7.14, which shows the daily sea ice volume between 2010 and 2015 for CPOM-CICE, reana_bt, reana_nt and reana_landy. The sea ice volume minima in September is decreased and close to, or below the sea ice volume minima estimated in CPOM-CICE. It is noticeable that the increments when the Landy CS2 product is assimilated are larger than

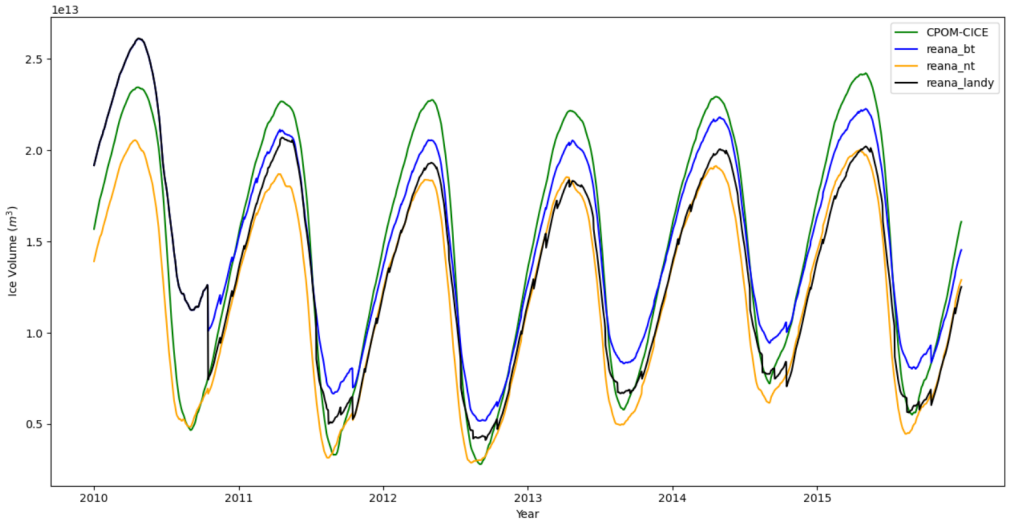

Fig. 7.14 Daily sea ice volume between 2010 and 2015 in CPOM-CICE, reana_bt, reana_nt and reana_landy (ensemble means).

those when the CPOM CS2 product is, which happens because of the greater differences between the CPOM-CICE estimates and Landy CS2 sea ice thickness observations in comparison to those from the CPOM CS2 product. There are large differences in sea ice volume in winter in particular, as high as $5 \times 10^{12} m^3$ during the winter peak between reana_landy and CPOM-CICE, with reana_bt lying in the middle of the two. In comparison with reana_nt, reana_landy has higher estimates of ice volume in summer, but in winter the two are more comparable, especially between 2012 and 2015.

The monthly mean sea ice volumes from reana_landy are compared to CPOM-CICE, reana_bt, reana_nt and PIOMAS for March, June, September and December in figure 7.15. In March reana_landy estimates of sea ice volume are similar to those from PIOMAS and reana_nt. In June reana_landy estimates are mainly lower than the other models except reana_nt. The ice melt in late May and June seems to be very strong in reana_nt. In September however PIOMAS sea ice volumes are the lowest alongside reana_nt. This must mean that melting in July and August is much more intense in PIOMAS than in reana_landy and reana_bt, so the thicker ice in PIOMAS is thinning to a much greater degree than in reana_landy and the other models. In December PIOMAS, reana_nt and reana_landy are comparable, as in March.

Although we now have an idea about the differences in total sea ice volume in a number of different models and observations, we also need to look at maps of the thickness to see

how it is distributed within the observations and the models. We show the March and October 2012 mean ice thickness from CPOM and Landy CS2 observations, PIOMAS, CPOM-CICE, reana_bt and reana_landy in figure 7.16. In March, there is good agreement on a region of thick ice between 2.4 m and 3.6 m off the north of Greenland and the Canadian Archipelago in CPOM CS2 observations, PIOMAS, reana_bt and reana_landy, while in the Landy CS2 observations this region is shifted slightly northward around the north pole. CPOM-CICE and Landy CS2 ice thickness agree well in both March and October except at the ice edges and the ice closest to the Canadian Archipelago, which is thinner in the Landy CS2 observations. The main region of disagreement in March sea ice thickness is in the Kara and Barents Seas. In October the observations have the thickest ice occurring away from North Greenland and the Canadian Archipelago and close to the North Pole, with very little ice above 1.4 m thick in the Landy CS2 observations. PIOMAS, reana_bt and reana_landy ice is thicker closer to North Greenland. The CPOM-CICE model differs significantly from the other data sets in how the sea ice is distributed across the Arctic, suggesting a need for improved or new sea ice model physics.

7.6 Shortcomings of the current reanalysis

We have striven to produce the best possible reanalyses in this study, but there are a number of issues we have identified in our data assimilation system that could be improved. As discussed in 2.2, there are now a range of different datasets available of sea ice concentration, using retrieval algorithms that make use of different brightness temperatures, frequencies and polarisations, or a combination of these. Sea ice concentration data sets can produce substantially different ice concentrations within the ice pack depending on the features of the retrievals, though they all have similar sea ice extents. We have found that assimilating two different sea ice concentration products have produced two remarkably different reanalyses. This is particularly true during the period when only sea ice concentration is assimilated: reana_bt has much higher ice thickness and volume estimates than reana_nt, CPOM-CICE and PIOMAS. When sea ice thickness and sea ice thickness distribution are assimilated, this difference is reduced substantially, primarily because the thickness and volume estimates in reana_bt are reduced. Assimilating Bootstrap sea ice concentration alone leads to particularly poor estimates of thickness and volume, though for long periods of our reanalyses it is

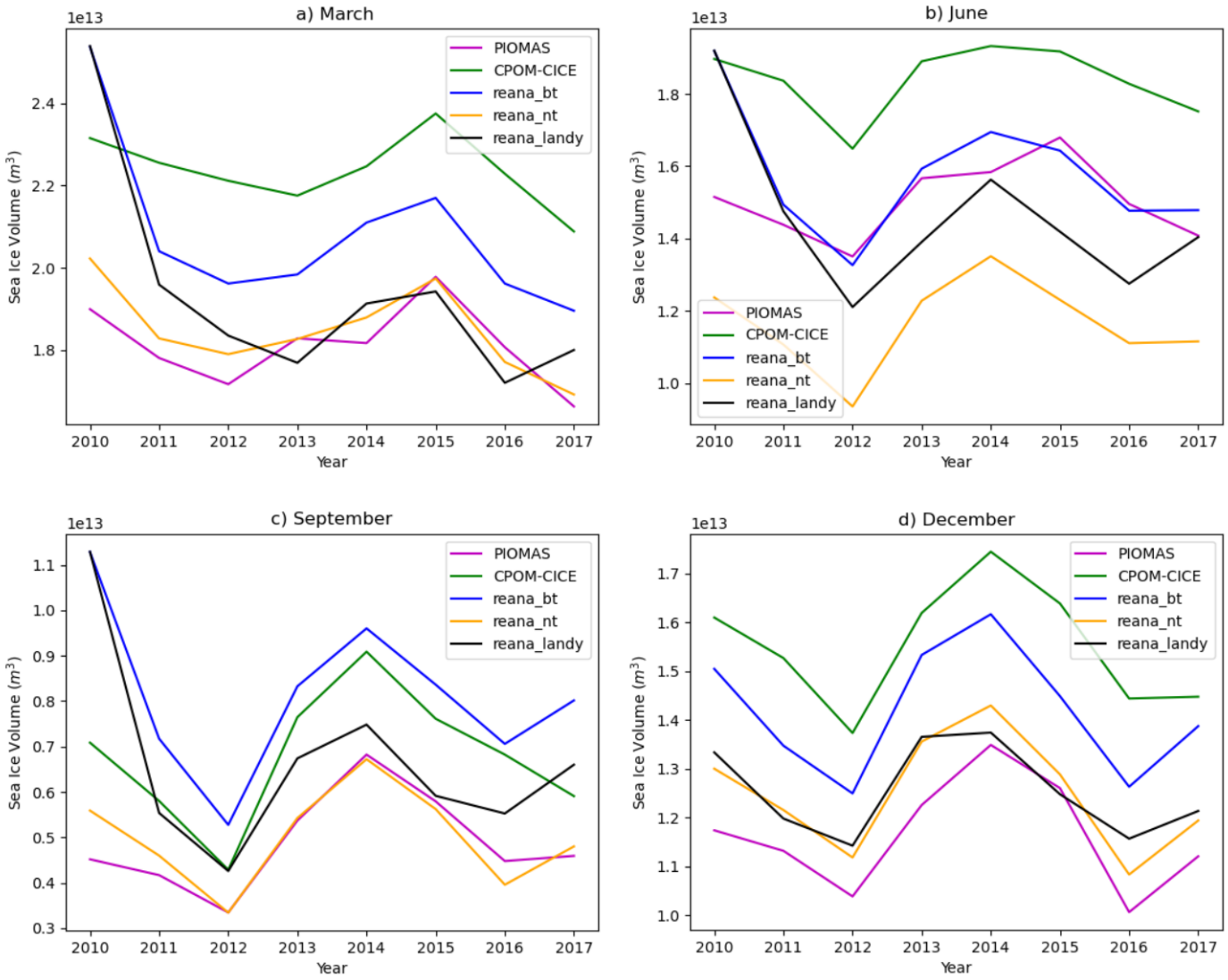

Fig. 7.15 Monthly mean sea ice volume in March, June, September and December between 2010 and 2017 in CPOM-CICE, reana_bt, reana_landy (ensemble means) and PIOMAS.

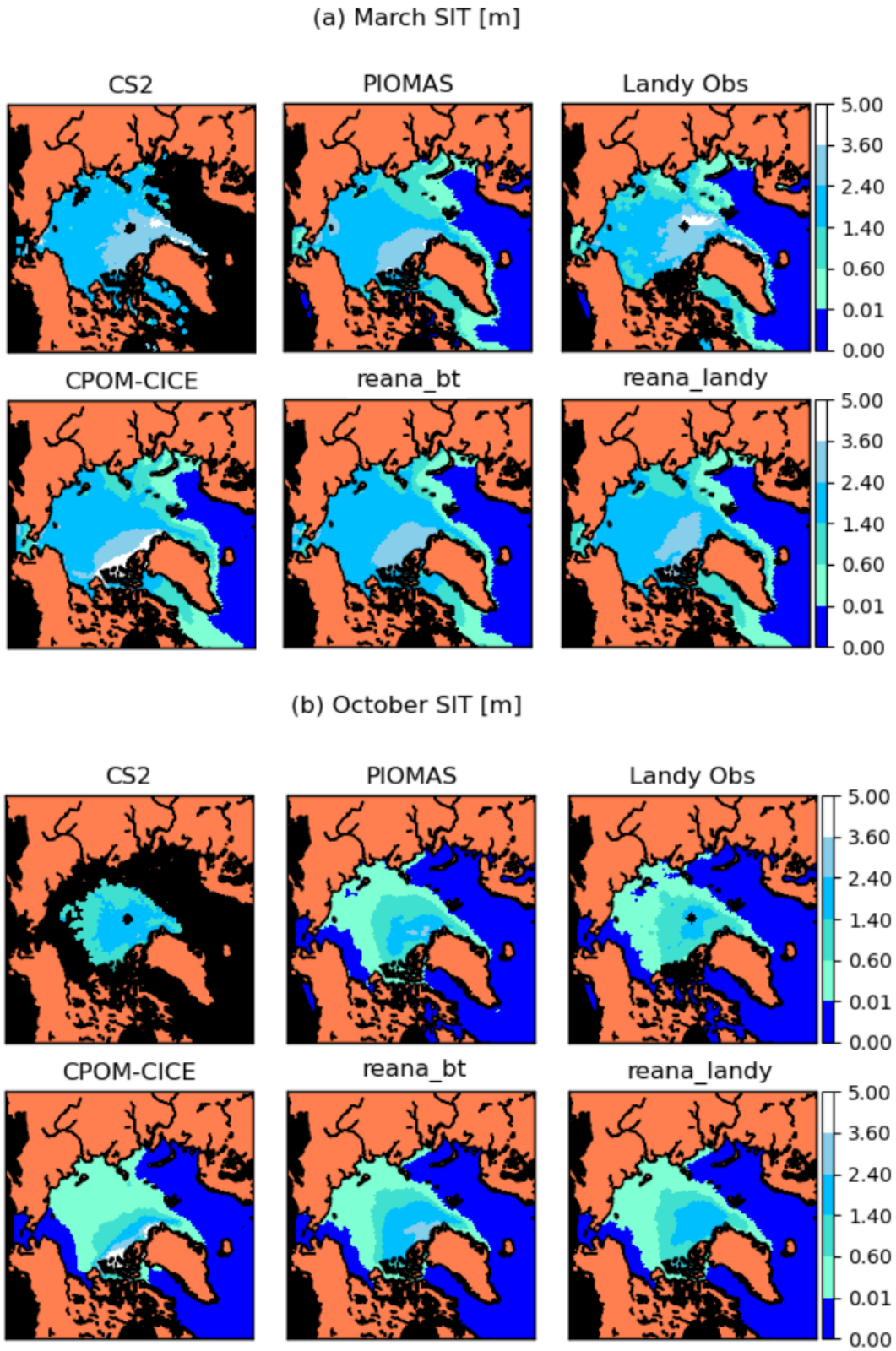

Fig. 7.16 Monthly mean sea ice thickness in March and October 2012 in the CPOM Cryosat-2 observations, Landy Cryosat-2 observations, PIOMAS, CPOM-CICE, reana_bt and reana_landy.

impossible to evaluate thickness or volume estimates because of the lack of observational products of these quantities. There may also be unrealistic estimates of thickness and volume in reana_nt during the 1981-2010 period which are difficult to identify.

7.6.1 Observation error covariances

Choosing the observation errors for sea ice concentration is difficult due to the uncertainties in the observation errors themselves. There are no observation errors provided with the datasets, with estimates on the uncertainties being between 5% and 30% depending on a number of factors (see section 2.2), and a lack of verification data. This means that the data assimilation is not well placed to optimally 'balance' the sea ice state between model and observation. A similar problem occurs regarding the CPOM CS2 observations of mean ice thickness observations, as observation errors are again not provided with the mean thickness data. CS2 mean thickness errors are difficult to quantify because of the long, complex processing chain that converts CS2 altimetry measurements into monthly mean gridded measurements of sea ice thickness. There is potential for assimilation of sea ice freeboard instead of thickness, and this would decrease the uncertainties in the observation products substantially. However, the model snow depth would then need to be used in the observation operator, so we are only moving away from the uncertainties in the observation to add additional uncertainty in the model (see section 2.3 for further details). As our sub-grid scale sea ice thickness distribution observations are derived from the same source as the mean thickness observations, they also have a highly uncertain observation error covariance matrix. There are even more uncertainties involved with quantifying the mean thickness errors than for the sea ice concentration. For the assimilation of sub-grid scale sea ice thickness distribution all observations within a category are assumed to have the same error, which means that some observations will be incorrectly weighted. This could also mean that within a grid cell there is imperfect weighting on the errors in the ice concentration (or ice thickness) across the thickness categories, which means that the analysis update is not ideal. Therefore further research into quantifying the errors in sea ice observation products would be useful for sea ice reanalysis studies so that the observation error covariance matrices are better known.

From October 2010 onwards, we assimilate three different types of observation (concentration, thickness and thickness distribution), these three types of observation are all correlated with one another, but we do not account for these correlations in the observation error covariance matrix (our R matrix is diagonal). The observation error correlations are important

because without them, we lose some of the information. In general data assimilation inclusion of error correlations has been shown to improve the accuracy of the observed variables in the analysis (Seaman, 1977) and to improved analyses (Miyoshi et al., 2013), and that they are also likely to be important for satellite observations (Stewart et al., 2013). However these error correlations are difficult to quantify, particularly for sea ice observations, which as we have discussed already contain a number of uncertainties. The observation error correlations are ignored in this study for simplicity, and outside the scope of this work.

7.6.2 Climatological Forcing

In this study we use the CICE default mixed layer model to prescribe the ocean temperature, salinity and currents using a climatology (Ferry et al., 2011). Therefore we are using an ocean that remains unchanged throughout the reanalysis period - with no trends in these variables. This is not realistic as there will be year-on-year changes and there are trends occurring over the whole period. For example the upper Arctic Ocean has warmed in the 21st century (Li et al., 2022), and its salinity has also decreased (Li and Fedorov, 2021) as the sea ice cover has retreated. There will also be inter-annual variability in the ocean which could not be represented in the climatology. For example in the circulation, which could affect regional distribution of the ice, e.g. in the Beaufort Gyre. This could also affect the export of sea ice in the Fram Strait, a region where we saw large differences both reanalyses and CPOM-CICE caused by the assimilation. Whether we use an ocean climatology or an ocean reanalysis to force the model, we are still lacking some of the ocean-ice feedback processes which would be present in a coupled ice-ocean model. However using a stand-alone forced sea ice model does mean it is easier to understand changes in the internal ice model processes caused by the data assimilation. Future work could involve employing this sea ice data assimilation system to an ocean model.

7.6.3 Spin-up of the assimilation

In our reanalyses we have run the model for a spin-up period of four years. The spin-up time is important for having a reasonable estimate of the sea ice state for the initialisation of the reanalyses, and for generating a sufficient ensemble spread so that the assimilation is effective. With regards to the ensemble spread, this choice of spin-up period appears to have been more than adequate, as we see a lot of movement by the ensemble mean towards

the observations in 1981 when sea ice concentration is first assimilated (see figures 6.3, 6.8 and 7.8). In terms of the spin-up for the initial estimate of the sea ice state to be reasonable, four years could be on the shorter side for the sea ice volume, because the ice in the thickest regions of the sea ice may not be adequately thick yet (although we believe that the model over-estimates ice thickness in this region anyway). It is more than adequate for estimates of sea ice concentration and extent, and for most other sea ice diagnostic variables, because there is very little memory in the sea ice cover inter-annually.

7.6.4 Special problems with CS2 thickness and CS2 thickness distribution data

In this study we assimilate observations from CS2 as monthly means, which appears to be necessary to reduce the uncertainties in these observations. We have chosen to assimilate the CS2 observations in the middle of the month, because the instantaneous model forecast at this time is expected to be the closest approximation to the monthly mean. In winter this is a reasonable approximation but during summer it is likely there are months when this is not the case, as during the peak melting season the ice cover is rapidly evolving in response to atmospheric and oceanic forcing. This may also be a problem in late Autumn and early winter when a lot of thin ice begins to form. However because we do not use CS2 thickness measurements below 1 m this is less of an issue. We assimilate CS2 observations between October and April only, so our choice to assimilate in the middle of the month should not be a big concern.

As the CS2 observations are assimilated monthly for only seven months of the year we also face an issue of large analysis increments occurring. There are two situations in the data assimilation that cause noticeable increments in parts of the sea ice state at certain points. The first occurs in October 2010, during the first assimilation time step of sea ice thickness, this causes noticeable increments in thickness, volume and a few other variables. For this reason it is important to avoid using this reanalysis to look at volume and thickness trends through 2010, as the thickness and volume estimates change significantly because of the impact of the sea ice thickness assimilation. Therefore we believe sea ice thickness and volume trends between 1981 and 2010, and trends from 2011 and later should be analysed separately. The second situation occurs every October after this year, due to the gap in summer sea ice thickness observations from CS2, these increments are noticeable but much

smaller than the one which occurs in the first situation, as this increment occurs every year on the same date it is also easier to account for when analysing trends in thickness or volume that occur after 2010.

Even after 2010, between May and September only sea ice concentration is assimilated because CPOM CS2 sea ice thickness does not have observational records during this time. This means that the sea ice concentration assimilation could possibly bring about the same effects it has before 2010 between May and September, whereby the thickness of the ice pack appears to gradually become too thick. However by looking at the beginning of the reanalysis in 1981, we see that this effect appears to occur during the freeze-up period, where the ice that forms during this time seems to be thicker than in the CPOM-CICE model. Although both reana_nt and reana_bt experiments only assimilated concentration between May and September the changes made to the model between October and April were significant such that the sea ice volume in these experiments did not converge. For these reasons we do not believe the lack of summer ice thickness observations from CPOM CS2 records to be an issue impacting the volume after 2010, though it does cause slightly larger increments to occur in some years in October during this period. It may cause slightly higher ice thicknesses in the Arctic than would appear if we had observations in this time period to assimilate, but this affect is likely negligible when compared with the substantial positive impacts from assimilating sea ice thickness in the first place.

7.6.5 Difficulties with the ensemble-inferred forecast error covariances

We have found that when the sea ice concentration assimilation causes positive increments to sea ice concentration, it tends to also thicken existing sea ice and create anomalously thick new ice in grid cells that were previously fully open. Although there should be ice in these grid cells according to the observations, the ice added is possibly too thick compared with reality. This effect appears to be particularly bad in July and August during our reanalyses. This problem is particularly apparent with reana_bt but lesser so with reana_nt. There may also be other unwanted effects caused by the correlations which are harder to identify. One way to prevent these problems might be to allow the ice concentration assimilation to add ice in the thinnest ice thickness category, though this would be impossible to implement if other observations are assimilated at the same time step as ice concentration. We could have implemented this strategy before 2010 and then not allow it afterwards, but this would cause further issues with the consistency of the reanalysis, in addition to those we have

highlighted above. The increased ice volumes in reana_bt have not been seen in other sea ice data assimilation studies that we know of (see section 3.5).

We have chosen to use a localisation radius of 100 km in our reanalysis, which is used at all locations on the model grid. This is not necessarily the ideal choice for localisation radius, which ideally needs to be tuned for each system depending on the the model and observation density, observation uncertainty and the ensemble size (Hamill et al., 2001). The localisation radius should correspond to the maximum distance at which meaningful correlations have a higher signal than those from spurious correlations (Ying et al., 2018). This means that finding the ideal localisation radius for each observation will require a significant amount of time and computing investment, which is outside the scope of this study. Depending on the ice thickness and concentration, the dominant factor in determining ice dynamics - which is important for determining the localisation radius - can be different. Close to the ice edge, in the MIZ, sea ice drift as a result of ice dynamics is key, whereas in the regions of thickest ice, the convergence of the ice by ridging is important. The correlation length scales will also change as the sea ice cover evolves throughout the seasons, a grid cell that is at the ice edge at the end of summer will be within the ice pack in winter, and this can change on an inter-annual basis. We chose a small localisation radius so that we avoid cases where the spurious correlations will be higher than those from true correlations almost anywhere, at anytime within the model. Other studies of sea ice-ocean data assimilation systems have used larger localisation radii, for example TOPAZ4 uses 300 km arctic-wide (Sakov et al., 2012), as does Fritzner et al. (2019). A study by Wang et al. (2017) found improvements by using a localisation radius dependent on latitude in a coupled ocean-sea ice model (assimilating both ocean and sea ice observations), but there has been little research in localisation radius choices for data assimilation in stand-alone sea ice models. By using a short localisation radius, it might mean that in some cases, information from some observations are lost, but any effects from spurious correlations should be almost entirely avoided for any region and season.

7.6.6 Evaluation of the reanalayses

In an attempt to evaluate our reanalysis we randomly chose around 25% of CS2 data that is not assimilated but is instead used to evaluate the ice thickness in the reanalyses. We do this because there is limited data available for which we can evaluate the system, but it is not ideal because we are decreasing sources of information for our reanalyses to use to improve our

estimates of the sea ice state. The primary issue with this is that the randomly chosen data for evaluation and the rest of the data which is assimilated will be correlated with one another in some way. As long as the assimilation system is functioning correctly then you would expect that the assimilation will decrease the RMSE in comparison to the non-assimilated data.

We also use Operation IceBridge data for evaluation, though it has severe restrictions. OIB data is limited mostly to March, with a few days of data also available in April each year. OIB measurements are made at a much smaller footprint than the model, which must be interpolated onto the CPOM-CICE model grid. The measurements are made using a lidar instrument which is flown on board an aircraft, with only one flight taking place each day, meaning that the data is also very sparse. There are also substantial differences between the CS2 observations that we assimilate and the OIB measurements, because there are significant uncertainties associated with each method of measuring ice thickness (Laxon et al., 2013). We use OIB data from 2012-2015 to assess the ice thickness estimates in both our reanalysis and the control CPOM-CICE model, and we find that the reduction in RMSE in the reanalyses is small but not non-negligible, with reana_nt seeing a greater reduction in RMSE than reana_bt.

7.7 Identification of key areas where model and observations disagree

As we stated in chapter 1, reanalyses can be a very useful tool for learning about model shortcomings. We have identified a substantial difference in the distribution of the ice thickness in the CPOM-CICE model in comparison with our reanalyses and other data sets. Although the Arctic sea ice volumes and its trends are not too dissimilar between CPOM-CICE and either reanalyses, the thickness distribution in the CPOM-CICE model is much more mounded, and tails off sharply initially from a central peak, and also covers a wider range of thicknesses (especially higher thicknesses - see figure 6.14). The sea ice cover is distributed more evenly around a smaller range of thicknesses in both reanalyses than in CPOM-CICE, especially in the early and middle periods of the freeze-up season, and in general there are too many grid cells with very thick ice. There are smaller differences between the ice cover in different regions between CPOM-CICE and our reanalyses, with CPOM-CICE underestimating the ice thickness in the Central Arctic and overestimating it in the Canadian Archipelago and north of Greenland. For this reason we will study and try to understand why these differences occur in each region in this section, focusing on the places where the sea ice cover is thickest

and the differences between CPOM-CICE and the reanalyses are largest, and suggest ways in which the modelling in these regions could be improved.

In CPOM-CICE most of the grid cells with very thick ice are in a region packed up against the Canadian Archipelago and north of Greenland. As we look at the ice cover spanning out from this region it becomes thin very quickly in summer, and so at the end of summer it has much lower ice extent than the reanalyses. This very thick ice (thicker than 4 m) is not seen in our reanalyses or observations (see section 6.7) in the past decade, and the model has not successfully captured the loss of this thick multi-year ice in the Canadian Archipelago (Howell and Brady, 2019). This seems to occur because of a lack of melting on the thickest ice in this region during the melting season, and the thick ice appears to be too resilient to melting in CPOM-CICE. It is difficult to discern why this is, because of the lack of sea ice thickness observations during the melting season. Basal melt was increased in the reanalysis in comparison to CPOM-CICE in both August and September, however top melt was increased in reana_bt but decreased in reana_nt, so the solutions offered by the reanalyses are not consistent. These changes to the volume fluxes could also be reactions by the model to the assimilation of the different sea ice concentration products. The estimation of top melt on the surface of the sea ice may be underestimated in CPOM-CICE, which would result in reduced melt pond coverage that cause enhanced melting. There has been research on improving the numerical models of melt ponds (Zhang, Schweiger, Webster, Light, Steele, Ashjian, Campbell and Spitz, 2018) and on developing observational data sets of melt ponds in the last decade with the use of imagery from the Moderate Resolution Imaging Spectroradiometer (MODIS) and machine learning (Lee et al., 2020) (Ding et al., 2020), since it was discovered that melt ponds are important in predicting summer sea ice loss (Schröder et al., 2014). The assimilation of melt pond observations may be important for improving estimates of sea ice cover during summer, and particularly for multi-year ice. The additional melt in thick ice regions may be accounted for by improved melt pond modelling or sea ice physics that are unknown or unaccounted for in the model. With the further development of melt pond observations it may be possible to assimilate melt pond fraction (area of a grid cell covered by melt ponds).

The Central Arctic ice cover, on the other hand, is generally much too thin throughout the 2010s in CPOM-CICE in comparison with observations. 2012 is a particular issue because much of the Central Arctic is ice free in CPOM-CICE, but this is in strong disagreement with observations and the reanalyses, where ice is still thicker than 2 m in many places. This problem could be related with the ice which is too thick close to the Canadian Archipelago,

with sea ice in the model converging too much toward the Canadian Archipelago away from the Central Arctic. The strong congelation ice growth that we saw in winter in section 7.2 could also be a cause, as the ice volume gain due to congelation is decreased a lot in both reanalyses in October and both reana_bt and reana_nt are closer to the evaluation data set from CS2 and independent observations from OIB.

In the freeze-up season, thin ice grows much quicker in the model than in observations, and ice extent and volume are overestimated throughout most of the year for this reason. The MIZ is generally larger in CPOM-CICE than in both reanalyses and observations, though reana_nt has an MIZ more comparable to CPOM-CICE in September, but not in March (see figure 6.6). It seems that this is more likely to be caused by less-than-ideal atmospheric and ocean forcing, especially as the sea ice at the ice edge is particularly sensitive to the ocean forcing. The modelled sea ice cover (and in particular volume) is more sensitive to changes in atmospheric forcing data sets than to changes in, for example, the melt pond parametrisations (Sterlin et al., 2021). There are large differences in reanalyses over the Arctic Ocean in many fields important for calculating air-sea and air-ice fluxes, especially for wind speeds and radiation, though there is more agreement in humidity and temperature. A comparison with reference observations shows that the uncertainties for all these fields however are quite similar, with no reanalysis clearly better (Chaudhuri et al., 2014). In this study we use a climatology to drive the ocean, but the sea ice concentration estimates at the ice edge and the total ice extent may be strongly improved by using a reanalysis. Recent improvements in wave modelling including the break up of ice from waves and the effects on lateral melt and the ice drift (Boutin et al., 2020) and floe size distribution (Bateson et al., 2020) should bring benefits to sea ice modelling at the ice edge.

In CPOM-CICE there is an issue with both overestimated freeze-up and melting of the sea ice. This means that the CPOM-CICE model estimates a sea ice cover which is much more seasonally varied than shown by observations of concentration or thickness. Though the ice growth is intense in CPOM-CICE through a single winter, the sea ice in a grid cell which was ice-free at the beginning of winter and then freezes over in winter is very unlikely to remain through the intense melting in summer. In particular we have identified some regions in the Arctic where the CPOM-CICE model and our reanalyses differ significantly. We have already talked about the differences in the thickest ice in the Canadian Archipelago and the Central Arctic, but there are also large differences in the Beaufort Sea, the Fram Strait and the Barents Sea. We also show that there are fundamental differences in the seasonal cycle seen in model and observations. Both ice thickness and ice concentration observations show

to some extent that both the melting and freezing begin earlier in the year, and because of this the assimilation increments are relatively very large in May and September in comparison with other months. Further work is needed to look at whether the annual cycle is wrong in the model (and why this is), or whether there are issues within the observational methods (uncertainties in measurements due to sea ice cover changes in the melt season) that cause this inconsistent annual cycle.

The sea ice estimates, and in particular the interseasonal changes of the sea ice in the Beaufort Sea differed substantially between the CPOM-CICE model and our reanalyses. This is probably the one region in which the ice cover went from multi-year ice to first-year ice in both reanalyses in the last decade, in particular, reana_nt saw strong melt in the Beaufort Sea. The Beaufort Gyre, one of the major ocean currents in the Arctic, means ice often becomes trapped in this region and this would lead to the formation of thick multi-year ice. In particular there is a loss of ice close to the Alaskan coast in summer, and the ice here is thinner year-round. Case studies have shown that an ice-free Beaufort Sea may be a result of high sea ice export and divergence (Babb et al., 2019), and both reanalyses do show an increased loss of ice volume due to dynamical processes. The negative trend of sea ice area in the Beaufort Sea is one of the highest of any regions, but this region is more stable in the CPOM-CICE model because the model is not able to melt the thick ice that builds up in this region during the 1980s. In both reanalyses the ice is also thicker than CPOM-CICE in winter, sometimes above 2 m thick in some grid cells, so although overall the CPOM-CICE model is more seasonal, in the Beaufort Sea it is not able to capture the large thickness changes in the sea ice cover which occur intra-annually.

The Barents and Kara Seas are probably the regions where sea ice models and observations differ the most, and for this reason we have seen that large differences between CPOM-CICE, reana_bt and reana_nt occur here where the largest differences have occurred within the last decade. The Barents Sea is of particular interest because observations of sea surface temperature (SST) suggest it has undergone rapid warming since 2000 (Kohnemann et al., 2017). This has helped to restrict sea ice formation in the Barents Sea and led to a lot of changes in water formation in the Barents Sea (commonly referred to as "Atlantification") (Barton et al., 2018). The Barents Sea is ice free in summer, but in winter is one of a number of seas at least partially covered with seasonal ice. In CPOM-CICE the ice in the Barents Sea is thin, with a mean thickness between 0 and 0.6 m in almost all grid cells. In the Kara Sea ice is slightly thicker but not above 1.4 m thick. In contrast the ice is thicker in the reanalyses (especially reana_bt) even though the extent of the sea ice is lower. In the Kara Sea there are

a lot more grid cells with a mean thickness between 1.4 m and 2.4 m in the reanalyses, and the Barents Sea also contains thicker ice than in CPOM-CICE. The CPOM CS2 observations are below 1 m in most of the Barents Sea, but the Kara Sea is covered with ice at least 1.5 m thick and in some cases 2.5 m thick. The Landy CS2 observations conversely show the Kara Sea and Barents Sea covered in ice thinner than 1 m. In PIOMAS the ice in the Barents and Kara is thin, interestingly quite similar to the CPOM-CICE estimates. The large differences in these data sets show there is a need for further observations and modelling improvements in the Barents Sea, especially when two different observational data sets produced from the same raw CS2 data give very different estimates of the sea ice in this region. Both reana_bt and reana_nt have thicker ice in the Kara Sea, but then the Barents Sea ice stays relatively thin. The reanalyses seem to show that the intense warming in the Barents Sea is thinning the ice in the Barents Sea but is not effecting the ice cover in the neighbouring Kara Sea so much, which is not captured in the models and is only reproduced by the assimilation of ice thickness.

In the Fram Strait there is also a large uncertainty in the ensemble spread in the reanalyses, and models and observations differ substantially. For this reason the assimilation is very effective in this region, and the reanalyses' estimates of sea ice in the Fram Strait are very different from CPOM-CICE. The thickness of the sea ice close to Greenland in the Fram Strait is increased, but there is less ice further away from the coast. The ice in this region is essentially export ice from the Transpolar drift stream and it is shifted in both reanalyses towards the eastern coast of Greenland. There is an increase in the ice thickness in this region in late summer in our reanalyses, but a decrease during the rest of the year. An analysis of long term trends in sea ice export in the Fram Strait by Smedsrud et al. (2017) showed that the September-February export was around 60% of the total export, with the remaining 40% between March-August, with no long term trends. Smedsrud et al. (2017) also showed that the Fram Strait export has increased during the last few decades, and that the export is responsible for 18% of the variance in the sea ice extent in September. It is important then that the Fram Strait is modelled well in CPOM-CICE for summer sea ice estimates, but in this area it appears to be poor. In terms of sea ice volume, Spreen et al. (2020) analysed volume export between 1992 and 2014 using observations of sea ice concentration, drift and thickness and found a decreasing trend in ice volume export through this time, however there were signals for years of very low sea ice volume like 2007 and 2012 where the export has contributed to overall ice volume loss. We saw that there is an increase in sea ice volume loss due to dynamics when analysing the volume fluxes in the 2010s (see section 7.2). It is possible that the estimates of sea ice in the Fram Strait could

already be improved by improving modelling of ice in the MIZ as mentioned previously in this section. If the reason for the displacement of the export region is because of ocean forcing, then it could be improved by coupling the model to an ocean model, or using more scientifically robust ocean forcing.

7.8 Summary

In this chapter we have investigated the reanalyses in greater detail. One of the primary reasons for producing a reanalysis is to study the changes to the processes in the model that occur as a result of the assimilation of observations which bring the model closer in line with the observations. We examined the changes in the volume budget and the differences in the fluxes between the reanalyses and CPOM-CICE. The detrimental impacts on the sea ice volume by assimilating sea ice concentration alone mean that there is a large discontinuity in October 2010, and so we look at the impacts only after 2010. We found that the most interesting differences occur in the early melting season, where there are changes to the top and basal melt which increase the ice melt in the reanalyses, showing that either the model is creating too much ice in winter or that the model misrepresents the melt in early summer, most likely a combination of both. This aligns with what was found in chapter 6, where the seasonality of the thinner thermodynamically driven ice was much different in the reanalyses than in the control. In September and October the ice formation is reduced in both reanalyses, and this prevents ice from becoming too thick in the Canadian Archipelago, and the excessive growth of thinner ice in CPOM-CICE which occurs in the early growth season.

The climatological trends in the reanalyses were investigated in much further detail in this chapter, and in particular the volume. Sea ice volume is closely tied to thickness and concentration, two key indicators of climate change in the Arctic Ocean, but there is little knowledge of its true state due to limited knowledge, primarily concerning the ice thickness, though ice concentration at the ice edge is also highly uncertain. In reana_nt we found decreasing trends in volume which were remarkably similar to those from PIOMAS in winter, spring and autumn. In summer the decreasing trend in reana_nt was much lower than PIOMAS, though there is still reasonable agreement, within the margin of error. All reanalyses agree with PIOMAS on the decreasing volume of Arctic sea ice over the last 40 years. In reana_bt the trends are much larger than seen in the other reanalyses, the control and PIOMAS, likely skewed by the large increments in thickness and volume that occur when

ice thickness began to be assimilated in 2010. We compared both our reanalyses in depth with PIOMAS, which has much lower sea ice volumes than reana_bt, but is comparable to reana_nt in many months. We speculated that the differences between PIOMAS and reana_bt are due to the different sea ice concentration observations chosen for assimilation and the different data assimilation scheme used. The reana_nt study was able to produce sea ice volumes very similar to those in PIOMAS in winter, and much lower than those in reana_bt. The assimilation of Bootstrap sea ice concentration alone clearly causes excessively high estimates of sea ice thickness in the Canadian Archipelago, but it is difficult to verify any sea ice volume reanalysis in the 1980s and 1990s because of a lack of thickness observations for evaluation. This means then that the sea ice volume in any reanalysis is strongly dependent upon which product is chosen to assimilate, and though assimilating NASA Team sea ice concentration leads to slightly better sea ice thickness estimates in the last decade than assimilating Bootstrap concentration, there could be unknown effects from data assimilation which could lead to sea ice state estimates substantially different from the truth in the 1980s and 1990s.

In this chapter we also looked at the assimilation of the very recently introduced Landy CS2 thickness observations, which use machine learning to produce year-round observations of sea ice thickness from CPOM CS2 data. The assimilation of this dataset provides the best results in comparison to independent observations by a substantial margin in comparison to the CPOM CS2 thickness observations. The reana_landy experiment assimilates Bootstrap observations but provides a closer match to PIOMAS than reana_bt, the year-round assimilation of sea ice thickness seems to correct for the high thickness bias caused by assimilation of the Bootstrap sea ice concentration dataset. This is the first time this observational product has been assimilated for use in a reanalysis product, and it shows highly promising results for use in sea ice reanalysis study, and should greatly improve knowledge of summer Arctic sea ice thickness with its use in combination with state-of-the-art sea ice models and data assimilation system. This is important because our knowledge of the summer sea ice state is much less confident than in winter, due to the lack of thickness observations and because of the increased uncertainty in the ice concentration observations due to melt pond interference.

Chapter 8

Concluding Remarks

The primary objective of this thesis was to produce and analyse a new Arctic sea ice reanalysis over the satellite era. In addition to assimilating ice concentration observations from Bootstrap or NASA Team and seasonally available mean sea ice thickness observations from Cryosat-2 (CPOM CS2), we also experimented with assimilating other recently developed observations from the CS2 satellite. These included assimilation of sub-grid scale sea ice thickness distribution and year-round observations of sea ice thickness (Landy CS2). The impacts and potential benefits of assimilating these new observational records in a new sea ice data assimilation system were investigated in chapter 5. In chapters 6 and 7 we identified a number of differences between the CPOM-CICE model and three reanalyses, investigated the potential causes of these differences and identified possible solutions for the sea ice modelling. In this chapter we lay out the conclusions of this thesis, and comment on implications in both sea ice data assimilation and wider questions in sea ice study, as well as future research potential.

8.1 An intercomparison of short-term sea ice data assimilation studies

We have developed a new sea ice data assimilation system CICE-PDAF, using the method of LETKF assimilation, in order to produce a new sea ice reanalysis and to identify and improve our current sea ice model CPOM-CICE. In chapter 2 we discussed presently available sea ice observation datasets including sea ice concentration, sea ice thickness, sea ice thickness distribution and recent advancements in making observations of snow depth and melt ponds. This includes a discussion of the errors in these products and the error statistics we use when assimilating any of these products. The sea ice model which is used in this study, CPOM-

CICE, is detailed in chapter 3. Data assimilation and the LETKF assimilation system used is also introduced in chapter 3, where we also discuss currently available sea ice reanalyses, including PIOMAS.

In chapter 4 we discussed the development of the coupled CICE-PDAF system and post-analysis step processing which is necessary under certain conditions due to the changes in the model sea ice state made by the assimilation. The method of generating ensemble spread is introduced, which follows from Brusdal et al. (2003). This method works by perturbing NCEP-2 atmospheric forcing fields using an EOF method, and then amplifying them. Using this data assimilation system we conducted experiments assimilating NASA Team Bootstrap daily sea ice concentration alongside CS2 products of monthly mean sea ice thickness in order to test and refine assimilation parameters for setting up the reanalysis studies. We used a localisation radius of 100 km, a forgetting factor of 0.995 and an ensemble size of 100.

In chapter 5 we performed short-term experiments comparing a control run (no assimilation) of the CICE-PDAF model alongside assimilation runs and found that the assimilation performed well for sea ice concentration, sea ice thickness and sub-grid scale sea ice thickness distribution. The best performing experiment in comparison to independent observations was assim_conc_hi_4hd, which assimilated sea ice concentration, mean sea ice thickness and the sea ice thickness distribution in the thinnest four categories of sea ice. For the first time we have assimilated a sub-grid scale sea ice thickness distribution, which caused significant changes in the ice thickness distribution across the ice cover in comparison to other reanalyses. By assimilating thickness distribution alongside mean thickness, there were important benefits to the thickness distribution and sea ice mass budget estimates in our sea ice model, primarily in the thickest category of sea ice, which saw a reduction in RMSE of 1.5 m that persisted throughout the experimental time period. This is the first time that a sub-grid scale sea ice thickness distribution product has been assimilated, and it shows that there are potentially benefits to assimilating it, though these are difficult to quantify due to a lack of independent verification data which have been processed in the same way as the CS2 ice thickness distribution observations.

We have shown that the assimilation of the CS2 products were highly beneficial when compared to the assimilation of concentration alone, when compared against randomly chosen CS2 evaluation data that were not assimilated. This has also been seen in Fritzner et al. (2019) and Fiedler et al. (2022). The assimilation of thickness distribution provides strong additional benefits for the ice thickness estimates in the thickest category. The large

(in some places over a metre) differences in ice thickness between assimilating only ice concentration and assimilating both ice concentration and ice thickness are striking and suggest that information about sea ice thickness is essential to produce a more realistic sea ice reanalysis data set. The assimilation of the Bootstrap concentration appeared to negatively effect CICE-PDAF estimates of sea ice thickness compared to these evaluation data, however many ocean-sea ice reanalyses have found positive impacts to sea ice thickness estimates (Chevallier et al., 2017). These differences may be a result of the use of the Bootstrap ice concentration dataset for assimilation, or the lack of a full ocean model in our reanalysis, and possibly a combination of both.

8.2 A Satellite Era Arctic Sea Ice Reanalysis

During the period of ice thickness assimilation in the reanalyses, particularly reana_nt and reana_bt, we find that the greatest improvement in sea ice thickness estimates in comparison to observations (independent and semi-independent) is in the central Arctic, around the North Pole, and in the Beaufort Sea. These areas are identified in Chevallier et al. (2017) as areas where current reanalyses of Arctic sea ice are deficient, so it is encouraging that our reanalysis shows significant improvement in these regions of the Arctic. They also note that many of the reanalyses use PIOMAS as calibration, despite the fact that PIOMAS does not use sea ice thickness assimilation for its sea ice reanalysis, but solely based on the fact that it has been verified with a wide range of in-situ data sources (Schweiger et al., 2011). Chevallier et al. (2017) mentions the need for further investigation into the observation errors which should be used for the data assimilation, which we also found to be the case, as many sea ice observational datasets do not provide fully quantified errors. Additionally Chevallier et al. (2017) also mentions that sea ice velocity biases are associated with ice thickness biases, so further work into successfully assimilating sea ice velocities might provide further benefits to ice thickness if assimilated alongside observations of sea ice thickness, so this could be an interesting, although challenging study, as early attempts at assimilating sea ice velocity alongside ice concentration showed there was little benefit, but assimilating sea ice velocity alongside ice thickness could provide some benefits.

As part of this thesis we have produced three new satellite era Arctic sea ice reanalyses, which we analyse, investigate and discuss in chapters 6 and 7. We assimilated Bootstrap and NASA Team sea ice concentration (separately), CPOM CS2 mean ice thickness, CPOM CS2 ice thickness distribution and Landy CS2 mean ice thickness. We found that assimilating Bootstrap concentration alone between 1981 and 2010 led to an excessive amount of sea ice being created in the late melting season (August and September), which, as with the study

we did on shorter reanalyses, led to higher sea ice volumes than in CPOM-CICE. When the CPOM CS2 products began to be assimilated in October 2010, there were significant increments to the ice thickness and ice volume in this case. We looked at differences in sea ice thickness between the free run and the reanalysis and found that the main differences were located in the Central Arctic, which is too thin in CPOM-CICE, and the Canadian Archipelago, where the ice is much too thick. There were also smaller differences in the Beaufort Sea, Barents Sea, Kara Sea and the Fram Strait. The differences in spatial distribution between the control run and the assimilation are important, as many studies note that a common bias in sea ice models is that ice is too thin near the Canadian Archipelago, and too thick in the central Arctic (near the north pole) and the Beaufort Sea, for example in Schweiger et al. (2011) it is found that PIOMAS overestimates the thickness of the thin ice and underestimates the thickness of thicker ice, this is also seen in the intercomparison study in Chevallier et al. (2017) and also noted in other studies such as Johnson et al. (2012), Kwok and Cunningham (2008), Chevallier et al. (2013), particularly showing a negative sea ice thickness bias in the regions of the thickest ice.

We discussed differences between the free model run, the reanalyses we produced and observations in the sea ice state in different regions of the Arctic. Generally, the model has a tendency to make the ice which packs up against the Canadian Archipelago too thick in comparison to the observations of thickness, and thus when thickness is assimilated we find that the reanalyses have thinner ice in this region, closer to estimates from independent OIB thickness observations. Conversely we find that ice in many regions surrounding the Canadian Archipelago is too thin in the model, and the reanalyses are able to improve estimates of thickness in these regions in comparison to the independent estimates. Assimilation of the Landy CS2 sea ice thickness data is particularly effective in this region in comparison to the OIB estimates in terms of the RMSE. In the Beaufort Sea, the sea ice cover in the reanalyses fluctuates much more throughout the seasons than in the free model run, reflecting some of the changes seen in observations (Kwok and Cunningham, 2010), particularly capturing the seasonal cycle here in an improved manner. The sea ice thickness estimates also differ in the regions of the Barents and Kara Seas, where ice is thicker in the reanalyses than in the CPOM-CICE model, and the reanalyses seem to capture the thinning ice in the Barents Sea, and also the thicker ice in the Kara Seas, in a way that is much closer to the observational estimates. In the Fram Strait there is an increase in the ice volume and a displacement of the ice export region in the reanalyses in the past decade in comparison to the free model run.

We investigated differences in components of the volume flux determining the local volume

budget between the free run and the reanalysis, to try and identify any particular problems in the sea ice modelling. We found that congelation ice growth was significantly higher in the free run than in the reanalysis in October, and that frazil ice growth is also higher between September and November. These differences appear to be partially responsible for the excess thickness that occurs in the Canadian Archipelago, and the increased sea ice extent that occurs in CPOM-CICE in winter. There were also differences in the early melting season in June between the free run and the reanalysis. In the Fram Strait, where sea ice is exported due to the Transpolar drift stream, the distribution of the ice was changed, with the ice closer to the eastern coast of Greenland becoming thicker, and ice further away thinning. The angle at which the sea ice is exported out of the Arctic is tilted closer towards Greenland, and there is an increased loss of sea ice due to dynamics in all months. The increase in sea ice volume loss due to dynamics is not completely due to changes in the sea ice drift in this region though, as there are also changes to convergence and divergence in the Central Arctic and the Beaufort Sea.

In section 7.4 we saw that in the freeze-up season the ensemble spread of the sea ice volume in the reanalysis was determined mainly by the uncertainty in the concentration (hence area and extent), and between May and September it was determined by the uncertainty in the sea ice thickness. In terms of improving the sea ice volume estimates in CPOM-CICE then, the sea ice concentration is important during the freeze-up season between October and April, and sea ice thickness is important during the melting season between May and September. Although the assimilation of the CPOM CS2 thickness observations does have an effect on sea ice volume estimates in summer, we have seen that there are also some negative effects from assimilating the Bootstrap sea ice concentration observations alone during the late melting season (August-September and parts of October). Assimilation of summer sea ice thickness observations then looks like it could be extremely useful for estimates of summer sea ice thickness and hence volume, which is important as the trends in declining sea ice are strongest during these months, and our knowledge of sea ice is not as strong in summer (Wunderling et al., 2020). Assimilation of summer sea ice thickness also appears to improve estimates of year-round ice thickness as well, as we see in this study.

We studied the distribution of mean thickness across the Arctic and found that the free run was overestimating the grid cells with very thick ice (> 4 m), and its shape was too peaked. The distribution of the mean thickness in the reanalysis was flatter than seen in the free run, with stark differences seen in September and particularly December. In December almost all grid cells in the reanalysis had a mean ice thickness between 0 and 3 m, whereas

CPOM-CICE was much more skewed towards ice less than 1 m thick, but also with a lot more grid cells with ice thicker than 3 m. This is further evidence of issues with the modelling of the early freeze-up season in CPOM-CICE. Future work in sea ice data assimilation should focus on further improving estimates of the thickness distribution using observations, and also producing a thickness distribution product from ICESat-2 which could be used as a validation tool with the CS2 measurements, or vice-versa.

We evaluated the new reanalyses produced in this thesis against evaluation (non-assimilated) observations from CS2, and independent observations from Operation IceBridge (OIB): all three reanalyses have lower RMSEs with respect to both sets of observations than the stand-alone CPOM-CICE model. Assimilating NASA Team and CPOM CS2 data led to marginally lower (2 cm) RMSEs than assimilating Bootstrap and CS2 data with respect to the evaluation data set from CS2. Assimilating Landy CS2 thickness data also resulted in a large decrease in RMSE, its RMSE was 7-9 cm higher than those which assimilated CPOM CS2 sea ice thickness. However in comparison with OIB ice thickness, the assimilation of Landy CS2 ice thickness resulted in the biggest decrease in RMSE, from 54 cm to 29 cm. Comparing the assimilation of Bootstrap and NASA Team SIC, assimilating NASA Team sea ice concentration decreased RMSE to 40 cm, whereas Bootstrap assimilation only reduced RMSE to 46 cm. The amount of OIB data is relatively small and restricted to March and a few days in April each year for a few years, but these results would indicate that assimilating NASA Team concentration alongside CPOM CS2 ice thickness performs slightly better than Bootstrap with CPOM CS2 since 2010.

The reanalyses were compared with PIOMAS, and it was found that there were large differences in sea ice volume estimates between PIOMAS and when assimilating Bootstrap sea ice concentration. When NASA Team observations were assimilated, the volume estimates were similar to PIOMAS estimates in the freeze-up season. However there were lower estimates of volume in the melting season (June and September) in comparison to PIOMAS. These differences in the melting season were smaller after 2005. As PIOMAS also assimilates NASA Team data we expect the differences should be small, so the differences in summer are surprising. When looking at the mean ice thickness, there are big differences in the distribution of the sea ice thickness across the Arctic, particularly in the Central Arctic and the Canadian Archipelago. Overall we identified five key regions where differences were the greatest between models, observations, our reanalyses and PIOMAS. PIOMAS has much thinner ice the Canadian Archipelago than the CPOM-CICE model all our reanalyses besides reana_landy, but then a more wide ranging region of ice over 1.4 m thick still covering

much of the Arctic Ocean. Baffin Bay is not mostly ice free in PIOMAS whereas it is in our reanalyses in late summer. The Barents and Kara Seas see the widest range of differences between models, observations and reanalyses. The reanalyses seem to show that the intense warming in the Barents Sea is thinning the ice in the Barents Sea but is not effecting the ice cover in the neighbouring Kara Sea so much, which is not captured in the models and is only reproduced by the assimilation of ice thickness. There is also strong disagreement about the thickness of the ice in the Central Arctic, with the CPOM-CICE model showing much thinner ice than in observations (which disagree themselves about how much thicker the ice should be). The consensus within sea ice reanalyses seems to be thicker ice in the Central Arctic than in sea ice models, which evaluates well against independent observations (particularly for reana_landy). In terms of sea ice extent PIOMAS has a slightly larger extent than all our reanalyses, primarily caused by the differences in the Barents Sea and Baffin Bay. This study has provided further evidence into the reduction of the Arctic sea ice cover over the satellite period. Of most importance is the increased evidence of the thinning of the Arctic sea ice that has taken place over the past 40 years. We find trends in the decreasing sea ice volume similar to those from PIOMAS (within the margin of error) in spring, autumn and winter, however we should be careful in extracting too many conclusions from this, as Chevallier et al. (2017) pointed out that reanalyses have calibrated themselves too much using PIOMAS, which still has considerable uncertainty associated and does not assimilate thickness. Here we have not calibrated these reanalyses in any way using PIOMAS, but as PIOMAS has been verified using in-situ data from a long time period, it is useful for comparison. A notable difference between our trends and those from PIOMAS is that the September trend in our reanalyses is much smaller, but the trend in June is greater.

As part of this thesis we introduced a new sea ice data assimilation system CICE-PDAF in order to investigate both short term sea ice data assimilation experiments and long term satellite era reanalyses. This system can be used to continue to produce the reanalysis for recent and future years when the observation and atmospheric/ocean forcing data become available, which will allow for further study of the current trends in the sea ice cover, and for further analysis of the long term impact of assimilating sea ice thickness observations in the system. There is also the potential for a lot of further study from this reanalysis. This includes the potential for further intercomparison studies with sea ice models, observations and reanalyses. There could be work arising from the data assimilation increments in the reanalysis, as well as how the assimilation parameters are working, and whether their refinement could improve the reanalysis. There are also a number of model diagnostic variables that we did not look at in this thesis, including ice age, melt ponds and ice strength - which

could provide important insight. There is also the potential for more in depth studies of this reanalysis on a smaller scale - looking at particular seas or areas of the sea ice cover - some of which we have identified and examined in some detail in this thesis. Parameter estimation using data assimilation (Hansen and Penland, 2007) could also provide a useful tool and provide a lot of insight into many of the uncertain parameters in sea ice models - in particular ice strength and albedo. Parameter estimation has been used very little in sea ice modelling studies thus far, but has a lot of potential in revealing more about important parameters in sea ice models, as was shown in Massonnet et al. (2014).

This thesis shows that with future work in producing new observations of sea ice, with improved spatiotemporal coverage, and with further work in sea ice data assimilation, there is a lot of potential for sea ice reanalyses to improve our understanding of the changing Arctic sea ice cover. For example, the assimilation of the summer sea ice thickness observations provided a marked improvement in ice thickness validation against independent observations. This is despite the fact that the independent observations used for validation are only available in March and April, meaning that the validation occurs 6 months after the end of the summer thickness assimilation. These results are also promising for sea ice forecasting using summer sea ice thickness. The assimilation of ice thickness distribution was able to significantly improve estimates of the sea ice thickness in category 5. There is also substantial room for improving and calibrating the data assimilation parameters used in the reanalyses, which is mentioned in Chevallier et al. (2017) as one area of sea ice data assimilation study where there is room for improvement. This was outside the scope of this study, though we did do a basic analysis in chapter 4 which showed how small changes in these parameters can be significant. In particular the uncertainties in both the observations and model, because the reliability and effectiveness of ensemble-based data assimilation is highly dependent on the use of accurate observation errors and a well-calibrated ensemble spread that represents the uncertainty in the model as close as possible (Rodwell et al., 2016). Further work could also include looking further back into the ice thickness record and assimilating ICESAT for ENVISAT ice thickness records, which although are highly uncertain could still provide benefits to a sea ice reanalysis, and would allow for a much longer (2002 onwards) period of ice thickness assimilation, for further consistency. Recent work by Tilling et al. (2019), which looked at creating a consistent longer term dataset of ice thickness by correcting issues with the ENVISAT ice thickness retrieval showed promise, and data like this produced in future could be used in a reanalysis system to lengthen the period where ice thickness can be assimilated, this could increase the length of a reanalysis assimilating sea ice thickness to 8 years. This work should also be useful for Arctic sea ice prediction.

We have shown that assimilating different sea ice concentration observations can lead to very different sea ice volume estimates, despite the similarities between the Bootstrap and NASA Team datasets. The strong disagreement in the seasonal cycle between the observations and model shows that future work is needed in this area, to decrease the uncertainty in sea ice observations in the transition periods between the melting and growth season, and to understand how the model physics cause the shift in the seasonal cycle. The differences in volume caused by assimilating different sea ice concentration datasets shows us the importance of additionally assimilating sea ice thickness observations, which can help constrain the influences of the sea ice concentration assimilation on the model. The findings of this thesis indicate that assimilating Landy CS2 ice thickness observations, which have been assimilated for the first time in this thesis, can further reduce the uncertainty in sea ice thickness and hence sea ice volume in model estimates of the sea ice state. This thesis shows that the assimilation of summer sea ice thickness and sea ice thickness distribution is extremely promising for future sea ice reanalysis and prediction studies, and can provide significant benefits to our estimates of the Arctic sea ice state and its trends over the satellite era.

References

Alexandrov, V., Sandven, S., Wahlin, J. and Johannessen, O. (2010), 'The relation between sea ice thickness and freeboard in the arctic', *The Cryosphere* **4**(3), 373–380.

Andersen, S., Tonboe, R., Kern, S. and Schyberg, H. (2006), 'Improved retrieval of sea ice total concentration from spaceborne passive microwave observations using numerical weather prediction model fields: An intercomparison of nine algorithms', *Remote Sensing of Environment* **104**(4), 374–392.

Anderson, J. L. and Anderson, S. L. (1999), 'A monte carlo implementation of the nonlinear filtering problem to produce ensemble assimilations and forecasts', *Monthly weather review* **127**(12), 2741–2758.

Armitage, T. W., Bacon, S., Ridout, A. L., Thomas, S. F., Aksenov, Y. and Wingham, D. J. (2016), 'Arctic sea surface height variability and change from satellite radar altimetry and grace, 2003–2014', *Journal of Geophysical Research: Oceans* **121**(6), 4303–4322.

Babb, D. G., Landy, J., Barber, D. and Galley, R. (2019), 'Winter sea ice export from the beaufort sea as a preconditioning mechanism for enhanced summer melt: A case study of 2016', *Journal of Geophysical Research: Oceans* **124**(9), 6575–6600.

Barber, D. G., Hop, H., Mundy, C. J., Else, B., Dmitrenko, I. A., Tremblay, J.-E., Ehn, J. K., Assmy, P., Daase, M., Candlish, L. M. et al. (2015), 'Selected physical, biological and biogeochemical implications of a rapidly changing arctic marginal ice zone', *Progress in Oceanography* **139**, 122–150.

Barton, B. I., Lenn, Y.-D. and Lique, C. (2018), 'Observed atlantification of the barents sea causes the polar front to limit the expansion of winter sea ice', *Journal of Physical Oceanography* **48**(8), 1849–1866.

Bateson, A. W., Feltham, D. L., Schröder, D., Hosekova, L., Ridley, J. K. and Aksenov, Y. (2020), 'Impact of sea ice floe size distribution on seasonal fragmentation and melt of arctic sea ice', *The Cryosphere* **14**(2), 403–428.

Beaven, S. G. (1995), *Sea ice radar backscatter modeling, measurements, and the fusion of active and passive microwave data*, University of Kansas.

Bishop, C. H. (2019), 'Data assimilation strategies for state-dependent observation error variances', *Quarterly Journal of the Royal Meteorological Society* **145**(718), 217–227.

Bishop, C. H., Etherton, B. J. and Majumdar, S. J. (2001), 'Adaptive sampling with the ensemble transform kalman filter. part i: Theoretical aspects', *Monthly weather review* **129**(3), 420–436.

Bitz, C., Holland, M., Weaver, A. and Eby, M. (2001), 'Simulating the ice-thickness distribution in a coupled climate model', *Journal of Geophysical Research: Oceans* **106**(C2), 2441–2463.

Bitz, C. M. and Lipscomb, W. H. (1999), 'An energy-conserving thermodynamic model of sea ice', *Journal of Geophysical Research: Oceans* **104**(C7), 15669–15677.

Blockley, E., Martin, M., McLaren, A., Ryan, A., Waters, J., Lea, D., Mirouze, I., Peterson, K., Sellar, A. and Storkey, D. (2014), 'Recent development of the met office operational ocean forecasting system: an overview and assessment of the new global foam forecasts', *Geoscientific Model Development* **7**(6), 2613–2638.

Blockley, E. W. and Peterson, K. A. (2018), 'Improving met office seasonal predictions of arctic sea ice using assimilation of cryosat-2 thickness', *The Cryosphere* **12**(11), 3419–3438.

Boutin, G., Lique, C., Ardhuin, F., Rousset, C., Talandier, C., Accensi, M. and Girard-Ardhuin, F. (2020), 'Towards a coupled model to investigate wave–sea ice interactions in the arctic marginal ice zone', *The Cryosphere* **14**(2), 709–735.

Briegleb, B. and Light, B. (2007), 'A delta-eddington multiple scattering parameterization for solar radiation in the sea ice component of the community climate system model', *NCAR technical note* pp. 1–108.

Brunt, K. M., Neumann, T. A., Amundson, J. M., Kavanaugh, J. L., Moussavi, M. S., Walsh, K. M., Cook, W. B. and Markus, T. (2016), 'Mabel photon-counting laser altimetry data in alaska for icesat-2 simulations and development', *The Cryosphere* **10**(4), 1707–1719.

Brusdal, K., Brankart, J.-M., Halberstadt, G., Evensen, G., Brasseur, P., van Leeuwen, P. J., Dombrowsky, E. and Verron, J. (2003), 'A demonstration of ensemble-based assimilation methods with a layered ogcm from the perspective of operational ocean forecasting systems', *Journal of Marine Systems* **40**, 253–289.

Buehner, M., Bertino, L., Caya, A., Heimbach, P., Smith, G., Lemieux, J., Toudal Pedersen, L. and Carrieres, T. (2017), 'Sea ice data assimilation', *Sea Ice Analysis and Forecasting: Towards an Increased Reliance on Automated Prediction Systems, eds T. Carrieres, M. Buehner, J.-F. Lemieux, and LT Pedersen (Cambridge: Cambridge University Press)* pp. 109–143.

Bunzel, F., Notz, D. and Pedersen, L. T. (2018), 'Retrievals of arctic sea-ice volume and its trend significantly affected by interannual snow variability', *Geophysical Research Letters* **45**(21), 11–751.

Castellani, G., Lüpkes, C., Hendricks, S. and Gerdes, R. (2014), 'Variability of a rctic sea-ice topography and its impact on the atmospheric surface drag', *Journal of Geophysical Research: Oceans* **119**(10), 6743–6762.

Cavalieri, D. J. (1991), 'Nasa sea ice validation program for the defense meteorological satellite program special sensor microwave imager', *Journal of Geophysical Research: Oceans* **96**(C12), 21969–21970.

Cavalieri, D. J., Gloersen, P. and Campbell, W. J. (1984), 'Determination of sea ice parameters with the nimbus 7 smmr', *Journal of Geophysical Research: Atmospheres* **89**(D4), 5355–5369.

Cavalieri, D. J. and Parkinson, C. L. (2012), 'Arctic sea ice variability and trends, 1979–2010', *The Cryosphere* **6**(4), 881–889.

Chassignet, E. P., Hurlburt, H. E., Smedstad, O. M., Halliwell, G. R., Hogan, P. J., Wallcraft, A. J., Baraille, R. and Bleck, R. (2007), 'The hycom (hybrid coordinate ocean model) data assimilative system', *Journal of Marine Systems* **65**(1-4), 60–83.

Chaudhuri, A. H., Ponte, R. M. and Nguyen, A. T. (2014), 'A comparison of atmospheric reanalysis products for the arctic ocean and implications for uncertainties in air–sea fluxes', *Journal of Climate* **27**(14), 5411–5421.

Chevallier, M., Salas y Mélia, D., Voldoire, A., Déqué, M. and Garric, G. (2013), 'Seasonal forecasts of the pan-arctic sea ice extent using a gcm-based seasonal prediction system', *Journal of Climate* **26**(16), 6092–6104.

Chevallier, M., Smith, G. C., Dupont, F., Lemieux, J.-F., Forget, G., Fujii, Y., Hernandez, F., Msadek, R., Peterson, K. A., Storto, A. et al. (2017), 'Intercomparison of the arctic sea ice cover in global ocean–sea ice reanalyses from the ora-ip project', *Climate Dynamics* **49**(3), 1107–1136.

Cohen, J., Screen, J. A., Furtado, J. C., Barlow, M., Whittleston, D., Coumou, D., Francis, J., Dethloff, K., Entekhabi, D., Overland, J. et al. (2014), 'Recent arctic amplification and extreme mid-latitude weather', *Nature geoscience* **7**(9), 627–637.

Cohen, J., Zhang, X., Francis, J., Jung, T., Kwok, R., Overland, J., Ballinger, T., Bhatt, U., Chen, H., Coumou, D. et al. (2020), 'Divergent consensuses on arctic amplification influence on midlatitude severe winter weather', *Nature Climate Change* **10**(1), 20–29.

Comiso, J. (2017), 'Bootstrap sea ice concentrations from nimbus-7 smmr and dmsp ssm/i-ssmis, version 3, boulder, colorado usa. nasa national snow and ice data center distributed active archive center'.

Comiso, J. C. (1995), *SSM/I sea ice concentrations using the bootstrap algorithm*, Vol. 1380, National Aeronautics and Space Administration, Goddard Space Flight Center.

Comiso, J. C., Cavalieri, D. J., Parkinson, C. L. and Gloersen, P. (1997), 'Passive microwave algorithms for sea ice concentration: A comparison of two techniques', *Remote sensing of Environment* **60**(3), 357–384.

Comiso, J. C., Grenfell, T. C., Lange, M., Lohanick, A. W., Moore, R. K. and Wadhams, P. (1992), 'Microwave remote sensing of the southern ocean ice cover', *Washington DC American Geophysical Union Geophysical Monograph Series* **68**, 243–259.

Coumou, D., Di Capua, G., Vavrus, S., Wang, L. and Wang, S. (2018), 'The influence of arctic amplification on mid-latitude summer circulation', *Nature Communications* **9**(1), 1–12.

Cox, M. D. (1984), 'A primitive equation, 3-dimensional model of the ocean.', *GFDL Ocean Group Technical Report No 1, GFDL, Princeton University* .

Curry, J. A., Schramm, J. L. and Ebert, E. E. (1995), 'Sea ice-albedo climate feedback mechanism', *Journal of Climate* **8**(2), 240–247.

Dai, A., Luo, D., Song, M. and Liu, J. (2019), 'Arctic amplification is caused by sea-ice loss under increasing co2', *Nature communications* **10**(1), 1–13.

David, C., Lange, B., Krumpen, T., Schaafsma, F., van Franeker, J. A. and Flores, H. (2016), 'Under-ice distribution of polar cod boreogadus saida in the central arctic ocean and their association with sea-ice habitat properties', *Polar Biology* **39**(6), 981–994.

Dawson, G., Landy, J., Tsamados, M., Komarov, A. S., Howell, S., Heorton, H. and Krumpen, T. (2022), 'A 10-year record of arctic summer sea ice freeboard from cryosat-2', *Remote Sensing of Environment* **268**, 112744.

Dee, D. P., Uppala, S. M., Simmons, A. J., Berrisford, P., Poli, P., Kobayashi, S., Andrae, U., Balmaseda, M., Balsamo, G., Bauer, d. P. et al. (2011), 'The era-interim reanalysis: Configuration and performance of the data assimilation system', *Quarterly Journal of the royal meteorological society* **137**(656), 553–597.

Ding, Y., Cheng, X., Liu, J., Hui, F., Wang, Z. and Chen, S. (2020), 'Retrieval of melt pond fraction over arctic sea ice during 2000–2019 using an ensemble-based deep neural network', *Remote Sensing* **12**(17), 2746.

Dulière, V. and Fichefet, T. (2007), 'On the assimilation of ice velocity and concentration data into large-scale sea ice models', *Ocean Science* **3**(2), 321–335.

Durkalec, A., Furgal, C., Skinner, M. W. and Sheldon, T. (2015), 'Climate change influences on environment as a determinant of indigenous health: Relationships to place, sea ice, and health in an inuit community', *Social science & medicine* **136**, 17–26.

Emery, W., Fowler, C., Hawkins, J. and Preller, R. (1991), 'Fram strait satellite image-derived ice motions', *Journal of Geophysical Research: Oceans* **96**(C3), 4751–4768.

England, M., Jahn, A. and Polvani, L. (2019), 'Nonuniform contribution of internal variability to recent arctic sea ice loss', *Journal of Climate* **32**(13), 4039–4053.

Evensen, G. (1994), 'Sequential data assimilation with a nonlinear quasi-geostrophic model using monte carlo methods to forecast error statistics', *Journal of Geophysical Research: Oceans* **99**(C5), 10143–10162.

Farrell, S. L., Kurtz, N., Connor, L. N., Elder, B. C., Leuschen, C., Markus, T., McAdoo, D. C., Panzer, B., Richter-Menge, J. and Sonntag, J. G. (2011), 'A first assessment of icebridge snow and ice thickness data over arctic sea ice', *IEEE Transactions on Geoscience and Remote Sensing* **50**(6), 2098–2111.

Feltham, D., Untersteiner, N., Wettlaufer, J. and Worster, M. (2006), 'Sea ice is a mushy layer', *Geophysical Research Letters* **33**(14).

Ferry, N., Masina, S., Storto, A., Haines, K., Valdivieso, M., Barnier, B. and Molines, J.-M. (2011), 'Product user manual globalreanalysisphys-001-004-a and b'.

Fiedler, E. K., Martin, M. J., Blockley, E., Mignac, D., Fournier, N., Ridout, A., Shepherd, A. and Tilling, R. (2022), 'Assimilation of sea ice thickness derived from cryosat-2 along-track freeboard measurements into the met office's forecast ocean assimilation model (foam)', *The Cryosphere* **16**(1), 61–85.

Flato, G. M. and Hibler III, W. D. (1995), 'Ridging and strength in modeling the thickness distribution of arctic sea ice', *Journal of Geophysical Research: Oceans* **100**(C9), 18611–18626.

Flocco, D., Feltham, D. L. and Turner, A. K. (2010), 'Incorporation of a physically based melt pond scheme into the sea ice component of a climate model', *Journal of Geophysical Research: Oceans* **115**(C8).

Francis, J. A., Vavrus, S. J. and Cohen, J. (2017), 'Amplified arctic warming and mid-latitude weather: new perspectives on emerging connections', *Wiley Interdisciplinary Reviews: Climate Change* **8**(5), e474.

Fritzner, S., Graversen, R., Christensen, K. H., Rostosky, P. and Wang, K. (2019), 'Impact of assimilating sea ice concentration, sea ice thickness and snow depth in a coupled ocean–sea ice modelling system', *The Cryosphere* **13**(2), 491–509.

Gaspari, G. and Cohn, S. E. (1999), 'Construction of correlation functions in two and three dimensions', *Quarterly Journal of the Royal Meteorological Society* **125**(554), 723–757.

Giles, K. A., Laxon, S. W. and Ridout, A. L. (2008), 'Circumpolar thinning of arctic sea ice following the 2007 record ice extent minimum', *Geophysical Research Letters* **35**(22).

Giles, K., Laxon, S., Wingham, D., Wallis, D., Krabill, W., Leuschen, C., McAdoo, D., Manizade, S. and Raney, R. (2007), 'Combined airborne laser and radar altimeter measurements over the fram strait in may 2002', *Remote Sensing of Environment* **111**(2-3), 182–194.

Gui, D., Lei, R., Pang, X., Hutchings, J. K., Zuo, G. and Zhai, M. (2020), 'Validation of remote-sensing products of sea-ice motion: A case study in the western arctic ocean', *Journal of Glaciology* **66**(259), 807–821.

Haas, C., Hendricks, S., Eicken, H. and Herber, A. (2010), 'Synoptic airborne thickness surveys reveal state of arctic sea ice cover', *Geophysical Research Letters* **37**(9).

Hamill, T. M., Whitaker, J. S. and Snyder, C. (2001), 'Distance-dependent filtering of background error covariance estimates in an ensemble kalman filter', *Monthly Weather Review* **129**(11), 2776–2790.

Hansen, J. A. and Penland, C. (2007), 'On stochastic parameter estimation using data assimilation', *Physica D: Nonlinear Phenomena* **230**(1-2), 88–98.

Hebert, D. A., Allard, R. A., Metzger, E. J., Posey, P. G., Preller, R. H., Wallcraft, A. J., Phelps, M. W. and Smedstad, O. M. (2015), 'Short-term sea ice forecasting: An assessment of ice concentration and ice drift forecasts using the us n avy's a rctic c ap n owcast/f orecast s ystem', *Journal of Geophysical Research: Oceans* **120**(12), 8327–8345.

Helm, V., Humbert, A. and Miller, H. (2014), 'Elevation and elevation change of greenland and antarctica derived from cryosat-2', *The Cryosphere* **8**(4), 1539–1559.

Hibler Iii, W. (1980), 'Modeling a variable thickness sea ice cover', *Monthly weather review* **108**(12), 1943–1973.

Hilmer, M. and Lemke, P. (2000), 'On the decrease of arctic sea ice volume', *Geophysical Research Letters* **27**(22), 3751–3754.

Holland, M. M., Bailey, D. A. and Vavrus, S. (2011), 'Inherent sea ice predictability in the rapidly changing arctic environment of the community climate system model, version 3', *Climate dynamics* **36**, 1239–1253.

Hollinger, J. P., Peirce, J. L. and Poe, G. A. (1990), 'Ssm/i instrument evaluation', *IEEE Transactions on Geoscience and Remote sensing* **28**(5), 781–790.

Houtekamer, P. L. and Mitchell, H. L. (1998), 'Data assimilation using an ensemble kalman filter technique', *Monthly Weather Review* **126**(3), 796–811.

Houtekamer, P. L. and Zhang, F. (2016), 'Review of the ensemble kalman filter for atmospheric data assimilation', *Monthly Weather Review* **144**(12), 4489–4532.

Howell, S. E. and Brady, M. (2019), 'The dynamic response of sea ice to warming in the canadian arctic archipelago', *Geophysical Research Letters* **46**(22), 13119–13125.

Hunke, E., Lipscomb, W., Turner, A., Jeffery, N. and Elliott, S. (2015), Cice: The los alamos sea ice model documentation and software user's manual 1568 version 5.1, Technical report, Los Alamos National Laboratory.

Hunt, B. R., Kostelich, E. J. and Szunyogh, I. (2007), 'Efficient data assimilation for spatiotemporal chaos: A local ensemble transform kalman filter', *Physica D: Nonlinear Phenomena* **230**(1-2), 112–126.

Hunter, C. M., Caswell, H., Runge, M. C., Regehr, E. V., Amstrup, S. C. and Stirling, I. (2010), 'Climate change threatens polar bear populations: a stochastic demographic analysis', *Ecology* **91**(10), 2883–2897.

Ivanova, N., Johannessen, O. M., Pedersen, L. T. and Tonboe, R. T. (2014), 'Retrieval of arctic sea ice parameters by satellite passive microwave sensors: A comparison of eleven sea ice concentration algorithms', *IEEE Transactions on Geoscience and Remote Sensing* **52**(11), 7233–7246.

Ivanova, N., Pedersen, L. T., Tonboe, R., Kern, S., Heygster, G., Lavergne, T., Sørensen, A., Saldo, R., Dybkjær, G., Brucker, L. et al. (2015), 'Inter-comparison and evaluation of sea ice algorithms: towards further identification of challenges and optimal approach using passive microwave observations', *The Cryosphere* **9**(5), 1797–1817.

Johnson, M., Proshutinsky, A., Aksenov, Y., Nguyen, A. T., Lindsay, R., Haas, C., Zhang, J., Diansky, N., Kwok, R., Maslowski, W. et al. (2012), 'Evaluation of arctic sea ice thickness simulated by arctic ocean model intercomparison project models', *Journal of Geophysical Research: Oceans* **117**(C8).

Kaleschke, L., Lüpkes, C., Vihma, T., Haarpaintner, J., Bochert, A., Hartmann, J. and Heygster, G. (2001), 'Ssm/i sea ice remote sensing for mesoscale ocean-atmosphere interaction analysis', *Canadian journal of remote sensing* **27**(5), 526–537.

Kalman, R. E. (1960), 'A new approach to linear filtering and prediction problems'.

Kanagaratnam, P., Markus, T., Lytle, V., Heavey, B., Jansen, P., Prescott, G. and Gogineni, S. P. (2007), 'Ultrawideband radar measurements of thickness of snow over sea ice', *IEEE Transactions on Geoscience and Remote Sensing* **45**(9), 2715–2724.

Kanamitsu, M., Ebisuzaki, W., Woollen, J., Yang, S.-K., Hnilo, J., Fiorino, M. and Potter, G. (2002), 'Ncep–doe amip-ii reanalysis (r-2)', *Bulletin of the American Meteorological Society* **83**(11), 1631–1644.

Kay, J. E., L'Ecuyer, T., Gettelman, A., Stephens, G. and O'Dell, C. (2008), 'The contribution of cloud and radiation anomalies to the 2007 arctic sea ice extent minimum', *Geophysical Research Letters* **35**(8).

Kern, S., Rösel, A., Pedersen, L. T., Ivanova, N., Saldo, R. and Tonboe, R. T. (2016), 'The impact of melt ponds on summertime microwave brightness temperatures and sea-ice concentrations', *The Cryosphere* **10**(5), 2217–2239.

Kerr, Y. H., Waldteufel, P., Wigneron, J.-P., Delwart, S., Cabot, F., Boutin, J., Escorihuela, M.-J., Font, J., Reul, N., Gruhier, C. et al. (2010), 'The smos mission: New tool for monitoring key elements ofthe global water cycle', *Proceedings of the IEEE* **98**(5), 666–687.

King, J., Howell, S., Derksen, C., Rutter, N., Toose, P., Beckers, J. F., Haas, C., Kurtz, N. and Richter-Menge, J. (2015), 'Evaluation of operation icebridge quick-look snow depth estimates on sea ice', *Geophysical Research Letters* **42**(21), 9302–9310.

Kohnemann, S. H., Heinemann, G., Bromwich, D. H. and Gutjahr, O. (2017), 'Extreme warming in the kara sea and barents sea during the winter period 2000–16', *Journal of Climate* **30**(22), 8913–8927.

Kovacs, K. M., Lydersen, C., Overland, J. E. and Moore, S. E. (2011), 'Impacts of changing sea-ice conditions on arctic marine mammals', *Marine Biodiversity* **41**(1), 181–194.

Krishfield, R. A., Proshutinsky, A., Tateyama, K., Williams, W. J., Carmack, E. C., McLaughlin, F. A. and Timmermans, M.-L. (2014), 'Deterioration of perennial sea ice in the beaufort gyre from 2003 to 2012 and its impact on the oceanic freshwater cycle', *Journal of Geophysical Research: Oceans* **119**(2), 1271–1305.

Kurtz, N., Farrell, S., Studinger, M., Galin, N., Harbeck, J., Lindsay, R., Onana, V., Panzer, B. and Sonntag, J. (2013), 'Sea ice thickness, freeboard, and snow depth products from operation icebridge airborne data', *The Cryosphere* **7**(4), 1035–1056.

Kurtz, N., M. Studinger, J., Harbeck, V., Onana, V. and Yi, D. (2015), 'Icebridge l4 sea ice freeboard, snow depth, and thickness, version 1'.
URL: *https://nsidc.org/data/IDCSI4/versions/1*

Kurtz, N., M. Studinger, J., Harbeck, V., Onana, V. and Yi, D. (2016), 'Icebridge sea ice freeboard, snow depth, and thickness quick look, version 1'.
URL: *https://nsidc.org/data/NSIDC-0708/versions/1*

Kurtz, N., Studinger, M., Harbeck, J., Onana, V. and Farrell, S. (2012), 'Icebridge sea ice freeboard, snow depth, and thickness', *Digital media, NASA Distributed Active Archive Center at the National Snow and Ice Data Center, Boulder, Colorado, USA, http://nsidc. org/data/idcsi2. html (last access: 6 December 2013)* .

Kurtz, N. T. and Farrell, S. L. (2011), 'Large-scale surveys of snow depth on arctic sea ice from operation icebridge', *Geophysical Research Letters* **38**(20).

Kwok, R. (2018), 'Arctic sea ice thickness, volume, and multiyear ice coverage: losses and coupled variability (1958–2018)', *Environmental Research Letters* **13**(10), 105005.

Kwok, R. and Cunningham, G. (2008), 'Icesat over arctic sea ice: Estimation of snow depth and ice thickness', *Journal of Geophysical Research: Oceans* **113**(C8).

Kwok, R. and Cunningham, G. (2010), 'Contribution of melt in the beaufort sea to the decline in arctic multiyear sea ice coverage: 1993–2009', *Geophysical Research Letters* **37**(20).

Kwok, R. and Cunningham, G. (2015), 'Variability of arctic sea ice thickness and volume from cryosat-2', *Philosophical Transactions of the Royal Society A: Mathematical, Physical and Engineering Sciences* **373**(2045), 20140157.

Kwok, R., Cunningham, G., Zwally, H. and Yi, D. (2007), 'Ice, cloud, and land elevation satellite (icesat) over arctic sea ice: Retrieval of freeboard', *Journal of Geophysical Research: Oceans* **112**(C12).

Kwok, R. and Morison, J. (2016), 'Sea surface height and dynamic topography of the ice-covered oceans from cryosat-2: 2011–2014', *Journal of Geophysical Research: Oceans* **121**(1), 674–692.

Kwok, R., Zwally, H. J. and Yi, D. (2004), 'Icesat observations of arctic sea ice: A first look', *Geophysical Research Letters* **31**(16).

Landy, J., Dawson, G., Tsamados, M. and et al (2022), 'A year-round satellite sea-ice thickness record from cryosat-2', *Nature* .

Lavergne, T., Eastwood, S., Teffah, Z., Schyberg, H. and Breivik, L.-A. (2010), 'Sea ice motion from low-resolution satellite sensors: An alternative method and its validation in the arctic', *Journal of Geophysical Research: Oceans* **115**(C10).

Lavergne, T., Sørensen, A. M., Kern, S., Tonboe, R., Notz, D., Aaboe, S., Bell, L., Dybkjær, G., Eastwood, S., Gabarro, C. et al. (2019), 'Version 2 of the eumetsat osi saf and esa cci sea-ice concentration climate data records', *The Cryosphere* **13**(1), 49–78.

Lawrence, I. R., Tsamados, M. C., Stroeve, J. C., Armitage, T. W. and Ridout, A. L. (2018), 'Estimating snow depth over arctic sea ice from calibrated dual-frequency radar freeboards', *The Cryosphere* **12**(11), 3551–3564.

Laxon, S. (1994), 'Sea ice altimeter processing scheme at the eodc', *International Journal of Remote Sensing* **15**(4), 915–924.

Laxon, S. W., Giles, K. A., Ridout, A. L., Wingham, D. J., Willatt, R., Cullen, R., Kwok, R., Schweiger, A., Zhang, J., Haas, C. et al. (2013), 'Cryosat-2 estimates of arctic sea ice thickness and volume', *Geophysical Research Letters* **40**(4), 732–737.

Lee, S., Stroeve, J., Tsamados, M. and Khan, A. L. (2020), 'Machine learning approaches to retrieve pan-arctic melt ponds from visible satellite imagery', *Remote Sensing of Environment* **247**, 111919.

Li, H. and Fedorov, A. V. (2021), 'Persistent freshening of the arctic ocean and changes in the north atlantic salinity caused by arctic sea ice decline', *Climate Dynamics* **57**(11), 2995–3013.

Li, Z., Ding, Q., Steele, M. and Schweiger, A. (2022), 'Recent upper arctic ocean warming expedited by summertime atmospheric processes', *Nature communications* **13**(1), 1–11.

Lindsay, R. and Zhang, J. (2006), 'Assimilation of ice concentration in an ice–ocean model', *Journal of Atmospheric and Oceanic Technology* **23**(5), 742–749.

Lipscomb, W. H. (2001), 'Remapping the thickness distribution in sea ice models', *Journal of Geophysical Research: Oceans* **106**(C7), 13989–14000.

Lipscomb, W. H. and Hunke, E. C. (2004), 'Modeling sea ice transport using incremental remapping', *Monthly weather review* **132**(6), 1341–1354.

Lipscomb, W. H., Hunke, E. C., Maslowski, W. and Jakacki, J. (2007), 'Ridging, strength, and stability in high-resolution sea ice models', *Journal of Geophysical Research: Oceans* **112**(C3).

Lisæter, K. A., Rosanova, J. and Evensen, G. (2003), 'Assimilation of ice concentration in a coupled ice–ocean model, using the ensemble kalman filter', *Ocean Dynamics* **53**(4), 368–388.

Mahesh, A., Spinhirne, J. D., Duda, D. P. and Eloranta, E. W. (2002), 'Atmospheric multiple scattering effects on glas altimetry. ii. analysis of expected errors in antarctic altitude measurements', *IEEE transactions on geoscience and remote sensing* **40**(11), 2353–2362.

Markus, T., Neumann, T., Martino, A., Abdalati, W., Brunt, K., Csatho, B., Farrell, S., Fricker, H., Gardner, A., Harding, D. et al. (2017), 'The ice, cloud, and land elevation satellite-2 (icesat-2): science requirements, concept, and implementation', *Remote sensing of environment* **190**, 260–273.

Maslanik, J. (1992), 'Effects of weather on the retrieval of sea ice concentration and ice type from passive microwave data', *International Journal of Remote Sensing* **13**(1), 37–54.

Massonnet, F., Fichefet, T. and Goosse, H. (2015), 'Prospects for improved seasonal arctic sea ice predictions from multivariate data assimilation', *Ocean Modelling* **88**, 16–25.

Massonnet, F., Goosse, H., Fichefet, T. and Counillon, F. (2014), 'Calibration of sea ice dynamic parameters in an ocean-sea ice model using an ensemble kalman filter', *Journal of Geophysical Research: Oceans* **119**(7), 4168–4184.

Mathiot, P., König Beatty, C., Fichefet, T., Goosse, H., Massonnet, F. and Vancoppenolle, M. (2012), 'Better constraints on the sea-ice state using global sea-ice data assimilation', *Geoscientific Model Development* **5**(6), 1501–1515.

Mauritzen, C. and Häkkinen, S. (1997), 'Influence of sea ice on the thermohaline circulation in the arctic-north atlantic ocean', *Geophysical Research Letters* **24**(24), 3257–3260.

Melia, N., Haines, K. and Hawkins, E. (2016), 'Sea ice decline and 21st century trans-arctic shipping routes', *Geophysical Research Letters* **43**(18), 9720–9728.

Melia, N., Haines, K., Hawkins, E. and Day, J. J. (2017), 'Towards seasonal arctic shipping route predictions', *Environmental Research Letters* **12**(8), 084005.

Mignac, D., Martin, M., Fiedler, E., Blockley, E. and Fournier, N. (2022), 'Improving the met office's forecast ocean assimilation model (foam) with the assimilation of satellite-derived sea-ice thickness data from cryosat-2 and smos in the arctic', *Quarterly Journal of the Royal Meteorological Society* .

Miyoshi, T., Kalnay, E. and Li, H. (2013), 'Estimating and including observation-error correlations in data assimilation', *Inverse Problems in Science and Engineering* **21**(3), 387–398.

Mu, L., Nerger, L., Tang, Q., Loza, S. N., Sidorenko, D., Wang, Q., Semmler, T., Zampieri, L., Losch, M. and Goessling, H. F. (2020), 'Toward a data assimilation system for seamless sea ice prediction based on the awi climate model', *Journal of Advances in Modeling Earth Systems* **12**(4), e2019MS001937.

Nerger, L. and Hiller, W. (2013), 'Software for ensemble-based data assimilation systems—implementation strategies and scalability', *Computers & Geosciences* **55**, 110–118.

Nerger, L., Hiller, W. and Schröter, J. (2005), Pdaf-the parallel data assimilation framework: experiences with kalman filtering, *in* 'Use of high performance computing in meteorology', World Scientific, pp. 63–83.

Nezhad, M. M., Neshat, M., Groppi, D., Marzialetti, P., Heydari, A., Sylaios, G. and Garcia, D. A. (2021), 'A primary offshore wind farm site assessment using reanalysis data: A case study for samothraki island', *Renewable Energy* **172**, 667–679.

Nose, T., Waseda, T., Kodaira, T. and Inoue, J. (2020), 'Satellite-retrieved sea ice concentration uncertainty and its effect on modelling wave evolution in marginal ice zones', *The Cryosphere* **14**(6), 2029–2052.

Parkinson, C. L. and Comiso, J. C. (2013), 'On the 2012 record low arctic sea ice cover: Combined impact of preconditioning and an august storm', *Geophysical Research Letters* **40**(7), 1356–1361.

Peacock, N. R. and Laxon, S. W. (2004), 'Sea surface height determination in the arctic ocean from ers altimetry', *Journal of Geophysical Research: Oceans* **109**(C7).

Perovich, D. K. and Richter-Menge, J. A. (2009), 'Loss of sea ice in the arctic', *Annual review of marine science* **1**, 417–441.

Petty, A. A., Kurtz, N. T., Kwok, R., Markus, T. and Neumann, T. A. (2020), 'Winter arctic sea ice thickness from icesat-2 freeboards', *Journal of Geophysical Research: Oceans* **125**(5), e2019JC015764.

Petty, A. A., Webster, M., Boisvert, L. and Markus, T. (2018), 'The nasa eulerian snow on sea ice model (nesosim) v1. 0: initial model development and analysis', *Geoscientific Model Development* **11**(11), 4577–4602.

Pham, D. T., Verron, J. and Roubaud, M. C. (1998), 'A singular evolutive extended kalman filter for data assimilation in oceanography', *Journal of Marine systems* **16**(3-4), 323–340.

Pringle, D., Eicken, H., Trodahl, H. and Backstrom, L. (2007), 'Thermal conductivity of landfast antarctic and arctic sea ice', *Journal of Geophysical Research: Oceans* **112**(C4).

Rhodes, R. H., Faïn, X., Stowasser, C., Blunier, T., Chappellaz, J., McConnell, J. R., Romanini, D., Mitchell, L. E. and Brook, E. J. (2013), 'Continuous methane measurements from a late holocene greenland ice core: Atmospheric and in-situ signals', *Earth and Planetary Science Letters* **368**, 9–19.

Ricker, R., Girard-Ardhuin, F., Krumpen, T. and Lique, C. (2018), 'Satellite-derived sea ice export and its impact on arctic ice mass balance', *The Cryosphere* **12**(9), 3017–3032.

Ricker, R., Hendricks, S., Helm, V., Skourup, H. and Davidson, M. (2014), 'Sensitivity of cryosat-2 arctic sea-ice freeboard and thickness on radar-waveform interpretation', *The Cryosphere* **8**(4), 1607–1622.

Ricker, R., Hendricks, S., Kaleschke, L., Tian-Kunze, X., King, J. and Haas, C. (2017), 'A weekly arctic sea-ice thickness data record from merged cryosat-2 and smos satellite data', *The Cryosphere* **11**(4), 1607–1623.

Rienecker, M. M., Suarez, M. J., Gelaro, R., Todling, R., Bacmeister, J., Liu, E., Bosilovich, M. G., Schubert, S. D., Takacs, L., Kim, G.-K. et al. (2011), 'Merra: Nasa's modern-era retrospective analysis for research and applications', *Journal of climate* **24**(14), 3624–3648.

Roberts, M. J., Wood, R. A., Marsh, R. and New, A. L. (1996), 'An intercomparison of a bryan–cox-type ocean model and an isopycnic ocean model. part i: The subpolar gyre and high-latitude processes', *Journal of Physical Oceanography* **26**(8), 1495–1527.

Rodwell, M., Lang, S., Ingleby, N., Bormann, N., Hólm, E., Rabier, F., Richardson, D. and Yamaguchi, M. (2016), 'Reliability in ensemble data assimilation', *Quarterly Journal of the Royal Meteorological Society* **142**(694), 443–454.

Rostosky, P., Spreen, G., Farrell, S. L., Frost, T., Heygster, G. and Melsheimer, C. (2018), 'Snow depth retrieval on arctic sea ice from passive microwave radiometers—improvements and extensions to multiyear ice using lower frequencies', *Journal of Geophysical Research: Oceans* **123**(10), 7120–7138.

Rothrock, D. A. (1975), 'The energetics of the plastic deformation of pack ice by ridging', *Journal of Geophysical Research* **80**(33), 4514–4519.

Sakov, P., Counillon, F., Bertino, L., Lisæter, K., Oke, P. and Korablev, A. (2012), 'Topaz4: an ocean-sea ice data assimilation system for the north atlantic and arctic', *Ocean Science* **8**(4), 633–656.

Sandu, I., Massonnet, F., Van Achter, G., Acosta Navarro, J. C., Arduini, G., Bauer, P., Blockley, E., Bormann, N., Chevallier, M., Day, J. et al. (2021), 'The potential of numerical prediction systems to support the design of arctic observing systems: Insights from the applicate and yopp projects', *Quarterly Journal of the Royal Meteorological Society* **147**(741), 3863–3877.

Santer, B. D., Wigley, T. M., Simmons, A. J., Kållberg, P. W., Kelly, G. A., Uppala, S. M., Ammann, C., Boyle, J. S., Brüggemann, W., Doutriaux, C. et al. (2004), 'Identification of anthropogenic climate change using a second-generation reanalysis', *Journal of Geophysical Research: Atmospheres* **109**(D21).

Scagliola, M., Fornari, M. and Tagliani, N. (2015), 'Pitch estimation for cryosat by analysis of stacks of single-look echoes', *IEEE Geoscience and Remote Sensing Letters* **12**(7), 1561–1565.

Schröder, D., Feltham, D. L., Flocco, D. and Tsamados, M. (2014), 'September arctic sea-ice minimum predicted by spring melt-pond fraction', *Nature Climate Change* **4**(5), 353–357.

Schröder, D., Feltham, D. L., Tsamados, M., Ridout, A. and Tilling, R. (2019), 'New insight from cryosat-2 sea ice thickness for sea ice modelling', *The Cryosphere* **13**(1), 125–139.

Schutz, B. E., Zwally, H. J., Shuman, C. A., Hancock, D. and DiMarzio, J. P. (2005), 'Overview of the icesat mission', *Geophysical Research Letters* **32**(21).

Schweiger, A., Lindsay, R., Zhang, J., Steele, M., Stern, H. and Kwok, R. (2011), 'Uncertainty in modeled arctic sea ice volume', *Journal of Geophysical Research: Oceans* **116**(C8).

Seaman, R. (1977), 'Absolute and differential accuracy of analyses achievable with specified observational network characteristics', *Monthly Weather Review* **105**(10), 1211–1222.

Serreze, M. C. and Barry, R. G. (2011), 'Processes and impacts of arctic amplification: A research synthesis', *Global and planetary change* **77**(1-2), 85–96.

Serreze, M. C. and Hurst, C. M. (2000), 'Representation of mean arctic precipitation from ncep–ncar and era reanalyses', *Journal of Climate* **13**(1), 182–201.

Sévellec, F., Fedorov, A. V. and Liu, W. (2017), 'Arctic sea-ice decline weakens the atlantic meridional overturning circulation', *Nature Climate Change* **7**(8), 604–610.

Sievers, I., Rasmussen, T. A. and Stenseng, L. (2023), 'Assimilating cryosat-2 freeboard to improve arctic sea ice thickness estimates', *The Cryosphere Discussions* pp. 1–23.

Smedsrud, L. H., Halvorsen, M. H., Stroeve, J. C., Zhang, R. and Kloster, K. (2017), 'Fram strait sea ice export variability and september arctic sea ice extent over the last 80 years', *The Cryosphere* **11**(1), 65–79.

Smith, D. (1996), 'Extraction of winter total sea-ice concentration in the greenland and barents seas from ssm/i data', *Remote Sensing* **17**(13), 2625–2646.

Smith, G. C., Roy, F., Reszka, M., Surcel Colan, D., He, Z., Deacu, D., Belanger, J.-M., Skachko, S., Liu, Y., Dupont, F. et al. (2016), 'Sea ice forecast verification in the canadian global ice ocean prediction system', *Quarterly Journal of the Royal Meteorological Society* **142**(695), 659–671.

Spreen, G., de Steur, L., Divine, D., Gerland, S., Hansen, E. and Kwok, R. (2020), 'Arctic sea ice volume export through fram strait from 1992 to 2014', *Journal of Geophysical Research: Oceans* **125**(6), e2019JC016039.

Spreen, G., Kaleschke, L. and Heygster, G. (2008), 'Sea ice remote sensing using amsr-e 89-ghz channels', *Journal of Geophysical Research: Oceans* **113**(C2).

Stark, J. D., Ridley, J., Martin, M. and Hines, A. (2008), 'Sea ice concentration and motion assimilation in a sea ice- ocean model', *Journal of Geophysical Research: Oceans* **113**(C5).

Sterlin, J., Fichefet, T., Massonnet, F., Lecomte, O. and Vancoppenolle, M. (2021), 'Sensitivity of arctic sea ice to melt pond processes and atmospheric forcing: A model study', *Ocean Modelling* **167**, 101872.

Stewart, L. M., Dance, S. L. and Nichols, N. K. (2013), 'Data assimilation with correlated observation errors: experiments with a 1-d shallow water model', *Tellus A: Dynamic Meteorology and Oceanography* **65**(1), 19546.

Stroeve, J., Hamilton, L. C., Bitz, C. M. and Blanchard-Wrigglesworth, E. (2014), 'Predicting september sea ice: Ensemble skill of the search sea ice outlook 2008–2013', *Geophysical Research Letters* **41**(7), 2411–2418.

Sundfjord, A., Fer, I., Kasajima, Y. and Svendsen, H. (2007), 'Observations of turbulent mixing and hydrography in the marginal ice zone of the barents sea', *Journal of Geophysical Research: Oceans* **112**(C5).

Swart, N. C., Fyfe, J. C., Hawkins, E., Kay, J. E. and Jahn, A. (2015), 'Influence of internal variability on arctic sea-ice trends', *Nature Climate Change* **5**(2), 86–89.

Thomas, D. N. (2017), *Sea ice*, John Wiley & Sons.

Tian-Kunze, X., Kaleschke, L., Maaß, N., Mäkynen, M., Serra, N., Drusch, M. and Krumpen, T. (2014), 'Smos-derived thin sea ice thickness: algorithm baseline, product specifications and initial verification', *The Cryosphere* **8**(3), 997–1018.

Tietsche, S., Notz, D., Jungclaus, J. and Marotzke, J. (2013), 'Assimilation of sea-ice concentration in a global climate model–physical and statistical aspects', *Ocean science* **9**(1), 19–36.

Tilling, R. L., Ridout, A. and Shepherd, A. (2016), 'Near-real-time arctic sea ice thickness and volume from cryosat-2', *The Cryosphere* **10**(5), 2003–2012.

Tilling, R. L., Ridout, A. and Shepherd, A. (2018), 'Estimating arctic sea ice thickness and volume using cryosat-2 radar altimeter data', *Advances in Space Research* **62**(6), 1203–1225.

Tilling, R. L., Ridout, A., Shepherd, A. and Wingham, D. J. (2015), 'Increased arctic sea ice volume after anomalously low melting in 2013', *Nature Geoscience* **8**(8), 643–646.

Tilling, R., Ridout, A. and Shepherd, A. (2019), 'Assessing the impact of lead and floe sampling on arctic sea ice thickness estimates from envisat and cryosat-2', *Journal of Geophysical Research: Oceans* **124**(11), 7473–7485.

Tippett, M. K., Anderson, J. L., Bishop, C. H., Hamill, T. M. and Whitaker, J. S. (2003), 'Ensemble square root filters', *Monthly weather review* **131**(7), 1485–1490.

Tiuri, M., Sihvola, A., Nyfors, E. and Hallikaiken, M. (1984), 'The complex dielectric constant of snow at microwave frequencies', *IEEE Journal of oceanic Engineering* **9**(5), 377–382.

Tonboe, R., Andersen, S. and Pedersen, L. T. (2006), 'Simulation of the ku-band radar altimeter sea ice effective scattering surface', *IEEE Geoscience and Remote Sensing Letters* **3**(2), 237–240.

Toyoda, T., Fujii, Y., Yasuda, T., Usui, N., Ogawa, K., Kuragano, T., Tsujino, H. and Kamachi, M. (2016), 'Data assimilation of sea ice concentration into a global ocean–sea ice model with corrections for atmospheric forcing and ocean temperature fields', *Journal of oceanography* **72**, 235–262.

Tsamados, M., Feltham, D. L. and Wilchinsky, A. (2013), 'Impact of a new anisotropic rheology on simulations of arctic sea ice', *Journal of Geophysical Research: Oceans* **118**(1), 91–107.

Tschudi, M. A., Meier, W. N. and Stewart, J. S. (2020), 'An enhancement to sea ice motion and age products at the national snow and ice data center (nsidc)', *The Cryosphere* **14**(5), 1519–1536.

Tschudi, M., Meier, W., Stewart, J., Fowler, C. and Maslanik, J. (2019), 'Polar pathfinder daily 25 km ease-grid sea ice motion vectors, version 4', *Boulder, CO: NASA National Snow and Ice Data Center Distributed Active Archive Center* **10**.

Verron, J., Sengenes, P., Lambin, J., Noubel, J., Steunou, N., Guillot, A., Picot, N., Coutin-Faye, S., Sharma, R., Gairola, R. et al. (2015), 'The saral/altika altimetry satellite mission', *Marine Geodesy* **38**(sup1), 2–21.

Vetra-Carvalho, S., Van Leeuwen, P. J., Nerger, L., Barth, A., Altaf, M. U., Brasseur, P., Kirchgessner, P. and Beckers, J.-M. (2018), 'State-of-the-art stochastic data assimilation methods for high-dimensional non-gaussian problems', *Tellus A: Dynamic Meteorology and Oceanography* **70**(1), 1–43.

Walsh, J. E., Chapman, W. L. and Portis, D. H. (2009), 'Arctic cloud fraction and radiative fluxes in atmospheric reanalyses', *Journal of Climate* **22**(9), 2316–2334.

Wang, H., Zhang, L., Chu, M. and Hu, S. (2020), 'Advantages of the latest los alamos sea-ice model (cice): evaluation of the simulated spatiotemporal variation of arctic sea ice', *Atmospheric and Oceanic Science Letters* **13**(2), 113–120.

Wang, X., Key, J., Kwok, R. and Zhang, J. (2016), 'Comparison of arctic sea ice thickness from satellites, aircraft, and piomas data', *Remote Sensing* **8**(9), 713.

Wang, Y., Counillon, F., Bethke, I., Keenlyside, N., Bocquet, M. and Shen, M.-l. (2017), 'Optimising assimilation of hydrographic profiles into isopycnal ocean models with ensemble data assimilation', *Ocean Modelling* **114**, 33–44.

Warren, S. G., Rigor, I. G., Untersteiner, N., Radionov, V. F., Bryazgin, N. N., Aleksandrov, Y. I. and Colony, R. (1999), 'Snow depth on arctic sea ice', *Journal of Climate* **12**(6), 1814–1829.

Welch, G., Bishop, G. et al. (1995), 'An introduction to the kalman filter'.

Wensnahan, M. and Rothrock, D. A. (2005), 'Sea-ice draft from submarine-based sonar: Establishing a consistent record from analog and digitally recorded data', *Geophysical research letters* **32**(11).

Whitaker, J. S. and Hamill, T. M. (2002), 'Ensemble data assimilation without perturbed observations', *Monthly weather review* **130**(7), 1913–1924.

Willatt, R., Laxon, S., Giles, K., Cullen, R., Haas, C. and Helm, V. (2011), 'Ku-band radar penetration into snow cover on arctic sea ice using airborne data', *Annals of Glaciology* **52**(57), 197–205.

Wingham, D., Francis, C., Baker, S., Bouzinac, C., Brockley, D., Cullen, R., de Chateau-Thierry, P., Laxon, S., Mallow, U., Mavrocordatos, C. et al. (2006), 'Cryosat: A mission to determine the fluctuations in earth's land and marine ice fields', *Advances in Space Research* **37**(4), 841–871.

Wunderling, N., Willeit, M., Donges, J. F. and Winkelmann, R. (2020), 'Global warming due to loss of large ice masses and arctic summer sea ice', *Nature Communications* **11**(1), 5177.

Xie, J., Bertino, L., Counillon, F., Lisæter, K. A. and Sakov, P. (2017), 'Quality assessment of the topaz4 reanalysis in the arctic over the period 1991–2013', *Ocean Science* **13**(1), 123–144.

Xie, J., Counillon, F. and Bertino, L. (2018), 'Impact of assimilating a merged sea-ice thickness from cryosat-2 and smos in the arctic reanalysis', *The Cryosphere* **12**(11), 3671–3691.

Xiu, Y., Min, C., Xie, J., Mu, L., Han, B. and Yang, Q. (2021), 'Evaluation of sea-ice thickness reanalysis data from the coupled ocean-sea-ice data assimilation system topaz4', *Journal of Glaciology* **67**(262), 353–365.

Yang, S. and Christensen, J. H. (2012), 'Arctic sea ice reduction and european cold winters in cmip5 climate change experiments', *Geophysical Research Letters* **39**(20).

Ying, Y., Zhang, F. and Anderson, J. L. (2018), 'On the selection of localization radius in ensemble filtering for multiscale quasigeostrophic dynamics', *Monthly Weather Review* **146**(2), 543–560.

Zhang, J. and Rothrock, D. A. (2003), 'Modeling global sea ice with a thickness and enthalpy distribution model in generalized curvilinear coordinates', *Monthly Weather Review* **131**(5), 845–861.

Zhang, J., Schweiger, A., Webster, M., Light, B., Steele, M., Ashjian, C., Campbell, R. and Spitz, Y. (2018), 'Melt pond conditions on declining arctic sea ice over 1979–2016: Model development, validation, and results', *Journal of Geophysical Research: Oceans* **123**(11), 7983–8003.

Zhang, J., Spitz, Y. H., Steele, M., Ashjian, C., Campbell, R., Berline, L. and Matrai, P. (2010), 'Modeling the impact of declining sea ice on the arctic marine planktonic ecosystem', *Journal of Geophysical Research: Oceans* **115**(C10).

Zhang, J., Thomas, D., Rothrock, D., Lindsay, R., Yu, Y. and Kwok, R. (2003), 'Assimilation of ice motion observations and comparisons with submarine ice thickness data', *Journal of Geophysical Research: Oceans* **108**(C6).

Zhang, Y.-F., Bitz, C. M., Anderson, J. L., Collins, N., Hendricks, J., Hoar, T., Raeder, K. and Massonnet, F. (2018), 'Insights on sea ice data assimilation from perfect model observing system simulation experiments', *Journal of Climate* **31**(15), 5911–5926.

Zhang, Y.-F., Bushuk, M., Winton, M., Hurlin, B., Yang, X., Delworth, T. and Jia, L. (2021), 'Assimilation of satellite-retrieved sea ice concentration and prospects for september predictions of arctic sea ice', *Journal of Climate* **34**(6), 2107–2126.

Zuo, H., Balmaseda, M. A. and Mogensen, K. (2017), 'The new eddy-permitting orap5 ocean reanalysis: description, evaluation and uncertainties in climate signals', *Climate Dynamics* **49**(3), 791–811.

Zwally, H. J., Yi, D., Kwok, R. and Zhao, Y. (2008), 'Icesat measurements of sea ice freeboard and estimates of sea ice thickness in the weddell sea', *Journal of Geophysical Research: Oceans* **113**(C2).